2021

An analytical method for finding exact Traveling wave solutions of some nonlinear Evolution equations (nlees) in biological and Mathematical problems

Ullah, Mohammad Safi

University of Rajshahi, Rajshahi

AN ANALYTICAL METHOD FOR FINDING EXACT TRAVELING WAVE SOLUTIONS OF SOME NONLINEAR EVOLUTION EQUATIONS (NLEES) IN BIOLOGICAL AND MATHEMATICAL PROBLEMS

Thesis submitted to the
Department of Mathematics, University of Rajshahi
For the partial fulfillment of the requirements for the degree of

MASTER OF PHILOSOPHY
IN
MATHEMATICS

Submitted by
Mohammad Safi Ullah
Examination Roll 1813021501
Registration No 1813021501
Session 2017-2018

Supervisor
Professor Dr. M. Zulfikar Ali
Department of Mathematics
University of Rajshahi
Rajshahi-6205

Co-Supervisor
Dr. Harun-Or-Roshid
Associate Professor
Department of Mathematics
Pabna University of Science and Technology, Pabna-6600

February, 2021

Dedicated
to
My Beloved Parents

ABSTRACT

Most of the natural happenings can be present by nonlinear modeling. The soliton theory is a highly effective section of nonlinear sciences that includes soliton, multi-soliton, rational, breather line, breather kinky, lump and rogue wave solutions. Such solutions are essential to realizing the internal properties of the nonlinear models. This dissertation presents exact traveling wave solutions of the three nonlinear models such as the (2+1) Bogoyavlenskii's breaking soliton (BBS) equation, the (2+1)-dimensional Benjamin-Bona-Mahony-Burgers (BBMB) equation and the (3+1)-dimensional Sharma–Tasso–Olver-like (STOL) equation by applying Hirota bilinear method. By this method, we construct the bilinear form and find the interaction solutions of the above three models. We determine the multi-soliton and their interaction solutions of the BBS model and STOL model. Various properties of the obtained solutions are illustrated clearly with a number of 3D plot, 2D plot, density plot, curve plot and contour plot by choosing suitable parametric values via the computational software Maple 18.

ACKNOWLEDGEMENT

I would like to start by thanking Almighty Allah, the Giver of Wisdom, Knowledge and Understanding, Whose divine help has been my source of sustenance.

I wish to express my deepest gratitude to my supervisor Professor Dr. M Zulfikar Ali and co-supervisor Dr. Harun-Or-Roshid for all their professional guidance, constructive feedback and motivations throughout my graduate study at the University of Rajshahi. They introduced me to the interesting and vibrant field of some nonlinear evolution equations and their connection to mathematics and physics. They have dedicated their time, knowledge and skills to guide and help me in my study. The preparation of this thesis would never have been possible without their help.

I would like to thank Professor Dr. Lutfor Rahman, Professor Dr. Kalyan Kumar Dey, Shikha Khatun, Dr. Fazlul Haque and Dr. Nur Alam for assisting me with so many mathematical and non-mathematical aspects of my MPhil study.

I am extremely grateful to the authority of Comilla University for giving me study leave to pursue my Mphil study in Rajshahi. Also I thank my colleagues and students in Comilla University, specially Zillur Rahman, Aman Mahbub and Dr. Abdul Hakim for their friendly support, great advice and encouragement throughout my study.

It is my great pleasure to thank my parents, wife, beloved children, brothers and sisters for supporting me spiritually throughout my study and my life in general. It would be a great happy moment to inform my father Abdus Sobhan and mother Mafia Aktar of my achievements in this higher degree research study.

Finally, I am also thankful to my friends, well-wishers and close ones who helped me directly or indirectly during this work.

Declaration by Author

I hereby announce that the work which is being presented in this thesis entitled ‘‘AN ANALYTICAL METHOD FOR FINDING EXACT TRAVELING WAVE SOLUTIONS OF SOME NONLINEAR EVOLUTION EQUATIONS (NLEES) IN BIOLOGICAL AND MATHEMATICAL PROBLEMS’’ submitted to the Department of Mathematics, University of Rajshahi in partial fulfillment of the requirements for decoration of the degree of Master of Philosophy in Mathematics, is an authentic record of own work.

The work of this thesis has not been submitted by me for the award of any other degree in this University or any other University

Mohammad Safi Ullah

Certificate

This is to certify that Mohammad Safi Ullah has completed his M. Phil thesis work entitled ‘‘AN ANALYTICAL METHOD FOR FINDING EXACT TRAVELING WAVE SOLUTIONS OF SOME NONLINEAR EVOLUTION EQUATIONS (NLEES) IN BIOLOGICAL AND MATHEMATICAL PROBLEMS’’ under my supervision and guidance in the department of mathematics, University of Rajshahi, Rajshahi-6205. During this work, I found him very sincere, energetic and hard working.

I wish him every success in life.

Dr. M Zulfikar Ali

Professor

Department of Mathematics

University of Rajshahi, Rajshahi-6205

Certificate

This is to certify that Mohammad Safi Ullah has completed his M. Phil thesis work entitled ‘‘AN ANALYTICAL METHOD FOR FINDING EXACT TRAVELING WAVE SOLUTIONS OF SOME NONLINEAR EVOLUTION EQUATIONS (NLEES) IN BIOLOGICAL AND MATHEMATICAL PROBLEMS’’ under my supervision and guidance in the department of mathematics, University of Rajshahi, Rajshahi-6205. During this work, I found him very sincere, energetic and hard working.

I wish him every success in life.

Dr. Harun-Or-Roshid

Associate Professor

Department of Mathematics

Pabna University of Science and Technology, Pabna

CONTENTS

INDEX OF FIGURES

Chapter One

Introduction

1.1. Literature review

Nonlinear evolution equations (NLEEs) applicable not only the areas of mathematical physics, but also other branches of nonlinear science for instance nonlinear optics, fluid dynamics, atmospheric, geochemistry, mathematical biology, ecology, chemical kinetics, chemical physics, plasma physics, oceanic scientific problems and others [1-20]. Therefore, searching for exact travelling wave solutions of NLEEs is a crucial concern for scientists and researchers. Soliton solution is a special type of traveling wave solution that is caused by a cancellation of nonlinear and dispersive effects in the medium. In mathematics and physics, a soliton is a self- reinforcing solitary wave packet that maintains its shape while it propagates at a constant velocity. In 1844, the Scottish John John Scott Russell was the first to observe the solitary waves [21]. The bulge of water, that he observed and called “great wave of translation”, was traveling along the channel of water for a long period of time while still retaining its shape. This single-humped wave of the bulge of water is now called solitary waves or solitons. The hot topics of solitons are lump, rogue, and breather waves.

Lump wave is one of the most important parts of solitary waves and has diverse properties. This wave is localized in all directions in the space which decays rationally and moves with a uniform velocity [22]. In 1977, the simplest lump wave solution was primarily reported by Manakov et. al. [23]. Up to now, more and more researcher has paid attention to the study of lump wave [24-28].

The rogue waves are localized in both time and space. Its amplitudes are at least two times higher than those of their surrounding waves, have been observed in the deep ocean.

This wave also arises in the fields of the ocean [29], atmospheric dynamics [30], Bose-Einstein condensates [31] etc.. It is well known that storms and tsunamis caused by typhoons can be predicated hours in advance, but the oceanic rogue waves suddenly appear from nowhere and disappear without a trace [32]. In 1965, the concept of freak rogue in the ocean was first introduced by Draper [33]. In 1983, a rational rogue wave solution was first introduced by a British applied mathematician Howell Peregrine [34].

Breather waves have been observed to be periodically or quasi-periodically localized in the time or space and also can be use to elaborate rogue wave phenomena [35]. In accordance with the distribution and propagation direction, breathers can be divided into the Akhmediev breathers [36] and Kuznetsov-Ma breathers [37]. Akhmediev breathers are space-periodic breather solutions, while Kuznetsov-Ma breathers are time-periodic breather solutions.

For investigating the characteristics of solitary waves, there are various reliable and effective approaches such as the (G'/G)-expansion method [38], the generalized Kudryashov method [39], the Hirota bilinear method [40], the $\tan(\varphi(\xi)/2)$-expansion scheme [41], the tan-cot method [42], the tanh-coth method [43], the direct algebraic method [44], and others [45-70].

Among the previous methods [38-70], the Hirota bilinear method is the best method for finding exact traveling wave solutions of the nonlinear model. This method was firstly discovered by a Japanese scholar Hirota, in 1971 [40]. This method becomes effective and reliable within a short time and used to derive soliton, multi soliton, lump wave, rogue wave, breather wave, and exciting localized formation of soliton solutions [71-78].

1.2. The objectives

The main purpose of this dissertation is to determine multi-solitons, lump, rogue, breather waves and their interaction solutions of the nonlinear models the (2+1) Bogoyavlenskii's breaking soliton (BBS) [79], the (2+1)-dimensional Benjamin-Bona-Mahony-Burgers (BBMB) [80] and the (3+1)-dimensional Sharma–Tasso–Olver-like (STOL) [81] equations by applying Hirota bilinear method.

1.3. The proposal of the dissertation

The total works of my dissertation are divided into eight chapters. Some review methods are included in chapter two, three and four, and then our main method is focused in chapter five, six, seven and eight with some applications to nonlinear models.

The ambition of **chapter two [2]** is to seek novel exact traveling wave solutions together with topological soliton, periodic cusp soliton, periodic bell solutions of the well-recognized Cahn-Allen model [54, 55, 60] and diffusive predator-prey model [61, 62] via MSE method.

In **chapter three [1]**, we incorporated optical soliton solutions that clarify the physical structures as beat phenomena, oscillating rhythm, oscillation together increasing and decreasing rhythm, and oscillation jointly increasing and decreasing rhythm of the Lakshmanan-Porsezian-Daniel (LPD) model [16] by using unified method [70].

In **chapter four [5]**, the generalized Kudryshov method [93, 95] is applied to determine exact solitary wave solutions for the time-fractional generalized Hirota–Satsuma coupled KdV (HSC KdV) model [82, 83]. Therefore, plentiful exact traveling wave solutions are achieved for this model. The succeeding chapters contain our main method with applications.

In **chapter five [6, 7],** the (2+1)-dimensional Bogoyavlenskii's breaking soliton (BBS) [79] and the (2+1)-dimensional Benjamin-Bona-Mahony-Burgers (BBMB) models [80] are considered and reduced to bilinear form by using the Hirota bilinear scheme. We analytically construct the collision of among lump waves, periodic waves, and one-, two-stripe soliton solutions. Finally, we graphically present the nature of the collision solutions of the model in 3D and contour plots.

In **chapter six [3]**, based on the Hirota bilinear form [40] and a "rational-cos-cosh'' type test function we will study new interaction solutions among the lump, periodic and kinky waves for the (3+1)-dimensional Sharma–Tasso–Olver-like (STOL) model [81]. Various types of interaction solutions even hybrid lump waves and fission fusion properties of the STOL model are also constructed. All dynamic properties of the obtained solutions are plotted with 3D and contour plots.

In chapter seven [4], the multi-soliton solution and their interaction solution of the (2+1) dimensional Bogoyavlenskii's breaking soliton (BBS) equation [79] are investigated by applying the Hirota bilinear approach [40]. From this multi-soliton solution, various forms of single kinky-lump type breather solitons, double kinky-lump type breather solitons, the collision of a kink line soliton with a kinky-type breather soliton, and collision of a pair of double kinky-lump breather solitons will be investigated. All the results are depicted by enough graphics.

In **chapter eight,** the Hirota bilinear integral technique [40] is applied to execute n-soliton solutions of the (3+1)-dimensional Sharma–Tasso–Olver-like (STOL) model [81]. We derive kinky-lump breather, combo line kink and kinky-lump breather, and a pair of kinky-lump breather wave solutions that degenerate from two-, three- and four-solitons respectively with both elastic/non-elastic fusion-fission of solitons. All special properties of these collision solutions are illustrated clearly with 3D and contour diagrams by Maple 18.

Chapter Two

Traveling wave solutions for two models by using the MSE Scheme

Acknowledgement

In this chapter [2], by employing modified simple equation (MSE) scheme we estimate the presence of stable kink soliton and kinky-periodic rogue wave solutions; unstable singular kink wave solutions of the biological dynamical models as a Cahn-Allen model and a diffusive predator-prey model. This model frequently occurs in various nonlinear science including quantum physics, plasmas and biophysics. We present some novel exact explicit solutions of the exponential form of both Cahn-Allen and diffusive predator-prey models with some free parametric values. We also derive particular solutions from the explicit solutions selecting some definite values of the free parametric values. As a result, kink, singular kink and kinky-periodic lump wave surfaces are achieved of the solutions. Lastly, the variety and graphic representations of the composition make the models dynamic. Stable and unstable situations are explained in detail from the analysis of the profiles.

2.1. Introduction

The mathematical representing of happenings in nature can be revealed by differential equations. It is well familiar that abundant categories of the physical occurrences in the field of fluid dynamics, quantum physics, chemical physics, electricity and plasmas are demonstrated by nonlinear models and the existence of solitary waves in nature is frequently. However, nonlinear behavior is a challenging due to some minor changes in time-related parametric values; it is not comfortable to manage the non-linear representative of the organism very quickly. Nonlinearity is responsible for the development of local waves and

has the ability to carry energy without wastage which is a very fascinating matter [10, 11]. Otherwise, rapidly growing the spread of infection may cause a disaster state in a community. To tackle the unavailable state or to remain a suitable state, we have to learn the dissimilar types of solutions of the dynamical system in a model of Cahn-Allen or any type of predator-prey model. As in tragedy state waves or to keep emerges location, the height and width of population size is very essential. If we resolve the model of dynamical systems of such difficulties by applying diverse approaches, we can find the best approach of appreciative such potential disasters and then earnings necessary precautions. Thus, the concern becomes more challenging and hence decisive solutions are needed. The solutions of the equation have a crucial impression on mathematical physics and engineering. Recently, there has been a tremendous increased to find the exact solutions of nonlinear models. Various effective schemes have been reputed and enriched, such as the bilinear scheme [40], the $\tan(\varphi(\xi)/2)$-expansion scheme [41], the Darboux transformation scheme [45], the (G'/G)-expansion scheme [46-47], the exp-$(-\varphi(\xi))$-expansion scheme [48], the extended F-expansion scheme [49], the simplest equation scheme [50], the MSE scheme [51–53], exp-function scheme [54], first integral scheme [55] and so on [56-62]. All most all of the above schemes are contingent on computational software except the MSE scheme. The MSE scheme is a very effective and reliable procedure settled successfully by Vitanov [51] and the reference therein [52-53].

The ambition of this chapter is to seek novel exact solutions together with topological soliton, periodic cusp soliton, periodic bell solutions of the well-recognized Cahn-Allen model [54, 55, 60] and diffusive predator-prey model [61, 62] via MSE scheme.

2.2. Description of the MSE scheme

Consider a general form of a nonlinear model as

$$H(u,u_t,u_x,u_{xt},u_{xx},\cdots\ \cdots)=0, \tag{2.1}$$

with real function $u(\xi)=u(x,t)$ and H is a polynomial of $u(x,t)$. We present the key steps of the scheme as follows:

Step 1: Let us combine the real variables x and t by a combined variable ξ as

$$u(\bar{r},t)=u(\xi),\quad \xi=\bar{P}.\bar{r}\pm wt, \tag{2.2}$$

where $\bar{P}=l\hat{i}+m\hat{j}+n\hat{k}$ and $\bar{r}=x\hat{i}+y\hat{j}+z\hat{k}$ with real constants l, m, n, wave amount k and wave velocity w.

By the above relation the Eq. (2.1) converted to the ordinary differential equation as follows

$$G(u,u',u''\cdots\ \cdots\ \cdots)=0\ , \tag{2.3}$$

where G is a polynomial in $u(\xi)$ and its derivatives.

Step 2: Consider the trial solution of Eq. (2.3) as

$$u(\xi)=\sum_{i=0}^{n}A_i\left(\frac{S'(\xi)}{S(\xi)}\right)^i, \tag{2.4}$$

with real constants $A_i(i=0,1,....,n)$ and unknown function $S(\xi)$.

Step 3: By balancing the derivative of highest order and nonlinear terms in Eq. (2.3), we can find the value of n in Eq. (2.4).

Step 4: From Eq. (2.4) and Eq. (2.3), we get a polynomial of $(S'(\xi)/S(\xi))$ and its derivatives and $(S(\xi))^{-i}$, $(i=0,1,2,\cdots,n)$, and then equating the coefficients of $(S(\xi))^{-i}$, $(i=0,1,2,\cdots,n)$ equal to zero. This produces gives an algebraic system which can be solved to obtain $A_i(i=0,1,2,\cdots,n)$, $S(\xi)$. Then we can find the solution of the Eq. (2.1).

Remark: In comparison the MSE scheme with the simple equation scheme [50], it is seen that simple equation scheme depend upon an auxiliary equation (Riccati equation) but MSE scheme is independent and can perform directly without help of any auxiliary equation. On the other hand, simple equation gives results which are special case of modified equation scheme.

2. 3. Illustrative Examples

Here, we include two examples to make clear the suitability of the MSE scheme to solve nonlinear models declared above.

2.3.1. Example-1: Traveling wave solution of Cahn-Allen Model

Let us consider nonlinear model given as

$$u_t = u_{xx} - u^m + u\,. \tag{2.5}$$

For $m = 3$, Eq. (2.5) suits to Cahn-Allen model [54, 55, 60]. This model occurs in various scientific areas including biophysics, quantum physics and plasmas. To solve this model, we use transformation $\xi = kx + wt$, for wave amount k and wave velocity w. Taking help of this transformation, Eq. (2.5) converts to an ordinary differential equation

$$wu' - k^2u'' + u^3 - u = 0\,. \tag{2.6}$$

Balancing u^3 with u'' we receive the unknown order of solution as $n = 1$. Hence the trial solution Eq. (2.4) takes the form as

$$u(\xi) = A_0 + A_1 \frac{S'(\xi)}{S(\xi)}\,. \tag{2.7}$$

Now, we can compute the terms:

$$u'(\xi) = A_1 \frac{S''(\xi)}{S(\xi)} - A_1\left(\frac{S'(\xi)}{S(\xi)}\right)^2, \tag{2.8}$$

$$u''(\xi) = A_1 \frac{S'''(\xi)}{S(\xi)} - 3A_1 \frac{S''(\xi)S'(\xi)}{S^2(\xi)} + 2A_1 \left(\frac{S'(\xi)}{S(\xi)} \right)^3 . \tag{2.9}$$

Putting Eq. (2.7)-Eq. (2.9) in the Eq. (2.6) and equating coefficients of same powers of $\frac{S'(\xi)}{S(\xi)}$, we gain:

Coefficient of $(S(\xi))^0$: $A_0^3 - A_0 = 0$, (2.10)

Coefficient of $(S(\xi))^{-1}$: $-k^2 A_1 S'''(\xi) + 3A_0^2 A_1 S'(\xi) + wA_1 S''(\xi) - A_1 S'(\xi) = 0$, (2.11)

Coefficient of $(S(\xi))^{-2}$: $-wA_1 (S'(\xi))^2 + 3k^3 A_1 S'(\xi) S''(\xi) + 3A_0 A_1^2 (S'(\xi))^2 = 0$, (2.12)

Coefficient of $(S(\xi))^{-3}$: $A_1 (A_1^2 - 2k^2)(S'(\xi))^3 = 0$. (2.13)

From Eq. (2.10), we achieve $A_0 = 0, 1, -1$ and from Eq. (2.13) we can receive the values $A_1 \neq 0$ and thus $A_1 = \pm\sqrt{2}k$ and

$$\frac{S'''}{S''} = \frac{3k^2(3A_0^2 - 1) + w(w - 3A_0 A_1)}{k^2(w - 3A_0 A_1)}. \tag{2.14}$$

Integrating we have

$$S'' = c_1 \exp\left(\frac{3k^2(3A_0^2 - 1) + w(w - 3A_0 A_1)}{k^2(w - 3A_0 A_1)} \xi\right). \tag{2.15}$$

From Eq. (2.12), we also get, $S' = \frac{3c_1 k^2}{w - 3A_0 A_1} \exp\left(\frac{3k^2(3A_0^2 - 1) + w(w - 3A_0 A_1)}{k^2(w - 3A_0 A_1)} \xi\right)$. (2.16)

Integrating Eq. (2.16) one time, we have

$$S = \frac{3c_1 k^4}{3k^2(3A_0^2 - 1) + w(w - 3A_0 A_1)} \exp\left(\frac{3k^2(3A_0^2 - 1) + w(w - 3A_0 A_1)}{k^2(w - 3A_0 A_1)} \xi\right) + c_2 . \tag{2.17}$$

Using Eqs. (2.16) and (2.17), we attain to the solution

$$u = A_0 + \frac{3c_1A_1k^2}{w-3A_0A_1} \times \exp\left(\frac{3k^2(3A_0^2-1)+w(w-3A_0A_1)}{k^2(w-3A_0A_1)}\xi\right) \Bigg/$$

$$\left(\frac{3c_1k^4}{3k^2(3A_0^2-1)+w(w-3A_0A_1)}\exp\left(\frac{3k^2(3A_0^2-1)+w(w-3A_0A_1)}{k^2(w-3A_0A_1)}\xi\right)+c_2\right), \quad (2.18)$$

where $\xi = k(x \pm \frac{3}{\sqrt{2}}t)$ with $w = \pm\frac{3}{\sqrt{2}}k$. Here c_1 and c_2 are arbitrary constants.

Case-I: For the set $A_0 = 0,\ A_1 = \pm\sqrt{2}k$, we get

$$u = \pm\frac{3\sqrt{2}c_1k^3}{w} \times \frac{\exp\left(\frac{w^2-3k^2)}{k^2w)}\xi\right)}{\frac{3c_1k^4}{w^2-3k^2}\exp\left(\frac{w^2-3k^2)}{k^2w)}\xi\right)+c_2}, \quad (2.19)$$

where $\xi = k(x \pm \frac{3}{\sqrt{2}}t)$ with $w = \pm\frac{3}{\sqrt{2}}k$.

If we choose $c_2 = \frac{3k^4c_1}{w^2-3k^2}$, then we arrive to the solution

$$u = \pm\frac{w^2-3k^2}{\sqrt{2}wk}\left\{1+\tanh\left(\frac{w^2-3k^2}{2wk^2}\xi\right)\right\}, \quad (2.20)$$

where $\xi = k(x \pm \frac{3}{\sqrt{2}}t)$ with $w = \pm\frac{3}{\sqrt{2}}k$.

If we choose $c_2 = -\frac{3k^4c_1}{w^2-3k^2}$, then we arrive to the solution

$$u = \pm\frac{w^2-3k^2}{\sqrt{2}wk}\left\{1+\coth\left(\frac{w^2-3k^2}{2wk^2}\xi\right)\right\}, \quad (2.21)$$

where $\xi = k(x \pm \frac{3}{\sqrt{2}}t)$.

Since c_1 and c_2 are free parameters, for various selections of c_1 and c_2 it provides abundant novel exact solutions of the Cahn-Allen model. The achieved solutions from Eq. (2.20) and Eq. (2.21) are depicted graphically in **Fig-2.1** and **Fig-2. 2.**

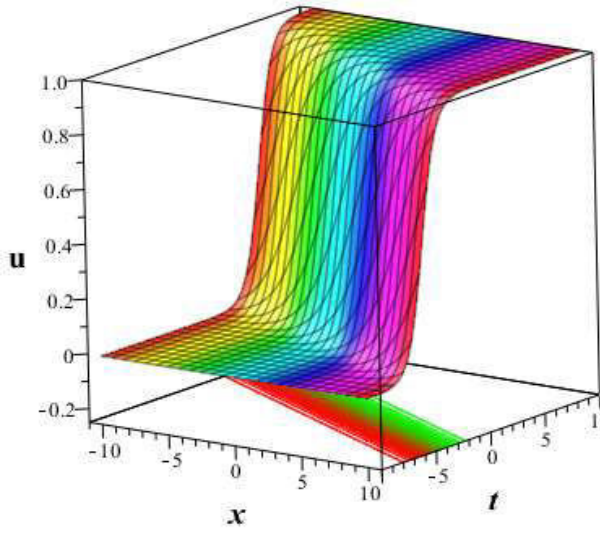

Fig-2.1: Kink wave of the solution Eq. (2.20) with $k=1$.

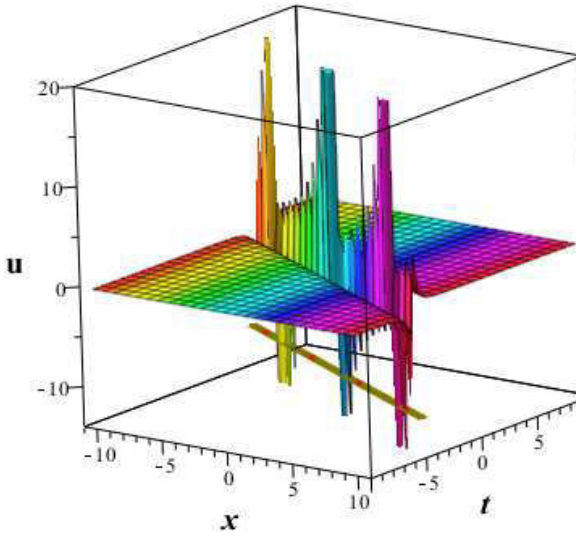

Fig-2.2: Single-kink soliton solution of the Eq. (2.21) with $k=1$.

Case-II: For the set $A_0=\pm 1,\ A_1=\pm\sqrt{2}k$, we get

$$u=\pm 1\pm\frac{3\sqrt{2}c_1k^3}{w-3\sqrt{2}k}\times\frac{\exp(\frac{6k^2+w(w-3\sqrt{2}k)}{k^2(w-3\sqrt{2}k)}\xi)}{\frac{3c_1k^4}{6k^2+w(w-3\sqrt{2}k)}\exp(\frac{6k^2+w(w-3\sqrt{2}k)}{k^2(w-3\sqrt{2}k)}\xi)+c_2}, \tag{2.22}$$

for $\xi=k(x\pm\frac{3}{\sqrt{2}}t)$ with $w=\pm\frac{3}{\sqrt{2}}k$. Here c_1 and c_2 are arbitrary parametric values.

If we choose $c_2=\frac{3k^4c_1}{6k^2+w(w-3\sqrt{2}k)}$, then we attain to the solution as

$$u=\pm 1\pm\frac{\sqrt{2}\{6k^2+w(w-3\sqrt{2}k)\}}{k(w-3\sqrt{2}k)}\left\{1+\tanh\left(\frac{6k^2+w(w-3\sqrt{2}k))}{k^2(w-3\sqrt{2}k)}\xi\right)\right\}, \tag{2.23}$$

where $\xi = k(x \pm \frac{3}{\sqrt{2}}t)$ with $w = \pm\frac{3}{\sqrt{2}}k$.

If we choose $c_2 = -\frac{3k^4 c_1}{6k^2 + w(w-3\sqrt{2}k)}$, then we attain to the solution as

$$u = \pm 1 \pm \frac{\sqrt{2}\{6k^2 + w(w-3\sqrt{2}k)\}}{k(w-3\sqrt{2}k)}\left\{1 + \tanh\left(\frac{6k^2 + w(w-3\sqrt{2}k))}{k^2(w-3\sqrt{2}k)}\xi\right)\right\}, \tag{2.24}$$

where $\xi = k(x \pm \frac{3}{\sqrt{2}}t)$ with $w = \pm\frac{3}{\sqrt{2}}k$.

Since c_1 and c_2 are free parameters, for different selections of c_1 and c_2 it provides abundant novel exact solutions of the Cahn-Allen model. The achieved solutions from Eq. (2.23) and Eq. (2.24) are similar in diagrams **Fig-2.1** and **Fig-2.2** respectively. So, we exclude these equations for convenience.

Again with commercial software, we can also get various solutions of the Cahn-Allen model (solving from Eqs. (2.11) and (2.12)).

For the set of solution $A_0 = 0,\ A_1 = \pm\sqrt{2}k$, we get $S(\xi) = a + b\exp(\pm\xi/\sqrt{2}k)$.

Thus arrive to the solution

$$u(x,t) = \pm\frac{b}{a\left\{\cosh\frac{\xi}{\sqrt{2}k} \mp \sinh\frac{\xi}{\sqrt{2}k}\right\} + b} \text{ with } \xi = k\left(x \pm 3t/\sqrt{2}\right). \tag{2.25}$$

If we consider $a/b = \exp(2c)$, then Eq. (2.25) reduces to well known solution

$$u(x,t) = \pm\frac{1}{2}\left\{1 + \tanh\left(\pm\frac{1}{\sqrt{2}}x + \frac{3}{2}t + c\right)\right\}. \tag{2.26}$$

For the set $A_0 = 1,\ A_1 = \pm\sqrt{2}k$, we get $S(\xi) = a + b\exp(\pm\xi/\sqrt{2}k)$.

Hence arrive to the solution

$$u(x,t)=1-\frac{b}{a\left\{\cosh\frac{\xi}{\sqrt{2}k}\pm\sinh\frac{\xi}{\sqrt{2}k}\right\}+b}\quad\text{with}\quad\xi=k\left(x\pm3t/\sqrt{2}\right).\tag{2.27}$$

If we consider $a/b=\exp(2c)$, then Eq. (2.27) reduces to well known solution

$$u(x,t)=\frac{1}{2}\left\{1+\tanh\left(\pm\frac{1}{\sqrt{2}}x+\frac{3}{2}t+c\right)\right\}.\tag{2.28}$$

For the set $A_0=-1,\ A_1=\pm\sqrt{2}k$, we get $S(\xi)=a+b\exp(\mp\xi/\sqrt{2}k)$.

Hence we attain to the solution

$$u(x,t)=-1-\frac{b}{a\left\{\cosh\frac{\xi}{\sqrt{2}k}\mp\sinh\frac{\xi}{\sqrt{2}k}\right\}+b}\quad\text{with}\quad\xi=k\left(x\mp3t/\sqrt{2}\right).\tag{2.29}$$

If we consider $a/b=\exp(2c)$, then Eq. (2.26) reduces to well known solution

$$u(x,t)=-\frac{1}{2}\left\{1+\tanh\left(\pm\frac{1}{\sqrt{2}}x+\frac{3}{2}t+c\right)\right\}.\tag{2.30}$$

Since a and b are free parameters, for different selections of a and b it provides abundant novel exact solutions of the Cahn-Allen model. Choosing $a/b=\exp(2c)$ we get special type solution like Eq. (2.28) and Eq. (2.30), but for other choose a and b in different way we can get dissimilar type of solutions. Thus Eq. (2.28) and Eq. (2.30) are particular type of our solutions. Graphs of the solutions Eq. (2.25), Eq. (2.27) and Eq. (2.29) represent kink type wave propagation (like **Fig-2.1)** for same positive/negative values of the arbitrary constants c_1 and c_2. But to get single soliton like wave propagation (like **Fig-2.2)** from the same solution, we have to pick opposite values of arbitrary constants c_1 and c_2.

2.3.2. Example 2: A diffusive predator-prey model

In the predator-prey model including any type of natural disaster, the cycle can be reflected as a flow that may be periodic or remain unchanged like soliton and may be considered as a nonlinear wave phenomenon allied to a large amount of significance in modern biophysics. Here, we deliberate a model of two combined nonlinear models relating the spatio-temporal kinetics of a predator-prey model [61]

$$\begin{cases} u_t = u_{xx} - \beta u + (1+\beta)u^2 - u^3 - uv \\ v_t = v_{xx} + kuv - mv - \delta v^3 \end{cases} \tag{2.31}$$

with positive constants k, δ, m and β. Research has been done from several angles to find a solution to the predator-prey model [61, 62]. For further convenience, to visualize the kinetics of the dispersive predator-prey model have expected the relations as $m = \beta$ and $k + 1/\sqrt{\delta} = \beta + 1$.

Hence the Eq. (2.31) converted to

$$\begin{cases} u_t = u_{xx} - \beta u + (k + 1/\sqrt{\delta})u^2 - u^3 - uv \\ v_t = v_{xx} + kuv - \beta v - \delta v^3 \end{cases} \tag{2.32}$$

Analogously, we bring in the variable $\eta = x - wt$, and make the transformation $u(x,t) = u(\eta)$, to convert Eq. (2.32) as the following form:

$$\begin{cases} u'' + cu' - \beta u + (k + 1/\sqrt{\delta})u^2 - u^3 - uv = 0 \\ v'' + cv' + kuv - \beta v - \delta v^3 = 0 \end{cases} \tag{2.33}$$

for $c \neq 0$.

To solve the Eq. (2.33), consider the relation $v = u/\sqrt{\delta}$ to convert the system to a single equation and we finally attain,

$$u'' + cu' - \beta u + ku^2 - u^3 = 0. \tag{2.34}$$

Balancing u^3 and u'' in Eq. (2.34), yields $m+2 = 3m \rightarrow m = 1$. So Eq. (2.34) has the following solution

$$u(\eta) = a_0 + a_1 \frac{\Omega'(\eta)}{\Omega(\eta)} \text{ and } a_1 \neq 0, \tag{2.35}$$

where a_0 and a_1 are constants and need to be determined. Inserting Eq. (2.35) in Eq. (2.34) and equating the coefficient of same powers of $(\Omega(\eta))^{-i}$, $i = 0,1,..,3$ and setting each of them is identical to zero; we have an algebraic system as below

$$ka_0^2 - \beta a_0 - a_0^3 = 0,$$

$$wa_1\Omega''(\eta) - (\beta a_1 + 3a_0^2 a_1 - 2ka_0 a_1)\Omega'(\eta) + a_1\Omega'''(\eta) = 0,$$

$$-3a_1(\Omega'(\eta))(\Omega''(\eta)) - (wa_1 - ka_1^2 + 3a_0 a_1^2)(\Omega'(\eta))^2 = 0,$$

$$(2A_1 - A_1^3)(\Omega'(\eta))^3 = 0.$$

From first and last equation of the above algebraic system, we get three types of solutions

$a_0 = 0, a_1 = \pm\sqrt{2}$ and $a_0 = \frac{1}{2}(k + \sqrt{k^2 - 4\beta})$, $a_1 = \pm\sqrt{2}$ and $a_0 = \frac{1}{2}(k - \sqrt{k^2 - 4\beta})$, $a_1 = \pm\sqrt{2}$.

Case1: When we consider $a_0 = 0$ and $a_1 = \pm\sqrt{2}$.

Set-1: For the solution $a_0 = 0$ and $a_1 = \sqrt{2}$, we get other parametric values $w = \frac{\sqrt{2}}{4}(k \pm 3\sqrt{k^2 - 4\beta})$ and $\Omega(\eta) = c_1 + c_2 e^{-\frac{1}{3}(w - \sqrt{2}k)\eta}$.

Using these parametric values in Eq. (35), we can find the solution of the Eq. (32) as follows

$$u=-\frac{\sqrt{2}}{3}\frac{c_2(w-\sqrt{2}k)}{c_2+c_1(\cosh\vartheta+\sinh\vartheta)} \tag{2.36}$$

where $\eta=x-\frac{\sqrt{2}}{4}(k\pm3\sqrt{k^2-4\beta})t$ and $\vartheta=\frac{1}{3}(w-\sqrt{2}k)\eta.$

Set-2: For the solution $a_0=0$ and $a_1=-\sqrt{2}$, we get remaining parametric values $w=-\frac{\sqrt{2}}{4}(k\pm3\sqrt{k^2-4\beta})$ and $\Omega(\eta)=c_1+c_2e^{-\frac{1}{3}(w+\sqrt{2}k)\eta}$.

Using these parametric values in Eq. (2.35), we can find the solution of the Eq. (2.32) as follows

$$u=\frac{\sqrt{2}}{3}\frac{c_2(w+\sqrt{2}k)}{c_2+c_1(\cosh\vartheta+\sinh\vartheta)}, \tag{2.37}$$

where $\eta=x+\frac{\sqrt{2}}{4}(k\pm3\sqrt{k^2-4\beta})t$ and $\vartheta=\frac{1}{3}(w+\sqrt{2}k)\eta$.

Case-2: When we consider $a_0=\frac{1}{2}(k+\sqrt{k^2-4\beta})$ and $a_1=\pm\sqrt{2}$.

Set-1: For the solution $a_0=\frac{1}{2}(k+\sqrt{k^2-4\beta})$ and $a_1=\sqrt{2}$, we get remaining parametric values $w=-\frac{1}{\sqrt{2}}k,\frac{\sqrt{2}}{4}(k-3\sqrt{k^2-4\beta})$ and $\Omega(\eta)=c_1+c_2e^{-\frac{\sqrt{2}}{6}(\sqrt{2}w+k+3\sqrt{k^2-4\beta})\eta}$.

Using these parametric values in Eq. (2.35), we can find the solution of the Eq. (2.32) as follows

$$u=\frac{1}{2}(k+\sqrt{k^2-4\beta})-\frac{1}{3}\frac{c_2(\sqrt{2}w+k+3\sqrt{k^2-4\beta})}{c_2+c_1(\cosh\vartheta+\sinh\vartheta)}, \tag{2.38}$$

where $\eta=x-\frac{\sqrt{2}}{4}(k-3\sqrt{k^2-4\beta})t$ or $\eta=x+\frac{1}{\sqrt{2}}kt$ and $\vartheta=\frac{\sqrt{2}}{6}(\sqrt{2}w+k+3\sqrt{k^2-4\beta})\eta$.

Set-2: For the solution $a_0=\frac{1}{2}(k+\sqrt{k^2-4\beta})$ and $a_1=-\sqrt{2}$, we get remaining parametric values $w=\frac{1}{\sqrt{2}}k,-\frac{\sqrt{2}}{4}(k-3\sqrt{k^2-4\beta})$ and $\Omega(\eta)=c_1+c_2e^{-\frac{\sqrt{2}}{6}(\sqrt{2}w-k-3\sqrt{k^2-4\beta})\eta}$.

Using these parametric values in Eq. (2.35), we can find the solution of the Eq. (2.32) as follows

$$u=\frac{1}{2}(k+\sqrt{k^2-4\beta})+\frac{1}{3}\frac{c_2(\sqrt{2}w-k-3\sqrt{k^2-4\beta})}{c_2+c_1(\cosh\vartheta+\sinh\vartheta)}, \tag{2.39}$$

where $\eta=x+\frac{\sqrt{2}}{4}(k-3\sqrt{k^2-4\beta})t$ or $\eta=x-\frac{1}{\sqrt{2}}kt$ and $\vartheta=\frac{\sqrt{2}}{6}(\sqrt{2}w-k-3\sqrt{k^2-4\beta})\eta$.

Case-3: When we consider $a_0=\frac{1}{2}(k-\sqrt{k^2-4\beta})$ and $a_1=\pm\sqrt{2}$.

Set-1: For the solution $a_0=\frac{1}{2}(k-\sqrt{k^2-4\beta})$ and $a_1=\sqrt{2}$, we get remaining parametric values $w=-\frac{1}{\sqrt{2}}k,\frac{\sqrt{2}}{4}(k+3\sqrt{k^2-4\beta})$ and $\Omega(\eta)=c_1+c_2e^{-\frac{\sqrt{2}}{6}(\sqrt{2}w+k-3\sqrt{k^2-4\beta})\eta}$.

Using these parametric values in Eq. (2.35), we can find the solution of the Eq. (2.32) as follows

$$u=\frac{1}{2}(k-\sqrt{k^2-4\beta})-\frac{1}{3}\frac{c_2(\sqrt{2}w+k-3\sqrt{k^2-4\beta})}{c_2+c_1(\cosh\vartheta+\sinh\vartheta)}, \tag{2.40}$$

where $\eta=x-\frac{\sqrt{2}}{4}(k+3\sqrt{k^2-4\beta})t$ or $\eta=x+\frac{1}{\sqrt{2}}kt$ and $\vartheta=\frac{\sqrt{2}}{6}(\sqrt{2}w+k-3\sqrt{k^2-4\beta})\eta$.

Set-2: For the solution $a_0=\frac{1}{2}(k-\sqrt{k^2-4\beta})$ and $a_1=-\sqrt{2}$, we get remaining parametric values $w=\frac{1}{\sqrt{2}}k,-\frac{\sqrt{2}}{4}(k+3\sqrt{k^2-4\beta})$ and $\Omega(\eta)=c_1+c_2e^{-\frac{\sqrt{2}}{6}(\sqrt{2}w-k+3\sqrt{k^2-4\beta})\eta}$.

Using these parametric values in Eq. (2.35), we can find the solution of the Eq. (2.32) as follows

$$u = \frac{1}{2}(k - \sqrt{k^2 - 4\beta}) + \frac{1}{3}\frac{c_2(\sqrt{2}w - k + 3\sqrt{k^2 - 4\beta})}{c_2 + c_1(\cosh\vartheta + \sinh\vartheta)}, \tag{2.41}$$

where $\eta = x + \frac{\sqrt{2}}{4}(k + 3\sqrt{k^2 - 4\beta})t$ or $\eta = x - \frac{1}{\sqrt{2}}kt$ and $\vartheta = \frac{\sqrt{2}}{6}(\sqrt{2}w - k + 3\sqrt{k^2 - 4\beta})\eta$.

If we plot Eq. (2.36) with particular choose of the constants such that $k^2 - 4\beta > 0$, then we achieved progress of spaces as kink type that is population density is stable and lies between two asymptotic state $u = 0$ to $u = 0.85$ with $c_1 = c_2 = w = \beta = 1,\ k = 2$ (see **Fig 2.3(a)**). But if we set the constants such that $k^2 - 4\beta < 0$, then most of the times population are stable except some times and periodic (see **Fig 2.3(b)** with $c_1 = c_2 = w = \beta = 1,\ k = 1$). On the other hand when c_1 *or* c_2 negative, then density of species unstable and increases unexpectedly (see **Fig 2.3(c)** with $c_1 = -1, c_2 = w = \beta = 1,\ k = 2$). **Fig 2.3(d)**: perspective view of Eq. (2.37) for $c_1 = c_2 = w = \beta = 1,\ k = 1$. The other solution gives the same type of situation with similar conditions on the parametric values. So we avoid the similar figures again.

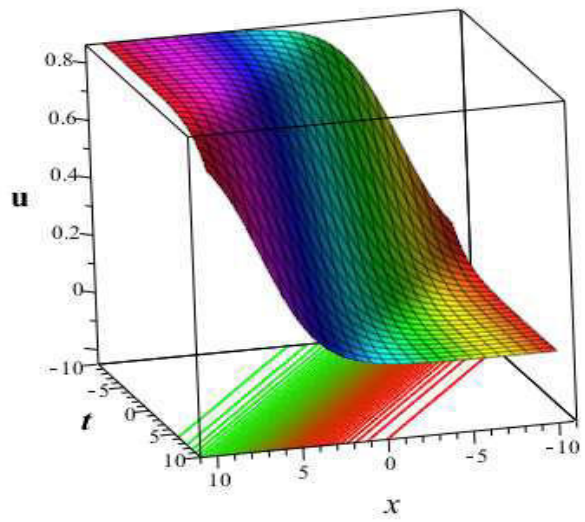

Fig-2.3(a) Kink wave view of Eq. (2.36) for $c_1 = c_2 = w = \beta = 1,\ k = 2$.

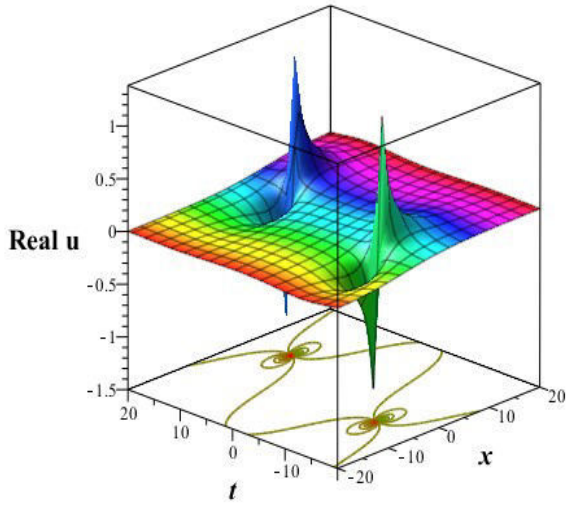

Fig-2.3(b) Kinky-periodic lump wave view of Eq. (2.36) for $c_1 = c_2 = w = \beta = 1,\ k = 1$.

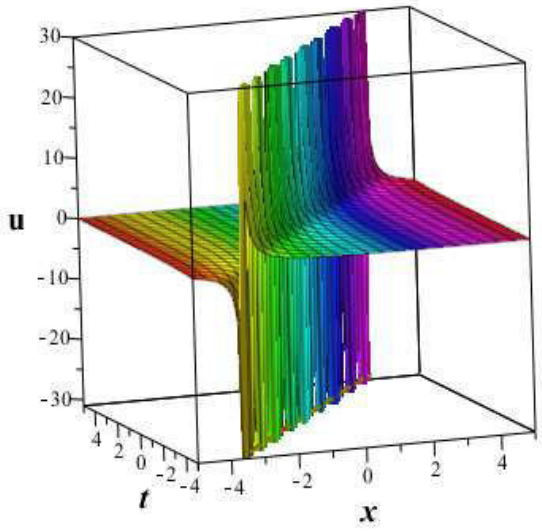

Fig-2.3(c) Singular-kink soliton view of Eq. (2.36) for $c_1 = -1, c_2 = w = \beta = 1,\ k = 2$.

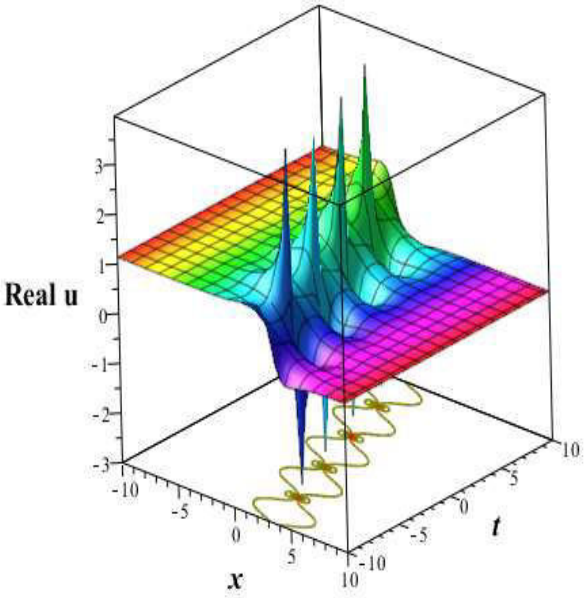

Fig-2.3(d) Kinky-periodic lump wave view of Eq. (2.37) for $c_1 = c_2 = w = \beta = 1,\ k = 1$.

2.4. Comparison

Here, we compare our solutions with the solutions of other researchers obtained by some renowned schemes as exp-function scheme, first integral scheme and Bernoulli sub-equation function scheme. The details are included as follows:

a) Comparison with Exp-function scheme Ref. [54]: Ugurlu [54] obtained some solutions of the Cahn-Allen model via exp-function scheme in which solutions u_8, u_9 are identical with our solution Eq. (2.25) when $b=1,\ a=b_0$ and the other solutions are different with their solutions (For more see the Ref. [53]).

b) Comparison with first integral scheme Ref. [55]**:** Tascan and Bekir [55] obtained some solutions of the Cahn-Allen model via first integral scheme in which solutions Eq. (2.20) are identical with our solutions Eq. (2.25) (when in our study $a=b=1,\ k=-1/\sqrt{2}$ and in their study $c_0=0$) and u_8, u_9 are identical with our solutions Eq. (2.25) when $b=1,\ a=b_0$ and the other solutions are different with their solutions.

c) Comparison with the Bernoulli sub-equation function scheme Ref. [60]**:** Bulut et. al. [60] derived six solutions of Cahn-Allen model and all of these are special case of our solutions. When we put $k=-\sqrt{2}/3,\ c_2=a_2,\ 2c_1k^2=E$; $k=-\sqrt{2}/3,\ c_2=2\sqrt{2}d,\ 2c_1k^2=E$ and $k=-\sqrt{2}/3,\ c_2=3\sqrt{2}d,\ 2c_1k^2=E$ in our solution (**Case-I** i.e., Eq. (2.19)) reduces to solutions u_1, u_4 and u_5 of Ref. [60] respectively. Similarly, we see that the solutions u_2, u_3, u_6 are special case of our solution (**Case-II** i.e., Eq. (2.22)). Our results have more free parameters which can be converted to diverse types of dynamical behavior for diverse choices of free parameters.

In contrast, by employing the MSE scheme in this manuscript we have achieved four solutions with simple calculations.

2.5. Conclusions

In this chapter, the MSE scheme has been effectively employed for finding the exact solutions and dynamics of the Cahn-Allen model and the dispersive predator-prey model. We presented abundant new exact explicit solutions of the exponential form of both Cahn-Allen and diffusive predator-prey models with some free parametric values. We derived particular solutions from the general exponential function such as stable kink soliton and kinky-periodic rogue wave solutions; unstable singular kink wave solutions of both models. We also derive particular solutions from the explicit solutions selecting some definite values of the free parametric values. Lastly, the variety and graphic representations of the composition make the models dynamic. Stable and unstable situations are explained in detail from the analysis of the profiles. By comparing the MSE scheme with different schemes, we can claim that the MSE scheme is frank, simple, proficient, and can be applied in numerous nonlinear models. In existing schemes, for example, the (G'/G)-expansion scheme, the exp-function scheme and the tanh-function scheme, it is essential to employ suggestive calculation software like Mathematica or Maple to solve the intricate algebraic equation. No auxiliary equations are needed to solve non-linear models by using the MSE scheme.

Chapter Three

Optical soliton polarization with LPD model by unified approach

Acknowledgement

In this chapter [1], we present the unified method and use it to integrate the Lakshmanan-Porsezian-Daniel (LPD) model to retrieve optical solitons in birefringent fibers. We first derive ordinary differential form of the model from its partial differential form via a variable transformation. Then the unified approach is carried out through computer on the model, by Maple-18 software. As outcomes, many new dynamical optical solitons in term of combo -trigonometric, -hyperbolic and -rational function solutions are added in the literature. The derived optical solitons solution exhibits some dynamics as beat phenomena, oscillating rhythm, oscillation together increasing and decreasing rhythm, and oscillation jointly increasing and decreasing rhythm even achieved a soliton solution which can changes its amplitude after a certain times. Besides this, various dynamical properties of the obtained solutions are presented graphically.

3.1. Introduction

Optical solitons are one of the rising research fields for the development of the telecommunication industry. We cannot imagine the operating of optical fiber, email, internet, mobile phones and many other communications except the idea of a solitary wave [12-15]. A renowned model which is familiar as the LPD model was primarily presented in 1988 [16]. Then, this model was extensively employed in various solitary wave propagation including, fiber optics. This model can describe the dynamical behavior of soliton transmission into optical fibers and photonic-crystal fiber. To express soliton solutions LPD model has been

studied by applying various reliable and effective integration algorithms such as Ricati equation scheme [63], $\exp(-\phi(\xi))$-expansion scheme [64], trial equation scheme [65] and many more [66-69].

The main purpose of this chapter is to optical solutions that clarify the physical structures as beat phenomena, oscillating rhythm, oscillation together increasing and decreasing rhythm, and oscillation jointly increasing and decreasing rhythm of the governing model by using a new scheme called unified method [70]. The details are demonstrated in the succeeding sections of this chapter.

3.2. Governing model

The dimensionless of LPD model with Kerr law nonlinearity has the follows form [66, 67]:

$$iu_t + au_{xx} + bu_{xt} + c|u|^2 u = \sigma u_{xxxx} + pu_x{}^2 u^* + q|u_x|^2 u + r|u|^2 u_{xx} + \lambda u^2 u_{xx}{}^* + s|u|^4 u . \tag{3.1}$$

The Eq. (3.1), the parameters a, b, c, σ and s signifies group velocity dispersion, spatio–temporal dispersion, coefficient of Kerr law nonlinearity, coefficient of fourth order dispersion and two–photon absorption correspondingly. Solitons are possible taking delicate balance of dispersion with nonlinear terms.

For birefringent fibers, the model can be divided into two parts of vector representation. Avoiding the properties of 4WM, the above model reduces to [64-65]:

$$\begin{aligned} iu_t + a_1u_{xx} + b_1u_{xt} + (c_1|u|^2 + d_1|v|^2)u = \sigma_1 u_{xxxx} + (p_1u_x{}^2 + q_1v_x{}^2)u^* \\ + (r_1|u_x|^2 + s_1|v_x|^2)u + (\lambda_1|u|^2 + \theta_1|v|^2)u_{xx} + (\chi_1u^2 + \eta_1v^2)u_{xx}{}^* \\ + (f_1|u|^4 + \phi_1|u|^2|v|^2 + \vartheta_1|v|^4)u . \end{aligned} \tag{3.2}$$

$$iu_t + a_2 v_{xx} + b_2 v_{xt} + (c_2|v|^2 + d_2|u|^2)v = \sigma_2 v_{xxxx} + (p_2 {v_x}^2 + q_2 {u_x}^2)v^*$$
$$+ (r_2|v_x|^2 + s_2|u_x|^2)v + (\lambda_2|v|^2 + \theta_2|u|^2)v_{xx} + (\chi_2 v^2 + \eta_2 u^2){v_{xx}}^*$$
$$+ (f_2|v|^4 + \phi_2|u|^2|v|^2 + \vartheta_2|u|^4)v. \quad (3.3)$$

In Eqs. (3.2), (3.3), c_j, f_j for $j = 1, 2$ represent the self-phase and d_j, ϕ_j, ϑ_j with $j = 1, 2$ stand for the cross-phase modulation effects, respectively.

3.3. Mathematical analysis

Consider the following transformation of this coupled system

$$u(x,t) = H_1(\zeta)\exp(i\varphi), \quad (3.4)$$

$$v(x,t) = H_2(\zeta)\exp(i\varphi). \quad (3.5)$$

where H_1 and H_2 are the soliton amplitude components and

$$\zeta = x - \varpi t \quad (3.6)$$

is the traveling wave variable with the soliton speed ϖ. The phase component φ is as below

$$\varphi = -kx + wt + \varepsilon. \quad (3.7)$$

with frequency k, wave number w and phase shift ε. Inserting Eq. (3.4) and Eq. (3.5) into Eq. (3.2) and Eq. (3.3) and sorting out the real and imaginary parts. The real part is

$$(w + a_n k^2 - b_n k w + k^4 \sigma_n)H_n - (c_n + k^2(p_n - r_n + \lambda_n + \chi_n))H_n{}^3$$
$$+ f_n H_n{}^5 - (d_n + k^2(q_n - s_n + \eta_n + \theta_n))H_n(H_{\bar{n}})^2 + \phi_n H_n{}^3(H_{\bar{n}})^2$$
$$+ \vartheta_n H_n(H_{\bar{n}})^4 + (p_n + r_n)H_n(H_n')^2 + (q_n + s_n)H_n(H_{\bar{n}}')^2$$
$$- (a_n - b_n\varpi + 6k^2\sigma_n)H_n'' + (\lambda_n + \chi_n)H_n{}^2 H_n'' + (\eta_n + \theta_n)H_{\bar{n}}{}^2 H_n'' + \sigma_n H_n{}^{(4)} = 0, \quad (3.8)$$

and the imaginary part is

$$(\varpi + 2a_n k - b_n(\varpi k + w) + 4k^3\sigma_n)H_n' - 2k(p_n + \lambda_n - \chi_n)H_n{}^2 H_n'$$
$$+ 2k(\eta_n - \theta_n)H_n'(H_{\bar{n}})^2 - 2q_n k H_n H_{\bar{n}} H_{\bar{n}}' - 4k\sigma_n H_n{}^{(3)} = 0 \quad (3.9)$$

with $n = 1, 2$ and $\bar{n} = 3 - n$. By the balancing principle, we can write

$$H_{\bar{n}} = H_n . \tag{3.10}$$

From Eq. (3.8) and Eq. (3.10), we can rewrite

$$(w + a_n k^2 - b_n kw + k^4 \sigma_n) H_n - (c_n + d_n + k^2 (h_n + R_n)) H_n{}^3 + J_n H_n{}^5$$

$$+ L_n H_n (H_n')^2 - (a_n - b_n \varpi + 6k^2 \sigma_n) H_n'' + R_n H_n{}^2 H_n'' + \sigma_n H_n{}^{(4)} = 0 , \tag{3.11}$$

where $J_n = f_n + \phi_n + \vartheta_n$, $h_n = p_n + q_n - r_n - s_n$, $L_n = p_n + q_n + r_n + s_n$,

$$R_n = \eta_n + \theta_n + \lambda_n + \chi_n . \tag{3.12}$$

From Eq. (3.9) and Eq. (3.10) we can rewrite

$$(\varpi + 2a_n k - b_n (\varpi k + w) + 4k^3 \sigma_n) H_n' - 2k(p_n + q_n - \eta_n + \theta_n + \lambda_n) H_n{}^2 H_n'$$

$$- 4k \sigma_n H_n{}^{(3)} = 0. \tag{3.13}$$

Thus, the third expression of Eq. (3.13) gives $\sigma_n = 0$. Hence the solutions of the couple system Eq. (3.2) and Eq. (3.3), will be presented for the fourth order dispersion omitted. The other functions of Eq.(13), yield the following relation

$$\eta_n + \chi_n = p_n + q_n + \theta_n + \lambda_n , \tag{3.14}$$

and therefore the soliton speed is

$$\varpi = \frac{b_n w - 2a_n k}{1 - b_n k} , \tag{3.15}$$

for $b_n \neq \frac{1}{k}$. Comparing the values of the soliton velocity Eq. (3.15) gives

$$(1 - b_1 k)(b_2 w - 2a_2 k) = (1 - b_2 k)(b_1 w - 2a_1 k) . \tag{3.16}$$

Therefore the Eq. (3.11) can be written as

$$(w + a_n k^2 - b_n kw) H_n - (c_n + d_n + k^2 (h_n + R_n)) H_n{}^3 + J_n H_n{}^5$$

$$+ L_n H_n (H_n')^2 - (a_n - b_n \varpi) H_n'' + R_n H_n{}^2 H_n'' = 0 . \tag{3.17}$$

3.4. Application of unified method to LPD model

Assume trial solution of Eq. (3.17) is

$$H_n(\zeta)=\sum_{i=0}^{N}[A_i^{(n)}S(\zeta)^i+B_i^{(n)}S(\zeta)^{-i}], \tag{3.18}$$

where $A_0^{(n)}$, $A_i^{(n)}$ and $B_i^{(n)}$ for $i=1,2,...,N$ are real constants and $S(\xi)$ satisfies Riccati equation:

$$S'(\zeta)=S^2(\zeta)+l\,. \tag{3.19}$$

Eq. (3.19) has nine solution categories according to three cases:

Case-01: Hyperbolic functions (when $l<0$):

$$S(\zeta)=\begin{cases}\dfrac{\sqrt{-\left(C^2+D^2\right)l}-C\sqrt{-l}\cosh\left(2\sqrt{-l}(\zeta+E)\right)}{C\sinh\left(2\sqrt{-l}(\zeta+E)\right)+D},\\ \dfrac{-\sqrt{-\left(C^2+D^2\right)l}-C\sqrt{-l}\cosh\left(2\sqrt{-l}(\zeta+E)\right)}{C\sinh\left(2\sqrt{-l}(\zeta+E)\right)+D},\\ \sqrt{-l}+\dfrac{2C\sqrt{-l}}{C+\cosh\left(2\sqrt{-l}(\zeta+E)\right)-\sinh\left(2\sqrt{-l}(\zeta+E)\right)},\\ -\sqrt{-l}+\dfrac{2C\sqrt{-l}}{C+\cosh\left(2\sqrt{-l}(\zeta+E)\right)-\sinh\left(2\sqrt{-l}(\zeta+E)\right)}.\end{cases} \tag{3.20}$$

Case-02: Trigonometric functions (when $l>0$):

$$S(\zeta)=\begin{cases}\dfrac{\sqrt{\left(C^2-D^2\right)l}-C\sqrt{l}\cos\left(2\sqrt{l}(\zeta+E)\right)}{C\sin\left(2\sqrt{l}(\zeta+E)\right)+D},\\ \dfrac{-\sqrt{\left(C^2-D^2\right)l}-C\sqrt{l}\cos\left(2\sqrt{l}(\zeta+E)\right)}{C\sin\left(2\sqrt{l}(\zeta+E)\right)+D},\\ i\sqrt{l}+\dfrac{-2iC\sqrt{l}}{C+\cos\left(2\sqrt{l}(\zeta+E)\right)-i\sin\left(2\sqrt{l}(\zeta+E)\right)},\\ -i\sqrt{l}+\dfrac{2iC\sqrt{l}}{C+\cos\left(2\sqrt{l}(\zeta+E)\right)+i\sin\left(2\sqrt{-l}(\zeta+E)\right)}.\end{cases} \tag{3.21}$$

where $C\neq 0$ and D, E are real arbitrary constant.

Case-03: Rational function solution (when $l=0$)

$$S(\zeta)=\frac{1}{\zeta+E}. \tag{3.22}$$

To identify value of N in Eq. (3.18), balancing $H_n^{\,2}H_n''$ with $H_n^{\,5}$ yields $N=1$. Eq.(3.18) takes the form

$$H_n(\zeta)=A_0^{(n)}+A_1^{(n)}S(\zeta)+B_i^{(n)}S(\zeta)^{-1}. \tag{3.23}$$

Then putting Eq. (3.23) along with Eq. (3.20) into Eq. (3.18) and after some calculations, we pose the following sets of solutions

Set 1: $A_0^{(n)}=0, A_1^{(n)}=M_n, B_1^{(n)}=0,$

$$\begin{aligned}
w=&(k^3J_na_nb_n-k\lambda^2L_n^{\,2}b_n-2kl^2L_nR_nb_n+2klJ_na_nb_n-k^2J_na_n\\
&+l^2L_n^{\,2}+2l^2L_nR_n+2lJ_na_n)/(J_n(k^2b_n^{\,2}+2lb_n^{\,2}-2kb_n+1)),\\
c_n=&-(k^4h_nL_nb_n^{\,2}+2k^4h_nR_nb_n^{\,2}+k^4L_nR_nb_n^{\,2}+2k^4R_n^{\,2}b_n^{\,2}+2k^2lh_nL_nb_n^{\,2}\\
&+4k^2lh_nR_nb_n^{\,2}-2k^2lL_n^{\,2}b_n^{\,2}-4k^2lL_nR_nb_n^{\,2}-2k^3h_nL_nb_n-4k^3h_nR_nb_n\\
&-2k^3L_nR_nb_n-4k^3R_n^{\,2}b_n+k^2L_nb_n^{\,2}d_n+2k^2R_nb_n^{\,2}d_n-2l^2L_n^{\,2}b_n^{\,2}\\
&-8l^2L_nR_nb_n^{\,2}-8l^2R_n^{\,2}b_n^{\,2}+4klL_n^{\,2}b_n+12klL_nR_nb_n+8klR_n^{\,2}b_n\\
&+2lL_nb_n^{\,2}d_n+4lR_nb_n^{\,2}d_n+k^2h_nL_n+2k^2h_nR_n+k^2L_nR_n+2k^2R_n^{\,2}\\
&-2kL_nb_nd_n-4kR_nb_nd_n-2lL_n^{\,2}-6lL_nR_n-4lR_n^{\,2}-2J_na_n+L_nd_n\\
&+2R_nd_n)/(k^2L_nb_n^{\,2}+2k^2R_nb_n^{\,2}+2lL_nb_n^{\,2}+4lR_nb_n^{\,2}-2kL_nb_n\\
&-4kR_nb_n+L_n+2R_n),
\end{aligned}$$

Set 2: $A_0^{(n)}=0, A_1^{(n)}=0, B_1^{(n)}=M_nl,$

$$\begin{aligned}
w=&(k^3J_na_nb_n-k\lambda^2L_n^{\,2}b_n-2kl^2L_nR_nb_n+2klJ_na_nb_n-k^2J_na_n\\
&+l^2L_n^{\,2}+2l^2L_nR_n+2lJ_na_n)/(J_n(k^2b_n^{\,2}+2lb_n^{\,2}-2kb_n+1)),
\end{aligned}$$

$$c_n = -(k^4 h_n L_n b_n^{\,2} + 2k^4 h_n R_n b_n^{\,2} + k^4 L_n R_n b_n^{\,2} + 2k^4 R_n^{\,2} b_n^{\,2} + 2k^2 l h_n L_n b_n^{\,2} + 4k^2 l h_n R_n b_n^{\,2} - 2k^2 l L_n^{\,2} b_n^{\,2} - 4k^2 l L_n R_n b_n^{\,2} - 2k^3 h_n L_n b_n - 4k^3 h_n R_n b_n - 2k^3 L_n R_n b_n - 4k^3 R_n^{\,2} b_n + k^2 L_n b_n^{\,2} d_n + 2k^2 R_n b_n^{\,2} d_n - 2l^2 L_n^{\,2} b_n^{\,2} - 8l^2 L_n R_n b_n^{\,2} - 8l^2 R_n^{\,2} b_n^{\,2} + 4klL_n^{\,2} b_n + 12klL_n R_n b_n + 8klR_n^{\,2} b_n + 2lL_n b_n^{\,2} d_n + 4lR_n b_n^{\,2} d_n + k^2 h_n L_n + 2k^2 h_n R_n + k^2 L_n R_n + 2k^2 R_n^{\,2} - 2kL_n b_n d_n - 4kR_n b_n d_n - 2lL_n^{\,2} - 6lL_n R_n - 4lR_n^{\,2} - 2J_n a_n + L_n d_n + 2R_n d_n)/(k^2 L_n b_n^{\,2} + 2k^2 R_n b_n^{\,2} + 2lL_n b_n^{\,2} + 4lR_n b_n^{\,2} - 2kL_n b_n - 4kR_n b_n + L_n + 2R_n),$$

Set 3: $A_0^{(n)} = 0, A_1^{(n)} = M_n, B_1^{(n)} = M_n l,$

$$w = -(8M_n^{\,2} l^2 k J_n L_n^{\,2} b_n + 16M_n^{\,2} l^2 k J_n L_n R_n b_n - 6M_n^{\,2} l k J_n^{\,2} a_n b_n - k^3 J_n L_n a_n b_n - 2k^3 J_n R_n a_n b_n + 8kl^2 L_n^{\,3} b_n + 32kl^2 L_n^{\,2} R_n b_n + 32kl^2 L_n R_n^{\,2} b_n - 8M_n^{\,2} l^2 J_n L_n^{\,2} - 16M_n^{\,2} l^2 J_n L_n R_n - 2klJ_n L_n a_n b_n - 4klJ_n R_n a_n b_n - 6M_n^{\,2} l J_n^{\,2} a_n + k^2 J_n L_n a_n + 2k^2 J_n R_n a_n - 8l^2 L_n^{\,3} - 32l^2 L_n^{\,2} R_n - 32l^2 L_n R_n^{\,2} - 2lJ_n L_n a_n - 4lJ_n R_n a_n)/(J_n(6J_n b_n^{\,2} M_n^{\,2} l + k^2 L_n b_n^{\,2} + 2k^2 R_n b_n^{\,2} + 2lL_n b_n^{\,2} + 4lR_n b_n^{\,2} - 2kL_n b_n - 4kR_n b_n + L_n + 2R_n)),$$

$$
\begin{aligned}
c_n = -(&6k^2h_nJ_nb_n^2M_n^2 - 6k^2J_nL_nb_n^2M_n^2l + 12kJ_nL_nb_nM_n^2l \\
&+ 12kJ_nR_nb_nM_n^2l + 2k^2lh_nL_nb_n^2 + 4k^2lh_nR_nb_n^2 - 4k^2lL_nR_nb_n^2 \\
&+ 12klL_nR_nb_n - 6J_nL_nM_n^2l - 6J_nR_nM_n^2l - 2a_nJ_n + 2k^2R_n^2 \\
&- 2lL_n^2 - 4lR_n^2 + L_nd_n + 2R_nd_n - 24l^2L_n^2b_n^2 + 2k^4R_n^2b_n^2 \\
&- 4k^3R_n^2b_n - 80l^2R_n^2b_n^2 + k^2h_nL_n + 2k^2h_nR_n + k^2L_nR_n \\
&- 6lL_nR_n - 88l^2L_nR_nb_n^2 + k^4h_nL_nb_n^2 + 2k^4h_nR_nb_n^2 + k^4L_nR_nb_n^2 \\
&- 2k^2lL_n^2b_n^2 - 2k^3h_nL_nb_n - 4k^3h_nR_nb_n - 2k^3L_nR_nb_n + k^2L_nb_n^2d_n \\
&+ 2k^2R_nb_n^2d_n + 4klL_n^2b_n + 8klR_n^2b_n + 2lL_nb_n^2d_n + 4lR_nb_n^2d_n \\
&- 2kL_nb_nd_n - 4kR_nb_nd_n - 8l^2J_nL_nb_n^2M^2 - 24l^2J_nR_nb_n^2M_n^2 \\
&+ 6J_nb_n^2d_nM_n^2l)/(6J_nb_n^2M_n^2l + k^2L_nb_n^2 + 2k^2R_nb_n^2 + 2lL_nb_n^2 \\
&+ 4lR_nb_n^2 - 2kL_nb_n - 4kR_nb_n + L_n + 2R_n)),
\end{aligned}
$$

for $M_n = \pm\dfrac{\sqrt{-J_n(L_n+2R_n)}}{J_n}$.

Using Eq. (3.20), Eq. (3.21), Eq. (3.22) and Eq. (3.4), Eq. (3.5), with the help of the solution **set-1,** we obtain the following eighteen exact solutions of Eq. (3.2) and Eq. (3.3)

$$u_{1,1}(x,t) = M_1\left(\frac{\sqrt{-(C^2+D^2)l} - C\sqrt{-l}\cosh\left(2\sqrt{-l}(\zeta+E)\right)}{C\sinh\left(2\sqrt{-l}(\zeta+E)\right)+D}\right)\times\exp[i(-kx+wt+\varepsilon)],$$

$$v_{1,1}(x,t) = M_2\left(\frac{\sqrt{-(C^2+D^2)l} - C\sqrt{-l}\cosh\left(2\sqrt{-l}(\zeta+E)\right)}{C\sinh\left(2\sqrt{-l}(\zeta+E)\right)+D}\right)\times\exp[i(-kx+wt+\varepsilon)],$$

$$u_{1,2}(x,t) = M_1\left(\frac{-\sqrt{-(C^2+D^2)l} - C\sqrt{-l}\cosh\left(2\sqrt{-l}(\zeta+E)\right)}{C\sinh\left(2\sqrt{-l}(\zeta+E)\right)+D}\right)\times\exp[i(-kx+wt+\varepsilon)],$$

$$v_{1,2}(x,t) = M_2\left(\frac{-\sqrt{-(C^2+D^2)l} - C\sqrt{-l}\cosh\left(2\sqrt{-l}(\zeta+E)\right)}{C\sinh\left(2\sqrt{-l}(\zeta+E)\right)+D}\right)\times\exp[i(-kx+wt+\varepsilon)],$$

$$u_{1,3}(x,t)=M_1\left(\sqrt{-l}+\frac{2C\sqrt{-l}}{C+\cosh\left(2\sqrt{-l}(\zeta+E)\right)-\sinh\left(2\sqrt{-l}(\zeta+E)\right)}\right)\times\exp\left[i(-kx+wt+\varepsilon)\right],$$

$$v_{1,3}(x,t)=M_2\left(\sqrt{-l}+\frac{2C\sqrt{-l}}{C+\cosh\left(2\sqrt{-l}(\zeta+E)\right)-\sinh\left(2\sqrt{-l}(\zeta+E)\right)}\right)\times\exp\left[i(-kx+wt+\varepsilon)\right].$$

$$u_{1,4}(x,t)=M_1\left(-\sqrt{-l}+\frac{2C\sqrt{-l}}{C+\cosh\left(2\sqrt{-l}(\zeta+E)\right)-\sinh\left(2\sqrt{-l}(\zeta+E)\right)}\right)\times\exp\left[i(-kx+wt+\varepsilon)\right],$$

$$v_{1,4}(x,t)=M_2\left(-\sqrt{-l}+\frac{2C\sqrt{-l}}{C+\cosh\left(2\sqrt{-l}(\zeta+E)\right)-\sinh\left(2\sqrt{-l}(\zeta+E)\right)}\right)\times\exp\left[i(-kx+wt+\varepsilon)\right],$$

$$u_{1,5}(x,t)=M_1\left(\frac{\sqrt{\left(C^2-D^2\right)}l-C\sqrt{l}\cos\left(2\sqrt{l}(\zeta+E)\right)}{C\sin\left(2\sqrt{l}(\zeta+E)\right)+D}\right)\times\exp\left[i(-kx+wt+\varepsilon)\right],$$

$$v_{1,5}(x,t)=M_2\left(\frac{\sqrt{\left(C^2-D^2\right)}l-C\sqrt{l}\cos\left(2\sqrt{l}(\zeta+E)\right)}{C\sin\left(2\sqrt{l}(\zeta+E)\right)+D}\right)\times\exp\left[i(-kx+wt+\varepsilon)\right],$$

$$u_{1,6}(x,t)=M_1\left(\frac{-\sqrt{\left(C^2-D^2\right)}l-C\sqrt{l}\cos\left(2\sqrt{l}(\zeta+E)\right)}{C\sin\left(2\sqrt{l}(\zeta+E)\right)+D}\right)\times\exp\left[i(-kx+wt+\varepsilon)\right],$$

$$v_{1,6}(x,t)=M_2\left(\frac{-\sqrt{\left(C^2-D^2\right)}l-C\sqrt{l}\cos\left(2\sqrt{l}(\zeta+E)\right)}{C\sin\left(2\sqrt{l}(\zeta+E)\right)+D}\right)\times\exp\left[i(-kx+wt+\varepsilon)\right],$$

$$u_{1,7}(x,t)=M_1\left(i\sqrt{l}+\frac{-2iC\sqrt{l}}{C+\cos\left(2\sqrt{l}(\zeta+E)\right)-i\sin\left(2\sqrt{l}(\zeta+E)\right)}\right)\times\exp\left[i(-kx+wt+\varepsilon)\right],$$

$$v_{1,7}(x,t)=M_2\left(i\sqrt{l}+\frac{-2iC\sqrt{l}}{C+\cos\left(2\sqrt{l}(\zeta+E)\right)-i\sin\left(2\sqrt{l}(\zeta+E)\right)}\right)\times\exp\left[i(-kx+wt+\varepsilon)\right],$$

$$u_{1,8}(x,t)=M_1\left(-i\sqrt{l}+\frac{2iC\sqrt{l}}{C+\cos\left(2\sqrt{l}(\zeta+E)\right)+i\sin\left(2\sqrt{-l}(\zeta+E)\right)}\right)\times\exp\left[i(-kx+wt+\varepsilon)\right],$$

$$v_{1,8}(x,t)=M_2\left(-i\sqrt{l}+\frac{2iC\sqrt{l}}{C+\cos\left(2\sqrt{l}(\zeta+E)\right)+i\sin\left(2\sqrt{-l}(\zeta+E)\right)}\right)\times\exp\left[i(-kx+wt+\varepsilon)\right],$$

$$u_{1,9}(x,t)=M_1\left(\frac{1}{\zeta+E}\right)\times\exp\left[i(-kx+wt+\varepsilon)\right],$$

$$v_{1,9}(x,t)=M_2\left(\frac{1}{\zeta+E}\right)\times\exp[i(-kx+wt+\varepsilon)],$$

where $M_n=\pm\frac{\sqrt{-J_n(L_n+2R_n)}}{J_n}$ and $w=(k^3J_na_nb_n-k\lambda^2L_n{}^2b_n-2kl^2L_nR_nb_n+2klJ_na_nb_n-k^2J_na_n+l^2L_n{}^2+2l^2L_nR_n+2lJ_na_n)/(J_n(k^2b_n{}^2+2lb_n{}^2-2kb_n+1)).$

Using Eq. (3.20), Eq. (3.21), Eq. (3.22) and Eq. (3.4), Eq. (3.5), with the help of the solution **set-2,** we obtain the following eighteen exact solutions of Eq. (3.2) and Eq. (3.3)

$$u_{2,1}(x,t)=\frac{M_1l}{\left(\frac{\sqrt{-(C^2+D^2)l}-C\sqrt{-l}\cosh\left(2\sqrt{-l}(\zeta+E)\right)}{C\sinh\left(2\sqrt{-l}(\zeta+E)\right)+D}\right)}\times\exp[i(-kx+wt+\varepsilon)],$$

$$v_{2,1}(x,t)=\frac{M_2l}{\left(\frac{\sqrt{-(C^2+D^2)l}-C\sqrt{-l}\cosh\left(2\sqrt{-l}(\zeta+E)\right)}{C\sinh\left(2\sqrt{-l}(\zeta+E)\right)+D}\right)}\times\exp[i(-kx+wt+\varepsilon)],$$

$$u_{2,2}(x,t)=\frac{M_1l}{\left(\frac{-\sqrt{-(C^2+D^2)l}-C\sqrt{-l}\cosh\left(2\sqrt{-l}(\zeta+E)\right)}{C\sinh\left(2\sqrt{-l}(\zeta+E)\right)+D}\right)}\times\exp[i(-kx+wt+\varepsilon)],$$

$$v_{2,2}(x,t)=\frac{Ml}{\left(\frac{-\sqrt{-(C^2+D^2)l}-C\sqrt{-l}\cosh\left(2\sqrt{-l}(\zeta+E)\right)}{C\sinh\left(2\sqrt{-l}(\zeta+E)\right)+D}\right)}\times\exp[i(-kx+wt+\varepsilon)],$$

$$u_{2,3}(x,t)=\frac{M_1l}{\left(\sqrt{-l}+\frac{2C\sqrt{-l}}{C+\cosh\left(2\sqrt{-l}(\zeta+E)\right)-\sinh\left(2\sqrt{-l}(\zeta+E)\right)}\right)}\times\exp[i(-kx+wt+\varepsilon)],$$

$$v_{2,3}(x,t)=\frac{M_2l}{\left(\sqrt{-l}+\frac{2C\sqrt{-l}}{C+\cosh\left(2\sqrt{-l}(\zeta+E)\right)-\sinh\left(2\sqrt{-l}(\zeta+E)\right)}\right)}\times\exp[i(-kx+wt+\varepsilon)],$$

$$u_{2,4}(x,t)=\frac{M_1 l}{\left(-\sqrt{-l}+\frac{2C\sqrt{-l}}{C+\cosh\left(2\sqrt{-l}(\zeta+E)\right)-\sinh\left(2\sqrt{-l}(\zeta+E)\right)}\right)}\times\exp\left[i\left(-kx+wt+\varepsilon\right)\right],$$

$$v_{2,4}(x,t)=\frac{M_2 l}{\left(-\sqrt{-l}+\frac{2C\sqrt{-l}}{C+\cosh\left(2\sqrt{-l}(\zeta+E)\right)-\sinh\left(2\sqrt{-l}(\zeta+E)\right)}\right)}\times\exp\left[i\left(-kx+wt+\varepsilon\right)\right],$$

$$u_{2,5}(x,t)=\frac{M_1 l}{\left(\frac{\sqrt{\left(C^2-D^2\right)l}-C\sqrt{l}\cos\left(2\sqrt{l}(\zeta+E)\right)}{C\sin\left(2\sqrt{l}(\zeta+E)\right)+D}\right)}\times\exp\left[i\left(-kx+wt+\varepsilon\right)\right],$$

$$v_{2,5}(x,t)=\frac{M_2 l}{\left(\frac{\sqrt{\left(C^2-D^2\right)l}-C\sqrt{l}\cos\left(2\sqrt{l}(\zeta+E)\right)}{C\sin\left(2\sqrt{l}(\zeta+E)\right)+D}\right)}\times\exp\left[i\left(-kx+wt+\varepsilon\right)\right],$$

$$u_{2,6}(x,t)=\frac{M_1 l}{\left(\frac{-\sqrt{\left(C^2-D^2\right)l}-C\sqrt{l}\cos\left(2\sqrt{l}(\zeta+E)\right)}{C\sin\left(2\sqrt{l}(\zeta+E)\right)+D}\right)}\times\exp\left[i\left(-kx+wt+\varepsilon\right)\right],$$

$$v_{2,6}(x,t)=\frac{M_2 l}{\left(\frac{-\sqrt{\left(C^2-D^2\right)l}-C\sqrt{l}\cos\left(2\sqrt{l}(\zeta+E)\right)}{C\sin\left(2\sqrt{l}(\zeta+E)\right)+D}\right)}\times\exp\left[i\left(-kx+wt+\varepsilon\right)\right],$$

$$u_{2,7}(x,t)=\frac{M_1 l}{\left(i\sqrt{l}+\frac{-2iC\sqrt{l}}{C+\cos\left(2\sqrt{l}(\zeta+E)\right)-i\sin\left(2\sqrt{l}(\zeta+E)\right)}\right)}\times\exp\left[i\left(-kx+wt+\varepsilon\right)\right],$$

$$v_{2,7}(x,t)=\frac{M_2 l}{\left(i\sqrt{l}+\frac{-2iC\sqrt{l}}{C+\cos\left(2\sqrt{l}(\zeta+E)\right)-i\sin\left(2\sqrt{l}(\zeta+E)\right)}\right)}\times\exp\left[i\left(-kx+wt+\varepsilon\right)\right],$$

$$u_{2,8}(x,t)=\frac{M_1 l}{\left(-i\sqrt{l}+\frac{2iC\sqrt{l}}{C+\cos\left(2\sqrt{l}(\zeta+E)\right)+i\sin\left(2\sqrt{-l}(\zeta+E)\right)}\right)}\times\exp\left[i\left(-kx+wt+\varepsilon\right)\right],$$

$$v_{2,8}(x,t)=\frac{M_2 l}{\left(-i\sqrt{l}+\frac{2iC\sqrt{l}}{C+\cos\left(2\sqrt{l}(\zeta+E)\right)+i\sin\left(2\sqrt{-l}(\zeta+E)\right)}\right)}\times\exp\left[i\left(-kx+wt+\varepsilon\right)\right],$$

$$u_{2,9}(x,t)=\frac{M_1 l}{\left(\frac{1}{\zeta+E}\right)}\times\exp[i(-kx+wt+\varepsilon)],$$

$$v_{2,9}(x,t)=\frac{M_2 l}{\left(\frac{1}{\zeta+E}\right)}\times\exp[i(-kx+wt+\varepsilon)],$$

where $M_n=\pm\frac{\sqrt{-J_n(L_n+2R_n)}}{J_n}$ and $w=(k^3J_na_nb_n-k\lambda^2L_n{}^2b_n-2kl^2L_nR_nb_n+2klJ_na_nb_n-k^2J_na_n+l^2L_n{}^2+2l^2L_nR_n+2lJ_na_n)/(J_n(k^2b_n{}^2+2lb_n{}^2-2kb_n+1)).$

Using Eq. (3.20), Eq. (3.21), Eq. (3.22) and Eq. (3.4), Eq. (3.5), with the help of the solution **set-3,** we obtain the following sixteen exact solutions of Eq. (3.2) and Eq. (3.3)

$$u_{3,1}(x,t)=\left(M_1\left(\frac{\sqrt{-(C^2+D^2)l}-C\sqrt{-l}\cosh\left(2\sqrt{-l}(\zeta+E)\right)}{C\sinh\left(2\sqrt{-l}(\zeta+E)\right)+D}\right)+\frac{M_1 l}{\left(\frac{\sqrt{-(C^2+D^2)l}-C\sqrt{-l}\cosh\left(2\sqrt{-l}(\zeta+E)\right)}{C\sinh\left(2\sqrt{-l}(\zeta+E)\right)+D}\right)}\right)\times\exp[i(-kx+wt+\varepsilon)],$$

$$v_{3,1}(x,t)=\left(M_2\left(\frac{\sqrt{-(C^2+D^2)l}-C\sqrt{-l}\cosh\left(2\sqrt{-l}(\zeta+E)\right)}{C\sinh\left(2\sqrt{-l}(\zeta+E)\right)+D}\right)+\frac{M_2 l}{\left(\frac{\sqrt{-(C^2+D^2)l}-C\sqrt{-l}\cosh\left(2\sqrt{-l}(\zeta+E)\right)}{C\sinh\left(2\sqrt{-l}(\zeta+E)\right)+D}\right)}\right)\times\exp[i(-kx+wt+\varepsilon)],$$

$$u_{3,2}(x,t)=\left(M_1\left(\frac{-\sqrt{-(C^2+D^2)l}-C\sqrt{-l}\cosh\left(2\sqrt{-l}(\zeta+E)\right)}{C\sinh\left(2\sqrt{-l}(\zeta+E)\right)+D}\right)+\frac{M_1 l}{\left(\frac{-\sqrt{-(C^2+D^2)l}-C\sqrt{-l}\cosh\left(2\sqrt{-l}(\zeta+E)\right)}{C\sinh\left(2\sqrt{-l}(\zeta+E)\right)+D}\right)}\right)\times\exp[i(-kx+wt+\varepsilon)],$$

$$v_{3,2}(x,t)=\left(\begin{array}{l} M_2\left(\dfrac{-\sqrt{-\left(C^2+D^2\right)l}-C\sqrt{-l}\cosh\left(2\sqrt{-l}(\zeta+E)\right)}{C\sinh\left(2\sqrt{-l}(\zeta+E)\right)+D}\right) \\ +\dfrac{M_2 l}{\left(\dfrac{-\sqrt{-\left(C^2+D^2\right)l}-C\sqrt{-l}\cosh\left(2\sqrt{-l}(\zeta+E)\right)}{C\sinh\left(2\sqrt{-l}(\zeta+E)\right)+D}\right)} \end{array}\right)\times\exp\left[i\left(-kx+wt+\varepsilon\right)\right],$$

$$u_{3,3}(x,t)=\left(\begin{array}{l} M_1\left(\sqrt{-l}+\dfrac{2C\sqrt{-l}}{C+\cosh\left(2\sqrt{-l}(\zeta+E)\right)-\sinh\left(2\sqrt{-l}(\zeta+E)\right)}\right) \\ +\dfrac{M_1 l}{\left(\sqrt{-l}+\dfrac{2C\sqrt{-l}}{C+\cosh\left(2\sqrt{-l}(\zeta+E)\right)-\sinh\left(2\sqrt{-l}(\zeta+E)\right)}\right)} \end{array}\right)\times\exp\left[i\left(-kx+wt+\varepsilon\right)\right],$$

$$v_{3,3}(x,t)=\left(\begin{array}{l} M_2\left(\sqrt{-l}+\dfrac{2C\sqrt{-l}}{C+\cosh\left(2\sqrt{-l}(\zeta+E)\right)-\sinh\left(2\sqrt{-l}(\zeta+E)\right)}\right) \\ +\dfrac{M_2 l}{\left(\sqrt{-l}+\dfrac{2C\sqrt{-l}}{C+\cosh\left(2\sqrt{-l}(\zeta+E)\right)-\sinh\left(2\sqrt{-l}(\zeta+E)\right)}\right)} \end{array}\right)\times\exp\left[i\left(-kx+wt+\varepsilon\right)\right],$$

$$u_{3,4}(x,t)=\left(\begin{array}{l} M_1\left(-\sqrt{-l}+\dfrac{2C\sqrt{-l}}{C+\cosh\left(2\sqrt{-l}(\zeta+E)\right)-\sinh\left(2\sqrt{-l}(\zeta+E)\right)}\right) \\ +\dfrac{M_1 l}{\left(-\sqrt{-l}+\dfrac{2C\sqrt{-l}}{C+\cosh\left(2\sqrt{-l}(\zeta+E)\right)-\sinh\left(2\sqrt{-l}(\zeta+E)\right)}\right)} \end{array}\right)\times\exp\left[i\left(-kx+wt+\varepsilon\right)\right],$$

$$v_{3,4}(x,t)=\left(\begin{array}{l} M_2\left(-\sqrt{-l}+\dfrac{2C\sqrt{-l}}{C+\cosh\left(2\sqrt{-l}(\zeta+E)\right)-\sinh\left(2\sqrt{-l}(\zeta+E)\right)}\right) \\ +\dfrac{M_2 l}{\left(-\sqrt{-l}+\dfrac{2C\sqrt{-l}}{C+\cosh\left(2\sqrt{-l}(\zeta+E)\right)-\sinh\left(2\sqrt{-l}(\zeta+E)\right)}\right)} \end{array}\right)\times\exp\left[i\left(-kx+wt+\varepsilon\right)\right],$$

$$u_{3,5}(x,t)=\left(\begin{array}{l} M_1\left(\dfrac{\sqrt{\left(C^2-D^2\right)l}-C\sqrt{l}\cos\left(2\sqrt{l}(\zeta+E)\right)}{C\sin\left(2\sqrt{l}(\zeta+E)\right)+D}\right) \\ +\dfrac{M_1 l}{\left(\dfrac{\sqrt{\left(C^2-D^2\right)l}-C\sqrt{l}\cos\left(2\sqrt{l}(\zeta+E)\right)}{C\sin\left(2\sqrt{l}(\zeta+E)\right)+D}\right)} \end{array}\right)\times\exp\left[i\left(-kx+wt+\varepsilon\right)\right],$$

$$v_{3,5}(x,t)=\left(\begin{array}{l} M_2\left(\dfrac{\sqrt{(C^2-D^2)l}-C\sqrt{l}\cos\left(2\sqrt{l}(\zeta+E)\right)}{C\sin\left(2\sqrt{l}(\zeta+E)\right)+D}\right) \\ +\dfrac{M_2 l}{\left(\dfrac{\sqrt{(C^2-D^2)l}-C\sqrt{l}\cos\left(2\sqrt{l}(\zeta+E)\right)}{C\sin\left(2\sqrt{l}(\zeta+E)\right)+D}\right)} \end{array}\right)\times\exp\left[i(-kx+wt+\varepsilon)\right],$$

$$u_{3,6}(x,t)=\left(\begin{array}{l} M_1\left(\dfrac{-\sqrt{(C^2-D^2)l}-C\sqrt{l}\cos\left(2\sqrt{l}(\zeta+E)\right)}{C\sin\left(2\sqrt{l}(\zeta+E)\right)+D}\right) \\ +\dfrac{M_1 l}{\left(\dfrac{-\sqrt{(C^2-D^2)l}-C\sqrt{l}\cos\left(2\sqrt{l}(\zeta+E)\right)}{C\sin\left(2\sqrt{l}(\zeta+E)\right)+D}\right)} \end{array}\right)\times\exp\left[i(-kx+wt+\varepsilon)\right],$$

$$v_{3,6}(x,t)=\left(\begin{array}{l} M_2\left(\dfrac{-\sqrt{(C^2-D^2)l}-C\sqrt{l}\cos\left(2\sqrt{l}(\zeta+E)\right)}{C\sin\left(2\sqrt{l}(\zeta+E)\right)+D}\right) \\ +\dfrac{M_2 l}{\left(\dfrac{-\sqrt{(C^2-D^2)l}-C\sqrt{l}\cos\left(2\sqrt{l}(\zeta+E)\right)}{C\sin\left(2\sqrt{l}(\zeta+E)\right)+D}\right)} \end{array}\right)\times\exp\left[i(-kx+wt+\varepsilon)\right],$$

$$u_{3,7}(x,t)=\left(\begin{array}{l} M_1\left(i\sqrt{l}+\dfrac{-2iC\sqrt{l}}{C+\cos\left(2\sqrt{l}(\zeta+E)\right)-i\sin\left(2\sqrt{l}(\zeta+E)\right)}\right) \\ +\dfrac{M_1 l}{\left(i\sqrt{l}+\dfrac{-2iC\sqrt{l}}{C+\cos\left(2\sqrt{l}(\zeta+E)\right)-i\sin\left(2\sqrt{l}(\zeta+E)\right)}\right)} \end{array}\right)\times\exp\left[i(-kx+wt+\varepsilon)\right],$$

$$v_{3,7}(x,t)=\left(\begin{array}{l} M_2\left(i\sqrt{l}+\dfrac{-2iC\sqrt{l}}{C+\cos\left(2\sqrt{l}(\zeta+E)\right)-i\sin\left(2\sqrt{l}(\zeta+E)\right)}\right) \\ +\dfrac{M_2 l}{\left(i\sqrt{l}+\dfrac{-2iC\sqrt{l}}{C+\cos\left(2\sqrt{l}(\zeta+E)\right)-i\sin\left(2\sqrt{l}(\zeta+E)\right)}\right)} \end{array}\right)\times\exp\left[i(-kx+wt+\varepsilon)\right],$$

$$u_{3,8}(x,t)=\left(\begin{array}{l} M_1\left(-i\sqrt{l}+\dfrac{2iC\sqrt{l}}{C+\cos\left(2\sqrt{l}(\zeta+E)\right)+i\sin\left(2\sqrt{-l}(\zeta+E)\right)}\right) \\ +\dfrac{M_1 l}{\left(-i\sqrt{l}+\dfrac{2iC\sqrt{l}}{C+\cos\left(2\sqrt{l}(\zeta+E)\right)+i\sin\left(2\sqrt{-l}(\zeta+E)\right)}\right)} \end{array}\right)\times\exp[i(-kx+wt+\varepsilon)],$$

$$v_{3,8}(x,t)=\left(\begin{array}{l} M_2\left(-i\sqrt{l}+\dfrac{2iC\sqrt{l}}{C+\cos\left(2\sqrt{l}(\zeta+E)\right)+i\sin\left(2\sqrt{-l}(\zeta+E)\right)}\right) \\ +\dfrac{M_2 l}{\left(-i\sqrt{l}+\dfrac{2iC\sqrt{l}}{C+\cos\left(2\sqrt{l}(\zeta+E)\right)+i\sin\left(2\sqrt{-l}(\zeta+E)\right)}\right)} \end{array}\right)\times\exp[i(-kx+wt+\varepsilon)],$$

where M_n and w are come from set 3.

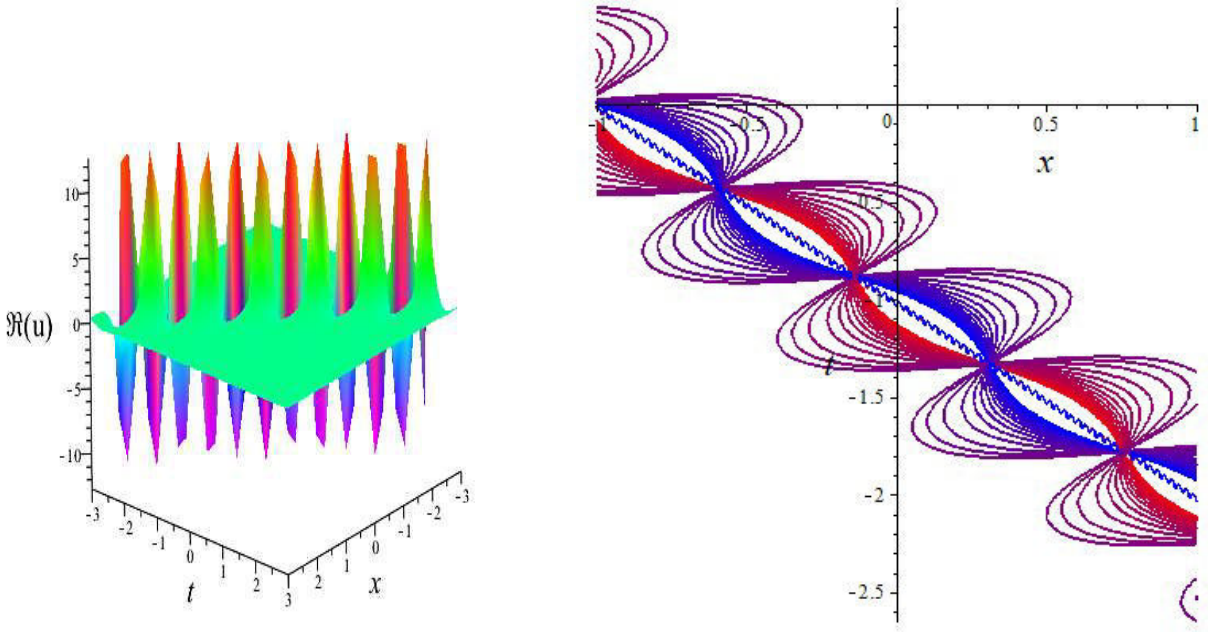

Fig-3.1: Outlook of rogue wave solution $u_{1,1}$ for $J_1=1,\ L_1=1,\ E=1,\ C=20,\ D=1,$ $l=-1,\ R_1=1,\ a_1=1,\ b_1=1,\ k=2,\ \varepsilon=0.$

For the physical description, it is observed that the solutions $u_{1,1}$, $u_{1,2}$, $v_{1,1}$, $v_{1,2}$, $u_{2,1}$, $u_{2,2}$, $v_{2,1}$, $v_{2,2}$, $u_{3,1}$, $u_{3,2}$, $v_{3,1}$, $v_{3,2}$ provide interaction of soliton and periodic wave degenerate rogue type breather optical soliton solutions. In particular, we depicted the graph of $u_{1,1}$ in **Fig. 3.1(a, b)**.

We also depicted 2d plots of the similar results by $u_{2,1}$ in **Fig 3.2(a, b, c)**. These graphs have different behavior for different conditions on parameter t as **(a)** represents oscillation with exponentially increasing amplitudes for $t \le 0$, **(b)** represents oscillations with exponentially decreasing amplitudes for $t > 1$, and **(c)** represents oscillations with exponentially decreasing amplitudes, then diminishes to zero and then again oscillations with exponentially increasing amplitudes $t = 1$. The solutions $u_{1,3}$, $u_{1,4}$, $v_{1,3}$, $v_{1,4}$, $u_{2,3}$, $u_{2,4}$, $v_{2,3}$, $v_{2,4}$, $u_{3,3}$, $u_{3,4}$, $v_{3,3}$, $v_{3,4}$ displayed similar behavior as combo periodic optical solitons and it has important properties to amplify or reduce amplitude of waves. This property is very much significant in optical communication systems. Particularly, we depicted the solution $u_{2,3}$ only in **Fig. 3.3(a, b)**. It is shown that when $\varpi = \frac{b_n w - 2a_n k}{1 - b_n k} > 0$ amplitudes of wave reduces after a certain times with a certain height. But when $\varpi = \frac{b_n w - 2a_n k}{1 - b_n k} < 0$ the reverse phenomena are causes as amplitudes of wave amplify after a certain time with a certain height.

The solutions $u_{1,5}$, $u_{1,6}$, $v_{1,5}$, $v_{1,6}$, $v_{2,5}$, $v_{2,6}$, $u_{3,5}$, $u_{3,6}$, $v_{3,5}$, $v_{3,6}$ exhibits double periodic optical solution which is depicted by the solutions $u_{1,5}$, $u_{1,6}$ in **Fig. 3.4** and **Fig. 3.5** respectively. The figures have a rhythm of oscillations with sub-harmonic beat i.e. not symmetric. The solutions $u_{1,7}$, $u_{1,8}$, $v_{1,7}$, $v_{1,8}$, $u_{2,7}$, $u_{2,8}$, $v_{2,7}$, $v_{2,8}$, $u_{3,7}$, $u_{3,8}$, $v_{3,7}$, $v_{3,8}$ exhibits double periodic optical solution which is depicted by the solutions $u_{1,8}$ in **Fig. 3.6**. The figures have a rhythm of oscillations with harmonic beat i.e. amplitudes are symmetric with maximum amplitude.

The solutions $u_{1,9}$, $v_{1,9}$, $u_{2,9}$, $v_{2,9}$ give the interaction of rational polynomial and periodic solitons, where polynomial function maintains it amplitude and exhibits periodic waves with increasing and decreasing amplitudes as depicted in **Fig 3.7(a, b)** for $u_{1,9}$.

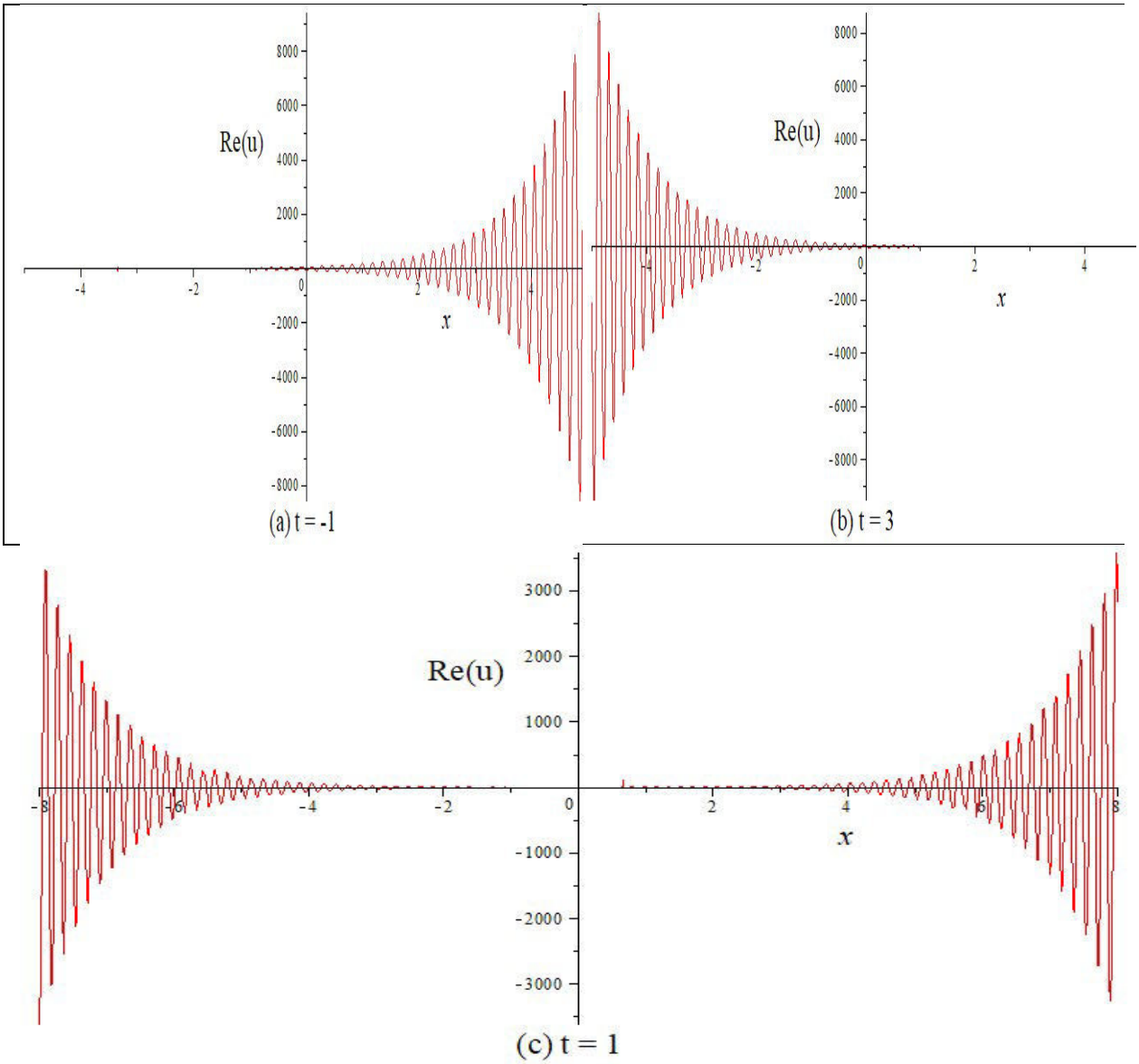

Fig-3.2: Outlook of rogue type breather optical soliton solutions $u_{2,1}$ for $J_1 = 1,\ L_1 = 1,\ E = 2,$ $C = 1,\ D = 1,\ l = -1,\ R_1 = 1,\ a_1 = 2,\ b_1 = 1,\ k = 35,\ \varepsilon = 0.$

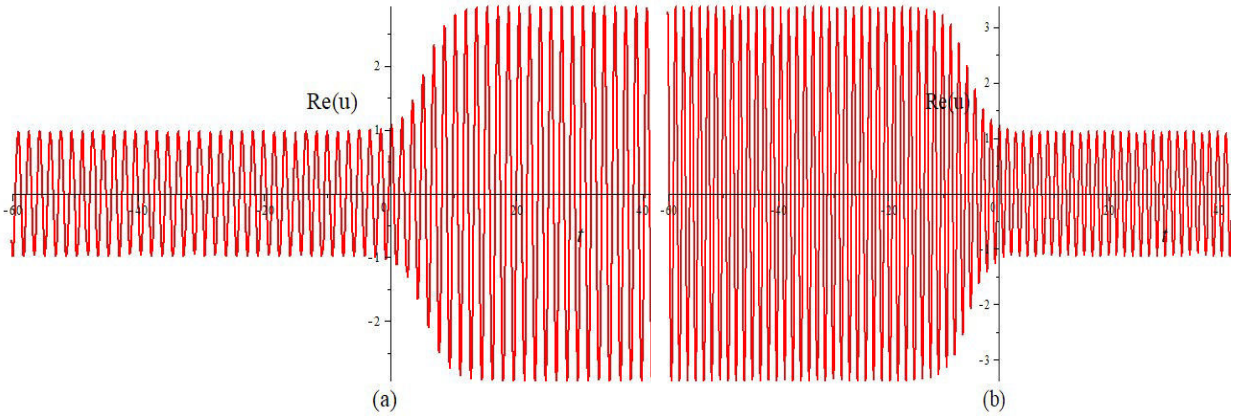

Fig-3.3: Outlook of optical solitary wave solution $u_{2,3}$ at $x=0$ for $J_1=1,\ L_1=0.2,\ E=1,$ $C=1,\ D=1,\ l=-1,\ R_1=4.2,\ a_1=1,\ b_1=1,\ k=2,\ \varepsilon=1$ **(a)** when $R_1=4.2$ **(b)** when $R_1=5.6.$

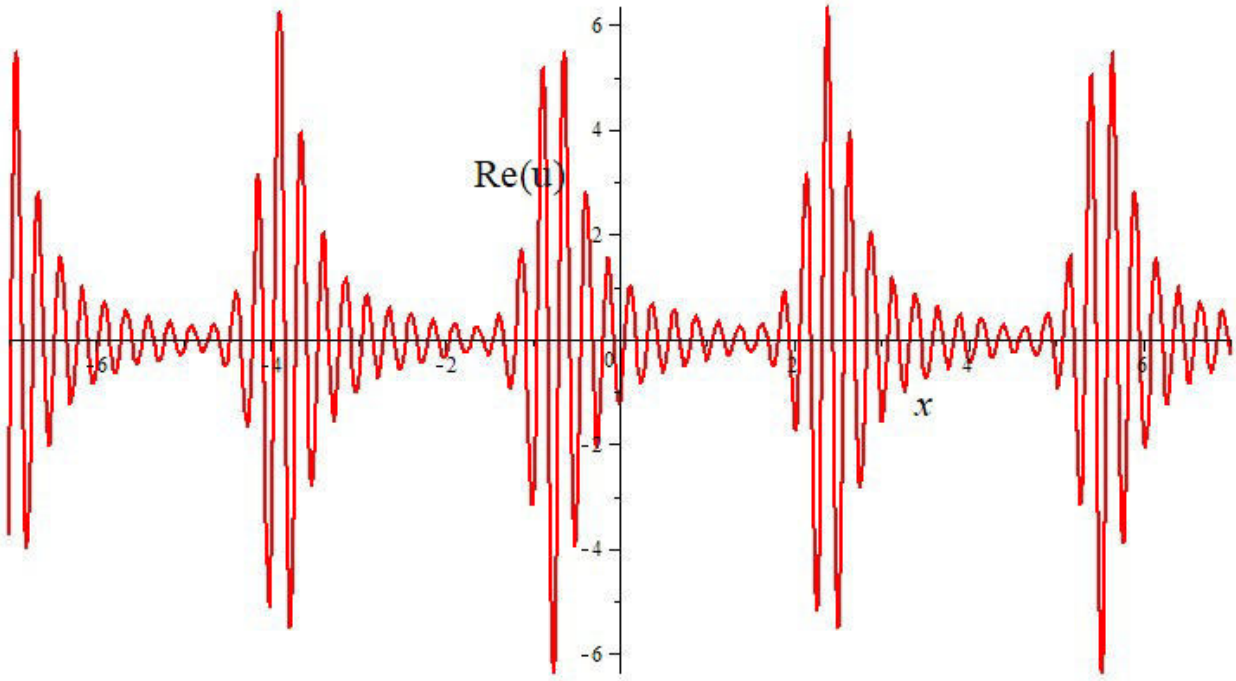

Fig-3.4: Outlook of optical solitary wave solution $u_{1,5}$ at $t=0$ for $J_1=1,\ L_1=1,\ E=0,$ $C=3,\ D=3.5,\ l=1,\ R_1=1,\ a_1=1,\ b_1=1,\ k=25,\ \varepsilon=0.$

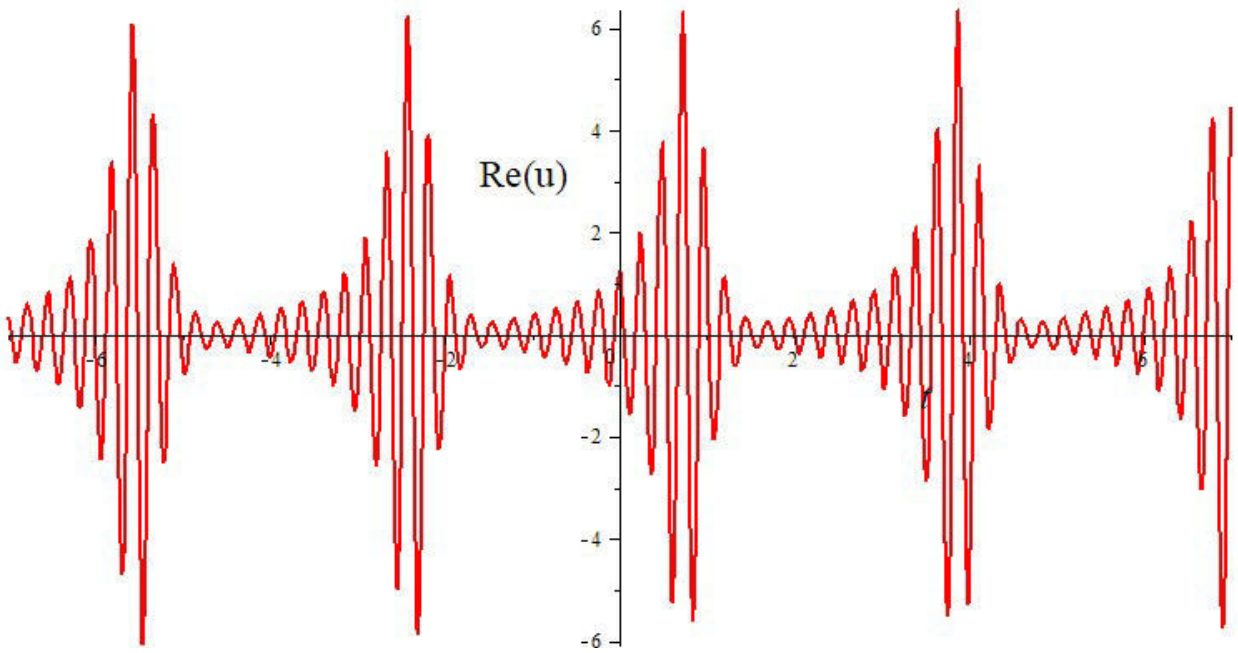

Fig-3.5: Outlook of optical solitary wave solution $u_{1,6}$ at $x = 0$ for $J_1 = 1,\ L_1 = 1,\ E = 0,$ $C = 3,\ D = 3.5,\ l = 1,\ R_1 = 1,\ a_1 = 1,\ b_1 = 1,\ k = 25,\ \varepsilon = 0.$

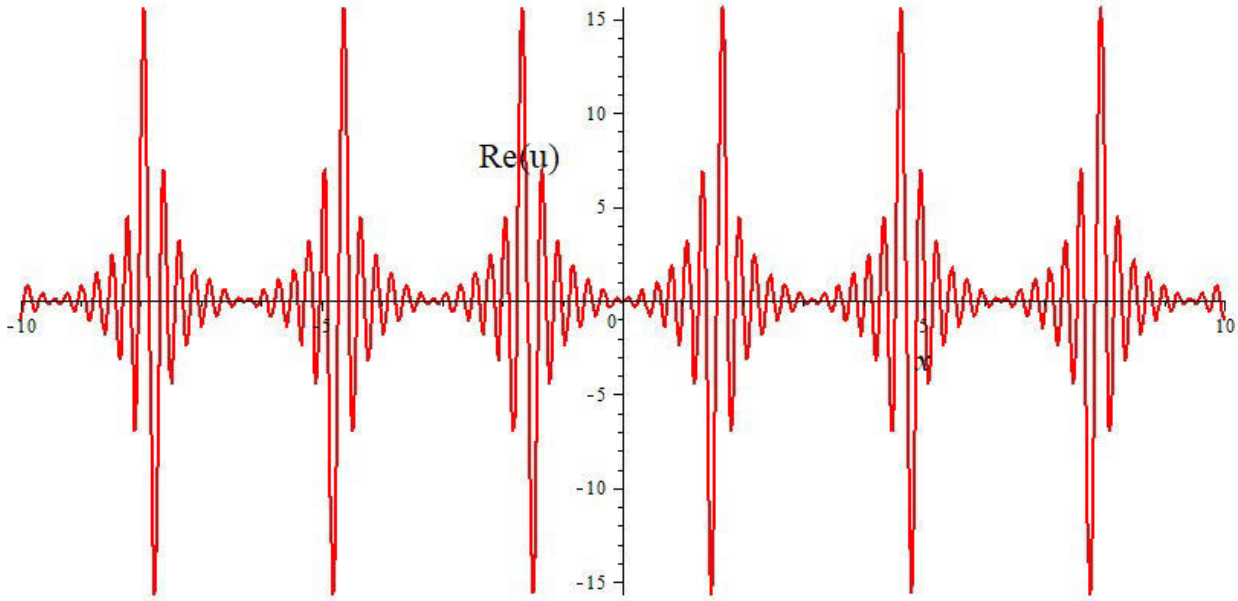

Fig-3.6: Outlook of optical solitary wave solution $u_{1,8}$ at $t = 0$ for $J_1 = 1,\ L_1 = 1,\ E = 0,\ C = 1.1,$ $D = 3.5,\ l = 1,\ R_1 = 1,\ a_1 = 1,\ b_1 = 1,\ k = 25,\ \varepsilon = 0.$

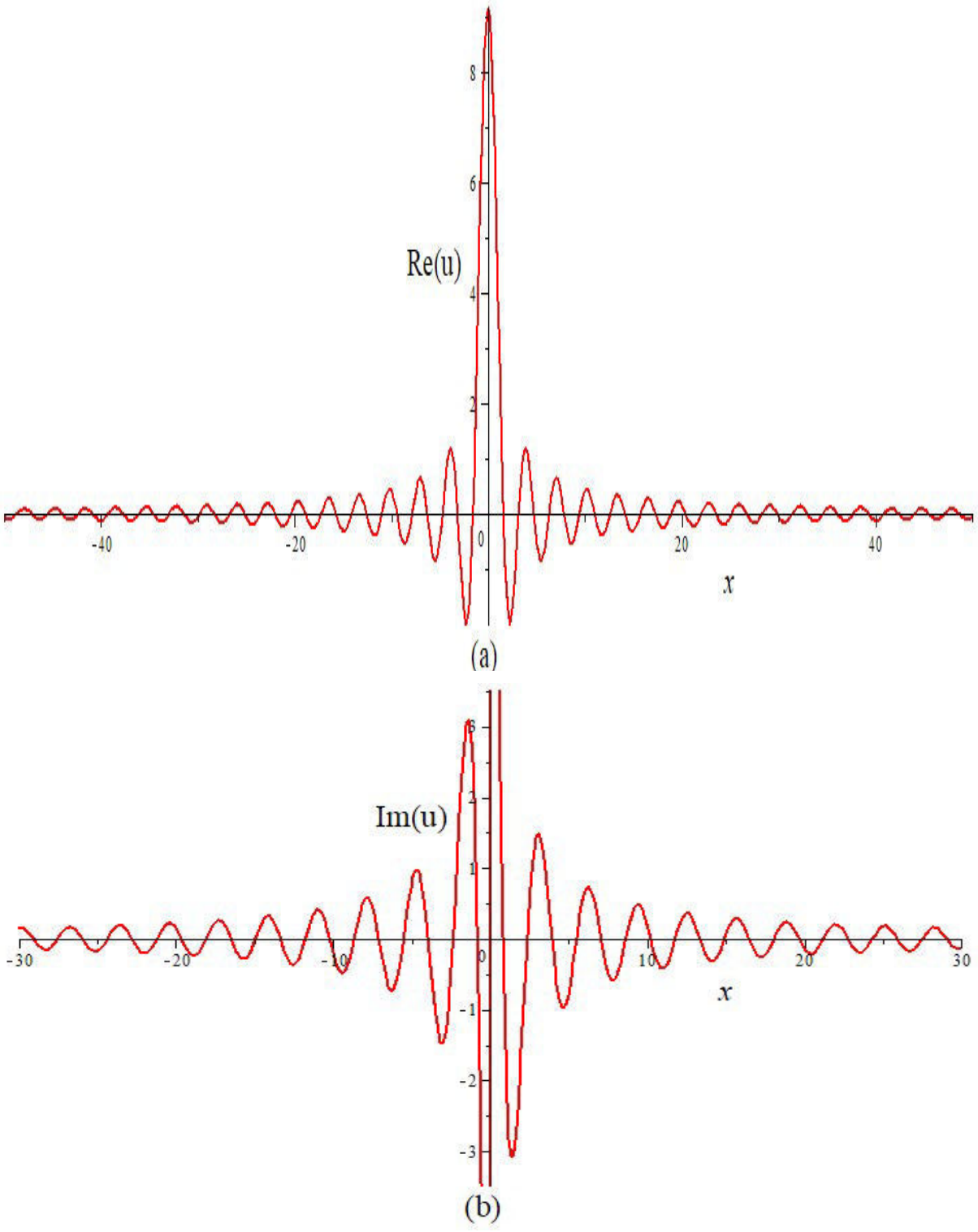

Fig-3.7: Outlook of rogue wave solution $u_{1,9}$ at $t=0$ for $J_1=1,\ L_1=1,\ E=0,\ C=1,$ $D=1,\ l=0,\ R_1=10,\ a_1=1,\ b_1=1,\ k=2,\ \varepsilon=0.$

3.5. Conclusion

This chapter has been presented the unified method to integrate the LPD model to retrieve optical solitons that can be used in birefringent fibers. We have derived optical solitons along with some dynamics as beat phenomena, oscillating rhythm, oscillation together increasing and decreasing rhythm, and oscillation jointly increasing and decreasing rhythm even achieved a soliton solution which can changes its amplitude after a certain times depicted in **Figs-3.2-3.7.** We also exhibits optical rogue wave in **Fig-3.1**. The results disclosed that the unified method is more effective and power tools to obtain optical solitons for nonlinear complex models which frequently arises in mathematical physics and engineering branches. Future works concerning extension and progress of the unified method to gain more dynamic structural solutions or applied in many models in diverse branches of engineering.

Chapter Four

Solitary wave solutions for the time fractional gHSC-KdV model

Acknowledgement

In this chapter [5], the generalized Kudryshov method is applied to determine exact solitary wave solutions for the time fractional generalized Hirota–Satsuma coupled KdV model. Here, fractional derivative is illustrated in the conformable derivative. Therefore, plentiful exact traveling wave solutions are achieved for this model, which encourage us to enlarge, a novel technique to gain unsteady solutions of autonomous nonlinear evolution models those occurs in physical and engineering branches. The obtained traveling wave solutions are expressed in terms of the exponential and rational functions. It is effortless to widen that this method is powerful and will be applied in further tasks to create advance exclusively innovative solutions to other higher-order nonlinear conformable fractional differential model in engineering problems.

4.1. Introduction

Nearby, great interest in fractional calculus applied in various fields such as electrical networks, control theory of dynamics, statistics, electro-chemistry of oxidization, acoustics, nonlinear optical fibre, plasma and solid state physics, chemical kinetics and geochemistry phenomena, signal processing and data mining can be effectively formed by means of nonlinear fractional order differential systems [17-20]. Modeling of a range of physical phenomena in terms of nonlinear time fractional evolution equations has played a significant factor in numerous efficient applications in the above mentioned fields.

The time fractional generalized HSC KdV system is vital nonlinear model occurs in the Toda lattice equation, a recognized (1+1) dimension soliton equation. This system can also be utilized as the model of interaction of neighboring particles of the same mass in a lattice formation with a crystal as well as illustrated basic characteristics of string dynamics in constant curvature space [82-85].

The more general form of time fractional generalized HSC KdV system can be written as follows [82, 83]:

$$\begin{cases} \dfrac{\partial^{\alpha} h}{\partial t^{\alpha}} = \dfrac{1}{4} h_{xxx} + 3hh_x + 3(w - v^2)_x \\ \dfrac{\partial^{\alpha} v}{\partial t^{\alpha}} = -\dfrac{1}{2} v_{xxx} - 3hv_x \\ \dfrac{\partial^{\alpha} w}{\partial t^{\alpha}} = -\dfrac{1}{2} w_{xxx} - 3hw_x \end{cases}, \qquad 0 < \alpha \le 1. \tag{4.1}$$

Recently, searching exact solutions of the system Eq. (4.1) was found by renowned researchers [84, 85]. Guo et. al. [84] applied the improved fractional sub-equation method to construct analytical solutions to the space–time fractional equations arises in fluid mechanics. The exact and complex traveling wave solutions to the time fractional generalized Hirota-Satsuma coupled KdV system are deliberated by Neirameh [85] using the direct algebraic method.

Considerable effort have been paid by many dynamical researchers to investigate exact solutions for FDEs such as the impulsive fractional differential equations with different boundary conditions [86-88], nonlinear impulsive hybrid boundary value problems involving fractional differential equations [89], space–time fractional Burgers equation [90], time fractional Burgers equation in fluid flow [91], the fractional coupled viscous Burgers' equation [92], time-fractional KdV equations [93] and so on.

The objective of this chapter is to apply the generalized Kudryashov method for finding the exact solitary wave solutions of the time fractional generalized HSC KdV system, which take part in a key task in mathematical physics.

This chapter is organized as follows: fundamental properties of conformable fractional derivative are presented in section 4.2. The brief description of the generalized Kudryashov methods is given in section 4.3. Then in section 4.4, this method has been applied to establish exact solutions for the time fractional general HSC KdV system. The obtained results are presented graphically and the relevant physical illustrations are provided in section 4.5. Finally, concluding remarks are drawn in section 4.6.

4.2. Conformable fractional derivative and its properties

For a function $\phi:(0,\infty)\to\Re$, the conformable fractional derivative of ϕ for order α is defined [94] as $\frac{\partial^\alpha \phi}{\partial t^\alpha}=\lim_{\varepsilon\to 0^+}\frac{\phi(t+\varepsilon t^{1-\alpha})-\phi(t)}{\varepsilon}$, $t>0$ and $0<\alpha\le 1$.

Some important properties of the conformable fractional derivative are as follows:

$$\frac{\partial^\alpha}{\partial t^\alpha}(a\phi+b\varphi)=a\frac{\partial^\alpha}{\partial t^\alpha}(\phi)+b\frac{\partial^\alpha}{\partial t^\alpha}(\varphi),\ \forall a,b\in\Re.$$

$$\frac{\partial^\alpha}{\partial t^\alpha}(t^\beta)=\beta t^{\beta-\alpha},\ \forall\beta\in\Re \text{ and } \frac{\partial^\alpha}{\partial t^\alpha}(\lambda)=0,\ \lambda=const.$$

$$\frac{\partial^\alpha}{\partial t^\alpha}(\phi\circ\varphi)(t)=t^{1-\alpha}\phi'(\varphi(t))\varphi'(t).$$

4.3. The Method

Let us assume a general nonlinear evolution equation in x and t as

$$\aleph(h,h_t,h_x,h_{xx},...)=0, x\in\Re, t>0, \tag{4.2}$$

where the function $h = h(x,t)$ is unknown and $\aleph$ is a polynomial function with respect to some functions or specified variables, which have nonlinear terms and highest order derivatives of the unknown function. The key steps of the generalized Kudryashov method are as [93, 95]:

Step 1: Consider the following traveling wave transformation

$$h(x,t) = H(\zeta), \quad \zeta = x - \frac{ct^{\alpha}}{\alpha}, \tag{4.3}$$

where c is the velocity of the relative wave mode. By using the above transformation the nonlinear partial differential equation Eq. (4.3) is reduced to a nonlinear ordinary differential equation (ODE):

$$\chi(H, H', H'', ...) = 0, \tag{4.4}$$

where the prime denotes the derivative of H with respect to ζ and χ is a polynomial of $H(\zeta)$.

Step 2: Let us assume that the solution of Eq. (4.4) has the following form:

$$H(\zeta) = \frac{\sum_{i=0}^{N} a_i \phi^i(\zeta)}{\sum_{j=0}^{M} b_j \phi^j(\zeta)}, \tag{4.5}$$

where a_i and b_j are real constants, N and M are positive integers such that a_N, $b_M \neq 0$ and $\phi(\zeta)$ satisfies the following ordinary differential equation:

$$\phi'(\zeta) = \phi^2(\zeta) - \phi(\zeta). \tag{4.6}$$

The general solution of Eq. (4.6) is of the following form:

$$\phi(\zeta) = \frac{1}{1 + Ae^{\zeta}}, \tag{4.7}$$

where A is any arbitrary constant.

Step 3: Determine the positive integers N and M in Eq. (4.5) by balancing the highest order derivative term with the nonlinear term of $H(\zeta)$ in Eq. (4.2) or Eq. (4.4). Moreover, we define the degree of $H(\zeta)$ as $D(H(\zeta)) = N - M$, which gives rise to the degree of other expression as $D(\frac{d^q H}{d\zeta^q}) = N - M + q, D(H^p(\frac{d^q H}{d\zeta^q})^s) = (N - M)p + s(N - M + q),$

where p, q, s are integer numbers.

Thus, we can find the value of N and M in Eq. (4.5).

Step 4: Inserting Eq. (4.5) along with Eq. (4.6) into Eq. (4.4) and collect all terms with the same powers of ϕ together. Setting each coefficients of this polynomial ϕ to zero, we obtain a system of algebraic equations for a_i, b_j and c.

Step 5: By inserting the values of parameters gained in previous step and $\phi(\zeta)$ into the Eq. (4.5), then the solutions of Eq. (4.2) can be constructed.

4.4. Applications

Consider the following traveling wave transformation:

$$\begin{cases} h(x,t) = \frac{1}{c}H^2(\xi) \\ v(x,t) = -c + H(\xi) \\ w(x,t) = 2c^2 - 2cH(\xi) \end{cases}, \tag{4.8}$$

where $\xi = x - \frac{c}{\alpha}.t^\alpha$.

Inserting Eq. (4.8) into Eq. (4.1) reduced into ordinary differential equations

$$c(H_\xi)^2 + cHH_{\xi\xi} + 3H^4 - 4c^2H^2 + 6c^4 + 2c^2R = 0 \tag{4.9}$$

and $cH_{\xi\xi} + 2H^3 - 2c^2H = 0,$ (4.10)

where R is an integration constant to be evaluated later.

Case 1: By balancing the highest order derivative term $HH_{\xi\xi}$ with the nonlinear term H^4 in Eq. (4.9) gives $N = M + 1$.

Setting $M = 1$, we have $N = 2$. Therefore Eq. (4.5) reduces to

$$H(\xi) = \frac{a_0 + a_1\phi + a_2\phi^2}{b_0 + b_1\phi}. \tag{4.11}$$

Inserting Eq. (4.11) along with Eq. (4.6) into Eq. (4.9), we have a polynomial of ϕ^k, $(k = 0,1,2,...)$. Equating the coefficients of this polynomial of the same powers of ϕ to zero, we obtain a system of equations yields the values for R, c, a_0, a_1, a_2, b_0 and b_1.

Set 1: $R = -\frac{5}{32}, c = -\frac{1}{4}, a_0 = -\frac{1}{4}b_0, a_1 = -\frac{1}{4}b_1 + \frac{1}{2}b_0, a_2 = \frac{1}{2}b_1, b_0, b_1 = const.$

Set 2: $R = -\frac{5}{2}, c = -1, a_0 = \frac{1}{2}b_1, a_1 = -b_1, a_2 = b_1, b_0 = -\frac{1}{2}b_1, b_1 = const.$

Set 3: $R = -\frac{5}{2}, c = -1, a_0 = -\frac{1}{2}b_1, a_1 = b_1, a_2 = -b_1, b_0 = -\frac{1}{2}b_1, b_1 = const.$

Set 4: $R = -\frac{5}{32}, c = -\frac{1}{4}, a_0 = \frac{1}{4}b_0, a_1 = \frac{1}{4}b_1 - \frac{1}{2}b_0, a_2 = -\frac{1}{2}b_1, b_0, b_1 = const.$

Set 5: $R = -\frac{3}{4}, c = \frac{1}{2}, a_0 = 0, a_1 = \mp\frac{i}{\sqrt{2}}b_1, a_2 = \pm\frac{i}{\sqrt{2}}b_1, b_0 = -\frac{1}{2}b_1, b_1 = const.$

For **set 1**, the time fractional generalized HSC KdV equations hold the solution as:

$$\begin{cases} h(x,t) = -\frac{1}{4}\left\{\frac{1 - Ae^{\xi}}{1 + Ae^{\xi}}\right\}^2 \\ v(x,t) = \frac{1}{2(1 + Ae^{\xi})} \\ w(x,t) = \frac{1}{4(1 + Ae^{\xi})} \end{cases}, \tag{4.12}$$

where $\xi = x + \frac{t^{\alpha}}{4\alpha}$.

For **set 2**, the time fractional generalized HSC KdV equations hold the solution as:

$$\begin{cases} h(x,t) = -\left\{\dfrac{1+A^2e^{2\xi}}{1-A^2e^{2\xi}}\right\}^2 \\ v(x,t) = \dfrac{2}{1-A^2e^{2\xi}} \\ w(x,t) = \dfrac{4}{1-A^2e^{2\xi}} \end{cases}, \tag{4.13}$$

where $\xi = x + \dfrac{t^\alpha}{\alpha}$.

For **set 3**, the time fractional generalized HSC KdV equations hold the solution as:

$$\begin{cases} h(x,t) = -\left\{\dfrac{1+A^2e^{2\xi}}{1-A^2e^{2\xi}}\right\}^2 \\ v(x,t) = -\dfrac{2A^2e^{2\xi}}{1-A^2e^{2\xi}} \\ w(x,t) = -\dfrac{4A^2e^{2\xi}}{1-A^2e^{2\xi}} \end{cases}, \tag{4.14}$$

where $\xi = x + \dfrac{t^\alpha}{\alpha}$.

For **set 4**, the time fractional generalized HSC KdV equations hold the solution as:

$$\begin{cases} h(x,t) = -\dfrac{1}{4}\left\{\dfrac{1-Ae^{\xi}}{1+Ae^{\xi}}\right\}^2 \\ v(x,t) = \dfrac{Ae^{\xi}}{2(1+Ae^{\xi})} \\ w(x,t) = \dfrac{Ae^{\xi}}{4(1+Ae^{\xi})} \end{cases}, \tag{4.15}$$

where $\xi = x + \dfrac{t^\alpha}{4\alpha}$.

For **set 5**, the time fractional generalized HSC KdV equations hold the solution as:

$$\begin{cases} h(x,t) = -4\left\{\dfrac{\pm(1+Ae^{\xi})\mp 1}{1-A^2e^{2\xi}}\right\}^2 \\ v(x,t) = \dfrac{-(1-A^2e^{2\xi})\mp i2\sqrt{2}(1+Ae^{\xi})\pm i2\sqrt{2}}{2(1-A^2e^{2\xi})}, \\ w(x,t) = \dfrac{1-A^2e^{2\xi}\mp i2\sqrt{2}(1+Ae^{\xi})\pm i2\sqrt{2}}{1-A^2e^{2\xi}} \end{cases} \tag{4.16}$$

where $\xi = x - \dfrac{t^{\alpha}}{2\alpha}$.

Case 2: Balancing $HH_{\xi\xi}$ with H^4 in equation Eq. (4.10) gives $N = M+1$. Setting $M = 1$, we obtain $N = 2$.

Therefore Eq. (4.5) reduces to

$$H(\xi) = \frac{a_0 + a_1\phi + a_2\phi^2}{b_0 + b_1\phi}. \tag{4.17}$$

Inserting Eq. (4.17) along with Eq. (4.5) into Eq. (4.10), we get a polynomial of ϕ^k, $(k = 0,1,2,...)$. Equating the coefficients of this polynomial of the same powers of ϕ to zero, we obtain a system of equations yields the values for c, a_0, a_1, a_2, b_0 and b_1.

Set 1: $c = -\dfrac{1}{4}, a_0 = -\dfrac{1}{4}b_0, a_1 = -\dfrac{1}{4}b_1 + \dfrac{1}{2}b_0, a_2 = \dfrac{1}{2}b_1, b_0, b_1 = const.$

Set 2: $c = -1, a_0 = \dfrac{1}{2}b_1, a_1 = -b_1, a_2 = b_1, b_0 = -\dfrac{1}{2}b_1, b_1 = const.$

Set 3: $c = -1, a_0 = -\dfrac{1}{2}b_1, a_1 = b_1, a_2 = -b_1, b_0 = -\dfrac{1}{2}b_1, b_1 = const.$

Set 4: $c = -\dfrac{1}{4}, a_0 = \dfrac{1}{4}b_0, a_1 = \dfrac{1}{4}b_1 - \dfrac{1}{2}b_0, a_2 = -\dfrac{1}{2}b_1, b_0, b_1 = const.$

Set 5: $c = \dfrac{1}{2}, a_0 = 0, a_1 = \pm i\sqrt{2}b_0, a_2 = \mp i\sqrt{2}b_0, b_0 = const., b_1 = 2b_0.$

From some simplification, we see that the **set-1** to **set-4** gives the same results as in **case-1**. But only **set-5** is different which gives solution as

$$\begin{cases} h(x,t) = -4\left\{\dfrac{\pm(1+Ae^{\xi})\mp 1}{-1+A^2e^{2\xi}}\right\}^2 \\ v(x,t) = \dfrac{1-A^2e^{2\xi} \pm i2\sqrt{2}(1+Ae^{\xi})\mp i2\sqrt{2}}{2(-1+A^2e^{2\xi})}, \\ w(x,t) = \dfrac{-1+A^2e^{2\xi} \mp i\sqrt{2}(1+Ae^{\xi})\pm i\sqrt{2}}{2(-1+A^2e^{2\xi})} \end{cases} \tag{4.18}$$

where $\xi = x - \dfrac{t^{\alpha}}{2\alpha}$.

4.5. Graphical representations

Ten set of results are achieved in this chapter. All of the results are analyzed and some of them depicted in the **Figs. 4.1, 4.2**. The graphs signify the change of amplitude, shape of wave and nature of the solitary waves for each acquired wave solutions in space x at time t. The solution $h(x,t)$ of Eq. (4.12) represents bright bell solitary wave (**Fig-4.1(a)**) for the physical parameters $A = 0.5,\ \alpha = 0.67$. The solution both $v(x,t)$ and $w(x,t)$ of Eq. (4.12) represents similar kink solitary wave. **Fig-4.1(b)** expressed the shape of the kink wave $v(x,t)$ of Eq. (4.12) for the physical parameters $A = 0.5,\ \alpha = 0.67$.

The solutions $h(x,t)$ of Eq. (4.15) represent bright bell solitary wave solutions and all of them are similar like to the graph **Fig-4.1(a)** of $h(x,t)$ in Eq. (4.12). We also see that the solutions $v(x,t),\ w(x,t)$ of Eq. (4.15) represent kink solitary wave solutions and all of them are similar like to the graph **Fig-4.1(b)** of $h(x,t)$ in Eq. (4.12). So we omit the similar type of figures.

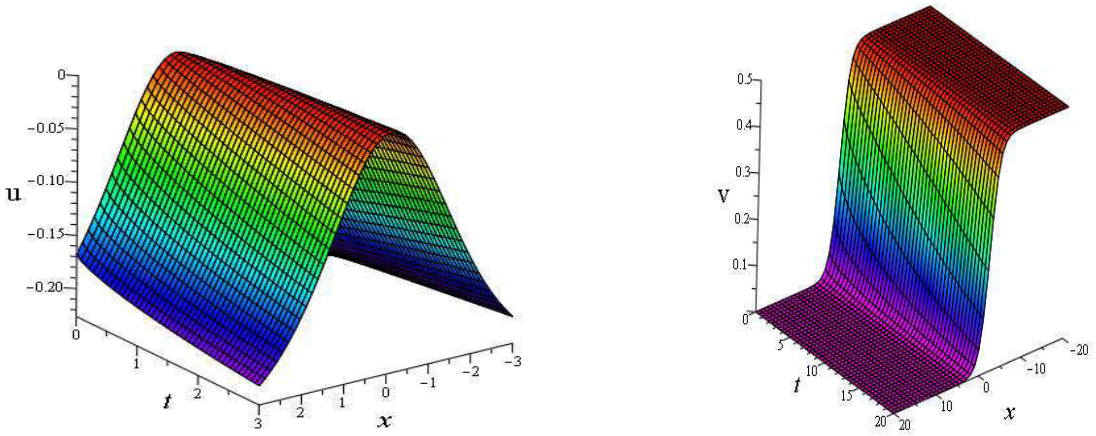

(a) (b)

Fig-4.1: (a) Represent bright bell solitary wave solution $h(x,t)$ of Eq. (4.12), and **(b)** Represent kink solitary wave solution $v(x,t)$ of Eq. (4.12) for the physical parametric values $A = 0.5,\ \alpha = 0.67$.

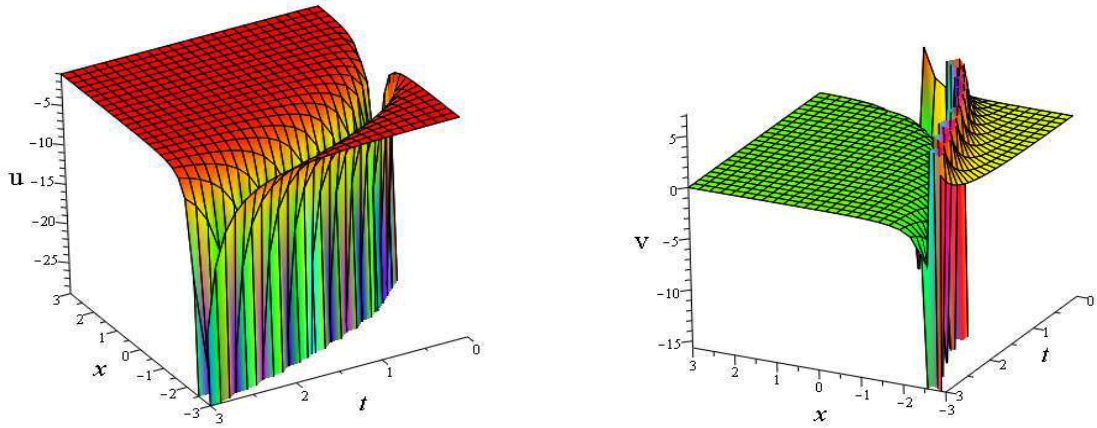

(a) (b)

Fig-4.2: (a) Represent dark bell solitary wave solution $h(x,t)$ of Eq. (4.13), and **(b)** Represent kink solitary wave solution $v(x,t)$ of Eq. (4.13) for the physical parametric values $A = 0.5,\ \alpha = 0.5$.

The solution $h(x,t)$ of Eq. (8.13) represents dark solitary wave (see **Fig-4.2(a)**) for the physical parameters $A = 0.5,\ \alpha = 0.5$ in space x at time t. The solution both $v(x,t)$ and $w(x,t)$ of Eq. (4.13) represents similar singular kink solitary wave. **Fig-4.2(b)** expressed the shape of the singular kink solitary wave $v(x,t)$ of Eq. (4.13) for the physical parameters $A = 0.5,\ \alpha = 0.5$. The solutions $h(x,t)$ of Eq. (4.14), Eq. (4.16) and Eq. (4.18) represent dark bell solitary wave solutions and all of them are similar to the graph **Fig-4.2(a)** of $h(x,t)$ in

Eq. (4.13). We also see that the solutions $v(x,t)$, $w(x,.t)$ of Eq. (4.14) and complex part of $v(x,t)$, $w(x,.t)$ of Eq. (4.16) and $v(x,t)$, $w(x,.t)$ of Eq. (4.18) represent singular kink solitary wave solutions and all of them are similar like to the graph **Fig-4.2(b)** of $h(x,t)$ in Eq. (4.13). So we omit the similar type of figures. Real part of $v(x,t)$, $w(x,.t)$ in Eq. (4.16) and Eq. (4.18) gives constant solution that represent in xt -plane.

4.6. Conclusions

In this chapter, we have successfully used a mathematical apparatus named the generalized Kudryashov method for creating exact solitary wave solutions to the time fractional generalized Hirota-Satsuma coupled KdV system. The achieved solitary wave solutions are expressed in terms of the exponential and rational functions. The acquired results will serve as a very important milestone in the study of interaction of neighboring particles of the same mass in a lattice formation with a crystal and long water wave phenomena. We also have demonstrated that the generalized Kudryashov method is an effective solvable tool for large classes of system of conformable nonlinear fractional differential equations.

Chapter Five

Interaction solutions of the (2+1)-D BBS and BBMB models

Acknowledgement

In this chapter [6, 7], the (2+1)-dimensional Bogoyavlenskii's breaking soliton (BBS) and Benjamin-Bona-Mahony-Burgers (BBMB) models are considered and reduced to bilinear form by using the Hirota bilinear approach. We analytically construct lump waves and collision of lump with periodic waves. We also present collision between lump wave and single-, double-kink soliton solutions, and the collision among lump, periodic and single-, double-kink soliton solutions of the BBS and BBMB models. In addition, we explain the fission properties of the lump and periodic waves, lump, periodic and single soliton, and lump, periodic and two solitons. Finally, we graphically present the nature of the collision solutions of both models in 3D and contour plots.

5.1. Introduction

The soliton theory, which is one of the three sections of nonlinear science, is broadly used in various areas of physical science such as fluid mechanics, nonlinear optics, mathematical biology, ecology, chemical kinetics, plasma waves and others [1-21]. Various reliable and effective approaches have been suggested to address the solitary waves such as the (G'/G)-expansion method [38], the generalized Kudryashov method [39], the Hirota bilinear method [40], the tan-cot method [42], the tanh-coth method [43], the direct algebraic method [44], the Darboux transformation method [45] etc. Recently the combination of quadratic functions with the exponential or trigonometric or hyperbolic functions to explain the nature of the collision of kink, lump, rogue and periodic waves for produce kinky-lump, kinky-rogue,

periodic-lump wave, periodic-rogue waves and kinky-periodic-rogue wave for the NLEEs [71-78]. Based on the motivation of the above study we consider the (2+1)-dimensional BBS [79] and BBMB [80] models for the study of new dynamic phenomena and the physical behavior of different collisions among lump, periodic and soliton solutions. Such structure solutions of two models are analyzed by applying the Hirota bilinear method.

5.2. The bilinear formation of the BBS model

Consider the (2+1)-dimensional BBS model is as follows [79]

$$\phi_{xxxy} + 4\phi_y\phi_{xx} + 4\phi_x\phi_{xy} + \phi_{xt} = 0, \tag{5.1}$$

where ϕ is the function of spatial variables x, y and time variable t.

Consider the conversion relation as below

$$\phi = \frac{3}{2}(\ln\psi)_x \tag{5.2}$$

with real function $\psi(x, y, t)$ to be determined.

Inserting the relation Eq. (5.2), in Eq. (5.1), then we can write

$$(\ln\psi)_{xxxxy} + 6(\ln\psi)_{xy}(\ln\psi)_{xxx} + 6(\ln\psi)_{xx}(\ln\psi)_{xxy} + (\ln\psi)_{xxt} = 0. \tag{5.3}$$

Integrating the equation Eq. (5.3) with respect to x, then we have

$$(\ln\psi)_{xt} + (\ln\psi)_{xxxy} + 6(\ln\psi)_{xy}.(\ln\psi)_{xx} = 0. \tag{5.4}$$

By considering the linear terms of Eq. (5.4), we have

$$(\ln\psi)_{xt} + (\ln\psi)_{xxxy} = 0. \tag{5.5}$$

By using the bilinear operator D, the Eq. (5.5) can be written as

$$(D_xD_t + D_yD_x^3)f.f = 0, \tag{5.6}$$

when the D-operator [71] is defined by

$$(D_x^{\,m} D_y^{\,k} D_t^{\,n}) f.g = (\frac{\partial}{\partial x_1} - \frac{\partial}{\partial x_2})^m (\frac{\partial}{\partial y_1} - \frac{\partial}{\partial y_2})^k (\frac{\partial}{\partial t_1} - \frac{\partial}{\partial t_2})^n [f(x_1, y_1, t_1).g(x_2, y_2, t_2)].$$

Thus Eq. (5.5) reduces to

$$\psi\psi_{xt} - \psi_t\psi_x + 3\psi_{xx}\psi_{xy} - 3\psi_x\psi_{xxy} + \psi\psi_{xxxy} - \psi_{xxx}\psi_y = 0. \tag{5.7}$$

Clearly if ψ satisfies Eq. (5.1), then $\phi = \frac{3}{2}(\ln\psi)_x$ directly generates the solutions of the governing model Eq. (5.1).

5.3. Lump wave solution of BBS model

To obtain the lump wave solutions of the BBS model, consider an ansatz of the following form

$$\psi = (p_1 x + p_2 y + p_3 t)^2 + (q_1 x + q_2 y + q_3 t)^2 + l, \tag{5.8}$$

where $p_1, p_2, p_3, q_1, q_2, q_3$ and l are free parameters. Setting Eq. (5.8) in Eq. (5.7), we have an algebraic system in $p_1, p_2, p_3, q_1, q_2, q_3$ and l. By solving this system via Maple 18, we have $p_3 = q_3 = 0,\ p_1 = p_1, p_2 = -\frac{q_1 q_2}{p_1}, q_1 = q_1, q_2 = q_2, l = l$, then the Eq. (5.8) can be written as

$$\psi = (p_1 x - \frac{q_1 q_2}{p_1} y)^2 + (q_1 x + q_2 y)^2 + l. \tag{5.9}$$

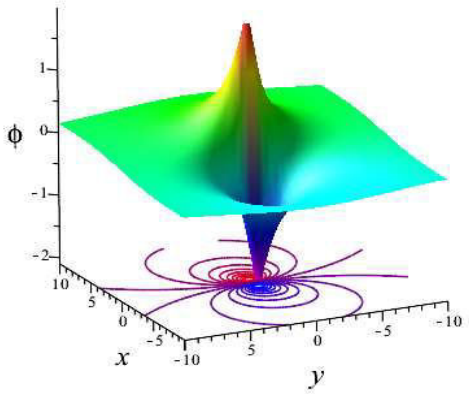

Fig-5.1: Profiles of the lump solution ϕ Eq. (5.1) for $p_1 = q_1 = q_2 = l = 1$.

By combining Eq. (5.9) and Eq. (5.7) and putting $p_1 = q_1 = q_2 = l = 1$, we have the solution of Eq. (5.1) as depicted in figure **Fig-1**. Due to guarantee ϕ is localized in every direction, l have to be considered as a positive constant. In this case, the optimum amplitude of the solution ϕ is occurred at the points $(\pm\sqrt{\frac{l}{{p_1}^2+{q_1}^2}},0)$ with the amplitudes $\frac{3}{2}\sqrt{\frac{{p_1}^2+{q_1}^2}{l}}$ and $-\frac{3}{2}\sqrt{\frac{{p_1}^2+{q_1}^2}{l}}$.

5.4. Collision among lumps, periodic waves, and soliton solutions

5.4.1. Collision between lumps and periodic waves: To study the collision scenarios between lump and periodic waves, consider a function constructed by double quadratic form and a sinusoidal function

$$\psi = (\alpha_1 x + \alpha_2 y + \alpha_3 t)^2 + (\beta_1 x + \beta_2 y + \beta_3 t)^2 + l + \lambda\cos(\gamma_1 x + \gamma_2 y + \gamma_3 t), \qquad (5.10)$$

where $\alpha_1,\alpha_2,\alpha_3,\beta_1,\beta_2,\beta_3,\gamma_1,\gamma_2,\gamma_3,l$ and λ are free parameters. Inserting Eq. (5.10) in Eq. (5.7), we have an algebraic system in $\alpha_1,\alpha_2,\alpha_3,\beta_1,\beta_2,\beta_3,\gamma_1,\gamma_2,\gamma_3,l$ and λ. By solving this system via Maple 18, we get the following results:

Case 1: $\alpha_2=\alpha_3=\beta_2=\beta_3=\gamma_2=\gamma_3=0,\lambda=\lambda,\alpha_1=\alpha_1,\beta_1=\beta_1,\gamma_1=\gamma_1,l=l$.

Case 2: $\alpha_1=\alpha_1,\alpha_2=-\frac{\beta_1\beta_2}{\alpha_1},\alpha_3=\beta_3=\gamma_1=\gamma_3=0,\lambda=\lambda,\beta_1=\beta_1,\beta_2=\beta_2,$
$\gamma_2=\gamma_2,l=l$.

For **case 1**, the Eq. (5.10) can be written as

$$\psi=(\alpha_1 x)^2+(\beta_1 x)^2+l+\lambda\cos(\gamma_1 x). \tag{5.11}$$

For **case 2**, the Eq. (5.10) can be written as

$$\psi=(\alpha_1 x-\frac{\beta_1\beta_2}{\alpha_1}y)^2+(\beta_1 x+\beta_2 y)^2+l+\lambda\cos(\gamma_2 y). \tag{5.12}$$

Using Eq. (5.11) and Eq. (5.7) and selecting $\alpha_1=\beta_1=\gamma_1=l=1$, we have the solution of Eq. (5.1) (see **Fig-5.2**). **Fig-5.2** exhibits as a single kinky-lump wave for $\lambda=1$ (see **Fig-5.2(a)**) but it is going to split into double kinky-lump waves even large number of kinky-lump waves due to fission of wave for the increase of λ (see the **Fig-5.2(b-d)**) gradually. Beside this, by choosing $\alpha_1=\beta_1=\beta_2=\gamma_2=l=1$ and setting Eq. (5.12) in Eq. (5.7), we have the solution of Eq. (5.1) (see **Fig-5.3**). The solution in **case-2** exhibits as a single lump wave for $\lambda=1$ (see **Fig-5.3(a)**) but it is going to split into double lump waves due to fission of lump wave for the increase of λ (see the **Fig-5.3(b-d)**) gradually. The energy distribution is symmetric over all the periodic lump waves while it travels (see **Fig-5.3**).

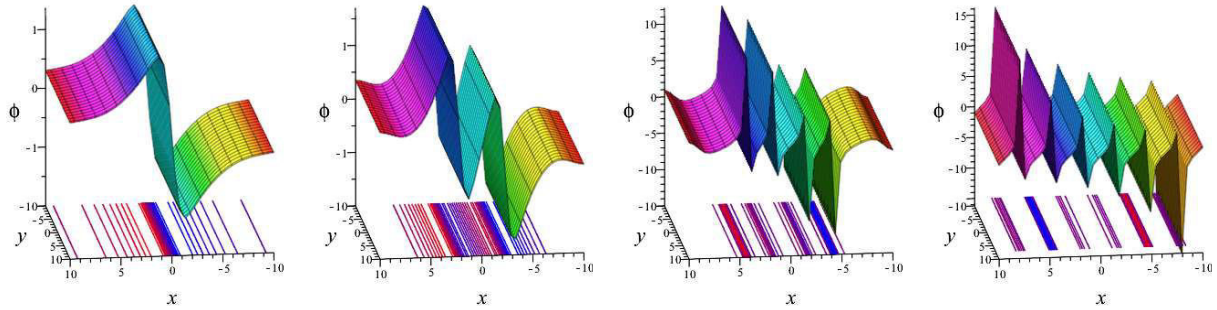

(a) $\lambda = 1$ (b) $\lambda = 10$ (c) $\lambda = 80$ (d) $\lambda = 50000$

Fig-5.2: Profiles of the kinky-lump wave degenerate into periodic kinky-lump wave gradually via solution ϕ of Eq. (5.1) for $\alpha_1 = \beta_1 = \gamma_1 = l = 1$.

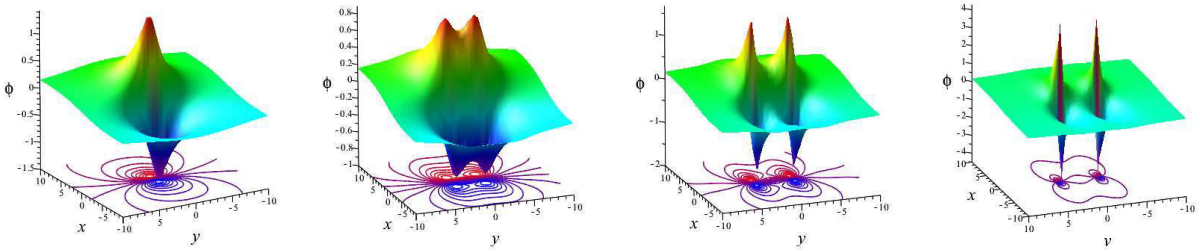

(a) $\lambda = 1$ (b) $\lambda = 8$ (c) $\lambda = 16$ (d) $\lambda = 17$

Fig-5.3: Profiles of collision solution ϕ of Eq. (5.1) for $\alpha_1 = \beta_1 = \beta_2 = \gamma_2 = l = 1$.

5.4.2. Collision between a lump and a single-kink soliton: To construct the collision of lump wave and a single kink soliton, we consider a function constructed by double quadratic form and an exponential function

$$\psi = (\alpha_1 x + \alpha_2 y + \alpha_3 t)^2 + (\beta_1 x + \beta_2 y + \beta_3 t)^2 + l + \lambda \exp(m_1 x + m_2 y + m_3 t), \qquad (5.13)$$

where $\alpha_1, \alpha_2, \alpha_3, \beta_1, \beta_2, \beta_3, m_1, m_2, m_3, l$ and λ are real free constants. Setting Eq. (5.13) into the Eq. (5.7), we have an algebraic system in $\alpha_1, \alpha_2, \alpha_3, \beta_1, \beta_2, \beta_3, m_1, m_2, m_3, l$ and λ. By solving these equations via Maple 18, we get $\alpha_1 = \alpha_1, \alpha_2 = -\frac{\beta_1 \beta_2}{\alpha_1}, \alpha_3 = \beta_3 = m_1 = m_3 = 0,$

$\beta_1 = \beta_1, \beta_2 = \beta_2, m_2 = m_2, l = l, \lambda = \lambda$, then the Eq. (5.13) can be written as

$$\psi = (\alpha_1 x - \frac{\beta_1\beta_2}{\alpha_1} y)^2 + (\beta_1 x + \beta_2 y)^2 + l + \lambda \exp(m_2 x). \quad (5.14)$$

Using Eq. (5.14) and Eq. (5.7) and selecting $\alpha_1 = \beta_1 = \beta_2 = m_2 = l = 1, \lambda = 10$, we have the solution of Eq. (5.1) (see **Fig-5.4**).The **Fig-5.4** exhibits the dynamic processes of collision between lump waves with a single kink wave solution. We observe that the lump wave is downed and consumed by the kink compare with single lump wave **Fig-5.1** and flow pattern being congested from one side.

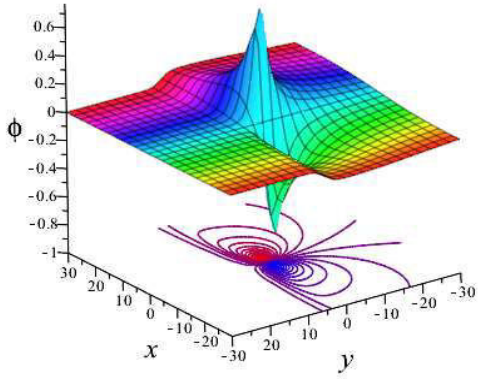

Fig-5.4: Profiles of collision lump solution ϕ of Eq. (5.1) for $\alpha_1 = \beta_1 = \beta_2 = m_2 = l = 1, \lambda = 10$.

4.3. Collision between a lump and a double kink soliton: To make the collision of lump wave and a two-kink soliton, we assume a function constructed by double quadratic form and a cosine hyperbolic function

$$\psi = (\alpha_1 x + \alpha_2 y + \alpha_3 t)^2 + (\beta_1 x + \beta_2 y + \beta_3 t)^2 + l + \lambda \cosh(\delta_1 x + \delta_2 y + \delta_3 t), \quad (5.15)$$

where $\alpha_1, \alpha_2, \alpha_3, \beta_1, \beta_2, \beta_3, \delta_1, \delta_2, \delta_3, l$ and λ are free parameters. Setting Eq. (5.15) in Eq.(5.7), we have a system of algebraic equations in $\alpha_1, \alpha_2, \alpha_3, \beta_1, \beta_2, \beta_3, \delta_1, \delta_2, \delta_3, l$ and λ.

By solving these equations via Maple 18, we obtain $\alpha_1 = \alpha_1, \alpha_2 = -\frac{\beta_1\beta_2}{\alpha_1}, \alpha_3 = \beta_3 = \delta_1 = \delta_3 = 0, \lambda = \lambda\ \beta_1 = \beta_1, \beta_2 = \beta_2, \delta_2 = \delta_2, l = l$, then the Eq. (5.15) can be written as

$$\psi = (\alpha_1 x - \frac{\beta_1\beta_2}{\alpha_1} x)^2 + (\beta_1 x + \beta_2 y)^2 + l + \lambda \cosh(\delta_2 y). \tag{5.16}$$

By combining Eq. (5.16) and Eq. (5.7) and setting $\alpha_1 = \beta_1 = \beta_2 = \delta_2 = l = 1, \lambda = 10$ and inserting, we have the solution of Eq. (5.1) (see **Fig-5.5**). The **Fig-5.5** exhibits the dynamic processes of collision between lump waves with two kink waves. We observe that the lump wave is downed and consumed by the kink waves compare with lump wave (see **Fig-5.1** and **Fig-5.4**) and flow pattern being congested from two sides.

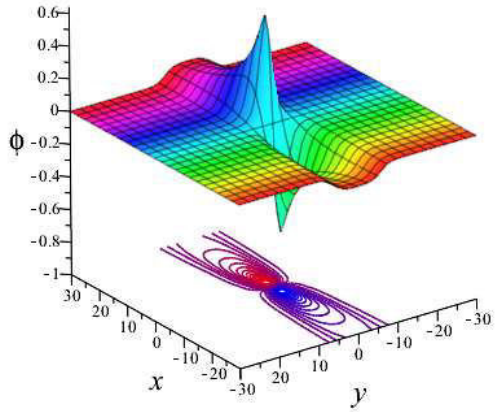

Fig-5.5: Profiles of collision lump solution ϕ of Eq. (5.1) for $\alpha_1 = \beta_1 = \beta_2 = \delta_2 = l = 1, \lambda = 10$.

5.4.4. Collision among lump, periodic and a single kink wave: To achieve the collision among a lump wave, a periodic and a single kink solution of Eq. (5.1), we assume a function constructed by double quadratic form, a cosine and an exponential function

$$\psi = (\alpha_1 x + \alpha_2 y + \alpha_3 t)^2 + (\beta_1 x + \beta_2 y + \beta_3 t)^2 + l$$
$$+ \lambda_1 \cos(\gamma_1 x + \gamma_2 y + \gamma_3 t) + \lambda_2 \exp(m_1 x + m_2 y + m_3), \tag{5.17}$$

where $\alpha_1,\alpha_2,\alpha_3,\beta_1,\beta_2,\beta_3,\gamma_1,\gamma_2,\gamma_3,m_1,m_2,m_3,l,\lambda_1$ and λ_2 are real free constants. Setting Eq. (5.17) in Eq. (5.7), we have a system of algebraic equations in $\alpha_1,\alpha_2,\alpha_3,\beta_1,\beta_2,\beta_3,$ $\gamma_1,\gamma_2,\gamma_3,m_1,m_2,m_3,l,\lambda_1$ and λ_2. By solving these equations via Maple 18, we have $\alpha_1=\alpha_1,$ $\beta_2=\beta_2,\ \alpha_2=-\frac{\beta_1\beta_2}{\alpha_1},\ \alpha_3=\beta_3=\gamma_1=\gamma_3=m_1=m_3=0,\ \lambda_1=\lambda_1,\ \lambda_2=\lambda_2,\ \alpha_2=\alpha_2,\ \beta_2=\beta_2,$ $\gamma_2=\gamma_2,m_2=m_2,l=l$, then the Eq. (5.17) can be written as

$$\psi=(\alpha_1 x-\frac{\beta_1\beta_2}{\alpha_1}y)^2+(\beta_1 x+\beta_2 y)^2+l+\lambda_1\cos(\gamma_2 y)+\lambda_2\exp(m_2 y). \tag{5.18}$$

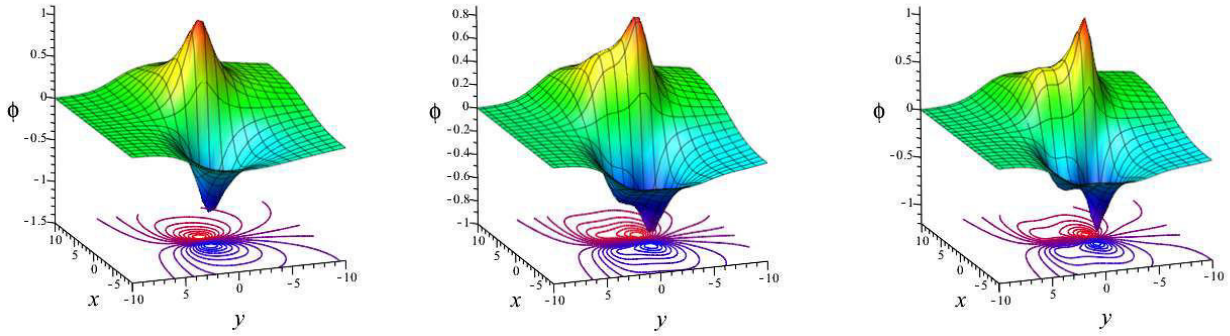

(a) $\lambda_1=1$ (b) $\lambda_1=9$ (c) $\lambda_1=12$

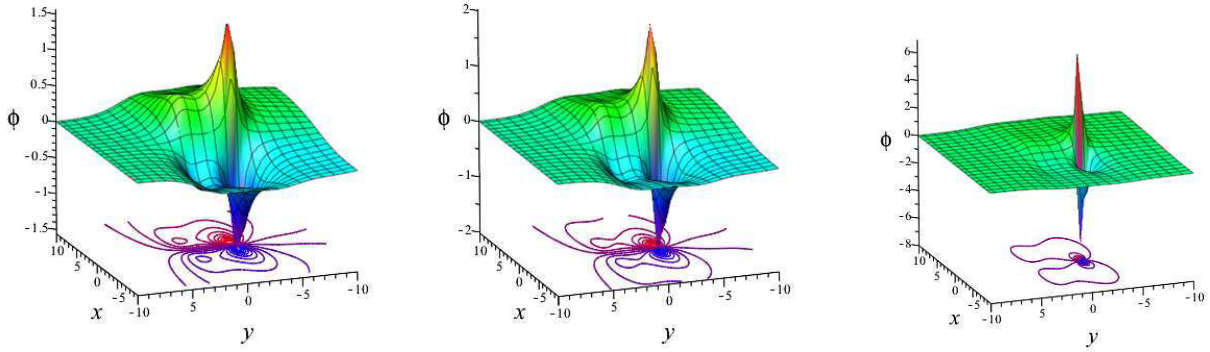

(d) $\lambda_1=15$ (e) $\lambda_1=16$ (f) $\lambda_1=17$

Fig-5.6: Profiles of collision solution ϕ of Eq. (5.1) for $\alpha_1=\beta_1=\beta_2=\gamma_2=m_2=l=1,\lambda_2=2$.

Using Eq. (5.18) and Eq. (5.7) and putting $\alpha_1 = \beta_1 = \beta_2 = \gamma_2 = m_2 = l = 1, \lambda_2 = 2$, we achieve the solution of Eq. (5.1) (see **Fig-5.6**). The **Fig-5.6** exhibits the dynamic processes of collision among lump waves with single kink and periodic wave solution. We observe that the lump wave is downed and consumed by the kink wave compare with lump wave (see **Fig-5.1** and **Fig-5.4**) and flow pattern being congested from one sides. Besides this, effect of periodic function makes the fission phenomena. The solution (see **Fig-5.6)** exhibits as a single lump wave for $\lambda_1 = 1$ **(**see **Fig-5.6(a))** but it is going to split into double lump waves with $\lambda_1 = 15$ **(**see the **Fig-5.6(b, c)** and **Fig-5.6(e, f))**. In fact, it is shown that one lump of them goes to diminish and another one still unchanged for $\lambda_1 = 17$ or more increasing values.

5.4.5. Collision among lump, periodic and a double kink soliton: To construct the collision among a lump wave, a periodic and a two-kink soliton, we assume a function constructed by double quadratic form, a cosine and cosine hyperbolic functions

$$\psi = (\alpha_1 x + \alpha_2 y + \alpha_3 t)^2 + (\beta_1 x + \beta_2 y + \beta_3 t)^2 + l$$
$$+ \lambda_1 \cos(\gamma_1 x + \gamma_2 y + \gamma_3 t) + \lambda_2 \cosh(\delta_1 x + \delta_2 y + \delta_3 t), \tag{5.19}$$

where $\alpha_1, \alpha_2, \alpha_3, \beta_1, \beta_2, \beta_3, \gamma_1, \gamma_2, \gamma_3, \delta_1, \delta_2, \delta_3, l, \lambda_1$ and λ_2 are free parameters. Setting Eq. (5.19) into the Eq. (5.7), we have an algebraic system in $\alpha_1, \alpha_2, \alpha_3, \beta_1, \beta_2, \beta_3, \gamma_1, \gamma_2, \gamma_3, \delta_1, \delta_2, \delta_3, l, \lambda_1$ and λ_2. By solving this system via Maple 18, we have $\alpha_1 = \alpha_1, \alpha_2 = -\frac{\beta_1\beta_2}{\alpha_1}$, $\alpha_3 = \beta_3 = \gamma_1 = \gamma_3 = \delta_1 = \delta_3 = 0, \lambda_1 = \lambda_1, \lambda_2 = \lambda_2, \beta_1 = \beta_1, \beta_2 = \beta_2, \gamma_2 = \gamma_2, \delta_2 = \delta_2, l = l$, then the Eq. (5.19) can be written as

$$\psi = (\alpha_1 x - \frac{\beta_1\beta_2}{\alpha_1} y)^2 + (\beta_1 x + \beta_2 y)^2 + l + \lambda_1 \cos(\gamma_2 y) + \lambda_2 \cosh(\delta_2 y). \tag{5.20}$$

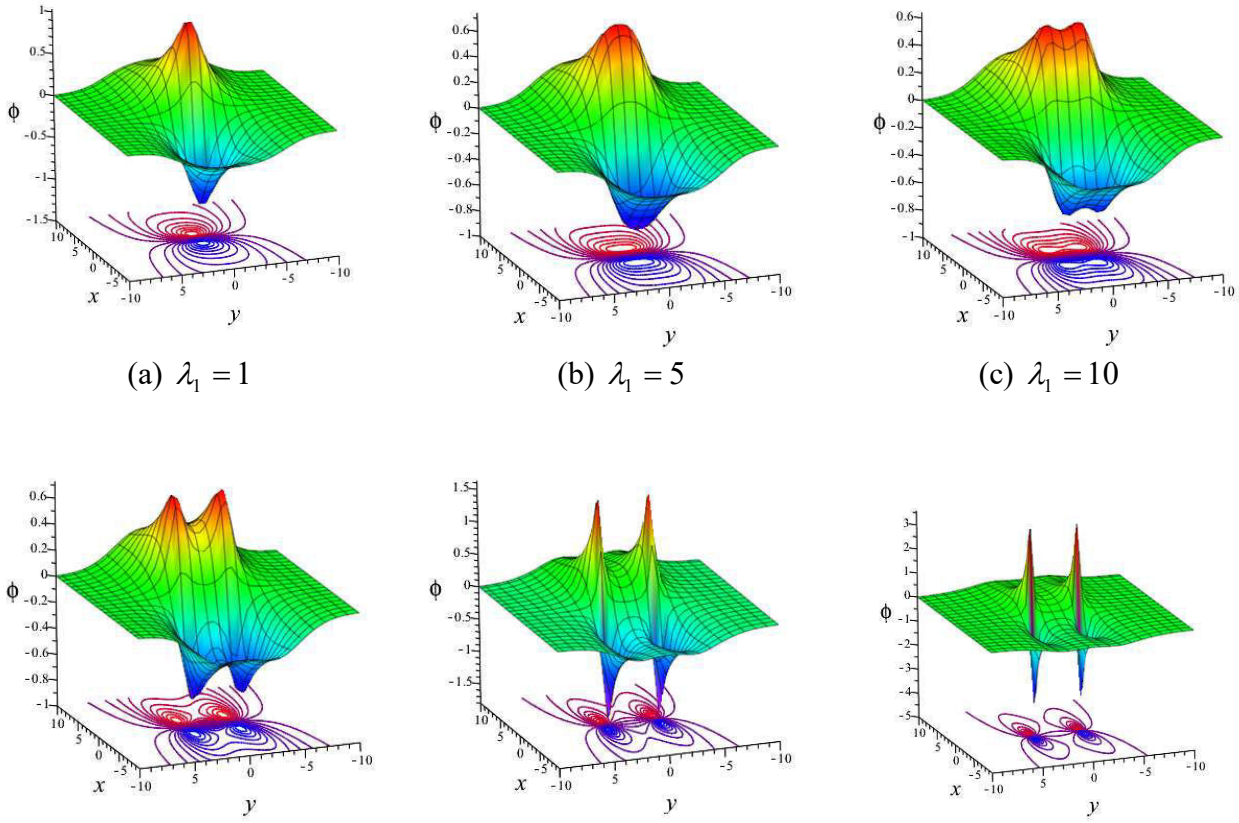

(a) $\lambda_1 = 1$ (b) $\lambda_1 = 5$ (c) $\lambda_1 = 10$

(d) $\lambda_1 = 20$ (e) $\lambda_1 = 30$ (f) $\lambda_1 = 32$

Fig-5.7: Profiles of collision solution ϕ of Eq. (5.1) for $\alpha_1 = \beta_1 = \beta_2 = \gamma_2 = \delta_2 = l = 1, \lambda_2 = 2$.

By using Eq. (5.20) and Eq. (5.7) and putting $\alpha_1 = \beta_1 = \beta_2 = \gamma_2 = \delta_2 = l = 1, \lambda_2 = 2$, then we acquire the solution of Eq. (5.1) (see **Fig-5.7**). The **Fig-5.7** exhibits the dynamic processes of collision among lump waves with double kink and a periodic wave solution. We observe that the lump wave is downed and consumed by the kink compare with lump wave (see **Fig-5.1** and **Fig-5.4**) and flow pattern being congested from two sides. Besides this, effect of periodic function makes the fission phenomena. The solution **Fig-5.7** exhibits as a single lump for $\lambda_1 = 1$ **(**see **Fig-5.7(a)),** but it is going to split into double lump with the increase of λ_1 (see the **Fig-5.7(b-f)**) gradually.

5.5. The bilinear structure of the BBMB model

Consider the (2+1) -dimensional BBMB model is as follows [80]

$$\phi_t + \phi_{xxx} - 3(\phi\eta)_x = 0, \phi_x = \eta_y, \tag{5.21}$$

where ϕ and η are the function of spatial variables x, y and time variable t.

We can rewrite the Eq. (5.21) as

$$\phi_t + \phi_{xxx} - 3(\phi_x\eta + \phi\eta_x) = 0,\ \phi_x = \eta_y. \tag{5.22}$$

Consider the conversion relation

$$\phi = -2(\ln\tau)_{xy} \text{ and } \eta = -2(\ln\tau)_{xx} \tag{5.23}$$

with real function $\tau(x, y, t)$ to be determined.

Through the relation Eq. (5.23), the Eq. (5.22) can be converted to

$$-2(\ln\tau)_{xyt} - 2(\ln\tau)_{xxxxy} - 12(\ln\tau)_{xxy}.(\ln\tau)_{xx} - 12(\ln\tau)_{xy}(\ln\tau)_{xxx} = 0,$$

$$-2(\ln\tau)_{xxy} = -2(\ln\tau)_{xxy}. \tag{5.24}$$

Integrating first equation of Eq. (5.24) with respect to x, yields

$$(\ln\tau)_{yt} + (\ln\tau)_{xxxy} - 12(\ln\tau)_{xy}.(\ln\tau)_{xx} = 0. \tag{5.25}$$

Now considering the linear terms, we have

$$(\ln\tau)_{yt} + (\ln\tau)_{xxxy} = 0. \tag{5.26}$$

Eq. (5.26) can be converted to the bilinear operator D as follows

$$(D_y D_t + D_x^3 D_y) f.f = 0, \tag{5.27}$$

while the D-operator [71] is defined by

$$(D_x^m D_y^k D_t^n) f.g = \left(\frac{\partial}{\partial x_1} - \frac{\partial}{\partial x_2}\right)^m \left(\frac{\partial}{\partial y_1} - \frac{\partial}{\partial y_2}\right)^k \left(\frac{\partial}{\partial t_1} - \frac{\partial}{\partial t_2}\right)^n [f(x_1, y_1, t_1).g(x_2, y_2, t_2)].$$

Thus Eq. (5.26) reduces to

$$\tau\tau_{ty} - \tau_t\tau_y + 3\tau_{xx}\tau_{xy} - 3\tau_x\tau_{xxy} + \tau\tau_{xxxy} - \tau_{xxx}\tau_y = 0\,. \tag{5.28}$$

It is clear that if τ satisfies Eq. (5.22), then $\phi = -2(\ln\tau)_{xy}$ and $\eta = -2(\ln\tau)_{xx}$ directly generates the solutions of the governing Eq. (5.21).

5.6. Lump wave solution of BBMB model

We now assume the following quadratic function

$$\tau = (\alpha_1 x + \alpha_2 y + \alpha_3 t)^2 + (\beta_1 x + \beta_2 y + \beta_3 t)^2 + l\,, \tag{5.29}$$

where $\alpha_1, \alpha_2, \alpha_3, \beta_1, \beta_2, \beta_3$ and l are free parameters. Setting Eq. (5.29) in the Eq. (5.28), we have a set of algebraic equations in $\alpha_1, \alpha_2, \alpha_3, \beta_1, \beta_2, \beta_3$ and l. By solving these equations via Maple 18, we have $\alpha_2 = \alpha_3 = \beta_1 = \beta_3 = 0, \alpha_1 = \alpha_1, \beta_2 = \beta_2, l = l$, then the Eq. (5.29) can be written as

$$\tau = (\alpha_1 x)^2 + (\beta_2 y)^2 + l\,. \tag{5.30}$$

Choosing $\alpha_1 = \beta_2 = l = 1$ and setting Eq. (5.30) in the Eq. (5.28), we obtain the figure **Fig-8** for the solution of Eq. (5.21). Due to guarantee ϕ, η are localized in every direction, l have to be considered as a positive constant. In this case, the optimum amplitude of the solution ϕ is occurred at the points $(0,0)$, $(\pm\frac{\sqrt{l/2}}{\alpha_1}, \pm\frac{\sqrt{l/2}}{\beta_2})$ with the amplitudes 0, $\frac{\alpha_1\beta_2}{l}$, $\frac{\alpha_1\beta_2}{l}$, $-\frac{\alpha_1\beta_2}{l}$, $-\frac{\alpha_1\beta_2}{l}$. For the potential function η, the optimum amplitudes are occurred at the points $(0,0)$, $(\pm\frac{\sqrt{3l}}{\alpha_1}, 0)$ with the amplitudes $-\frac{4\alpha_1^2}{l}$, $\frac{\alpha_1^2}{2l}$ and $\frac{\alpha_1^2}{2l}$.

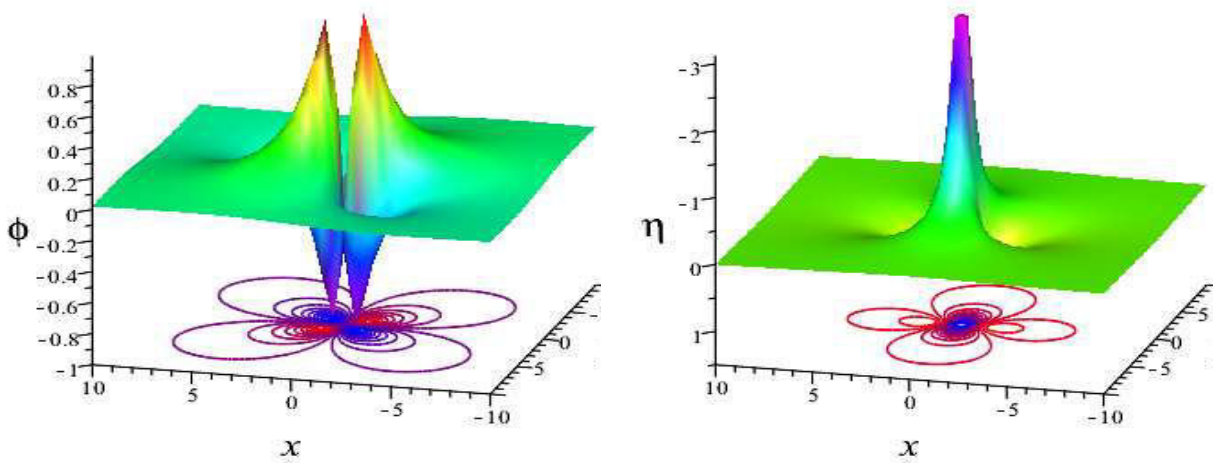

(a) (b)

Fig-5.8: Profiles of the lump solution ϕ and η of Eq. (5.21) for $\alpha_1 = \beta_2 = l = 1$.

5.7. Collision among lumps, periodic waves, and soliton solutions

5.7.1. Collision of lump and periodic waves: Due to produce collision of lump and periodic waves, we assume a function constructed by double quadratic form and a sinusoidal function

$$\tau = (\alpha_1 x + \alpha_2 y + \alpha_3 t)^2 + (\beta_1 x + \beta_2 y + \beta_3 t)^2 + l + \lambda \cos(\gamma_1 x + \gamma_2 y + \gamma_3 t), \tag{5.31}$$

where $\alpha_1, \alpha_2, \alpha_3, \beta_1, \beta_2, \beta_3, \gamma_1, \gamma_2, \gamma_3, l$ and λ are free parameters. Setting Eq. (5.31) into the Eq. (5.28), we have a system of algebraic equations in $\alpha_1, \alpha_2, \alpha_3, \beta_1, \beta_2, \beta_3, \gamma_1, \gamma_2, \gamma_3, l$ and λ. By solving these equations via Maple 18, we get the following results:

Case 1: $\alpha_2 = \alpha_3 = \beta_2 = \beta_3 = \gamma_1 = \gamma_3 = 0, \lambda = \lambda, \alpha_1 = \alpha_1, \beta_1 = \beta_1, \gamma_1 = \gamma_1, l = l$.

Case 2: $\alpha_1 = -\dfrac{\beta_1 \beta_2}{\alpha_2}, \alpha_3 = \beta_3 = \gamma_1 = \gamma_3 = 0, \lambda = \lambda, \alpha_2 = \alpha_2, \beta_1 = \beta_1, \beta_2 = \beta_2,$

$\gamma_2 = \gamma_2, l = l$.

For **case 1**, the Eq. (5.31) can be written as

$$\tau = (\alpha_1 x)^2 + (\beta_1 x)^2 + l + \lambda \cos(\gamma_2 y). \tag{5.32}$$

For **case 2**, the Eq. (5.31) can be written as

$$\tau = (-\frac{\beta_1 \beta_2}{\alpha_2} x + \alpha_2 y)^2 + (\beta_1 x + \beta_2 y)^2 + l + \lambda \cos(\gamma_2 y). \tag{5.33}$$

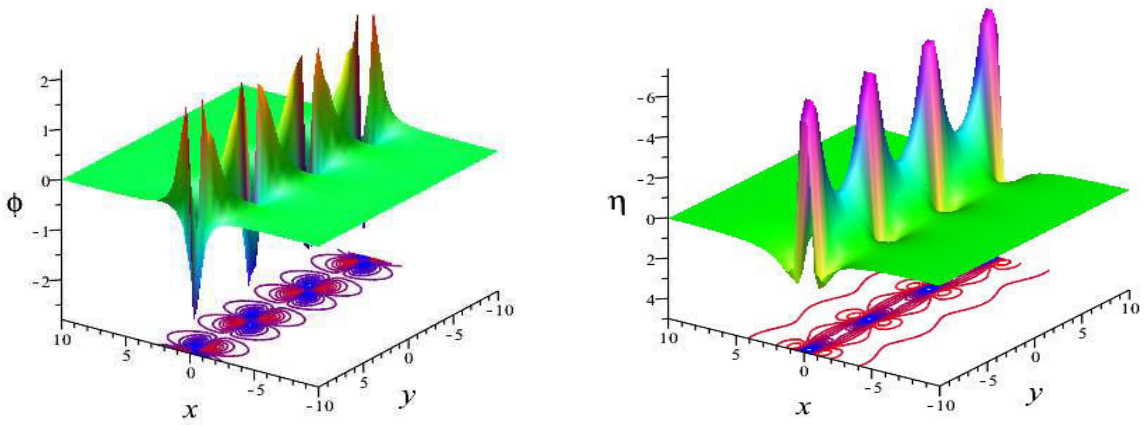

(a) (b)

Fig-5.9: Profiles of the periodic lump wave solution ϕ and η of Eq. (5.21) for $\alpha_1 = \beta_1 = \gamma_1 = l = 1$.

Choosing $\alpha_1 = \beta_1 = \gamma_1 = l = 1$ and setting Eq. (5.32) in Eq. (5,28), we have the figures **Fig-5.9** for the solution of Eq. (5.21). By choosing $\alpha_2 = \beta_1 = \beta_2 = \gamma_2 = l = 1$ and setting Eq. (5.33) in Eq. (5.28), we have the figures **Fig-5.10** for the solution of Eq. (5.21). The energy distribution is symmetric over all the periodic lump waves while it travels (see **Fig-5.9**). Beside this, the solution in **case-2** exhibits as a single lump wave for $\lambda = 1$ (see **Fig-5.10(a, d)**) but it is going to split into double lump waves due to fission of lump wave for the increase of λ (see the **Fig-5.10(b, c)** and **(e, f)**) gradually.

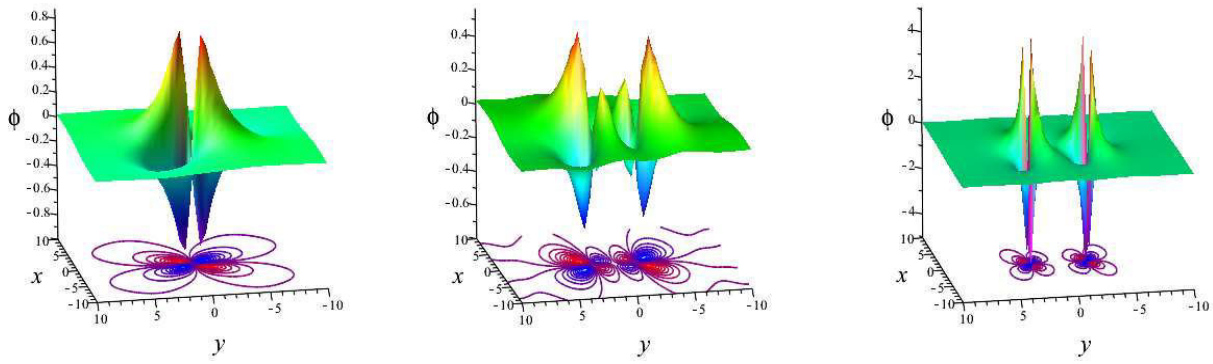

(a) $\lambda = 1$ (b) $\lambda = 8$ (c) $\lambda = 16$

(d) $\lambda = 1$ (e) $\lambda = 8$ (f) $\lambda = 16$

Fig-5.10: (a-c) Profiles of collision solution ϕ and (d-e), profiles of collision solution η of Eq. (5.21) for $\alpha_2 = \beta_1 = \beta_2 = \gamma_2 = l = 1$.

5.7.2. Collision of lump wave and a strip solution: Due to produce collision of lump wave and a stripe soliton, we assume a function constructed by double quadratic form and an exponential function

$$\tau = (\alpha_1 x + \alpha_2 y + \alpha_3 t)^2 + (\beta_1 x + \beta_2 y + \beta_3 t)^2 + l + \lambda \exp(m_1 x + m_2 y + m_3 t), \qquad (5.34)$$

where $\alpha_1, \alpha_2, \alpha_3, \beta_1, \beta_2, \beta_3, m_1, m_2, m_3, l$ and λ are real free constants. Setting Eq. (5.34) into the Eq. (5.28), we have a system of algebraic equations in $\alpha_1, \alpha_2, \alpha_3, \beta_1, \beta_2, \beta_3, m_1, m_2, m_3, l$

and λ. By solving these equations via Maple 18, we get $\alpha_1 = -\frac{\beta_1\beta_2}{\alpha_2}, \alpha_3 = \beta_3 = m_1 = m_3 = 0,$

$\lambda = \lambda, \alpha_2 = \alpha_2, \beta_1 = \beta_1, \beta_2 = \beta_2, m_2 = m_2, l = l$, then the Eq. (5.34) can be written as

$$\tau = (-\frac{\beta_1\beta_2}{\alpha_2}x + \alpha_2 y)^2 + (\beta_1 x + \beta_2 y)^2 + l + \lambda \exp(m_2 y). \tag{5.35}$$

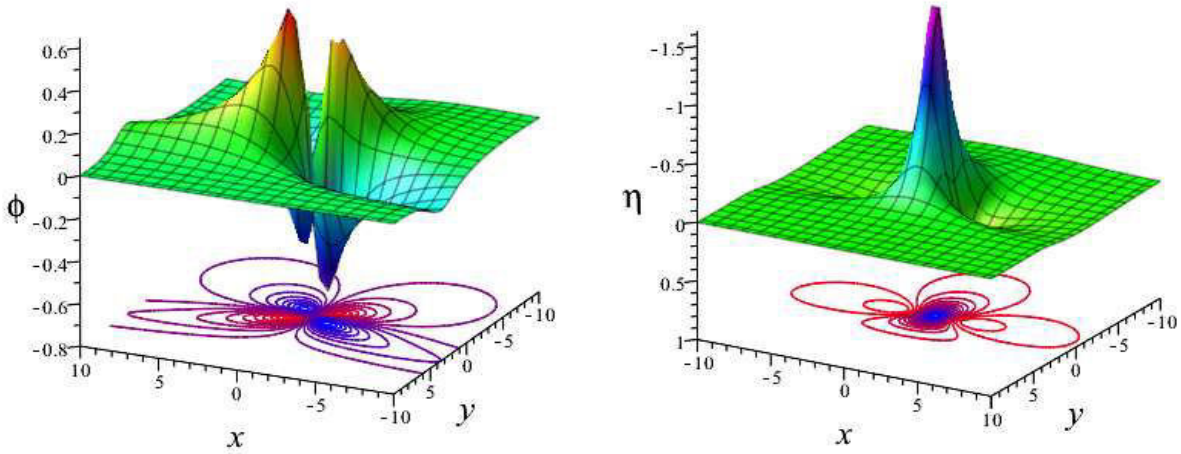

(a) (b)

Fig-5.11: Profiles of collision lump solution ϕ and η of Eq. (5.21) for $\alpha_2 = \beta_1 = \beta_2 = \gamma_2 = m_2 = l = 1, \lambda = 5.$

Choosing $\alpha_2 = \beta_1 = \beta_2 = m_2 = l = 1, \lambda = 5$ and inserting Eq. (5.35) in Eq. (5.28), we have the figures **Fig-5.11** for the solution of Eq. (5.21). The **Fig-5.11** exhibits the dynamic processes of interaction between lump waves with a stripe solution. We observe that the lump wave is downed and consumed by the stripe compare with single lump wave **Fig-5.8** and flow pattern being congested from one side.

5.7.3. Collision of lump wave and a double stripes solution: Due to produce collision of lump wave and a double stripes soliton, we assume a function constructed by double quadratic form and a cosine hyperbolic function

$$\tau = (\alpha_1 x + \alpha_2 y + \alpha_3 t)^2 + (\beta_1 x + \beta_2 y + \beta_3 t)^2 + l + \lambda \cosh(\delta_1 x + \delta_2 y + \delta_3 t), \quad (5.36)$$

where $\alpha_1, \alpha_2, \alpha_3, \beta_1, \beta_2, \beta_3, \delta_1, \delta_2, \delta_3, l$ and λ are free parameters. Setting Eq. (5.36) in the Eq. (5.28), we have a system of algebraic equations in $\alpha_1, \alpha_2, \alpha_3, \beta_1, \beta_2, \beta_3, \delta_1, \delta_2, \delta_3, l$ and λ. By solving these equations via Maple 18, we obtain $\alpha_1 = -\frac{\beta_1\beta_2}{\alpha_2}, \alpha_3 = \beta_3 = \delta_1 = \delta_3 = 0$, $\lambda = \lambda$, $\alpha_2 = \alpha_2, \beta_1 = \beta_1, \beta_2 = \beta_2, \delta_2 = \delta_2, l = l$, then the Eq. (5.36) can be written as

$$\tau = (-\frac{\beta_1\beta_2}{\alpha_2} x + \alpha_2 y)^2 + (\beta_1 x + \beta_2 y)^2 + l + \lambda \cosh(\delta_2 y). \quad (5.37)$$

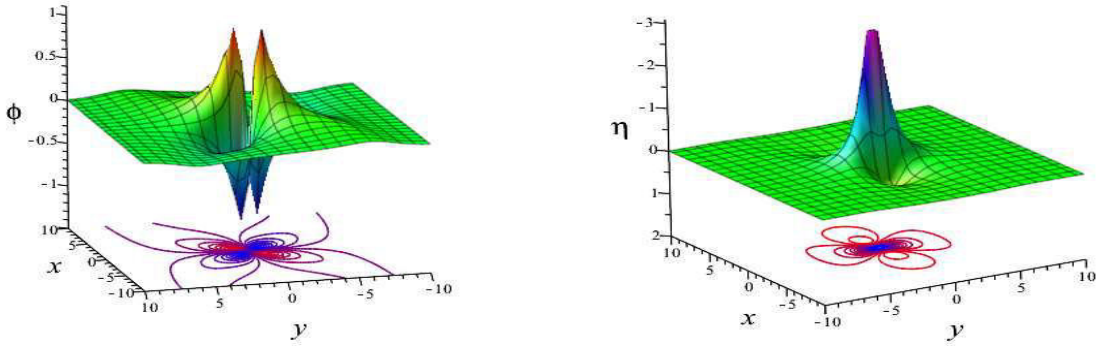

(a) (b)

Fig-5.12: Profiles of collision lump solution ϕ and η of Eq. (5.21) for $\alpha_2 = \beta_1 = \beta_2 = \delta_2 = l = 1$.

Choosing $\alpha_2 = \beta_1 = \beta_2 = \delta_2 = l = 1$ and setting Eq. (5.37) in Eq. (5.28), we have the figures **Fig-5.12** for the solution of Eq. (5.21). The **Fig-5.12** exhibits the dynamic processes of collision between lump waves with two stripes solution. We observe that the lump wave is downed and swallowed by the stripes compare with lump wave (see **Fig-5.8** and **Fig-5.11**) and flow pattern being congested from two sides.

5.7.4. Collision among lump, periodic and a stripe solution: Due to produce interaction among a lump wave, a periodic and a stripe soliton, we assume a function constructed by double quadratic form, a cosine and a exponential functions

$$\tau = (\alpha_1 x + \alpha_2 y + \alpha_3 t)^2 + (\beta_1 x + \beta_2 y + \beta_3 t)^2 + l$$

$$+ \lambda_1 \cos(\gamma_1 x + \gamma_2 y + \gamma_3 t) + \lambda_2 \exp(m_1 x + m_2 y + m_3), \quad (5.38)$$

where $\alpha_1, \alpha_2, \alpha_3, \beta_1, \beta_2, \beta_3, \gamma_1, \gamma_2, \gamma_3, m_1, m_2, m_3, l, \lambda_1$ and λ_2 are real free constants. Setting Eq. (5.38) in the Eq. (5.28), we have a system of algebraic equations in $\alpha_1, \alpha_2, \alpha_3, \beta_1, \beta_2, \beta_3, \gamma_1, \gamma_2, \gamma_3, m_1, m_2, m_3, l, \lambda_1$ and λ_2. By solving these equations via Maple 18, we have $\alpha_1 = -\frac{\beta_1\beta_2}{\alpha_2}, \alpha_3 = \beta_3 = \gamma_1 = \gamma_3 = m_1 = m_3 = 0, \lambda_1 = \lambda_1, \lambda_2 = \lambda_2, \alpha_2 = \alpha_2, \beta_1 = \beta_1, \beta_2 = \beta_2, \gamma_2 = \gamma_2, m_2 = m_2, l = l$, then the Eq. (3.18) can be written as

$$\tau = (-\frac{\beta_1\beta_2}{\alpha_2} x + \alpha_2 y)^2 + (\beta_1 x + \beta_2 y)^2 + l + \lambda_1 \cos(\gamma_2 y) + \lambda_2 \exp(m_2 y). \quad (3.39)$$

Choosing $\alpha_2 = \beta_1 = \beta_2 = \gamma_2 = m_2 = l = 1, \lambda_2 = 3$ and inserting Eq. (5.39) in Eq. (5.28), we have the figures **Fig-5.13** for the solution of Eq. (5.21). The **Fig-5.13** exhibits the dynamic processes of collision among rogue waves with one stripe and periodic wave solution. We observe that the lump wave is downed and consumed by the stripe compare with lump wave (see **Fig-5.8** and **Fig-5.11**) and flow pattern being congested from one sides. Besides this, effect of periodic function makes the fission phenomena. The solution **Fig-5.13** exhibits as a single lump-stripe wave for $\lambda_1 = 1$ **(**see **Fig-5.13(a, d))** but it is going to split into double lump-stripe waves with $\lambda_1 = 11$ **(**see the **Fig-5.13(b, c)** and **Fig-5.13(e, f))**. In fact, it is shown that one lump of them goes to diminish and another one still unchanged for $\lambda_1 = 16$ or more increasing values.

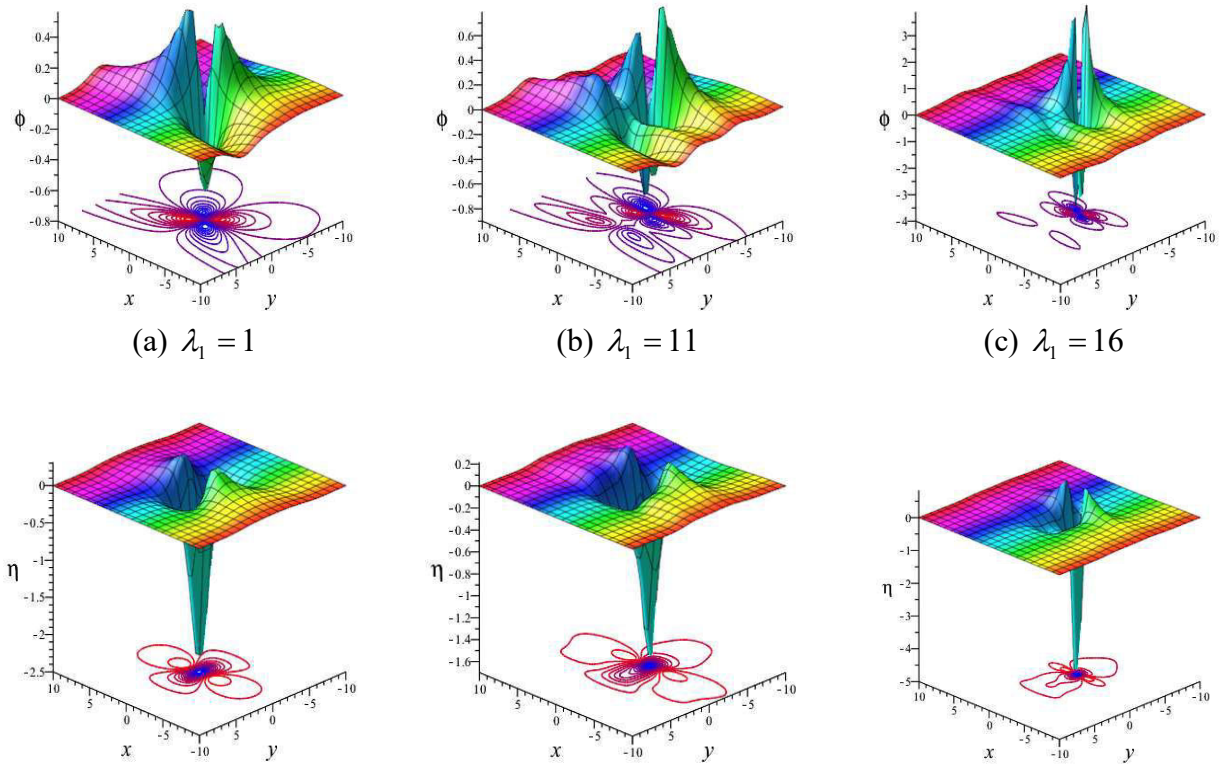

(a) $\lambda_1 = 1$ (b) $\lambda_1 = 11$ (c) $\lambda_1 = 16$

(d) $\lambda_1 = 1$ (e) $\lambda_1 = 11$ (f) $\lambda_1 = 16$

Fig-5.13: (a-c) Profiles of collision solution ϕ and (d-e) Profiles of collision solution η of Eq. (5.21) for $\alpha_2 = \beta_1 = \beta_2 = \gamma_2 = m_2 = l = 1, \lambda_2 = 3$.

5.7.5. Collision among lump, periodic and a double stripes solution: Due to produce collision among a lump wave, a periodic and a double stripes soliton, we assume a function constructed by double quadratic form, a cosine and cosine hyperbolic functions

$$\tau = (\alpha_1 x + \alpha_2 y + \alpha_3 t)^2 + (\beta_1 x + \beta_2 y + \beta_3 t)^2 + l$$

$$+ \lambda_1 \cos(\gamma_1 x + \gamma_2 y + \gamma_3 t) + \lambda_2 \cosh(\delta_1 x + \delta_2 y + \delta_3 t), \qquad (5.40)$$

where $\alpha_1, \alpha_2, \alpha_3, \beta_1, \beta_2, \beta_3, \gamma_1, \gamma_2, \gamma_3, \delta_1, \delta_2, \delta_3, l, \lambda_1$ and λ_2 are free parameters. Setting Eq. (5.40) into the Eq. (5.28), we have a system of algebraic equations in $\alpha_1, \alpha_2, \alpha_3, \beta_1, \beta_2, \beta_3, \gamma_1, \gamma_2, \gamma_3, \delta_1, \delta_2, \delta_3, l, \lambda_1$ and λ_2. By solving these equations via Maple

18, we have $\alpha_1 = -\frac{\beta_1\beta_2}{\alpha_2}, \alpha_3 = \beta_3 = \gamma_1 = \gamma_3 = \delta_1 = \delta_3 = 0, \lambda_1 = \lambda_1, \lambda_2 = \lambda_2, \alpha_2 = \alpha_2, \beta_1 = \beta_1,$

$\beta_2 = \beta_2$, $\gamma_2 = \gamma_2, \delta_2 = \delta_2, l = l$, then the Eq. (5.40) can be written as

$$\tau = (-\frac{\beta_1\beta_2}{\alpha_2}x + \alpha_2 y)^2 + (\beta_1 x + \beta_2 y)^2 + l + \lambda_1 \cos(\gamma_2 y) + \lambda_2 \cosh(\delta_2 y). \quad (5.41)$$

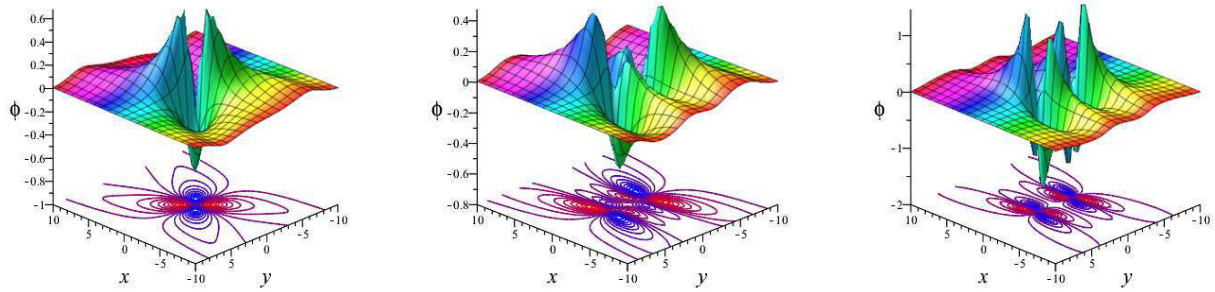

(a) $\lambda_1 = 1$ (b) $\lambda_1 = 10$ (c) $\lambda_1 = 20$

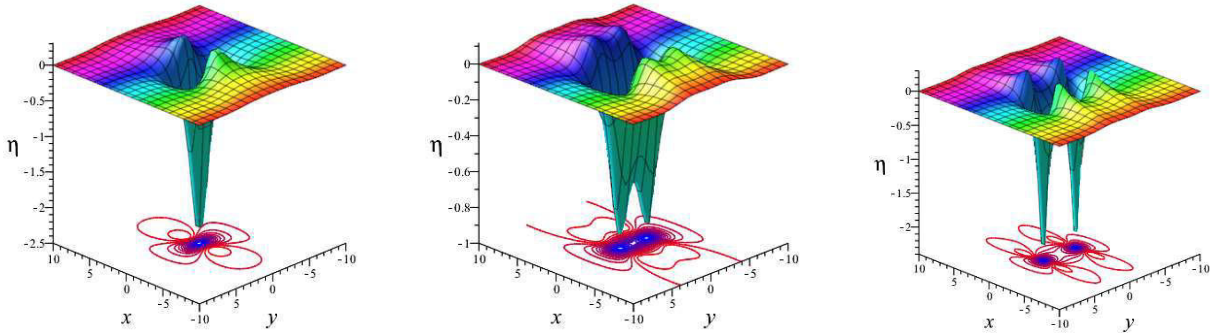

(d) $\lambda_1 = 1$ (e) $\lambda_1 = 10$ (f) $\lambda_1 = 20$

Fig-5.14: (a-c) Profiles of collision solution ϕ and (d-e) Profiles of collision solution η of Eq. (5.21) for $\alpha_2 = \beta_1 = \beta_2 = \gamma_2 = \delta_2 = l = \lambda_2 = 1$.

Choosing $\alpha_2 = \beta_1 = \beta_2 = \gamma_2 = \delta_2 = l = \lambda_2 = 1$ and setting Eq. (5.41) in Eq. (5.28), we have the figures **Fig-5.14** for the solution of Eq. (5.21). The **Fig-5.14** exhibits the dynamic processes of collision among lump waves with double stripes and a periodic wave solution. We observe that the lump wave is downed and consumed by the stripe compare with lump wave (see **Fig-5.8** and **Fig-5.11**) and flow pattern being congested from two sides. Besides

this, effect of periodic function makes the fission phenomena. The solution **Fig-5.14** exhibits as a single lump-stripe wave for $\lambda_1 = 1$ **(**see **Fig-5.14(a, d))** but it is going to split into double lump-stripe waves with the increase of λ_1 (see the **Fig-5.14(b, c)** and **Fig-5.14(e, f)**) gradually.

5.8. Conclusion

The main result in this chapter is the procedure of obtaining the lump wave solutions and a class of interactions among lump, periodic and the soliton solutions of the BBS and BBMB models by using different ansatz functions. In particular, for the double quadratic polynomials in the structure of the solution provide a lump wave solution that profiles are depicted in **Fig-5.1** and **Fig-5.8**. We explicitly present interactions between lump and periodic waves, lump and single-, double-kink soliton solutions of the model. We also show how to interact lump with periodic waves, and single-, double- kink solitons, and to produce dynamical various structures such as periodic kinky-lump waves, periodic lump waves, lump-single, -double kink solitions, periodic-single, -double kink solitons. All interaction solitons are depicted in figures **Fig-5.2** to **Fig-5.7** and **Fig-5.9** to **Fig-5.14**. It is observed that the results are much interesting as they present the causes of fission properties of the lump waves, which are presented in the figures **Fig-5.3, Fig-5.6, Fig-7, Fig-5.10, Fig-5.13** and **Fig-5.14**. It is included that the new dynamics may be enriched nonlinear behavior of the model and even can be found to others nonlinear models.

Chapter Six

Interaction solutions of the (3+1)-D STOL equation

Acknowledgement

In this chapter [3], we consider a (3+1)-dimensional Sharma–Tasso–Olver-like (STOL) model describing dynamical propagation of nonlinear dispersive waves in inhomogeneous media. Applying Hirota's bilinear technique and a trial function, we explore nonlinear dynamical properties of basic solutions to the STOL model. We find that the fission fusion pattern occurs in the collision between the lump and kink waves, the collision between the lump and periodic waves, and the collision among the lump, kink and periodic waves, which is a novel fascinating collision pattern. We also observe that a large value of the coefficient in the periodic function produces a hybrid lump wave by fission in the collision solution. To better understand the dynamic properties of the obtained collision solutions, we plot a number of 3D and contour diagrams by choosing suitable parametric values with the aid of the computational software Maple 18.

6.1. Introduction

Nonlinear evolution equations (NLEEs) applicable not only the areas of mathematical physics, but also other branches of nonlinear science for instance optics, plasma physics, atmospheric, geochemistry and oceanic sciences etc. [1-21]. Complication of NLEES and challenges in their analytical study has engrossed lots of effort from renowned scientists who are involved with nonlinear dynamics. As a result, exploration of exact solutions of NLEEs is a vital anxiety for dynamical researchers. There are diverse categories of exact solutions mainly soliton, multi-soliton, rational, periodic, breather line, breather kinky, lump and rogue

wave solutions through the generalized Kudryashov method [39], the Hirota bilinear method [40], the tan-cot method [42], the tanh-coth method [43], the direct algebraic method [44], the Darboux transformation method [45] etc. In mathematical physics, the interaction of lump wave with other soliton/periodic wave is a kind of remarkable task in nonlinear sciences which are localized both in position and time. Recently, combination of positive quadratic polynomial functions with the exponential/trigonometric functions i.e. collision of kink, lump, rogue and periodic waves produce kinky-lump, kinky-rogue, periodic-lump wave, periodic-rogue waves and kinky-periodic rogue wave for the NLEEs and their nonlinear dynamics concerned a lot of interest [71-78].

Motivated by the above works, we would like to derive novel higher order collision solutions of the (3+1)-dimensional classical STOL equation [81]

$$u_t + a[(3uu_x + u^3)_x + u_{xxx}] + b[(2uu_y + u_x\partial_x^{-1}u_y + u^2\partial_x^{-1}u_y)_x + u_{xxy}]$$
$$+ c[(2uu_z + u_x\partial_x^{-1}u_z + u^2\partial_x^{-1}u_z) + u_{xxz}] = 0 \qquad (6.1)$$

with real function $u(x, y, z, t)$ and real constants a, b, c. Here ∂_x^{-1} indicate integral operator and inverse of ∂_x.

In this chapter, our main goal is to construct more novel exact collision among lump, periodic and kinky wave solutions that degenerate into periodic line breather waves, kinky periodic waves, double kinky periodic waves, periodic lump waves, double kinky lump waves, kinky periodic lump waves, hybrid lump waves and fission fusion properties of the Eq. (6.1).

6.2. Interaction solutions and dynamics of the solutions for STOL equation

Through the relation $u = (\ln f)_x$, the Eq. (6.1) can be expressed as the form

$$aff_{xxxx} + bff_{xxxy} + cff_{xxxz} - af_xf_{xxx} - bf_xf_{xxy} - cf_xf_{xxz} + ff_{xt} - f_xf_t = 0 \qquad (6.2)$$

with real function $f(x,y,z,t)$ to be determine. When f satisfies Eq. (6.2), $u=(\ln f)_x$ directly generates a solution of the main Eq. (6.1).

In order to evaluate f explicitly, we assume an ansatz of the following form

$$\begin{aligned} f &= (m_1x+m_2y+m_3z+m_4t+m_5)^2+(m_6x+m_7y+m_8z+m_9t+m_{10})^2 \\ &\quad + m_{11}+l_1\cos(m_{12}x+m_{13}y+m_{14}z+m_{15}t+m_{16}) \\ &\quad + l_2\cosh(m_{17}x+m_{18}y+m_{19}z+m_{20}t+m_{21}), \end{aligned} \tag{6.3}$$

where $m_1,m_2,m_3,.....m_{16}$, l_1 and l_2 are real free constants, $m_{17},.....m_{21}$ are real/completely imaginary constants. Inserting Eq. (6.3) to Eq. (6.2), collect every coefficients of x, y, z, t, cos, sin, cosh, sinh together and setting each of these expression equal zero, we gain a system of equations in $m_1,m_2,m_3,.....m_{21}$, l_1 and l_2. Solving this system of algebraic equations by using Maple 18, we obtain the following four results,

Case 1:

$$l_1=0,l_2=0,m_4=0,m_9=0,\ m_i=m_i(i=1,2,3,5,6,7,8,10,11,\cdots,21). \tag{6.4}$$

Inserting Eq. (6.4) into the Eq. (6.3), we obtain

$$f=(m_1x+m_2y+m_3z+m_5)^2+(m_6x+m_7y+m_8z+m_{10})^2+m_{11}. \tag{6.5}$$

Using the relation $u=(\ln f)_x$, Eq. (6.5) offer the result

$$\begin{aligned} u_1 &= [2(m_1x+m_2y+m_3z+m_5)m_1+2(m_6x+m_7y+m_8z+m_{10})m_6]/ \\ &\quad [(m_1x+m_2y+m_3z+m_5)^2+(m_6x+m_7y+m_8z+m_{10})^2+m_{11}]. \end{aligned} \tag{6.6}$$

The result Eq. (6.6) contains nine free arbitrary constants and exhibits lump wave with the condition $m_{11}>0$ in the xy plane. The line soliton solution that is definitely dissimilar starting a moving line soliton, arise very quickly and disappear in the constant background

within tiny time but in the intermediate time it gives highest peak. It is well known that $u \to 0$ as the two quadratic functions tend to positive or negative infinity. It maximum minimum amplitude occurs at the points $(\frac{m_2 m_{10} - m_5 m_7}{m_1 m_7 - m_2 m_6} \pm \sqrt{\frac{m_{11}}{m_1^{\,2} + m_6^{\,2}}}, \frac{m_5 m_6 - m_1 m_{10}}{m_1 m_7 - m_2 m_6})$ when $z = 0$. The **Fig-6.1** represent stretch of the lump wave solution Eq. (6.6), consists of one deep hole and one high crest for the particular values $m_1 = 2, m_2 = 3, m_3 = 2, m_5 = 1, m_6 = 5,$ $m_7 = 1, m_8 = 5,\ m_{10} = 1, m_{11} = 10$, in the xy plane with $t = 0, z = 0$. The peak of the lump wave locates at $(-\frac{2}{13} + \frac{\sqrt{290}}{29}, -\frac{3}{13})$, the valley locates at $(-\frac{2}{13} - \frac{\sqrt{290}}{29}, -\frac{3}{13})$ and maximum amplitude is $\frac{\sqrt{290}}{10}$ and deep is equal distance i.e. $-\frac{\sqrt{290}}{10}$.

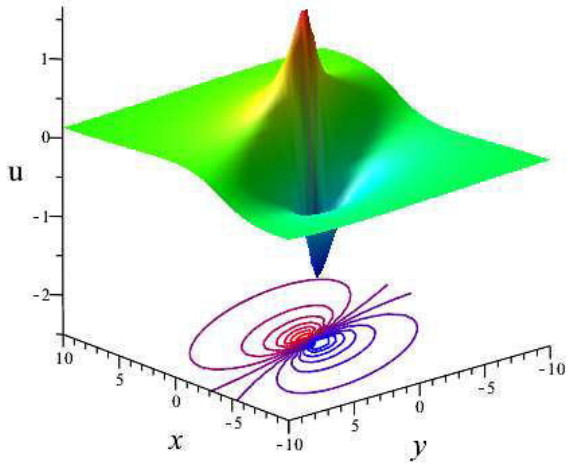

Fig-6.1: Outlook of lump wave solution u_1 of the Eq. (6.6).

Case 2:

$$l_1 = 0, m_4 = 0, m_9 = 0, m_{20} = -m_{17}^{\,2}(am_{17} + bm_{18} + cm_{19})$$

$$l_2 = l_2, m_i = m_i\ (i = 1,2,3,5,6,7,8,10,11,17,18,19,21), \qquad (6.7)$$

where a, b and c can take arbitrary values.

Inserting Eq. (6.7) into the Eq. (6.3), we emerge to

$$f = (m_1x + m_2y + m_3z + m_5)^2 + (m_6x + m_7y + m_8z + m_{10})^2 + m_{11}$$

$$+ l_2 \cosh\{m_{17}x + m_{18}y + m_{19}z - m_{17}^2(am_{17} + bm_{18} + cm_{19})t + m_{21}\}. \quad (6.8)$$

Using the relation $u = (\ln f)_x$, Eq. (6.8) provides the result

$$u_2 = [2(m_1x + m_2y + m_3z + m_5)m_1 + 2(m_6x + m_7y + m_8z + m_{10})m_6$$

$$+ l_2m_{17} \sinh\{m_{17}x + m_{18}y + m_{19}z - m_{17}^2(am_{17} + bm_{18} + cm_{19})t + m_{21}\}]/$$

$$[(m_1x + m_2y + m_3z + m_5)^2 + (m_6x + m_7y + m_8z + m_{10})^2 + m_{11}$$

$$+ l_2 \cosh\{m_{17}x + m_{18}y + m_{19}z - m_{17}^2(am_{17} + bm_{18} + cm_{19})t + m_{21}\}]. \quad (6.9)$$

In the solutions Eq. (6.9), we explore collision of the lump and a double kink waves through demonstration of the **Fig-6.2**. It is seen that only a double kink waves is visible in **Fig-6.2 (a)** at the time $t = -16$ and a small wave initiate at the lower kink (see from contour plot of **Fig-6.2(a)**) but in its propagation a lump wave come out at the time $t = -6$ from the lower kink (see **Fig-6.2(b)**). So, the fission phenomenon of lower kink is happened. As time goes, it moves to the upper kink and then get highest amplitude at $t = 0$ as well as lump reach in the middle of the two kinks (see **Fig-6.2(c)**). Then the lump wave goes to the upper kink and amplitude of lump decreases again as time increase (see **Fig-6.2(d)**) and finally diminished to the upper kink at $t = 16$ (see **Fig-6.2(e)**). So, the fusion phenomenon of upper kink is occurred. From the overall observation, we see the height of the double kink waves remain same in the overall propagation before and after the collision.

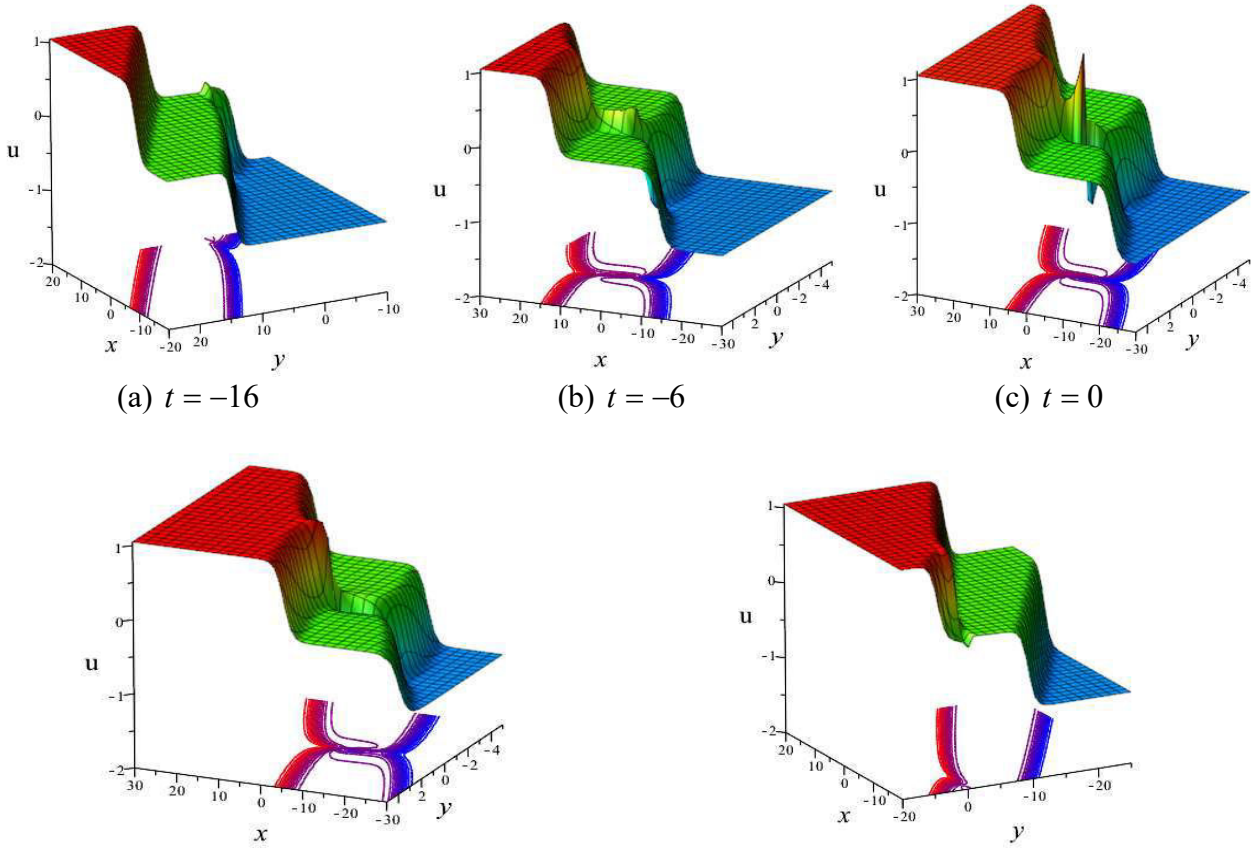

(a) $t=-16$ (b) $t=-6$ (c) $t=0$

(d) $t=6$ (e) $t=16$

Fig-6.2: Fission-fusion profiles of the lump wave get into a duel kinky waves for the solutions Eq. (6.9) with $l_2=a=b=1, c=-1, m_1=3, m_2=-146, m_3=-4.4, m_5=4, m_6=3, m_7=-3.9, m_8=10.24,\ m_{10}=1,\ m_{11}=8.82, m_{17}=1.05, m_{18}=2.1, m_{19}=4.6, m_{21}=0$ at $z=0$.

Case 3:

$$l_2=0, m_4=0, m_9=0, m_{15}={m_{12}}^2(am_{12}+bm_{13}+cm_{14})$$

$$l_1=l_1, m_i=m_i\ (i=1,2,3,5,6,7,8,10,11,12,13,14,16)\,. \tag{6.10}$$

where a, b and c can take arbitrary real values.

Setting Eq. (6.10) to the Eq. (6.3), we acquire

$$f=(m_1x+m_2y+m_3z+m_5)^2+(m_6x+m_7y+m_8z+m_{10})^2+m_{11}$$

$$+l_1\cos\{m_{12}x+m_{13}y+m_{14}z+{m_{12}}^2(am_{12}+bm_{13}+cm_{14})t+m_{16}\}\,. \tag{6.11}$$

Using the relation $u = (\ln f)_x$, Eq. (6.11) offers the result

$$u_3 = [2(m_1x + m_2y + m_3z + m_5)m_1 + 2(m_6x + m_7y + m_8z + m_{10})m_6$$

$$- l_1 m_{12} \sin\{m_{12}x + m_{13}y + m_{14}z + m_{12}^2(am_{12} + bm_{13} + cm_{14})t + m_{16}\}m_{12}]/$$

$$[(m_1x + m_2y + m_3z + m_5)^2 + (m_6x + m_7y + m_8z + m_{10})^2 + m_{11}$$

$$+ l_1 \cos\{m_{12}x + m_{13}y + m_{14}z + m_{12}^2(am_{12} + bm_{13} + cm_{14})t + m_{16}\}]. \quad (6.12)$$

For $l_1 = 0$, u_3 reduce to single lump only like **case-1** but for $l_1 \neq 0$, u_3 comes in-terms of two quadratic polynomials and a sinusoidal function (i.e. collision of lump and periodic wave), as depicted in the **Fig.-6.3, Fig. 6.4** and **Fig. 6.5**. Here, three sub cases are arises in the followings.

(i) When $m_{12} = 0$ and $m_{13} \neq 0$, u_3 reduces to collision solution with following dynamics: It is well-known that the lump form with a crest and a trough (observe **Fig. 6.3(a)**). But as the value of l_1 increases, the collision of lump and periodic waves create a fission of lump wave i.e. a crest and a trough progressively split into two crest and two trough having the same height (observe **Fig. 6.3(b-d)**) and propagate along y-direction initially. Thus the fission of lump wave is happened. We also observe that fission of the lump wave is continuous process as for large values of $l_1 = 355$, the lump wave again generate fission and split into four lump waves propagate along both in the x and y-directions, even if for $l_1 = 1045$, it gives six lump (hybrid lump) waves (see **Fig.-6.3(e, f)**) and so on.

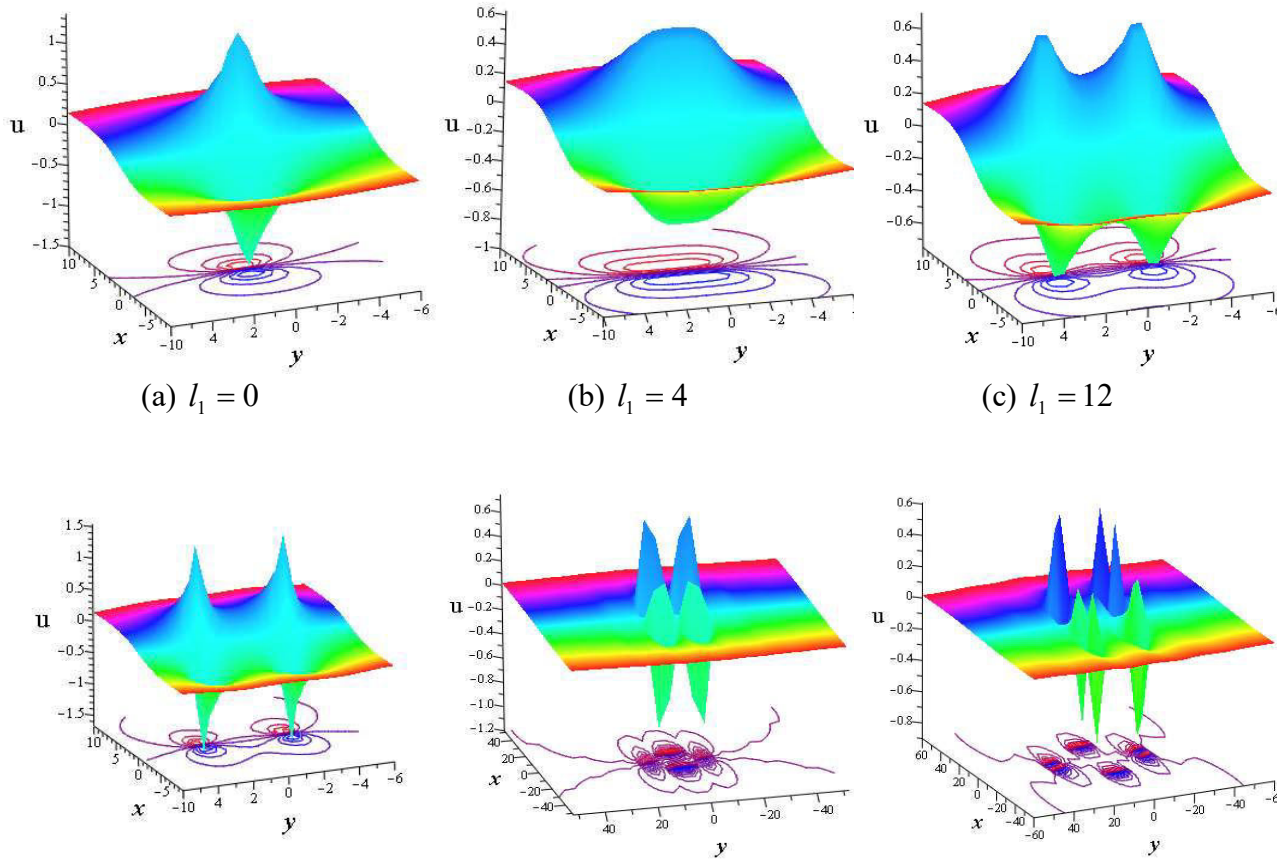

(a) $l_1 = 0$ (b) $l_1 = 4$ (c) $l_1 = 12$

(d) $l_1 = 16$ (e) $l_1 = 355$ (f) $l_1 = 1045$

Fig-6.3: Diagrams of collision solution u_3 of Eq. (6.12) for the values $a = 3, b = 3, c = -4,$ $m_1 = -1, m_2 = 1,\ m_3 = -2, m_5 = -0.1, m_6 = 1, m_7 = 1, m_8 = 2, m_{10} = 0.1, m_{11} = 1, m_{12} = 0, m_{13} = 1,$ $m_{14} = -2, m_{16} = 0.$

(ii) When $m_{12} \neq 0$ and $m_{13} = 0$, u_3 reduces to collision solution with following dynamics: It gives the similar collision solution (fission of lump) in the figures **Fig. 6.4.(b-f)** and produces more lump waves propagate periodically toward the x-axis and also the extreme amplitude of the crests and the troughs gradually enlarges as l_1 increases. In contrast the **Fig.-6.3** with **Fig.-6.4**, we observe that the lump wave in the collision solution locates toward the y-axis in **Fig.-6.3** but the lump wave in the collision solution locates toward the x-axis in the **Fig.-6.4**.

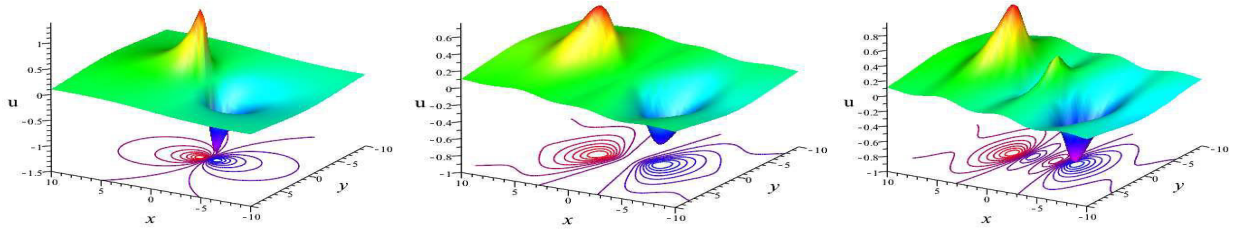

(a) $l_1 = 0$ (b) $l_1 = 4$ (c) $l_1 = 8$

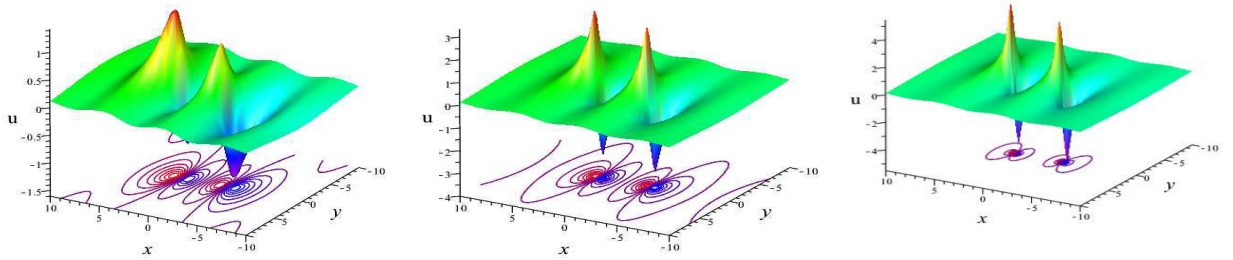

(d) $l_1 = 12$ (e) $l_1 = 16$ (f) $l_1 = 17$

Fig-6.4: Diagrams of the collision solution u_3 of Eq. (4.12) for the values $a = 3, b = 3, c = -4$, $m_1 = -1, m_2 = 1, m_3 = -2, m_5 = -0.1, m_6 = 1, m_7 = 1, m_8 = 2, m_{10} = 0.1, m_{11} = 1, m_{12} = 1, m_{13} = 0$, $m_{14} = -2, m_{16} = 0$.

(iii) When $m_{12} \neq 0$ and $m_{13} \neq 0$, u_3 reduces to collision solution with following dynamics: In fact, some interesting phenomenon can also be observed when both $m_{12} \neq 0$ and $m_{13} \neq 0$ and the values coefficient l_1 increases the trigonometric function that dominate on the values of coefficients in quadratic functions (lump wave) as depicted in **Fig-6.5(a)-(d)**. We display the corresponding 3D plot (3D as in upper and contour plot as in lower), density and 2D profile in the xy-plane (for $y = -3, 0, 3$ in **Fig-6.5(c)**) of the lump-periodic wave. Anyone can see that at $y = 0$ amplitude of the lump gives highest peak (observe **Fig-6.5(c)**). On the other hand, another periodic-lump wave can be observed in xt-plane as in the **Fig-6.5(d)**.

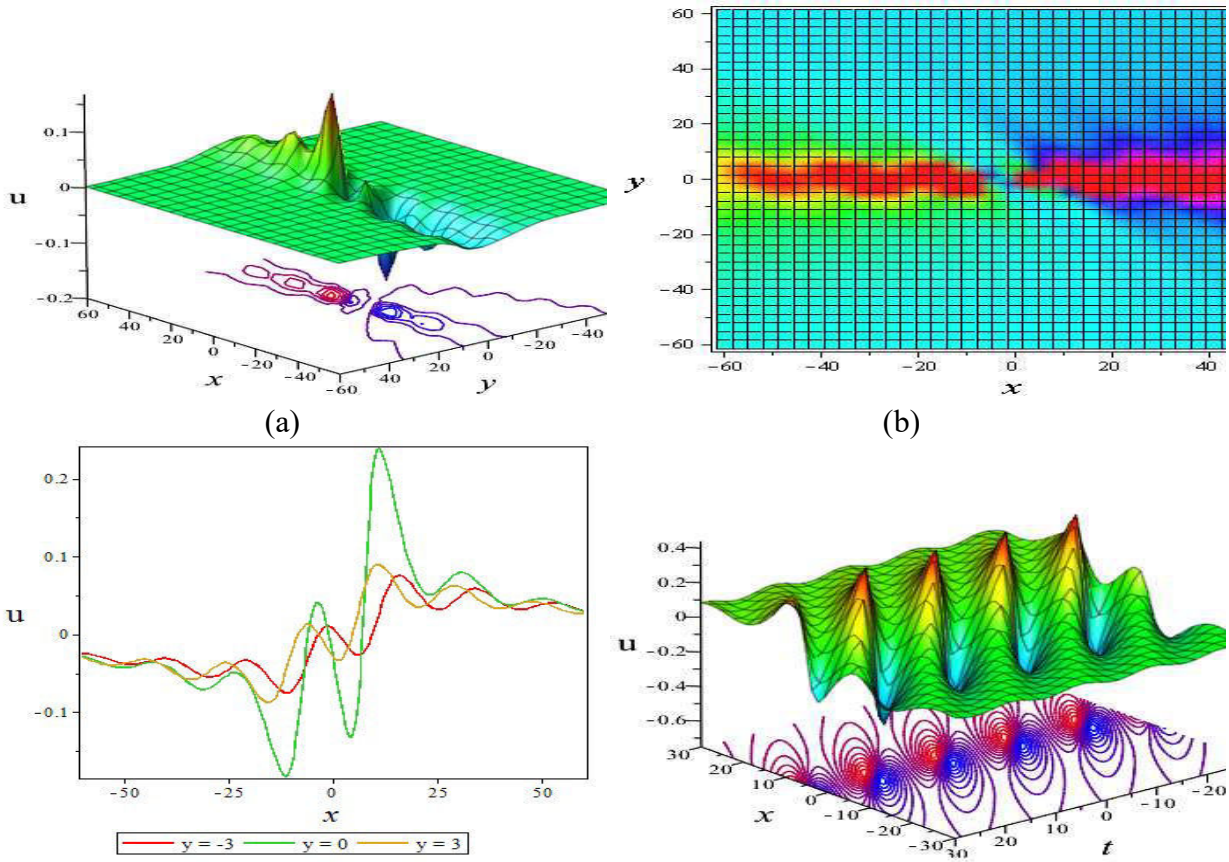

Fig-6.5: Profile of the collision of lump and periodic waves solution u_3 of Eq. (6.12) for $l_1 = 15$, $a = 1, b = 2, c = -4, m_1 = 0.5, m_2 = -1$, $m_3 = 1, m_5 = -0.5, m_6 = -0.25, m_7 = -3$, $m_8 = -3.5$, $m_{10} = 1$, $m_{11} = 20, m_{12} = 1/3, m_{13} = 4/15$, $m_{14} = -0.8, m_{16} = 0$: (a) the 3D plot, (b) the density plot and (c) the similar curve plot at $z = 0, t = 0$; (d) Periodic lump wave at $z = 0, y = 0$.

Case 4:

$$m_4 = 0, m_9 = 0, m_{15} = m_{12}^{\,2}(am_{12} + bm_{13} + cm_{14}), m_{20} = -m_{17}^{\,2}(am_{17} + bm_{18} + cm_{19})$$

$$l_1 = l_1, l_2 = l_2, m_i = m_i \ (i = 1,2,3,5,6,7,8,10,11,12,13,14,16,17,18,19,21), \tag{6.13}$$

where a, b and c can take any arbitrary values.

Putting Eq. (6.13) into the Eq. (6.3), offers the result

$$f = (m_1x + m_2y + m_3z + m_5)^2 + (m_6x + m_7y + m_8z + m_{10})^2 + m_{11}$$
$$+ l_1 \cos\{m_{12}x + m_{13}y + m_{14}z + m_{12}^{\,2}(am_{12} + bm_{13} + cm_{14})t + m_{16}\}$$
$$+ l_2 \cosh\{m_{17}x + m_{18}y + m_{19}z - m_{17}^{\,2}(am_{17} + bm_{18} + cm_{19})t + m_{21}\}. \tag{6.14}$$

Using the relation $u = (\ln f)_x$, Eq. (6.14) offers the result

$$\begin{aligned} u_4 &= [2(m_1x + m_2y + m_3z + m_5)m_1 + 2(m_6x + m_7y + m_8z + m_{10})m_6 \\ &- l_1 m_{12} \sin\{m_{12}x + m_{13}y + m_{14}z + m_{12}{}^2(am_{12} + bm_{13} + cm_{14})t + m_{16}\} \\ &+ l_2 m_{17} \sinh\{m_{17}x + m_{18}y + m_{19}z - m_{17}{}^2(am_{17} + bm_{18} + cm_{19})t + m_{21}\}]/ \\ &[(m_1x + m_2y + m_3z + m_5)^2 + (m_6x + m_7y + m_8z + m_{10})^2 + m_{11} \\ &+ l_1 \cos\{m_{12}x + m_{13}y + m_{14}z + m_{12}{}^2(am_{12} + bm_{13} + cm_{14})t + m_{16}\} \\ &+ l_2 \cosh\{m_{17}x + m_{18}y + m_{19}z - m_{17}{}^2(am_{17} + bm_{18} + cm_{19})t + m_{21}\}]. \end{aligned} \tag{6.15}$$

In the solution Eq. (6.15), comes in terms of two quadratic polynomials, a periodic and a hyperbolic function which exhibits double kinky-periodic-lump type wave propagation for $l_2 \neq 0, l_1 \neq 0$. In this case, three clusters are arises in the followings.

Cluster-1 - Taking l_2 very small as $l_2 \to 0$:

Taking l_2 very small, a dynamical situation viewed in the **Figs. 6.6-6.8** for the values $a = 5, b = 1, c = -1,\ m_3 = m_5 = m_8 = m_{10} = m_{11} = m_{14} = 1,\ m_{16} = 0.1,\ m_{19} = 7, m_{21} = 1$ at $z = 0$. The solution u_4 provides double kinky-periodic lump wave in which some x-periodic-lump with period $2\pi / m_{12}$ get into the double kink and kinky wave moves through x axis with time increases for the values as depicted in the **Fig-6.6(a)-(c)**. In this case number of lump wave remains same with the same value of $l_2 = 0.0001$. But when $l_2 \to 0$, the number of lump wave gradually increases as the values of l_2 decreases (observe **Fig-6.6(d)-(e)**), even if, kink vanishes and only periodic lump exist for $l_2 = 0$ (observe **Fig-6.6(f)**) at $t = 0$. Actually, changing different parametric constraint of the solution Eq. (6.15) distinguish characteristics again exhibits in **Fig-6.7(a)-(d)** as $y-$periodic lump with period $2\pi / m_{13}$ get into the kink

that arise with a constant background and decay go back to the same previous background at a longer time.

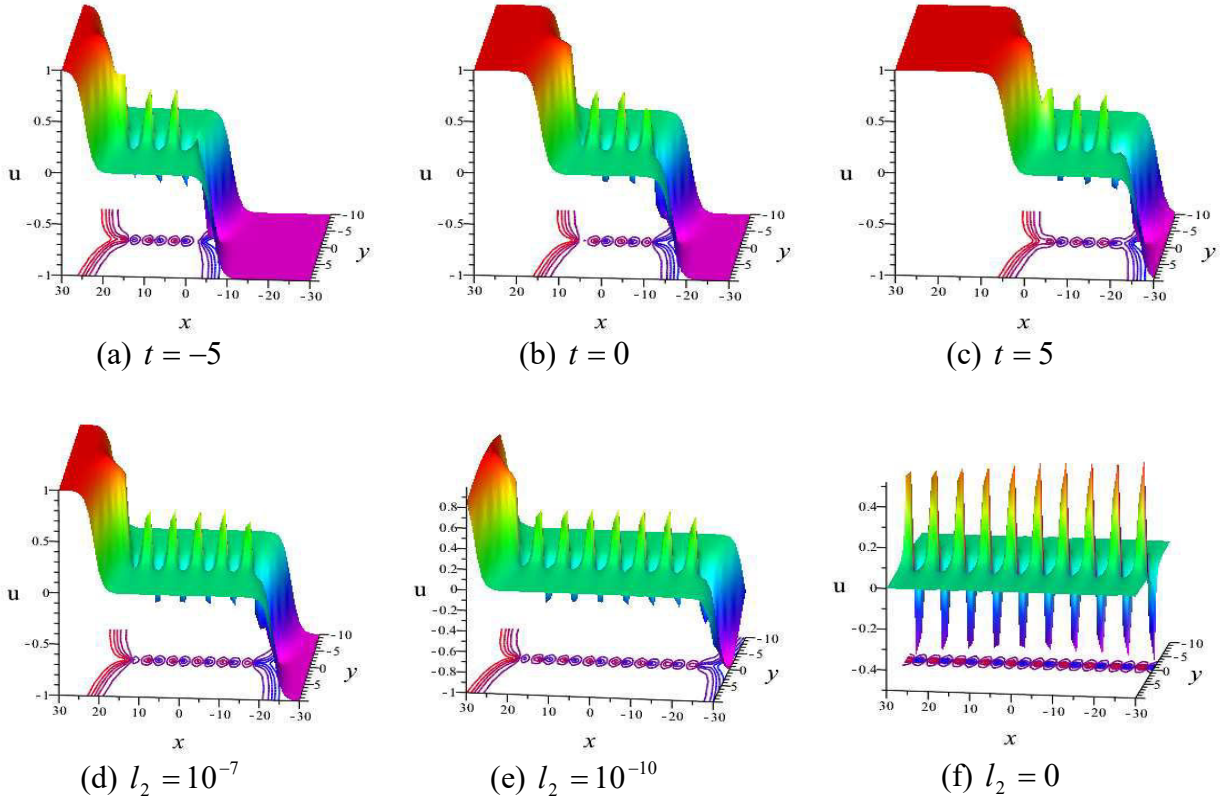

(a) $t=-5$ (b) $t=0$ (c) $t=5$

(d) $l_2=10^{-7}$ (e) $l_2=10^{-10}$ (f) $l_2=0$

Fig-6.6: Profiles of collision solution u_4 of Eq. (6.15) for the parameters $m_1=m_6=m_{13}=m_{18}=0$, $m_2=m_7=m_{12}=m_{17}=1$, $l_1=0.5$: (a)-(c) the periodic lump get into the double kinky wave for $l_2=10^{-4}$; (d)-(e) increases of periodic lump into the double kinky wave for $l_2\to 0$; **(f)** x - periodic lump wave for $l_2=0$.

On the other hand, same behavior can be observed in line soliton in the **Fig-6.7(e)-(h)**. Interesting characteristics can also be experienced when constant coefficients vanishes (i.e., $m_5=m_{10}=m_{11}=m_{16}=m_{21}=0$) as depicted in the **Fig-6.8(a)-(c)** that behaved $y-$periodic bright-dark lump waves get into the double kink waves with period $2\pi/m_{13}$. The bright lumps get into the lower kink and dark lumps get into the upper kink. Both kinks give the fission phenomena and produce hybrid lump waves in which height and number of lump

increases as l_1 increase (observe **Fig-6.8(a)-(c)**). These novel nonlinear phenomena are the first report for the (3+1)-dimension STOL equation.

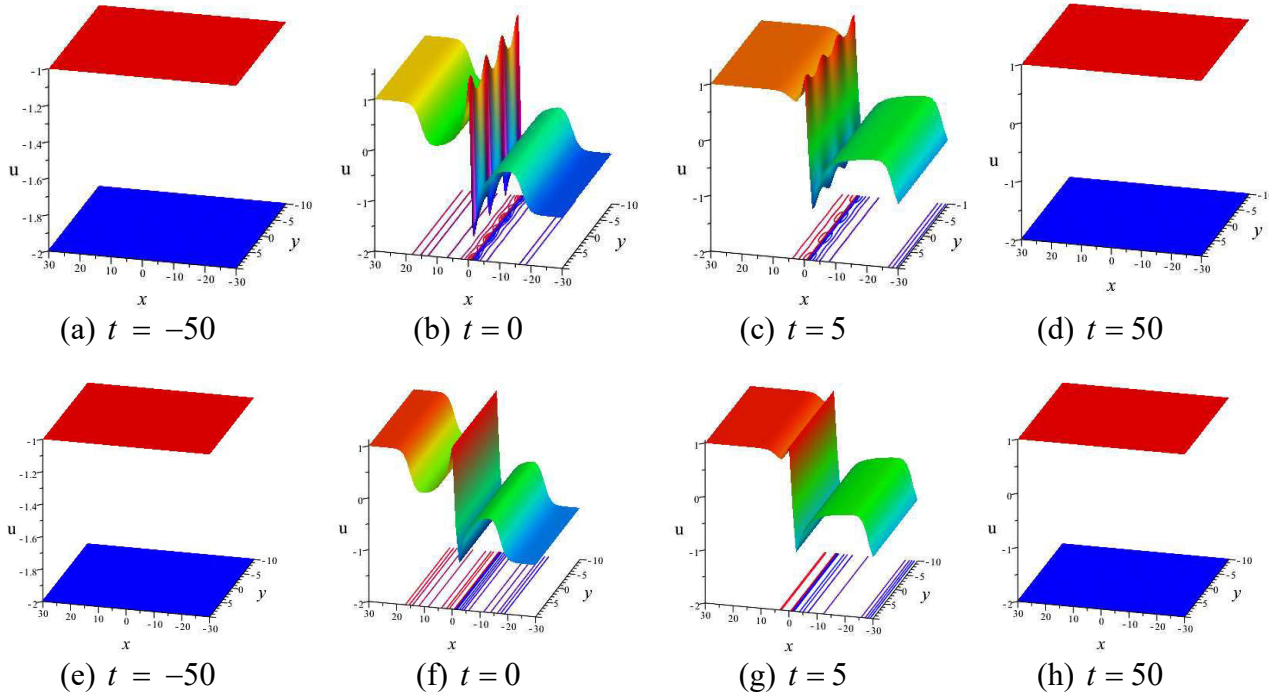

(a) $t = -50$ (b) $t = 0$ (c) $t = 5$ (d) $t = 50$

(e) $t = -50$ (f) $t = 0$ (g) $t = 5$ (h) $t = 50$

Fig-6.7: Profiles of collision solution u_4 of Eq. (6.15) for $l_1 = 0.5, l_2 = 10^{-4}$ at $z = 0$; (a)-(d) y – periodic lump wave get into the kinky wave for $m_2 = m_7 = m_{12} = m_{18} = 0, m_1 = m_6 = m_{13} = m_{17} = 1$; (e)-(h) x - periodic lump get into the kink wave for $m_2 = m_7 = m_{13} = m_{18} = 0$, $m_1 = m_6 = m_{12} = m_{17} = 1$.

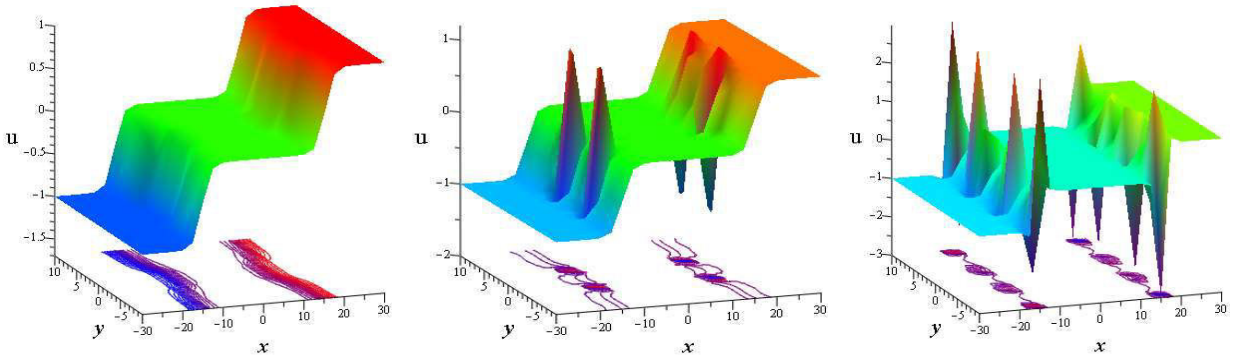

(a) $l_1 = 5$ (b) $l_1 = 50$ (c) $l_1 = 500$

Fig-6.8: Profiles of collision solution u_4 of Eq. (6.15) for $l_2 = 10^{-4}, a = 5, b = 1, c = -1, m_1 = m_6 = m_{12} = m_{18} = 0, m_{19} = 7, m_2 = m_3 = m_7 = m_8 = m_{13} = m_{14} = m_{17} = 1$ at $t = 0, z = 0$

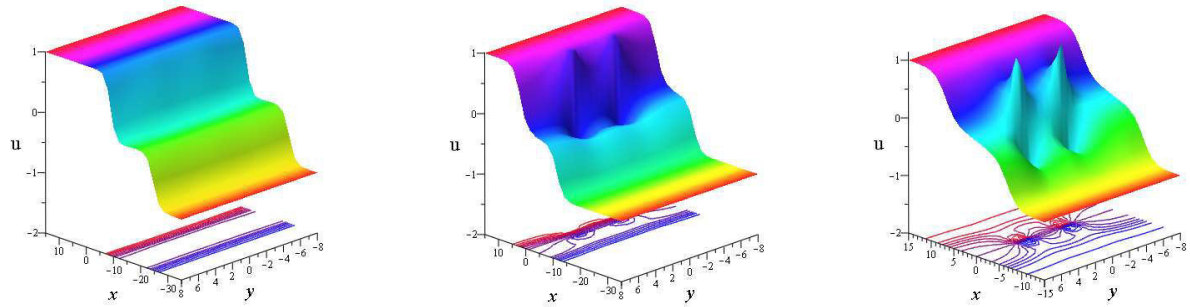

(a) $t=-16$ (b) $t=-4$ (c) $t=0$

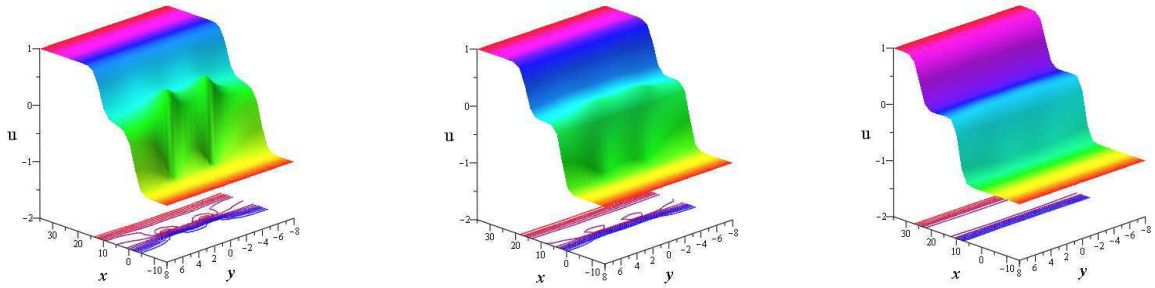

(d) $t=4$ (e) $t=8$ (f) $t=16$

Fig-6.9: Fission-fusion profile of y -periodic lump wave with the double kink wave of solution Eq. (6.15) for $m_{13}=1$.

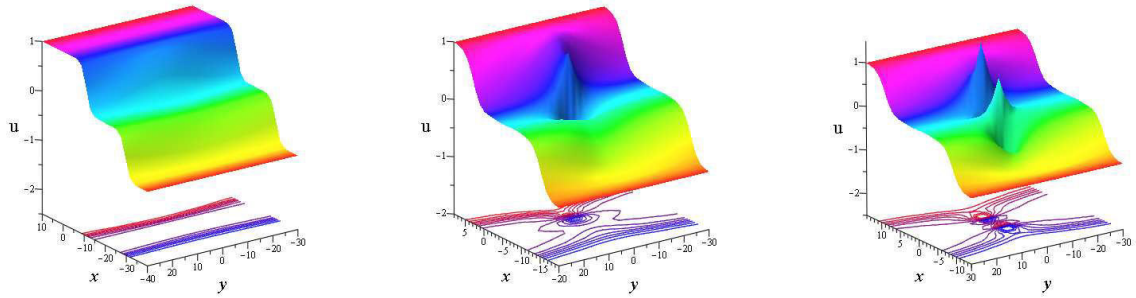

(a) $t=-20$ (b) $t=-6$ (c) $t=0$

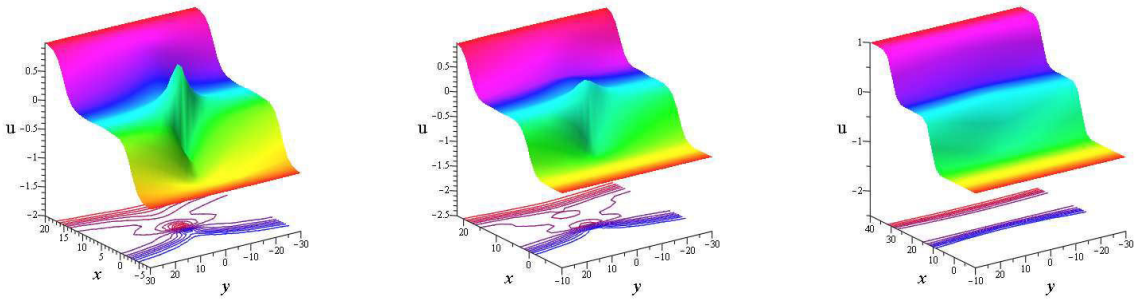

(d) $t=6$ (e) $t=9$ (f) $t=20$

Fig-6.10: Fission-fusion profile of x -periodic lump wave with the double kink wave of solution Eq. (6.15) for $m_{12}=1$.

Cluster-2 - Taking l_2 not so small:

Taking l_2 not so small, a dynamical situation viewed to the solution u_4, provides double kinky waves in which two lump waves periodically get into the kink waves and exhibits fission fusion phenomena. Solution Eq. (6.15), exhibits fission-fusion phenomena as depicted in the **Fig-6.9(a)-(f)** and **Fig-6.10(a)-(f)** which are similar to the fission-fusion phenomena of the **Fig-6.2**. But the only different is that y periodic two lumps causes fission from the upper kink and then fused into the lower kink when $m_{12}=0, m_{13}\neq 0$ (observe **Fig-6.9(a)-(e)**) and x periodic two lumps causes fission from the upper kink and then fused into the lower kink when $m_{12}\neq 0, m_{13}=0$ (observe **Fig-6.10(a)-(f)**). Both the figures **Fig-6.9(a)-(f)** and **Fig-6.10(a)-(f)** are sketch with specific parameters $l_1=16, l_2=0.5, a=-3, b=2, c=1,\ m_1=-1,$ $m_2=1,\ m_3=-2,\ m_5=0, m_6=1, m_7=1,\ m_8=4,\ m_{10}=0,\ m_{11}=1, m_{14}=1,\ m_{16}=0,\ m_{17}=1,$ $m_{18}=0, m_{19}=2,\ m_{21}=0$ at $z=0$. These novel nonlinear phenomenon is the first report for the (3+1)-dimension STOL equation.

Cluster-3 - Taking lump vanish (i.e., $m_i=0; i=1,2,3,5,6,7,10$):

when $m_i=0,\ (i=1,2,3,5,6,7,10)$; lump waves being diminished and then collision between the kinky and periodic wave are appeared in the solution Eq. (6.15), then we find

$$f = m_{11} + l_1 \cos\{m_{12}x + m_{13}y + m_{14}z + m_{12}{}^2(am_{12} + bm_{13} + cm_{14})t + m_{16}\}$$
$$+ l_2 \cosh\{m_{17}x + m_{18}y + m_{19}z - m_{17}{}^2(am_{17} + bm_{18} + cm_{19})t + m_{21}\}. \qquad (6.16)$$

The solution Eq. (6.16) can convert to diverse collision solutions, selecting the constants $m_{17}, m_{18}, m_{19}, m_{21}$ are real/purely imaginary value.

(i) For $m_{17}, m_{18}, m_{19}, m_{21}$ are real valued, we acquire a collision wave of the Eq. (6.1) using the relation $u = (\ln f)_x$ as:

$$u_5 = [-l_1 m_{12} \sin\{m_{12}x + m_{13}y + m_{14}z + m_{12}{}^2(am_{12} + bm_{13} + cm_{14})t + m_{16}\}$$

$$+ l_2 m_{17} \sinh\{m_{17}x + m_{18}y + m_{19}z - m_{17}{}^2(am_{17} + bm_{18} + cm_{19})t + m_{21}\}]/$$

$$[m_{11} + l_1 \cos\{m_{12}x + m_{13}y + m_{14}z + m_{12}{}^2(am_{12} + bm_{13} + cm_{14})t + m_{16}\}$$

$$+ l_2 \cosh\{m_{17}x + m_{18}y + m_{19}z - m_{17}{}^2(am_{17} + bm_{18} + cm_{19})t + m_{21}\}]. \quad (6.17)$$

Characteristics of the solution u_5 for the Eq. (6.17) are explained for the involve parametric values $a = 1, b = -2, c = 3, m_{11} = 1500, m_{14} = -2, m_{16} = 1, m_{17} = 1, m_{19} = -1/12, m_{21} = 1$ and $l_2 = 100$ in the figure **Fig. 6.11** and corresponding contour line of the diagram are drawn bellow of the figures in **Fig. 6.11**. For $l_1 = 0$, u_5 reduces to double kinky waves (see **Fig. 6.11(a)**) but for $l_1 \neq 0$, u_5 is collision of a y - kinky periodic breather wave (see **Fig.-6.11(b-d)**). Evidently, as t changes the collision wave moves toward the $x-$axis and the phase of the periodic wave changes after $\frac{2\pi}{m_{13}}$ along y -axis.

we also observe that changing different parametric constraint in the solution Eq. (6.17) distinguish characteristics again exhibits which are periodic line breather waves proceed in various directions as depicted in the **Fig-6.11(e)-(h), (i)-(l), (m)-(p)**. Each group of periodic line breather waves begins with a constant background and decay return to the same previous background at a longer time. Therefore the annihilation properties are obtained in this case.

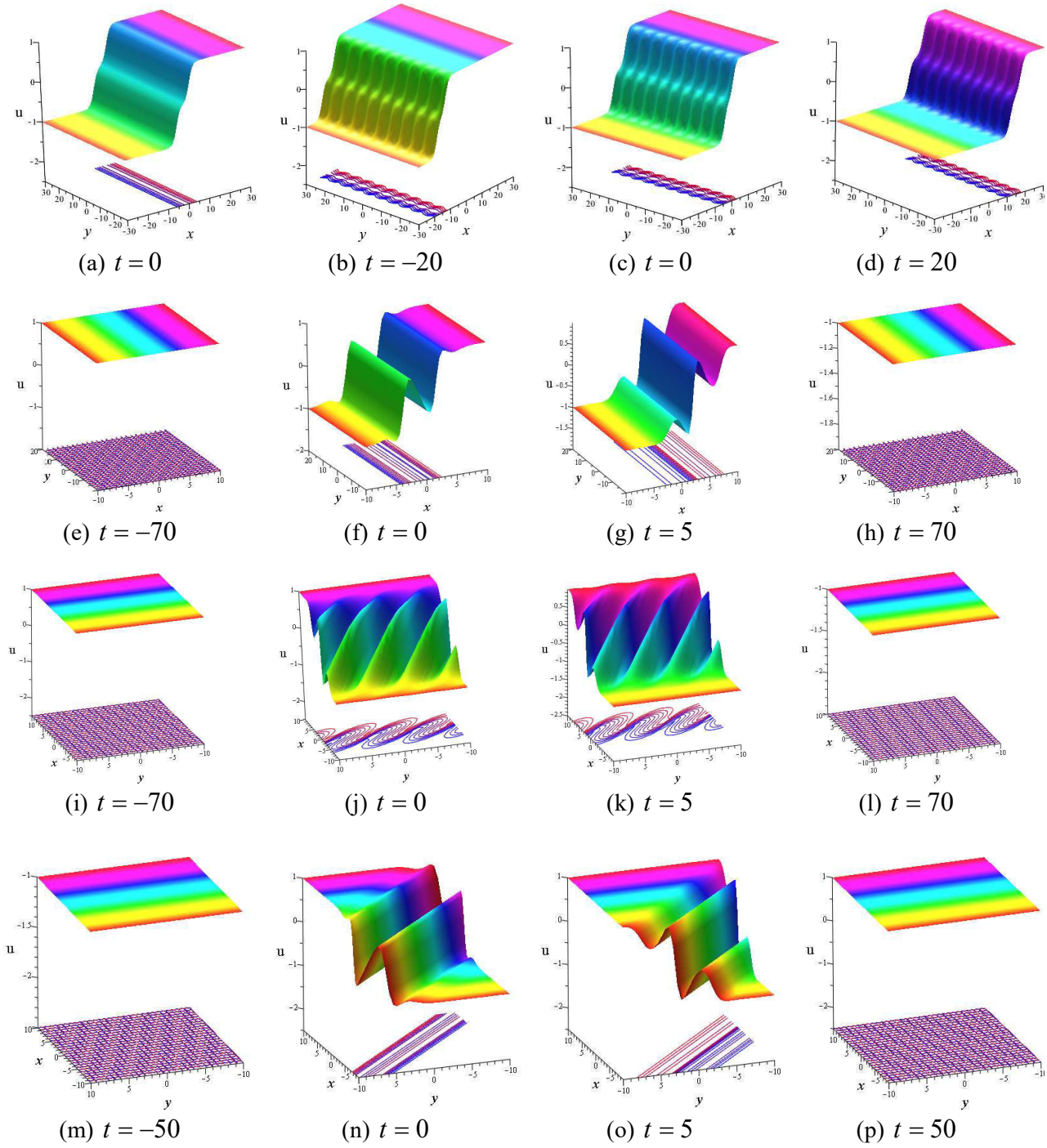

(a) $t = 0$ (b) $t = -20$ (c) $t = 0$ (d) $t = 20$

(e) $t = -70$ (f) $t = 0$ (g) $t = 5$ (h) $t = 70$

(i) $t = -70$ (j) $t = 0$ (k) $t = 5$ (l) $t = 70$

(m) $t = -50$ (n) $t = 0$ (o) $t = 5$ (p) $t = 50$

Fig-6.11: Annihilation properties of the collision solution u_5 of Eq. (6.17): **(a)** double kinky waves for $l_1 = m_{12} = m_{18} = 0,\ m_{13} = 1$; **(b)-(d)** y - periodic and double kinky waves for $l_1 = 1000,\ m_{12} = m_{18} = 0,\ m_{13} = 1$; **(e)-(h)** x - periodic and double kinky waves for $l_1 = 1000,\ m_{13} = m_{18} = 0,\ m_{12} = 1$; **(i)-(l)** (x, y) - periodic and double kinky waves for $l_1 = 1000,\ m_{18} = 0,\ m_{12} = m_{13} = 1$; **(m)-(p)** (x, y) - periodic and double kinky waves for $l_1 = 1000,\ m_{12} = m_{13} = m_{18} = 1$.

(ii) For $m_{17}, m_{18}, m_{19}, m_{21}$ are pure imaginary valued, i.e., $m_{17} = i\tilde{m}_{17}, m_{18} = i\tilde{m}_{18}$, $m_{19} = i\tilde{m}_{19}$, $m_{21} = i\tilde{m}_{21}$ with $\tilde{m}_{17}, \tilde{m}_{18}, \tilde{m}_{19}$ and $\tilde{m}_{21}$ are real valued, we acquire a collision of two breather waves of the Eq. (6.1) using the relation $u = (\ln f)_x$ as:

$$\tilde{u}_5 = [-l_1 m_{12} \sin\{m_{12}x + m_{13}y + m_{14}z + m_{12}^{\,2}(am_{12} + bm_{13} + cm_{14})t + m_{16}\}$$

$$- l_2 \tilde{m}_{17} \sin\{\tilde{m}_{17}x + \tilde{m}_{18}y + \tilde{m}_{19}z + \tilde{m}_{17}^{\,2}(a\tilde{m}_{17} + b\tilde{m}_{18} + c\tilde{m}_{19})t + \tilde{m}_{21}\}]/$$

$$[m_{11} + l_1 \cos\{m_{12}x + m_{13}y + m_{14}z + m_{12}^{\,2}(am_{12} + bm_{13} + cm_{14})t + m_{16}\}$$

$$+ l_2 \cos\{\tilde{m}_{17}x + \tilde{m}_{18}y + \tilde{m}_{19}z + \tilde{m}_{17}^{\,2}(a\tilde{m}_{17} + b\tilde{m}_{18} + c\tilde{m}_{19})t + \tilde{m}_{21}\}]. \quad (6.18)$$

Lastly, the solution represented by Eq. (6.18) are different periodic waves for different chooses of parameters in $\tilde{u}_5$. When $l_1 = 0$, $\tilde{u}_5$ is a one periodic wave that confine in the position and time directions (observe **Fig. 6.12(a)**). Otherwise, when $l_1 \neq 0$, then $\tilde{u}_5$ exhibits the dual periodic waves in both xy and xz- planes (observe **Fig. 6.12(b, c)**).

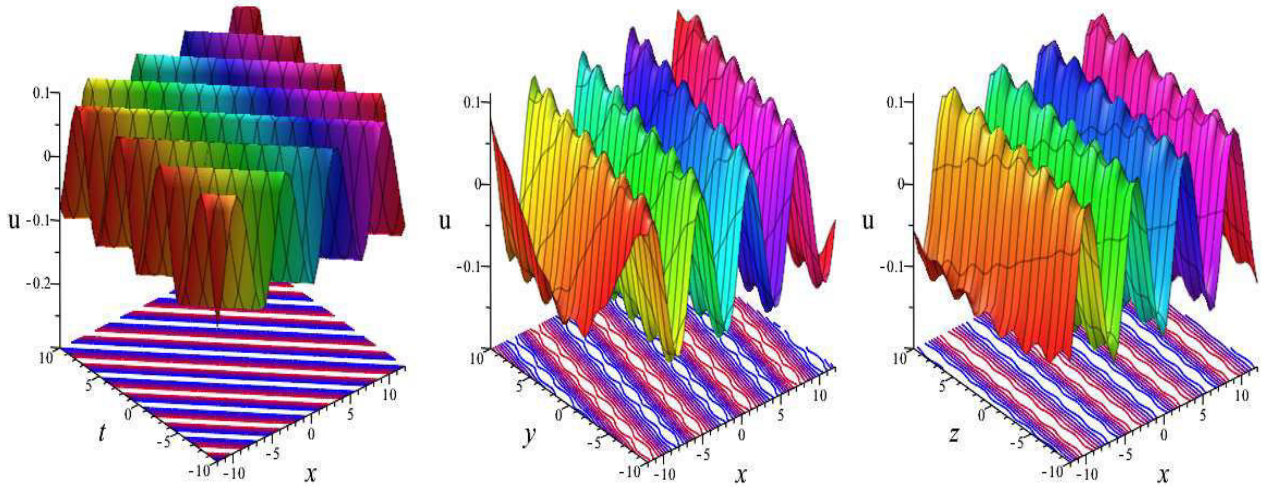

(a) $y = 0, z = 0$ (b) $t = 0, z = 0$ (c) $t = 0, y = 0$

Fig-6.12: Diagrams of the collision solution $\tilde{u}_5$ of Eq. (6.18) for $a = -1, b = 1, c = -0.6, m_{11} = 1$, $m_{12} = 0$, $m_{13} = 2$, $m_{14} = -2$, $m_{16} = 1, l_2 = 0.1$ and $\tilde{m}_{17} = 1, \tilde{m}_{18} = -0.25, \tilde{m}_{19} = -1/12, \tilde{m}_{21} = 1$: **(a)** one periodic wave at $l_1 = 0$; **(b)-(c)** dual periodic wave at $l_1 = 0.1$.

6.3. Conclusion

In summary, interaction solutions of the (3+1)-dimensional STOL equation have been determined successfully. With the aid of Maple software, a test function is carefully used to derive different nonlinear dynamical properties. As a result, some novel collision solutions among the lump, periodic and kinky waves are derived for the STOL model. We also established fission fusion properties for the collision of lump and kink waves, lump and periodic waves and among the collision of lump, kink and periodic waves. We also observe that fission and fusion properties exist in presence and without presence of sinusoidal function that produces hybrid lump waves. By taking purely imaginary values of some parameters, we derived line breather and double periodic breather wave solutions. To better understand the dynamic natures of the obtained collision solutions, we depict adequate 3d plots and contour diagrams by choosing suitable parametric values with the aid of computational software Maple 18. It is expected that our achieved solutions can improve the dynamical characteristics of the other higher order models.

Chapter Seven

Multi -Soliton and interaction solutions to the (2+1)-D BBS model

Acknowledgement

In this chapter [4], we derive a multi-soliton solution for the Bogoyavlenskii's breaking soliton (BBS) equation by utilizing the simplified Hirota's approach. From this multi-soliton solution, we investigate various forms of single kinky-lump type breather solitons, double kinky-lump type breather solitons, collision of a kink line soliton with a kinky-type breather soliton, and collision of a pair of double kinky-lump breather solitons by the appropriate selection of the involved parameters. These breathers hold unlike features in various planes even in various times. Elastic and non-elastic collisions for double kinky type lump breather are experienced in various planes and in various times. The effect and control of the propagation direction, energies, phase shifts and shape of waves by the parameters are also analyzed. Some figures are given to illustrate the dynamics of the achieved solutions. The acquired results can enrich the dynamical properties of the higher dimensional nonlinear scenarios in the engineering fields.

7.1. Introduction

Nonlinear partial differential models are extensively employed to interpret many complicated areas of sciences and engineering issue for instance optical connections, oceanic scientific problems, fluid dynamics, atmospheric, geochemistry, chemical physics, plasma physics and others [1-21]. It has three sections specifically soliton, chaos and fractal. Concepts of solitons are very significant and effective research area in nonlinear science. The hot topics of solitons are lump, kink, rogue and breather solitary waves. To explore the features of solitary wave numerous reputed scientists have been developed various reliable and fruitful approaches mainly the Hirota bilinear method [40], tan-cot

method [42], direct algebraic method [44], Darboux transformation [45], (G'/G)-expansion method [47], F-expansion method [49], exp-function method [54], homogeneous balance method [56], Homotopy perturbation method [57], the inverse scattering transform [58] and so forth. In 1971, a well known approach called Hirota bilinear method was firstly discovered by Hirota [40]. This method become effective and reliable within the short time and used to derive soliton, multi soliton, lump waves, rogue waves, breather waves and exciting localized formations of soliton solutions [71-78].

The prime aim of this chapter is to determine multiple soliton solutions and then construct various new kinds of localized wave solutions to the following Bogoyavlenskii's breaking soliton (BBS) equation [79] via the Hirota bilinear technique

$$\Phi_{xxxy} + 4\Phi_y\Phi_{xx} + 4\Phi_x\Phi_{xy} + \Phi_{xt} = 0. \tag{7.1}$$

To reach our goal, this chapter is arranged as follows: we employ the Hirota bilinear technique to determine the n-soliton solutions of the BBS equation in section **7.2**. In section **7.3** offers the lump, breather soliton and their collision solutions of the BBS equation. Finally some conclusions are drown in the section **7.4**.

7.2. Multi-soliton of the BBS equation

Dispersion relation for the BBS Eq. (7.1) can be evaluated considering a trial solution in an exponential form as:

$$\Phi(x,y,t) = \exp(\vartheta_i), \ \vartheta_i = a_i x + b_i y - \varpi_i t. \tag{7.2}$$

Exerting the Eq. (7.2) into the linear terms of the Eq. (7.1), we get hold of the dispersion relation ϖ_i as

$$\varpi_i = a_i^{\,2} b_i, \ i = 1,2,\cdots\cdots,n \tag{7.3}$$

and the resultant variables take place as

$$\vartheta_i = a_i x + b_i y - a_i^{\,2} b_i t\,,\ i = 1,2,\cdots\ \cdots, n\,. \tag{7.4}$$

Let us consider the conversion relation

$$\Phi(x,y,t) = R(\ln \tau(x,y,t))_x\,. \tag{7.5}$$

Now exerting the Eq. (7.5) with $\tau(x,y,t) = 1 + \exp(\vartheta)$ into the Eq. (7.1) and then resolve R, we acquire

$$R = \frac{3}{2}\,. \tag{7.6}$$

To evaluate n soliton solution, we must consider the supplementary function $\tau(x,y,t)$ in the following:

$$\tau(x,y,t) = 1 + \sum_{i=1}^{n} \exp(\vartheta_i) + \sum_{i<j}^{n} A_{ij} \exp(\vartheta_i + \vartheta_j)$$

$$+ \sum_{i<j<k}^{n} A_{ij} A_{ik} A_{jk} \exp(\vartheta_i + \vartheta_j + \vartheta_k) + ... + (\prod_{i<j} A_{ij}) \exp(\sum_{i=1}^{n} \vartheta_i)\,. \tag{7.7}$$

Here we consider trial solution for two soliton as

$$\tau(x,y,t) = 1 + \exp(\vartheta_1) + \exp(\vartheta_2) + A_{12} \exp(\vartheta_1 + \vartheta_2)\,. \tag{7.8}$$

Setting Eq. (7.8) with Eq. (7.5) and Eq. (7.6) into the Eq. (7.1), then solving for unknown A_{12} we gain

$$A_{12} = \frac{(a_1 - a_2)(a_1^{\,2} b_2 + 2a_1 b_1 a_2 - 2a_1 a_2 b_2 - b_1 a_2^{\,2})}{(a_1 + a_2)(a_1^{\,2} b_2 + 2a_1 b_1 a_2 + 2a_1 a_2 b_2 + b_1 a_2^{\,2})}. \tag{7.9}$$

In the similar way, we can get three, four and more soliton solution from Eq. (7.7), where the unknowns are given by

$$A_{ij} = \frac{(a_i - a_j)(a_i^{\,2} b_j + 2a_i b_i a_j - 2a_i a_j b_j - b_i a_j^{\,2})}{(a_i + a_j)(a_i^{\,2} b_j + 2a_i b_i a_j + 2a_i a_j b_j + b_i a_j^{\,2})}, i, j = 1,2,\cdots\ \cdots, n\,. \tag{7.10}$$

providing $(a_i + a_j)(a_i^{\,2} b_j + 2a_i b_i a_j + 2a_i a_j b_j + b_i a_j^{\,2}) \neq 0$.

Profile of the solution Eq. (7.7) exhibits multi-soliton solutions or n kink soliton solutions as depicted into the **Fig-7.1**. Taking $n = 1,\ 2$ and $n = 3$, we get single kink wave (observe

Fig-7.1(a)), double kink solitons (observe Fig-7.1(b)) and triple kink solitons (observe Fig-7.1(c)) respectively. It evidently observe from Figs-7.1(b) and 7.1(c) that before ($t < 0$) and after ($t > 0$) collision multi-kink solitons remains their own properties (height, width and speed) are same. That is the collisions are elastic.

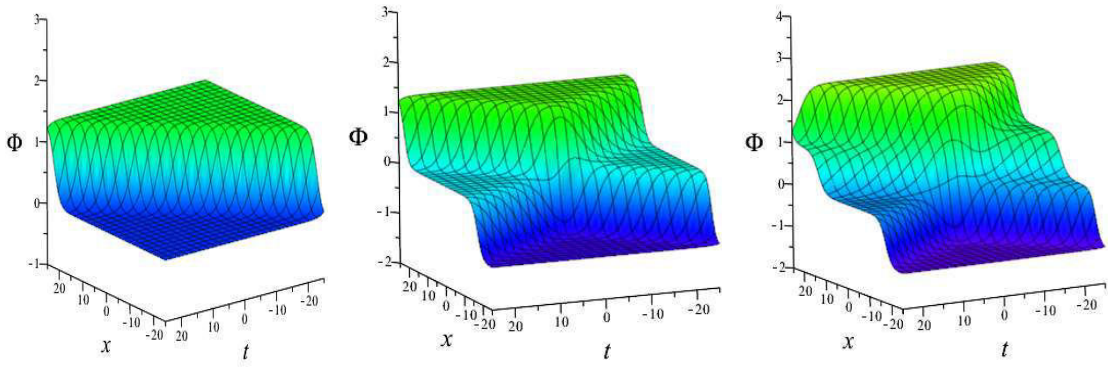

(a) (b) (c)

Fig-7.1: Sketch of the Eq. (7.5) with Eq. (7.7) and Eq. (7.10) for the values $a_1 = .88,\ a_2 = -.77,\ a_3 = .66,\ b_1 = 1,\ b_2 = .9,\ b_3 = .8$ **(a)** 3D shape of single kink soliton ($n = 1$); **(b)** 3D shape of double kink or two solitons ($n = 2$); **(c)** 3D shape of triple kink or three solitons ($n = 3$).

7.3. Lump and breather soliton solution of the BBS equation

This section recalls the multi-soliton solutions to derive lump type breather solution; collision of a soliton and a lump type breather soliton; and collision between two lump type breather solitons in the succeeding subsections.

7.3.1. Lump type breather soliton solutions from two solitons: Here, we would like to create lump type breather wave propagation. To perform that, we have to assume at least two soliton solutions by putting $n = 2$ and then let $a_1 = l_1 + im_1,\ a_2 = l_1 - im_1,\ b_1 = p_1 + iq_1,\ b_2 = p_1 - iq_1$ into the Eq. (7.8) and Eq. (7.9) and then Eq. (7.5) gives

$$\Phi(x,y,t) = \frac{3}{2}\{\ln(1 + 2\exp(M_1)\cos(\sigma_1) + A_{12}\exp(2M_1)\}_x, \tag{7.11}$$

where

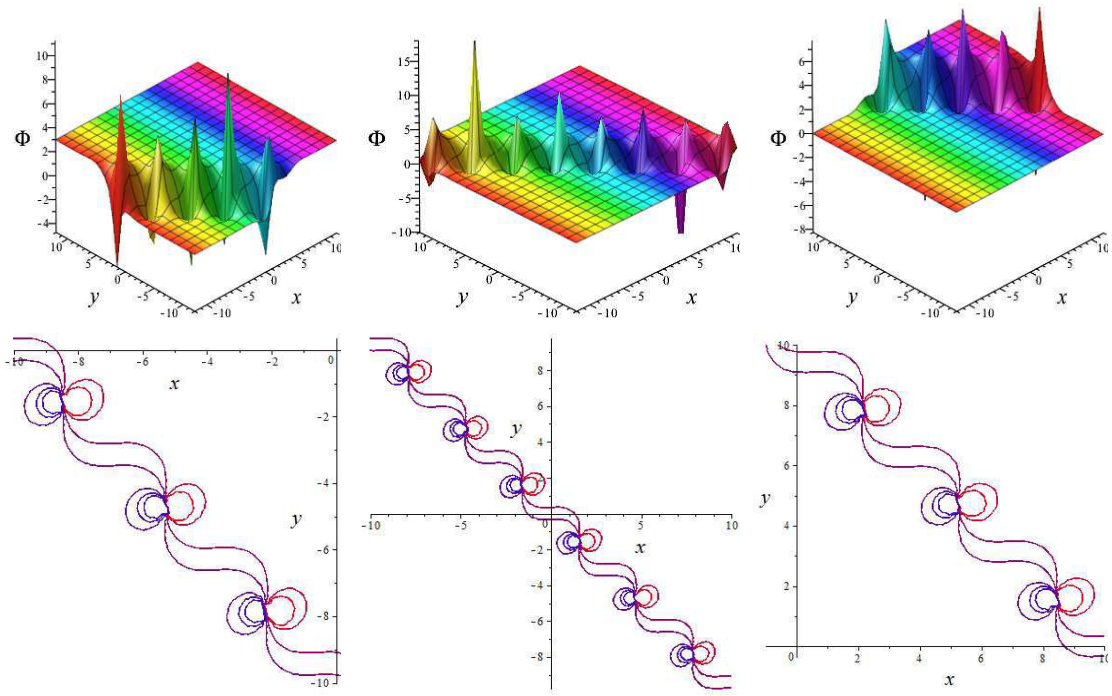

(a) $t=-5$ (b) $t=0$ (c) $t=5$

Fig-7.2: Outlook of the Eq. (7.11) with the parametric values $l_1=1,\ m_1=-1,\ p_1=1,\ q_1=1$: 3D plot (upper) and its contour plot (below).

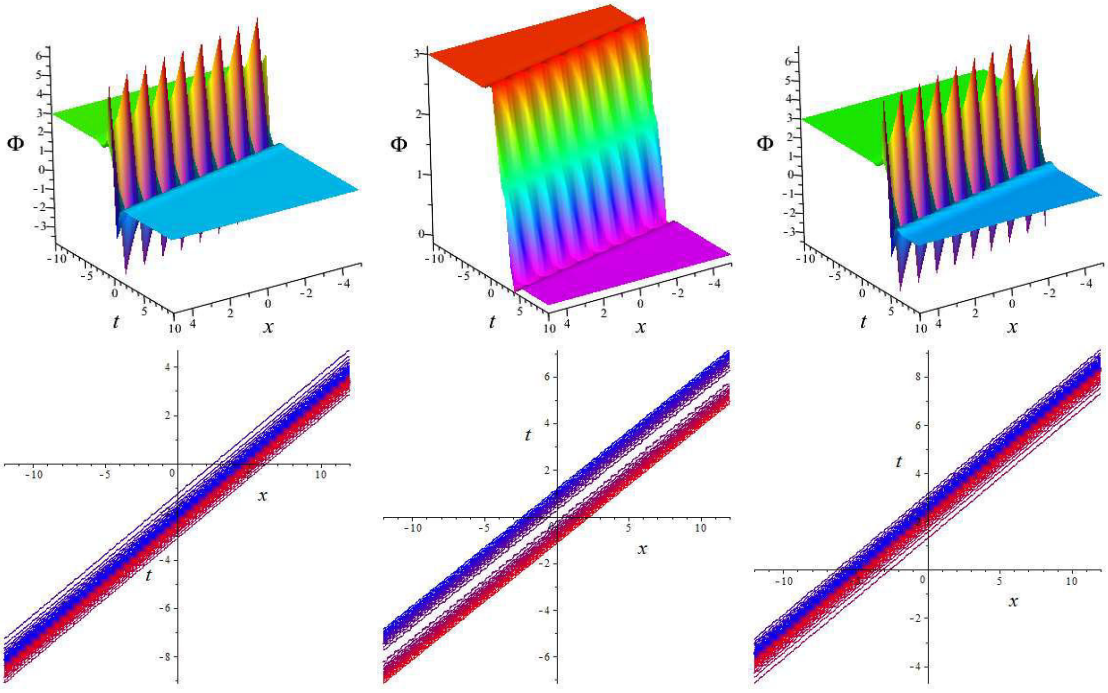

(a) $y=-5$ (b) $y=0$ (c) $y=5$

Fig-7.3: Outlook of the Eq. (7.11) with the parametric values $l_1=1,\ m_1=-1,\ p_1=1,\ q_1=1$: 3D plot (upper) and its contour plot (below).

$M_1 = l_1 x + p_1 y - (l_1^2 p_1 - m_1^2 p_1 - 2 l_1 m_1 q_1)t$, $\sigma_1 = m_1 x + q_1 y - (l_1^2 q_1 - m_1^2 q_1 + 2 l_1 m_1 p_1)t$

and $A_{12} = -\dfrac{m_1(2p_1 l_1 m_1 + q_1 l_1^2 + 3q_1 m_1^2)}{l_1(2q_1 l_1 m_1 + p_1 m_1^2 + 3p_1 l_1^2)}$.

The solution Eq. (7.11) comes from two solitons solution and gives lump type breather propagation. Features of the solution Eq. (7.11) (observe **Fig.-7.2** 3D (upper) & its contour (below)) for the values $l_1 = 1$, $m_1 = -1$, $p_1 = 1$, $q_1 = 1$. Figures show that the solution exhibits as lump type breather propagations along the paradox c at $t = 0$ (observe **Fig.-7.2(b)**), for different times ($t \neq 0$) it propagate not along paradox in the xy-plane but parallel to the paradox (observe **Fig.-7.2(a, c)**) and in every case all lump get into a kink wave. We also observe that the kink waves as well as periodic lump lie in the negative quadrant for $t < 0$, moves toward the paradox with time increases and reach along paradox at $t = 0$, and then moves away from the paradox into the positive quadrant for as $t > 0$ with increase time. Its swiftness, breadth and direction remain unchanged on the whole dynamical system and periodic lump occur equidistance from each other in each system.

Alternatively, we experience different phenomena when profile observes in the xt-plane. In this case, the solution Eq. (7.11) exhibits as multi-lump waves periodically get into a single kink wave when $y \neq 0$ (observe **Fig-7.3(a, c)**), but exhibits double kinky wave at $y = 0$ (observe **Fig-7.3(b)**) and periodic lump type scratch are also viewed in the both kink wave.

7.3.2. Interaction of a soliton and a lump type breather soliton from three soliton solutions: In this case, we would like to determine a collision solution between periodic lump type breather waves comes from two solitons and a kink soliton. In this regard, consider the three solitons solution by putting $n = 3$ into the Eq. (7.7) with Eq. (7.10), and

then let $a_1 = l_1 + im_1$, $a_2 = l_1 - im_1$, $a_3 = c$, $b_1 = p_1 + iq_1$, $b_2 = p_1 - iq_1$, $b_3 = d$ into the Eq. (7.7) together with the Eq. (7.5), Eq. (7.6) and Eq. (7.10) gives the resultant solution as

$$\Phi(x,y,t) = \frac{3}{2}\ln\{1 + 2\exp(M_1)\cos(\sigma_1) + A_{12}\exp(2M_1) + \exp(cx + dy - c^2dt) + 2\rho_1\exp(M_1 + cx + dy - c^2dt)\cos(\sigma_1 + \xi_1) + A_{12}\rho_1^2\exp(2M_1 + cx + dy - c^2dt)\}_x \quad (7.12)$$

where $A_{12} = -\frac{m_1(2p_1l_1m_1 + q_1l_1^2 + 3q_1m_1^2)}{l_1(2q_1l_1m_1 + p_1m_1^2 + 3p_1l_1^2)}$, $M_1 = l_1x + p_1y - (l_1^2p_1 - m_1^2p_1 - 2l_1m_1q_1)t$,

$\sigma_1 = m_1x + q_1y - (l_1^2q_1 - m_1^2q_1 + 2l_1m_1p_1)t$ and $A_{23} = P_1 + iQ_1 = \rho_1\exp(i\xi_1)$ (say), then $A_{13} = P_1 - iQ_1 = \rho_1\exp(-i\xi_1)$ in which $\rho_1 = \sqrt{P_1^2 + Q_1^2}$ and $\xi_1 = \tan^{-1}(\frac{Q_1}{P_1})$.

In the Eq. (7.12), solution comes in terms of the combination of exponential and periodic sinusoidal function exhibits collision of a kinky periodic lump type breather soliton and a kink shaped line soliton, as viewed in the **Figs-7.4, 7.5** and **7.6** for the values $l_1 = 1$, $m_1 = -1$, $p_1 = 1$, $q_1 = 1$, $c = 1$. There are two sub-cases existed depending on interaction direction.

Case (i): For $d > 0$, we observe (see **Fig-7.4** 3D (upper) and its contour (below)) that the two waves are always parallel to each other, even at the time of interaction (see the contour plots **Fig-7.4** (below)). We also observe that the two waves (display as a double kink wave) contains periodically lump waves get into the lower kink (see **Fig.-7.4(a)** (upper)) before ($t < 0$) collision and upper kink (see **Fig.-7.4(c)** (upper)) after ($t > 0$) collision in the xy-plane respectively. They are overlapped entirely at $t = 0$ where highest amplitude comes into sight (see **Fig.-7.4(b)** (upper)). Actually the whole collision processes is completely elastic which is evidently observed in the contour plots **Fig.-7.4** (below) in the same plane.

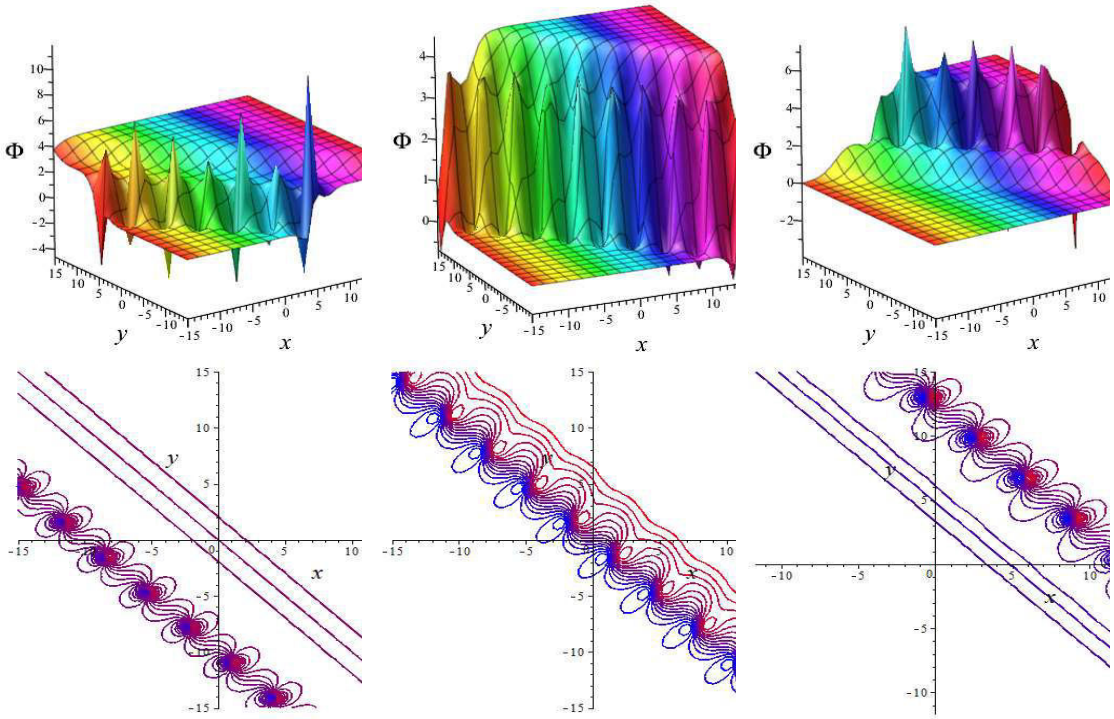

(a) $t=-5$ (b) $t=0$ (c) $t=5$

Fig-7.4: Collision between breather lump soliton and kink line soliton of the Eq. (7.12) for $l_1=1$, $m_1=-1$, $p_1=1$, $q_1=1$, $c=1$, $d=1$: 3D plot (upper) and its contour plot (below).

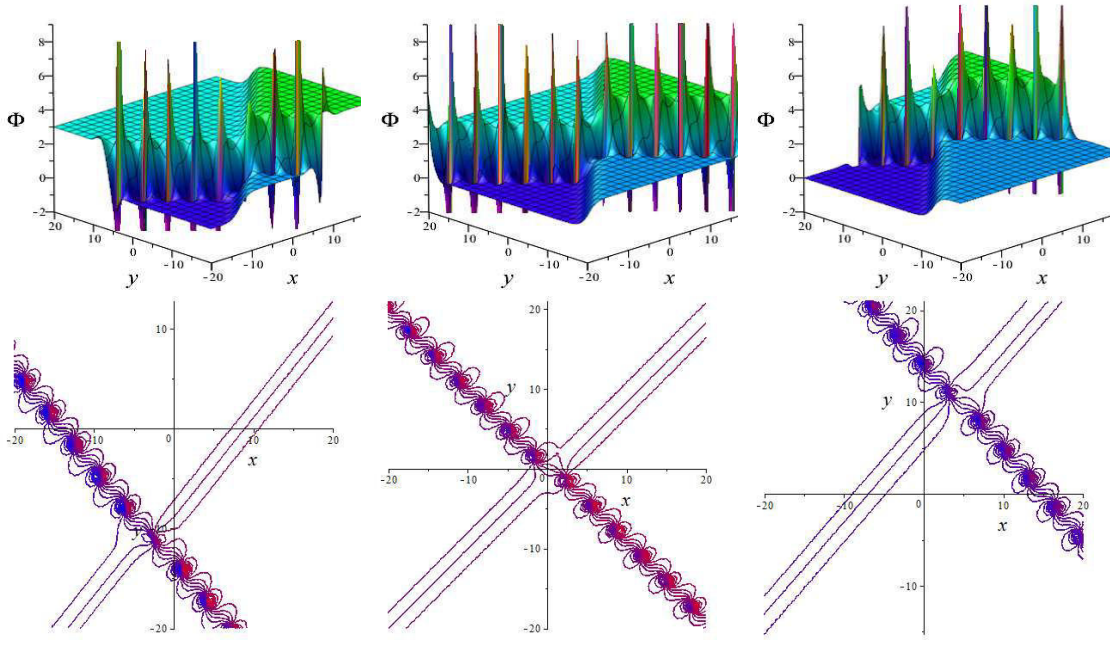

(a) $t=-7$ (b) $t=0$ (c) $t=7$

Fig-7.5: Collision between breather lump soliton and kink line soliton of the Eq. (7.12) for $l_1=1$, $m_1=-1$, $p_1=1$, $q_1=1$, $c=1$, $d=-1$: 3D plot (upper) and its contour plot (below).

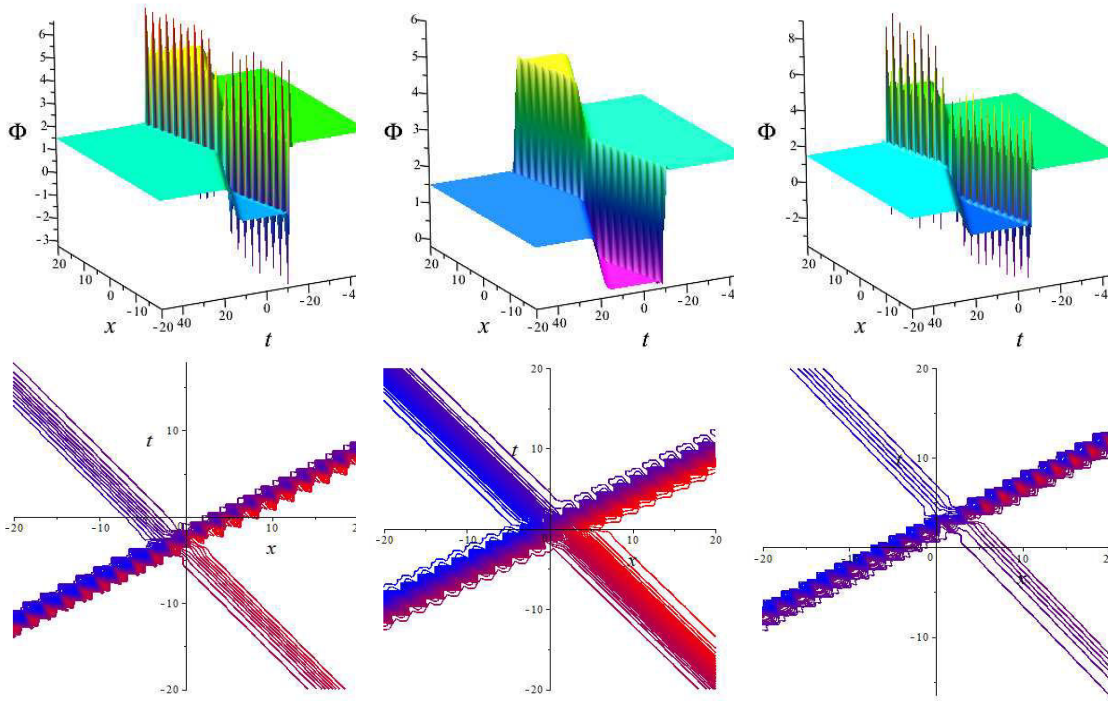

(a) $y=-5$ (b) $y=0$ (c) $y=5$

Fig-7.6: Collision between breather lump soliton and kink line soliton of the Eq. (7.12) for $l_1=1$, $m_1=-1$, $p_1=1$, $q_1=1$, $c=1$, $d=-1$: 3D plot (upper) and its contour plot (below).

Case (ii): For $d<0$, we observe (see **Fig-7.5** 3D (upper) and its contour (below)) that the two waves (a kinky periodic lump type breather soliton and a kink shaped line soliton) interact at a certain angle. We see that a kink wave interact the breather wave and shifting of the collision changes along negative of y-axis (observe **Fig-7.5(a)**) to positive of y-axis (observe **Fig-7.5(c)**), but at the intermediate time they interact at the origin (observe **Fig-7.5(b)**). The overall propagation process is elastic. Beside this, when we take the plot into the xt-plane similar elastic collision are also observed in the double kink waves with the same parametric values (observe **Fig.-7.6** 3D (upper) and its contour (below)).

7.3.3. Four solitons and Interaction of two lump type breather solitons: To determine interaction of two lump type breather solitons, we have to consider at four

soliton solutions. In this regard, consider the three solitons solution by putting $n=4$ in Eq. (7.7) with Eq. (7.10), and then let $a_1=l_1+im_1$, $a_2=l_1-im_1$, $a_3=l_2+im_2$, $a_4=l_2-im_2$, $b_1=p_1+iq_1$, $b_2=p_1-iq_1$, $b_3=p_2+iq_2$, $b_4=p_2-iq_2$ into the Eq. (7.7) together with Eqs. (7.5), (7.6) and (7.10) gives the resultant solution as

$$\begin{aligned}\Phi(x,y,t)=\frac{3}{2}\ln\{&1+2\exp(M_1)\cos(\sigma_1)+2\exp(M_2)\cos(\sigma_2)\\&+A_{12}\exp(2M_1)+A_{34}\exp(2M_2)\\&+2\rho_1\cos(\xi_1+\sigma_1+\sigma_2)\exp(M_1+M_2)\\&+2\rho_2\cos(\xi_2+\sigma_1-\sigma_2)\exp(M_1+M_2)\\&+2A_{12}\rho_1\rho_2\exp(2M_1+M_2)\cos(\sigma_2+\xi_1-\xi_2)\\&+2A_{34}\rho_1\rho_2\exp(M_1+2M_2)\cos(\sigma_1+\xi_1+\xi_2)\\&+A_{12}A_{34}\exp(2M_1+2M_2)\}_x\end{aligned}\tag{7.13}$$

where $M_1=l_1x+p_1y-(l_1^{\,2}p_1-m_1^{\,2}p_1-2l_1m_1q_1)t$,

$\sigma_1=m_1x+q_1y-(l_1^{\,2}q_1-m_1^{\,2}q_1+2l_1m_1p_1)t$,

$M_2=l_2x+p_2y-(l_2^{\,2}p_2-m_2^{\,2}p_2-2l_2m_2q_2)t$,

$\sigma_2=m_2x+q_2y-(l_2^{\,2}q_2-m_2^{\,2}q_2+2l_2m_2p_2)t$,

$A_{12}=-\dfrac{m_1(2p_1l_1m_1+q_1l_1^{\,2}+3q_1m_1^{\,2})}{l_1(2q_1l_1m_1+p_1m_1^{\,2}+3p_1l_1^{\,2})}$, $A_{34}=-\dfrac{m_2(2p_2l_2m_2+q_2l_2^{\,2}+3q_2m_2^{\,2})}{l_2(2q_2l_2m_2+p_2m_2^{\,2}+3p_2l_2^{\,2})}$,

$A_{24}=P_1+iQ_1=\rho_1\exp(i\xi_1)$ (say) and $A_{14}=P_2+iQ_2=\rho_2\exp(i\xi_2)$ (say), then $A_{13}=P_1-iQ_1=\rho_1\exp(-i\xi_1)$ and $A_{23}=P_2-iQ_2=\rho_2\exp(-i\xi_2)$.

To find the values of ρ_1, ρ_2, ϑ_1 and ϑ_2 we apply $\rho=\sqrt{P^2+Q^2}$ and $\vartheta=\tan^{-1}(\frac{Q}{P})$.

In the solution Eq. (7.13), comes in-terms of exponential and periodic sinusoidal function exhibits collision of a pair of periodic lump type breather waves, as viewed in the **Fig-7.7** with the values $l_1=1$, $m_1=-1$, $p_1=1$, $q_1=1$, $l_2=-1.001$, $m_2=1$, $p_2=1$, $q_2=1$ at $t=0$. It is fascinating that collision of these breathers own unlike dynamic natures in distinct planes. Both elastic (observe **Fig-7.7(a)** 3D (upper) & its contour (below)) and non-elastic (observe **Fig-7.7(b, c)** 3D (upper) & its contour (below)) collision own for

different times and different planes. **Fig-7.7(a)** exhibits double kink type X-shaped breather soliton for elastic collision as before and after collision each lump type breather wave remains their same solitonic natures and interacts at the origin coming along opposite paradox in the xy-plane. It is observed that the some lump waves are periodically got into each soliton, being at equal distance from each other. On the other hand, when we take the same plot in the same xy-plane but in different time at $t=-4$ it exhibits non-elastic fusion phenomena after collision as propagate from negative to positive along y direction (observe **Fig-7.7(b)** 3D (upper) and its contour (below)). Other behaviour is also own the collision when observed in the xt-plane. It is seen that a breather lump wave interact at $t=0$ and then causes fission as it split into two breather type lump waves (observe **Fig-7.7(c)** 3D (upper) & its contour (below)) times goes by.

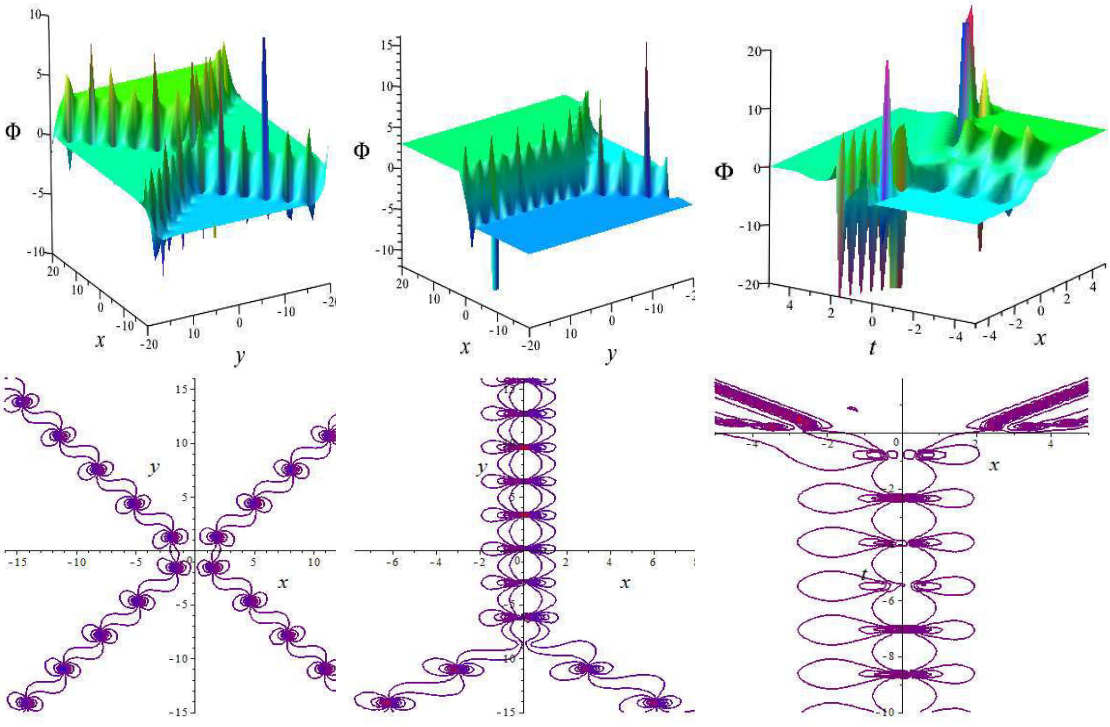

(a) $t=0$ (b) $t=-4$ (c) $y=0$

Fig-7.7: Collision of periodic lump and periodic line waves of the Eq. (7.13) for $l_1=1$, $m_1=-1$, $p_1=1$, $q_1=1$, $l_2=-1.001$, $m_2=1$, $p_2=1$, $q_2=1$: 3D plot (upper) and its contour plot (below).

7.4. Conclusions

In the summery, we have been successfully used Hirota bilinear method to gian multi-soliton solutions Eq. (7.7) of the BBS equation, see **Figs-7.1**. Various parametric values have been selected to get distinguish dynamical characteristics single kinky-lump type breather solitons (see **Figs-7.2, 7.3(a, c))**, double kinky-lump type breather solitons (see **Figs-7.3 (b), 7.4, 7.5, 7.6** and **7.7(a)**), collision of a kink line soliton with a kinky-type breather soliton (see **Figs-7.4, 7.5, 7.6**), and collision of a pair of kinky-lump breather solitons (see **Fig-7.7(a)**) by the appropriate selection of exist parameters from the multi soliton solutions of the models. These breathers hold unlike features in various planes even in various times. Elastic (see see **Figs-7.1-7.6, 7.7(a)**) and non-elastic (see **Fig-7.7 (b, c)**) collisions for double kinky type lump breather are experienced in various plane and in various times. Some figures are given to illustrate the dynamics of the achieved solutions. This will also prompt us to explore new approach to obtain more extensive and accurate solution to the models. The acquired results can enhance the dynamical properties of higher dimensional nonlinear scenarios in the engineering fields.

Chapter Eight

Multi-solitons and interaction solution to the (3+1)-D STOL model

Acknowledgement

In this chapter, the Hirota bilinear integral technique is applied to execute n-soliton solutions of the (3+1)-dimensional Sharma–Tasso–Olver-like (STOL) model. We also reveal the interactions are non-elastic fusion or fission phenomena that more kink waves fused or a single kink wave split into more kink waves due to soliton fission. We derive kinky-lump breather, combo line kink and kinky-lump breather, and a pair of kinky-lump breather wave solutions that degenerate from two-, three- and four-solitons respectively by choosing complex conjugate values involving free parameters. We reveal the interactions are non-elastic fusion phenomena that kink and breather waves fused into a kinky-lump breather from the collision of line kink and combo kinky-lump breather, a single kinky-lump breather from a pair of kinky-lump breather waves after interaction respectively. The fission phenomena also observe from the same interaction with the reverse condition on parameters. All special properties of these collision solutions are illustrated clearly with 3D and contour plots.

8.1 Introduction

Nonlinear evolution models can illustrate various complicated happening in various branches including fluid mechanics, optical fiber communications, plasmas, mathematical biology, and so on [1-21]. With the improvement of the soliton concept, numerous effective and reliable schemes to achieve exact and analytical solutions of the models have been presented in the literature [38-70]. A novel integral technique which is familiar as Hirota bilinear scheme was primarily presented in 1971 [40], by Hirota, and was effectively applied in huge amount of nonlinear models [71-78].

The primary purpose of this chapter is to find some novel exact multi-solutions and collision solutions of the following STOL model [81]

$$\psi_t + p[(3\psi\psi_x + \psi^3)_x + \psi_{xxx}] + q[(2\psi\psi_y + \psi_x\partial_x^{-1}\psi_y + \psi^2\partial_x^{-1}\psi_y)_x + \psi_{xxy}]$$

$$+ r[(2\psi\psi_z + \psi_x\partial_x^{-1}\psi_z + \psi^2\partial_x^{-1}\psi_z) + \psi_{xxz}] = 0. \quad (8.1)$$

where p, q, r are free parametric values and ψ is the function that contains the space variables x, y, z, and time variable t. The integral operator ∂_x^{-1} is the inverse of ∂_x. The STOL model Eq. (8.1) can explain the extension of nonlinear dispersive waves in the inhomogeneous medium [96]. This model can also illustrate various difficult sciences areas for instance optics, plasmas, quantum physics, and others [97–100].

The design of this chapter is given as: firstly we apply the Hirota bilinear transformation to establish the multi-soliton solutions of the STOL model in section **8.2**. Section **8.3** discusses the interaction solutions of the STOL model. Lastly, conclusions and some comments are provided in section **8.4**.

8.2. Multi-solitons of the STOL model

To achieve dispersion relation of the STOL model Eq. (8.1), we consider an exponential function solution as bellow:

$$\psi(x,y,z,t) = \exp(\vartheta_i), \ \vartheta_i = a_i x + b_i y + c_i z - \varpi_i t. \quad (8.2)$$

Putting Eq. (8.2) in the linear parts of the Eq. (8.1), then we have

$$\varpi_i = aa_i^3 + ba_i^2 b_i + ca_i^2 c_i, \ i = 1,2,\cdots,n. \quad (8.3)$$

Thus we reach to

$$\vartheta_i = a_i x + b_i y + c_i z - (aa_i^3 + ba_i^2 b_i + ca_i^2 c_i)t, \ i = 1,2,\cdots,n. \quad (8.4)$$

Now, consider the bilinear conversion relation

$$\psi(x,y,z,t) = A(\ln\varphi(x,y,z,t))_x. \quad (8.5)$$

Inserting Eq. (8.5) and $\varphi = 1 + \exp(\vartheta)$ in the Eq. (8.1), then solve A yields

$$A = 1. \tag{8.6}$$

For n multi-soliton solution, suppose the trial function as follows:

$$\varphi(x,y,z,t) = 1 + \sum_{i=1}^{n} \exp(\vartheta_i) + \sum_{i<j}^{n} P_{ij} \exp(\vartheta_i + \vartheta_j) + \sum_{i<j<k}^{n} P_{ij} P_{ik} P_{jk} \exp(\vartheta_i + \vartheta_j + \vartheta_k)$$

$$+ .... + (\prod_{i<j} P_{ij}) \exp(\sum_{i=1}^{n} \vartheta_i). \tag{8.7}$$

Now suppose the trial solution for 2-soliton as follows

$$\varphi(x,y,z,t) = 1 + \exp(\vartheta_1) + \exp(\vartheta_2) + P_{12} \exp(\vartheta_1 + \vartheta_2). \tag{8.8}$$

Putting Eq. (8.8) including Eq. (8.5) and Eq. (8.6) in the Eq. (8.1), then solve P_{12} yields

$$P_{12} = 0. \tag{8.9}$$

Similarly, we can find 3-soliton, 4-soliton and all other soliton solutions from Eq. (8.7), with the following conditions

$$P_{ij} = 0,\ i, j = 1,2,\cdots,n. \tag{8.10}$$

Shapes of the wave equation Eq. (8.7) together with Eq. (8.5) & Eq. (8.10) for $n = 1$, 2 and 3 exhibits one-, two- and three-soliton solutions respectively as described in the **Fig-8.1** with the parametric values $p = 1$, $a_1 = b_1 = b_2 = c_1 = c_2 = c_3 = 1$, $a_2 = -1$, $a_3 = 0.5$, $b_3 = 0.5$. It is experienced that $n = 1$ displays a single kink wave (view **Fig-8.1(a, d)**) only, but in the interaction solutions: single kink wave split into two kink waves ($n = 2$) (view **Fig-8.1(b)**) and single kink wave split into three kink waves ($n = 3$) (view **Fig-8.1(c)**) after ($t > 0$) interactions due to non-elastic collisions fission phenomena. The reverse phenomena also observed for reverse conditions on involve parameters depicted in **Fig-8.1(e-f)**.

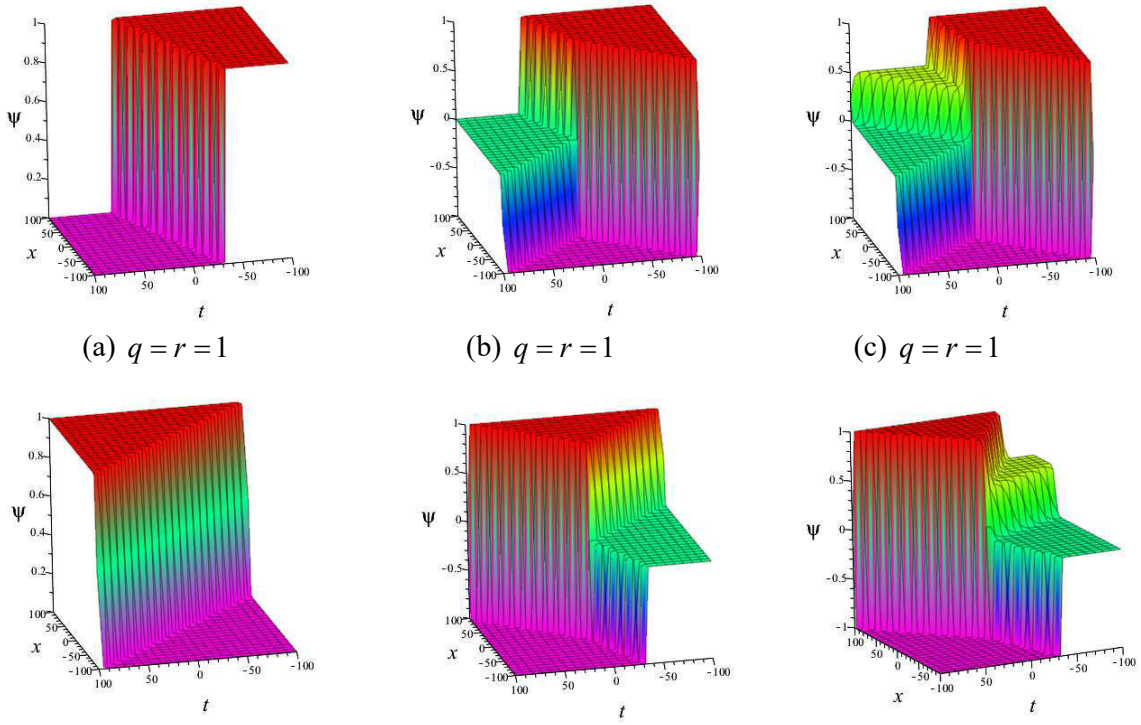

(a) $q = r = 1$ (b) $q = r = 1$ (c) $q = r = 1$

(d) $q = r = -1$ (e) $q = r = -1$ (f) $q = r = -1$

Fig-8.1: Shape of the wave solution Eq. (8.7) with $y = 0,\ z = 0$: **(a, d)** single kink soliton ($n = 1$); **(b, e)** dual kink solitons ($n = 2$); **(c, f)** triple kink solitons ($n = 3$).

8.3. Interaction solutions of the STOL model

For retrieving lump breather; the interaction between single soliton and single lump breather; and interaction of double lump breather solitons we address the Eq. (8.7) again in the next subdivisions.

8.3.1. Collisions of 2-soliton degenerate into a lump shape breather solitons: Here, we spotlight on lump shape breather wave propagation from the two solitons solution. To present that, we have to assume $n = 2$ in Eq. (8.7) and then place $a_1 = \alpha_1 + i\beta_1$, $a_2 = \alpha_1 - i\beta_1$, $b_1 = \gamma_1 + i\delta_1$, $b_2 = \gamma_1 - i\delta_1$, $c_1 = \eta_1 + i\rho_1$, $c_2 = \eta_1 - i\rho_1$ into the Eq. (8.8) and Eq. (8.9) together with Eq. (8.5), yields

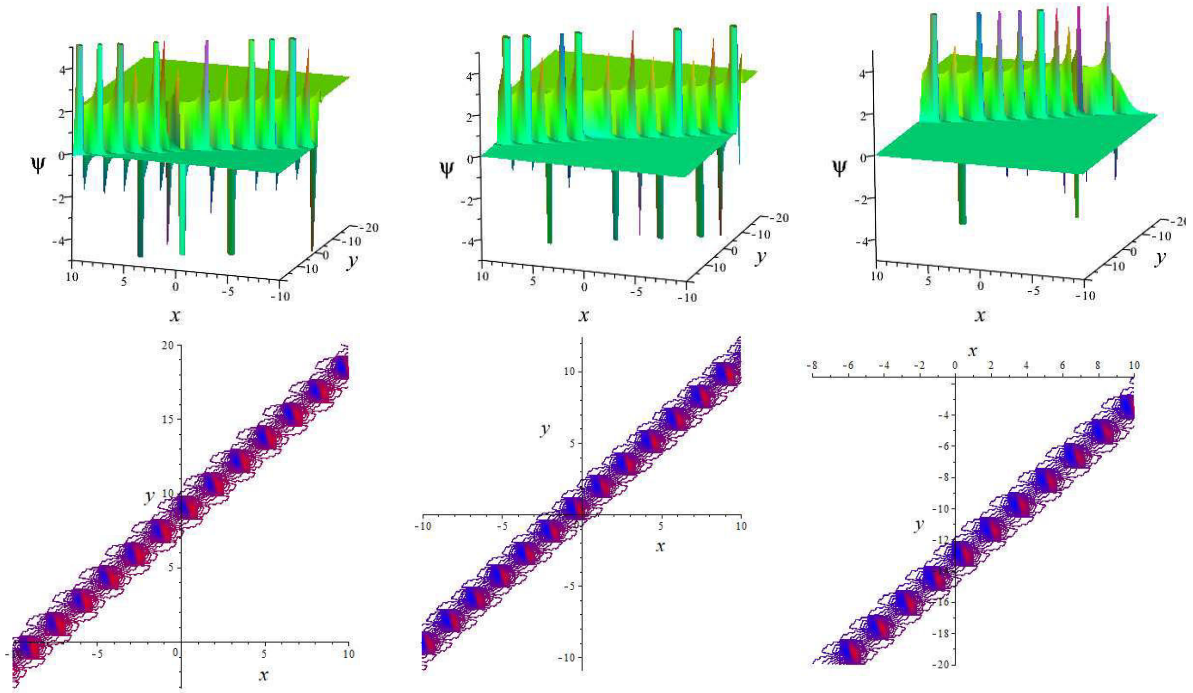

(a) $t=-4$ (b) $t=0$ (c) $t=7$

Fig-8.2: Outlook of the Eq. (8.11) for $a=1,\ b=1,\ c=1,\ \alpha_1=2,\ \beta_1=0,\ \gamma_1=-2,\ \delta_1=4,$ $\eta_1=1,\ \rho_1=1$ at $z=1$: 3D plot (upper) and its contour plot (below).

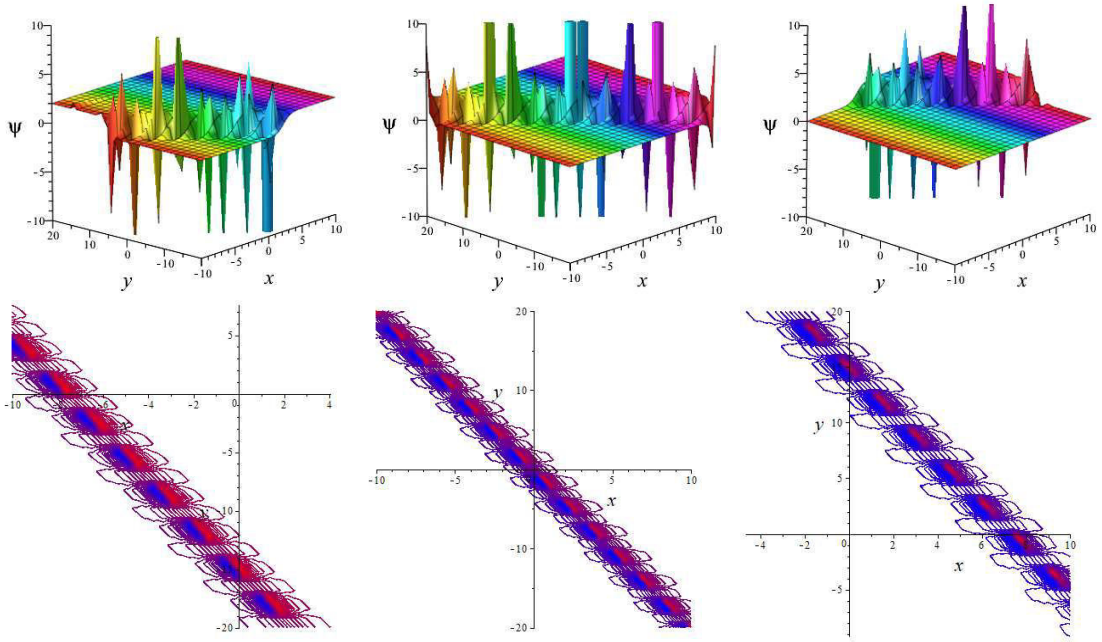

(a) $z=-3$ (b) $z=0$ (c) $z=3$

Fig-8.3: Outlook of the Eq. (8.11) for $a=1,\ b=1,\ c=1,\ \alpha_1=2,\ \beta_1=0.001,\ \gamma_1=1,$ $\delta_1=-2,\ \eta_1=-5,\ \rho_1=0.5$ at $t=0$: 3D plot (upper) and its contour plot (below).

$$\psi(x,y,z,t) = \{\ln(1+2\exp(M)\cos(\sigma), \tag{8.11}$$

where $M = \alpha_1 x + \gamma_1 y + \eta_1 z - (a(\alpha_1^3 - 3\alpha_1\beta_1^2) + b(\alpha_1^2\gamma_1 - 2\alpha_1\beta_1\delta_1 - \beta_1^2\gamma_1)$

$+ c(\alpha_1^2\eta_1 - 2\alpha_1\beta_1\rho_1 - \beta_1^2\eta_1))t$

and $\sigma = \beta_1 x + \delta_1 y + \rho_1 z - (a(3\alpha_1^2\beta_1 - \beta_1^3) + b(\alpha_1^2\delta_1 + 2\alpha_1\beta_1\gamma_1 - \beta_1^2\delta_1)$

$+ c(\alpha_1^2\rho_1 + 2\alpha_1\beta_1\eta_1 - \beta_1^2\rho_1))t.$

Here the wave equation Eq. (8.11) appears from 2-soliton solution degenerate into a lump shape breather wave by taking complex conjugate of free parameters. Actually, it comes with the combinations of exponential and sinusoidal functions. Dynamics of the wave equation Eq. (8.11) is viewed in **Fig-8.2** (3D diagram (above) & corresponding contour diagram (below)). Figures display that the solution reveals as lump style breather waves in the xy-plane with $z = 0$ and it moves towards the paradox ($t < 0$) with time goes (view **Fig-8.2(a)**), arrive at the paradox for $t = 0$ (view **Fig-8.2(b)**), and then go away from the paradox with times ($t > 0$) (view **Fig-8.2(c)**) and overall its movement each lump occur on a kink wave. Its direction, width and velocity remain the same in the overall propagation process and periodic lump occur equal distance from one another. Besides this, we skilled a similar phenomena when sketch viewed in the same xy-plane for $t = 0$. Here, the lump breather wave moves towards the paradox ($z < 0$) from negative quadrant with value of z increases (view **Fig-8.3(a)**), reach along the paradox at $z = 0$ (view **Fig-8.3(b)**), and then go away from the paradox through positive quadrant with increase of z (view **Fig-8.3(c)**) and overall its movement each lump occur on a kink wave.

8.3.2. Collision of single soliton with a lump style breather wave from 3-soliton solutions: Here, this subsection decides a collision between kink type line soliton and a lump style breather waves degenerate from other two solitons. From consider the three solitons $n = 3$, one soliton remain same and the other two solitons take its parameters as the complex conjugate new parametric values like $a_1 = \alpha_1 + i\beta_1$, $a_2 = \alpha_1 - i\beta_1$, $b_1 = \gamma_1 + i\delta_1$,

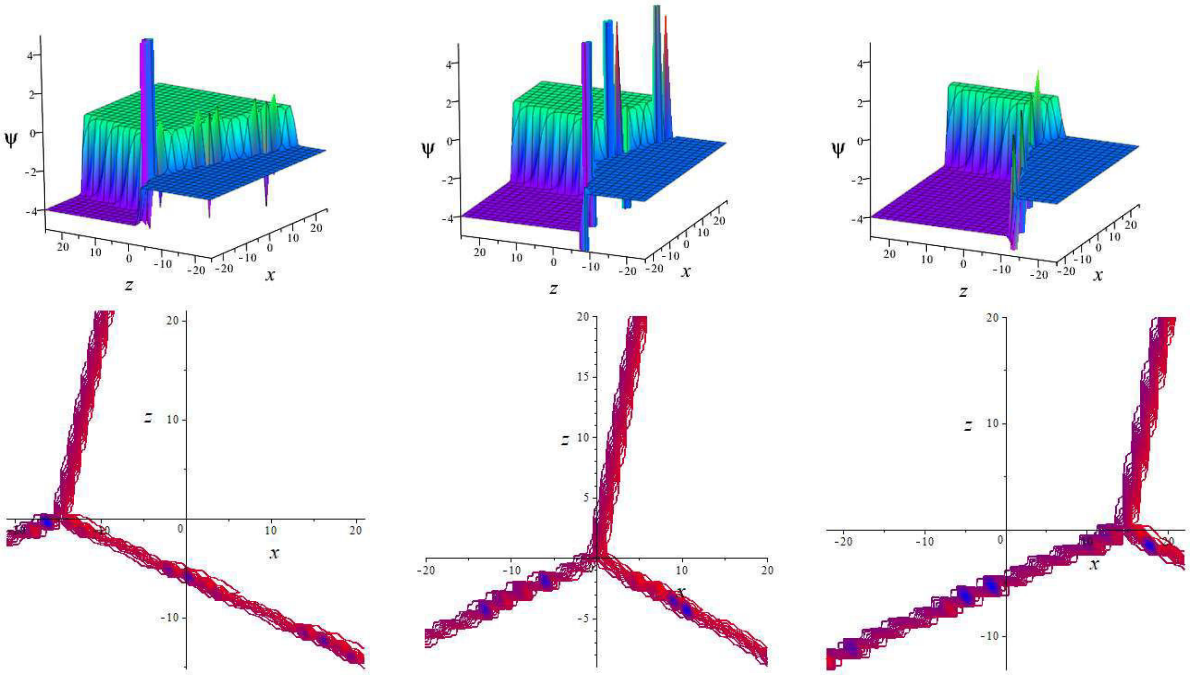

(a) $t=-1$ (b) $t=0$ (c) $t=1$

Fig-8.4: Interaction of single soliton with a lump shape breather wave of the Eq. (8.12) at $y=0$: 3-dimensional diagram (above) and corresponding contour diagram (under).

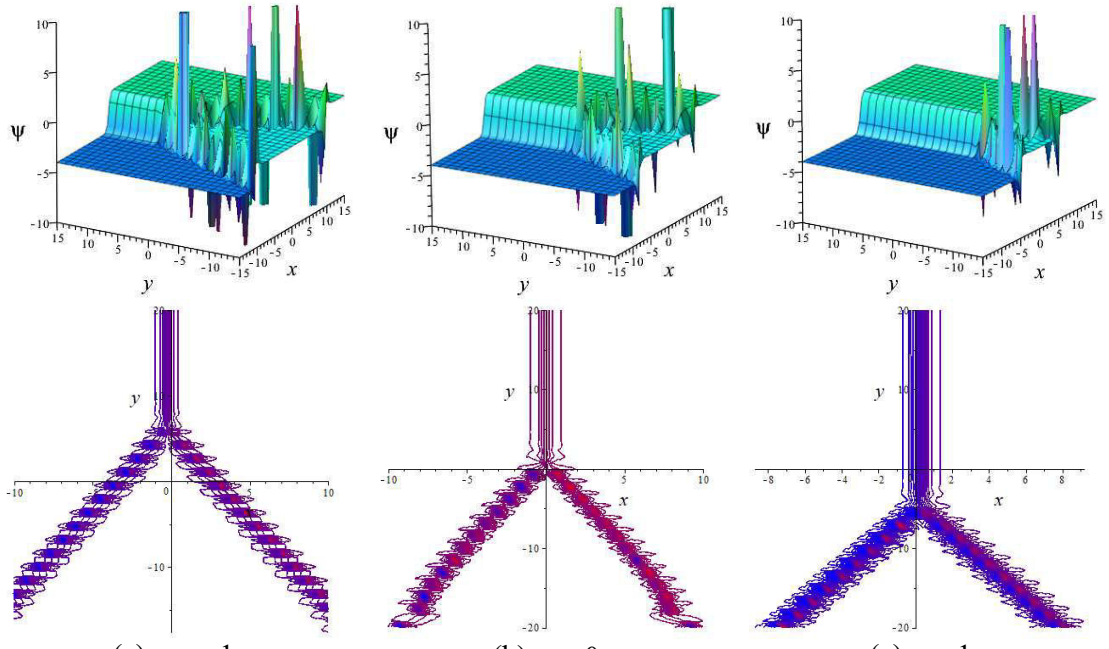

(a) $z=-1$ (b) $z=0$ (c) $z=1$

Fig-8.5: Interaction profile of single soliton with a lump shape breather wave of the Eq. (8.12) at $t=0$: 3-dimensional diagram (above) and corresponding contour diagram (under).

$b_2=\gamma_1-i\delta_1,\ c_1=\eta_1+i\rho_1,\ c_2=\eta_1-i\rho_1,\ a_3=d,\ b_3=e,\ c_3=k$ into the Eq. (8.7) along with the Eq. (8.5), Eq. (8.6) and Eq. (8.10) yields

$$\psi(x,y,z,t)=\ln\{1+2\exp(M)\cos(\sigma)+\exp(\lambda)\}_x, \tag{8.12}$$

where $M=\alpha_1x+\gamma_1y+\eta_1z-(a(\alpha_1^{\,3}-3\alpha_1\beta_1^{\,2})+b(\alpha_1^{\,2}\gamma_1-2\alpha_1\beta_1\delta_1-\beta_1^{\,2}\gamma_1)$

$+c(\alpha_1^{\,2}\eta_1-2\alpha_1\beta_1\rho_1-\beta_1^{\,2}\eta_1))t,$

$\sigma=\beta_1x+\delta_1y+\rho_1z-(a(3\alpha_1^{\,2}\beta_1-\beta_1^{\,3})+b(\alpha_1^{\,2}\delta_1+2\alpha_1\beta_1\gamma_1-\beta_1^{\,2}\delta_1)$

$+c(\alpha_1^{\,2}\rho_1+2\alpha_1\beta_1\eta_1-\beta_1^{\,2}\rho_1))t$

and $\lambda=dx+ey+kz-(ad^3+bd^2e+cd^2k)t$

The Eq. (8.12), exhibits a solution of the combo exponential and sinusoidal functions, demonstrate interaction of a line soliton (kink) and lump shape breather soliton arises into a kink wave, as sighted in the **Fig-8.4** and **Fig-8.5** for the values $p=1,\ q=1,\ r=1/3,$ $\alpha_1=-2,\ \beta_1=0.001,\ \gamma_1=-1,\ \delta_1=4,\ \eta_1=-5,\ \rho_1=1,\ d=-4,\ e=0.001,\ k=1.$

Figures display that the solution reveals as a kink and combo kinky-lump breather wave (few lump get in each kink wave) interact and degenerate into a kinky-lump breather wave (see 3D plots of **Fig-8.4(a-c)**) after interaction ($x>0$). Besides this, we skilled a similar phenomena when sketch viewed in the xy-plane with $t=0$ in the figures (**Fig-8.5**).

8.3.3. Collision of double kinky-lump shape breather waves degenerate into a single kinky-lump shape breather wave: To establish collision of double kinky-lump shape breather waves, we recall the four solitons solution from the general multi-soliton solution Eq. (8.7). Here, the four solitons solution ($n=4$) take its parameters as the complex conjugate new parametric values like then let $a_1=\alpha_1+i\beta_1,\ a_2=\alpha_1-i\beta_1,\ a_3=\alpha_2+i\beta_2,$ $a_4=\alpha_2-i\beta_2,\ b_1=\gamma_1+i\delta_1,\ b_2=\gamma_1-i\delta_1,\ b_3=\gamma_2+i\delta_2,\ b_4=\gamma_2-i\delta_2,\ c_1=\eta_1+i\rho_1,$ $c_2=\eta_1-i\rho_1,\ c_3=\eta_2+i\rho_2,\ c_4=\eta_2-i\rho_2$ into the Eq. (8.7) together with Eq. (8.5), Eq. (8.6) and Eq. (8.10) yields

$$\psi(x,y,t) = \ln\{1 + 2\exp(M_1)\cos(\sigma_1) + 2\exp(M_2)\cos(\sigma_2)\}_x, \tag{8.13}$$

where $M_1 = \alpha_1 x + \gamma_1 y + \eta_1 z - (a(\alpha_1^3 - 3\alpha_1\beta_1^2) + b(\alpha_1^2\gamma_1 - 2\alpha_1\beta_1\delta_1 - \beta_1^2\gamma_1)$
$+ c(\alpha_1^2\eta_1 - 2\alpha_1\beta_1\rho_1 - \beta_1^2\eta_1))t,$

$\sigma_1 = \beta_1 x + \delta_1 y + \rho_1 z - (a(3\alpha_1^2\beta_1 - \beta_1^3) + b(\alpha_1^2\delta_1 + 2\alpha_1\beta_1\gamma_1 - \beta_1^2\delta_1)$
$+ c(\alpha_1^2\rho_1 + 2\alpha_1\beta_1\eta_1 - \beta_1^2\rho_1))t,$

$M_2 = \alpha_2 x + \gamma_2 y + \eta_2 z - (a(\alpha_2^3 - 3\alpha_2\beta_2^2) + b(\alpha_2^2\gamma_2 - 2\alpha_2\beta_2\delta_2 - \beta_2^2\gamma_2)$
$+ c(\alpha_2^2\eta_2 - 2\alpha_2\beta_2\rho_2 - \beta_2^2\eta_2))t$

and $\sigma_2 = \beta_2 x + \delta_2 y + \rho_2 z - (a(3\alpha_2^2\beta_2 - \beta_2^3) + b(\alpha_2^2\delta_2 + 2\alpha_2\beta_2\gamma_2 - \beta_2^2\delta_2)$
$+ c(\alpha_2^2\rho_2 + 2\alpha_2\beta_2\eta_2 - \beta_2^2\rho_2))t.$

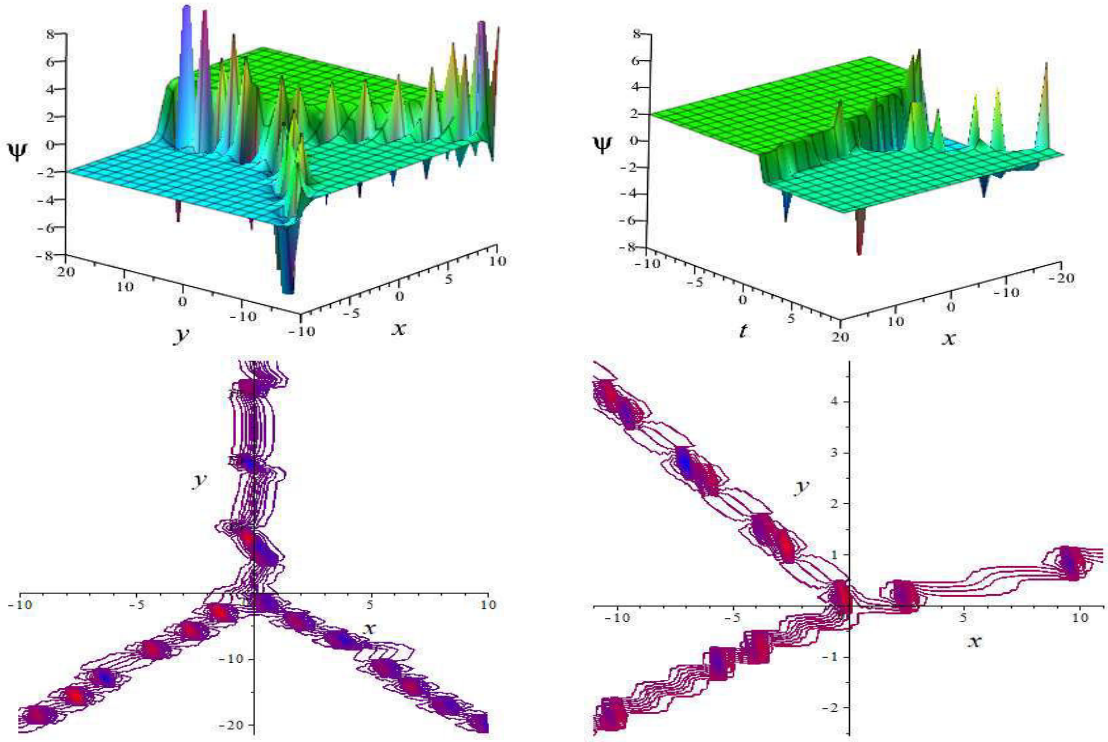

(a) $z = 0, t = 0$ (b) $y = 0, z = 0$

Fig-8.6: Interaction profile of two kinky-lump breather solitons of the Eq. (8.13): 3 dimensional diagram (above) and corresponding contour diagram (under).

The Eq. (8.13), exhibits a solution of combo exp-sinusoidal function, demonstrate interaction of double kinky-lump shape breather waves, as sighted in the **Fig-8.6** for the

values $p=2,\ q=-5,\ r=7,\ \alpha_1=2,\ \beta_1=0.001,\ \gamma_1=1,\ \delta_1=-2,\ \eta_1=1,\ \rho_1=0.5,$ $\alpha_2=-2,\ \beta_2=0.001,\ \gamma_2=1,\ \delta_2=-7,\ \eta_2=1/3,\ \rho_2=0.5$. **Fig-8.6** display that the solution reveals as a pair of combo kinky-lump breather waves degenerate into a single combo kinky-lump wave after interaction ($y>0$) (see 3D plots of **Fig-8.6(a)**) and after interaction ($x>0$) (see 3D plots of **Fig-8.6(b)**). After $y=0$ i.e., when $y>0$ **Fig-8.6(a)**, combo kinky-lump fused and degenerated into a single kinky-lump breather wave is cleared from its corresponding contour plots. After $x=0$ i.e., when $x>0$ **Fig-8.6(b)**, combo kinky-lump fused and degenerated into a single kinky-lump breather wave is cleared from its corresponding contour plots.

8.4. Conclusion

Hirota bilinear integral technique has been used successfully to derive n-soliton solutions of the STOL model **Fig-8.1**. We have obtained a kinky-lump breather (**Fig-8.2** & **Fig-8.3**), combo line kink and kinky-lump breather degenerate into single breather wave (**Fig-8.4** & **Fig-8.5**), and a pair of kinky-lump breather degenerate into single breather wave (**Fig-8.6**) solutions from two-, three- and four-solitons respectively by selecting complex conjugate values of involved parameters. We have been experienced with fission-fusion phenomena in **Fig-8.1, Fig-8.4, Fig-8.5** & **Fig-8.6** from interactions of multi-solitons, and kink-breather waves. The 3-dimensional and contour diagrams are presented to illustrate the dynamics of new properties of these collision solutions. The integral scheme can also be used to derive distinguish complex nonlinear models.

Chapter Nine

Conclusions

This dissertation has been presented exact traveling wave solutions of the three nonlinear models namely, the (2+1) Bogoyavlenskii's breaking soliton (BBS) equation, the (2+1)-dimensional Benjamin-Bona-Mahony-Burgers (BBMB) equation and the (3+1)-dimensional Sharma–Tasso–Olver-like (STOL) equation by applying Hirota bilinear method. We have successfully obtained the bilinear form and interaction solutions of the above three models. We also obtained multi-soliton solutions and their interaction solutions of the BBS and STOL model. We evaluated various characteristic of the solutions including, lump wave, fission-fusion and annihilation properties of lump wave. It is very interesting that we have the three new dynamics for BBMB and STOL models which are still unexplored in the literature. First one comes from the interaction of kink and lump wave degenerate a kinky-lump wave for the BBMB model. This kinky-lump wave split into double, triple, even large numbers of kinky-lump waves due to fission for the increase of the coefficient of cosine function gradually **(**See the **Fig-5.2)**. The second property is comes from the interaction of two quadratic polynomials (lump wave) and a periodic sinusoidal function degenerated a periodic-lump wave solutions of the STOL model gives hybrid lump wave solutions (see **Fig-6.3**) as increases of the coefficient of cosine function gradually. Third property is interaction among lump, kink and periodic waves provides a double kinky-periodic lump waves (see **Fig-6.8**). The lump into the double kink wave split due to fission produces a hybrid lump wave into a double kinky wave. All special properties of the obtained solutions are illustrated clearly with a number of 3D plot, 2D plot, density plot, curve plot and contour plot by choosing suitable parametric values with the aid of the computational software Maple 18. The acquired results can enrich the dynamical properties of the higher dimensional nonlinear scenarios in the engineering fields.

References

[1] **M. S. Ullah**, H. O. Roshid, M. Z. Ali, A. Biswas, M. Ekici, S. Khan, L. Moraru, A. K. Alzahrani, M. R. Belic, Optical soliton polarization with Lakshamanan-Porsezian-Daniel model by unified approach, Results Phys., 22 (2021) 103958.

[2] **M. S. Ullah**, H. O. Roshid, M. Z. Ali, N. F. M. Noor, Novel dynamics of wave solutions for Cahn-Allen and diffusive predator-prey models using MSE scheme, Partial Differ. Equ. Appl. Math., 3 (2021) 100017.

[3] **M. S. Ullah**, H. O. Roshid, W. X. Ma, M. Z. Ali, Z. Rahman, Interaction phenomena among lump, periodic and kink wave solutions to a (3+1)-dimensional Sharma-Tasso-Olver-like equation, Chin. J. Phys., 68 (2020) 699-711.

[4] **M. S. Ullah**, H. O. Roshid, M. Z. Ali, Z. Rahman, Dynamical structures of multi-soliton solutions to the Bogoyavlenskii's breaking soliton equations, Eur. Phys. J. Plus, 135(3) (2020) 282.

[5] **M. S. Ullah**, H. O. Roshid, M. Z. Ali, Z. Rahman, Novel exact solitary wave solutions for the time fractional generalized Hirota–Satsuma coupled KdV model through the generalized Kudryshov method, Contemp. Math., 1(1) (2019) 25-32.

[6] **M. S. Ullah**, M. Z. Ali, H. O. Roshid, A. R. Seadawy, D. Baleanu, Collision phenomena among lump, periodic and soliton solutions to a (2+1)-dimensional Bogoyavlenskii's breaking soliton model, Phys. Lett. A, 397 (2021) 127263.

[7] **M. S. Ullah**, M. Z. Ali, H. O. Roshid, M. F. Hoque, Collision phenomena among lump, periodic and stripe soliton solutions to a (2+1)-dimensional Benjamin-Bona-Mahony-Burgers Model, Eur. Phys. J. Plus, 136 (2021) Revisions Being Processed.

[8] B. Q. Li, Y. L. Ma, Rogue waves for the optical fiber system with variable coefficients, Optik, 158 (2018) 177-184.

[9] O. A. Ilhan, T. A. Sulaiman, H. Bulut, H. M. Baskonus, On the new wave solutions to a nonlinear model arising in plasma physics, Eur. Phys. J. Plus, 133(1) (2018) 27.

[10] M. Aguero, M. Najera and M. Carrillo, Nonclassic solitonic structures in DNA's vibrational dynamics, International Journal of Modern Physics B, 22 (2008) 2571-2582.

[11] W. Alka, A. Goyal and C.N. Kumar, Nonlinear dynamics of DNA-Riccati generalized solitary wave solutions, Phys. Lett. A, 375 (2011) 480-483.

[12] H. Triki, A. Biswas, S. P. Moshokoa, M. Belic, Optical solitons and conservation laws with quadratic-cubic nonlinearity, Optik, 128 (2017) 63–70.

[13] B. Q. Li, Y. L. Ma, Periodic solutions and solitons to two complex short pulse (CSP) equations in optical fiber, Optik, 144 (2017) 149–155.

[14] M. F. Hoque, H. O. Roshid, Optical soliton solutions of the Biswas-Arshed model by the $\tan(\theta/2)$ expansion approach, Phys. Scr., 95 (2020) 075219.

[15] B. Kibler, J. Fatome, C. Finot, G. Millot, F. Dias, G. Genty, N. Akhmediev, J. M. Dudley, The Peregrine soliton in nonlinear fibre optics, Nat. Phys., 6 (2010) 790–795.

[16] M. Lakshmanan, K. Porsezian, M. Daniel, Effect of discreteness on the continuum limit of the Heisenberg spin chain, Phys. Lett. A, 133(9) (1988)483–488.

[17] K. Diethelm, N. J. Ford, J. Math. Anal. Appl., 265(2) (2002) 229-248.

[18] H. Rezazadeh, H. Aminikhah, A. R. Sheikhani, Stability analysis of Hilfer fractional differential systems, Math. Commun., 21 (1) (2016) 45-64.

[19] I. Podlubny, Fractional differential equations, Academic Press, New York, 198 (1998).

[20] K. B. Oldham, J. Spanier, The fractional calculus, Academic Press, New York, (1974).

[21] J. S. Russell, Report on waves: 14th meeting of the British association for the advancement of science, John Murray, London, (1844) 311–390.

[22] J. Villarroel, J. Prada, P. G. Estévez, Dynamics of lump solutions in a 2+1 NLS equation, Stud Appl Math, 122 (2009) 395–410.

[23] S. V. Manakov, V. E. Zakharov, L. A. Bordag, A. R. Its, V. B. Matveev, Two-dimensional solitons of the Kadomstev-Petviashvili equation and their interaction, Phys. Lett. A, 63(3) (1977) 205-206.

[24] H. O. Roshid, Lump solutions to a (3+ 1)-dimensional potential-Yu–Toda–Sasa–Fukuyama (YTSF) like equation, Int. J. Appl. Comput. Math., 3 (2017) 1455-1461.

[25] W. X. Ma, Lump solutions to the Kadomtsev–Petviashvili equation, Phys. Lett. A, 379 (2015) 1975–1978.

[26] J. P. Yu, Y. L. Sun, Study of lump solutions to dimensionally reduced generalized KP equations, Nonlinear Dynam., 87 (2017) 2755-2763.

[27] S. T. Chen, W. X. Ma, Lump solutions to a generalized Bogoyavlensky-Konopelchenko equation, Front. Math. China, 13(3) (2018) 525-534.

[28] Z. Xu, H. Chen, Z. Dai, Rogue wave for the (2+1)-dimensional Kadomtsev–Petviashvili equation, Appl. Math. Lett., (37) (2014) 34–38.

[29] C. Kharif, E. Pelinovsky, A. Slunyaev, Rogue waves in the ocean, Springer, Berlin, Germany, (2009).

[30] L. Stenflo, M. Marklund, Rogue waves in the atmosphere, Plasma Phys., 76(3-4) (2010) 293–295.

[31] L. C. Zhao, Dynamics of nonautonomous rogue waves in Bose–Einstein condensate, Annals of Physics, 329 (2013) 73-79.

[32] N. Akhmediev, A. Ankiewicz, M. Taki, Waves that appear from nowhere and disappear without a trace, Phys. Lett. A, 373 (2009) 675–678.

[33] L. Draper, Freak wave, Mar. Obs., 35 (1965) 193–195.

[34] D. H. Peregrine, Water waves, nonlinear Schrödinger equations and their Solutions, J. Aust. Math. Soc. Ser. B, 25 (1983) 16-43.

[35] D. J. Kedziora, A. Ankiewicz, N. Akhmediev, Second-order nonlinear Schrödinger equation breather solutions in the degenerate and rogue wave limits, Phys. Rev. E, 85 (2012) 066601.

[36] N. Akhmediev, V. I. Korneev, Modulation instability and periodic solutions of the nonlinear Schrödinger equation, Theoret. Math. Phys., 69 (1986) 1089–1093.

[37] Y. C. Ma, On the multi-soliton solutions of some nonlinear evolution equations, Stud. Appl. Math., 60 (1979) 73–82.

[38] M. L. Wang, X. Z. Li, J. L. Zhang, The (G'/G)-expansion method and travelling wave solutions of nonlinear evolution equations in mathematical physics, Phys. Lett. A, 372(4) (2008) 417−423.

[39] A. A. Gaber, A. F. Aljohani, A. Ebaid, J. T. Machado , The generalized Kudryashov method for nonlinear space–time fractional partial differential equations of Burgers type, Nonlinear Dynam., 95 (2019) 361–368.

[40] R. Hirota, Exact Solution of the Korteweg-de Vries Equation for Multiple Collisions of Solitons, Phys. Rev. Lett. 27 (1971) 1192–1194.

[41] Z. Hammouch, T. Mekkaoui, P. Agarwal, Optical solitons for the Calogero–Bogoyavlenskii–Schiff equation in (2 + 1) dimensions with time-fractional conformable derivative, Eur Phys J Plus, 133(7) (2018) 248.

[42] R. Kumar, M. Kumar, A. Kumar, Some soliton solutions of non linear partial differential equations by tan-cot method, IOSR J. Math., 6(6) (2013) 23–28.

[43] A. M. Wazwaz, The tanh-coth method for solitons and kink solutions for nonlinear parabolic equations, Appl. Math. Comput., 188 (2007) 1467-1475.

[44] A. R. Seadawa, The solutions of the Boussinesq and generalized fifth-order KdV equations by using the direct algebraic method, Appl. Math. Sci., 6(82) (2012) 4081-4090.

[45] V. B. Matveev, M. A. Salle, Darboux transformation and solitons, Springer, Berlin, 1991.

[46] H. O. Roshid, M. F. Hoque, M. A. Akbar, New extended (G'/G)-expansion method for traveling wave solutions of nonlinear partial differential equations (NPDEs) in mathematical physics, Italian Journal of pure and applied mathematics, 33 (2014) 175-190.

[47] H. O. Roshid, N. Rahman, M.A. Akbar, Traveling wave solutions of nonlinear Klein-Gordon equation by extended (G'/G)-expansion method, Annals of pure and applied mathematics, 3(1) (2013) 10-16.

[48] H. O. Roshid, M. A. Rahman, The $\exp(-\Phi(\eta))$-expansion method with application in the (1+1)-dimensional classical Boussinesq equations, Results in Physics, 4 (2014) 150-155.

[49] M. A. Abdou, The extended F-expansion method and its application for a class of nonlinear evolution equations, Chaos, Solitons and Fractals, 31(1) (2007) 95–104.

[50] H. Jafari, N. Kadkhoda, Application of simplest equation method to the (2+ 1)-dimensional nonlinear evolution equations, New Trends in Mathematical Sciences, 2(2) (2014) 64-68.

[51] N. K. Vitanov, Z. I. Dimitrova, H. Kantz, Modified method of simplest equation and its application to nonlinear PDEs, Appl. Math. Comput., 216 (2010) 2587- 2595.

[52] A. J. M. Jawad, M. D. Petkovic, A. Biswas, Modified simple equation method for nonlinear evolution equations, Appl. Math. Comput., 217 (2010) 869–77.

[53] E.M.E. Zayed, A note on the modified simple equation method applied to Sharma–Tasso–Olver equation, Appl. Math. Comput., 218 (2011) 3962–4.

[54] Y. Ugurlu, Exp-function method for the some nonlinear partial differential equations. Mathematica Aeterna, 3(1) (2013) 57-70.

[55] Tascan, A. Bekir, A traveling wave solutions of the Cahn-Allen equation by using first integral method, Appl. Math. Comput., 207 (2007) 279-282.

[56] E. Fan, H. Zhang, A note on the homogeneous balance method, Phys. Lett. A, 246 (1998) 403–406.

[57] D. Arseven, T. Zi, An analytical study for Fisher type equations by using homotopy perturbation method, Comput. Math. Appl., 60(3) (2010) 602–609.

[58] M. J. Ablowitz, M. A. Ablowitz, P. A. Clarkson, Solitons, Nonlinear evolution equations and inverse scattering (Cambridge University Press, Cambridge, 1991).

[59] M. R. Miura, Backlund transformation, Springer, Berlin, 1978.

[60] H. Bulut, S. S. Atas, H. M. Baskonus, Some novel exponential function structures to the Cahn–Allen equation, Cogent Phys, 3(1) (2016) 1240886.

[61] S. V. Petrovskii, H. Malchow and B. L. Li, An exact solution of a diffusive predator-prey system, Proceedings of the Royal Society A, 461 (2005) 1029-1053.

[62] R. A. Kraenkel, K. Manikandan and M. Senthivelan, On certain new exact solutions of a diffusive predator-prey system, Commun Nonlinear Sci Numer Simul, 18 (2013) 1269-1274.

[63] A. A. Al-Qarni, A. Ebaid, A. A. Alshaery, H. O. Bakodah, A. Biswas, S. Khan, M. Ekici, Q. Zhou, S. P. Moshokoa, M. R. Belic, Optical solitons for Lakshmanan–Porsezian–Daniel model by Riccati equation approach, Optik, 182 (2019) 922–929.

[64] S. Arshed, A. Biswas, F. B. Majid, Q. Zhou, S. P. Moshokoa, M. Belic, Optical solitons in birefringent fibers for Lakshmanan-Porsezian-Daniel model using $\exp(-\phi(\xi))$-expansion method, Optik, 170 (2018) 555–560.

[65] A. Biswas, Y. Yildirim, E. Yasar, R. T. Alqahtani, Optical solitons for Lakshmanan-Porsezian-Daniel model with dual-dispersion by trial equation method, Optik, 168 (2018) 432–439.

[66] A. Bansal, A. Biswas, H. Triki, Q. Zhou, S. P. Moshokoa, M. Belic, Optical solitons and group invariant solutions to Lakshmanan-Porsezian-Daniel model in optical fibers and PCF, Optik, 160 (2018) 86–91.

[67] R. T. Alqahtani, M. M. Babatin, A. Biswas, Bright optical solitons for Lakshmanan-Porsezian-Daniel model by semi-inverse variational principle, Optik, 154 (2018) 109–114.

[68] A. Biswas, M. Ekici, A. Sonmezoglu, M. M. Babatin, Optical solitons with differential group delay and dual-dispersion for Lakshmanan-Porsezian-Daniel model by extended trial function method, Optik, 170 (2018) 512–519.

[69] J. V. Guzman, R. T. Alqahtani, Q. Zhou, M. F. Mahmood, S. P. Moshokoa, M. Z. Ullah, A. Biswas, M. Belic, Optical solitons for Lakshmanan-Porsezian-Daniel model with spatio-temporal dispersion using the method of undetermined coefficients, Optik, 144 (2017) 115–123.

[70] S. Akcagil, T. Aydemir, A new application of the unified method, NTMSCI, 6 (2018) 185-199.

[71] R. Hirota, The Direct method in soliton theory, Camb. Uni. Press: Cambridge, (2004).

[72] J. B. Zhang, W. X. Ma, Mixed lump-kink solutions to the BKP equation, Comput. Math. Appl., 74(3) (2017) 591–596.

[73] H. Q. Zhao, W. X. Ma, Mixed lump–kink solutions to the KP equation, Comput. Math. Appl., 74(6) (2017) 1399–1405.

[74] W. X. Ma, X. Yong, H. Q. Zhang, Diversity of interaction solutions to the (2+1)-dimensional Ito equation, Comput. Math. Appl., 75(1) (2018) 289–295.

[75] H. O. Roshid, W. X. Ma, Dynamics of mixed lump-solitary waves of an extended (2 + 1)-dimensional shallow water wave model, Phys. Lett. A, 382 (2018) 3262-3268.

[76] W. Liu, Y. Zhang, Multiple rogue wave solutions for a (3+1)-dimensional Hirota bilinear equation, Appl. Math. Lett., 98 (2019) 184-190.

[77] G. F. Deng, Y. T. Gao, J. J. Su, C. C. Ding, Multi-breather wave solutions for a generalized (3+1)-dimensional Yu–Toda–Sasa–Fukuyama equation in a two-layer liquid, Appl. Math. Lett., 98 (2019) 177-183.

[78] W. X. Ma, Interaction solutions to the Hirota-Satsuma-Ito equation in (2+1)-dimensions, Front. Math. China, 14(3) (2019), 619-629.

[79] T. Xia, S. Xiong, Exact solutions of (2+1) -dimensional Bogoyavlenskii's breaking soliton equation with symbolic computation, Compu. Math. Appl., 60 (3) (2010) 919-923.

[80] M. Kazeminia, P. Tolou, J. Mahmoudi, I. Khatami, Solitary and periodic solutions of BBMB equation via exp-function method, Adv. studies Theor. Phys., 3 (2009) 461-471.

[81] A. M. Wazwaz, S. A. E. Tantawy, New (3+1)-dimensional equations of Burgers type and Sharma-Tasso-Olver type: multiple-soliton solutions, Nonlinear Dyn., 87 (2017) 2457−2461.

[82] Z. Z. Ganji, D. D. Gangi, Y. Rostamiyan, Solitary wave solutions for a time-fraction generalized Hirota–Satsuma coupled KdV equation by an analytical technique, Appl. Math. Model., 33(7) (2009) 3107-3113.

[83] M. Shateri, D. D. Ganji, Solitary wave solutions for a time-fraction generalized Hirota-Satsuma coupled KdV equation by a new analytical technique, Int. J. Differ. Equ. (2010) 954674.

[84] S. Guo , L. Mei , Y. Li , Y. Sun , The improved fractional sub-equation method and its applications to the space–time fractional differential equations in fluid mechanics, Phys. Lett. A, 376(4) (2012) 407–411.

[85] A. Neirameh, Soliton solutions of the time fractional generalized Hirota-Satsuma coupled KdV system, Appl. Math. Inf. Sci., 9(4) (2015) 1847-1853.

[86] G. M. Mophou, Existence and uniqueness of mild solutions to impulsive fractional differential equations , Nonlinear Anal., 72 (2010) 1604-1615.

[87] G. Wang, B. Ahmad, L. Zhang, Some existence results for impulsive nonlinear fractional differential equations with mixed boundary conditions, Comput. Math. Appl., 62(3) (2011) 1379-1397.

[88] X. Zhang, X. Huang, Z. Liu, The existence and uniqueness of mild solutions for impulsive fractional equations with nonlocal conditions and infinite delay, Nonlinear Anal. Hybrid Syst., 4 (2010) 775-781.

[89] B. Ahmad, S. Sivasundaram, Existence results for nonlinear impulsive hybrid boundary value problems involving fractional differential equations, Nonlinear Anal.: Hybrid Syst., 3 (2009) 251-258.

[90] A. B. Emad, A. Salamand, J. H. Ahmed, Solutions of the (2+1) space–time fractional Burgers equation, American Journal of Computational and Applied Mathematics, 6(2) (2016) 109-117.

[91] A. Yokus, D. Kaya, Numerical and exact solutions for time fractional Burgers' equation, J. Nonlinear Sci. Appl., 10 (2017) 3419–3428.

[92] T. A. Sulaiman, M. Yavuz, H. Bulut, H. M. Baskonus, Investigation of the fractional coupled viscous Burgers' equation involving Mittag-Leffler kernel, Physica A, 527(1) (2019) 121-126.

[93] H. Bulut, Y. Pandir, S. T. Demiray, Exact solutions of time-fractional KdV equations by using generalized Kudryashov method, International Journal of Modeling and Optimization, 4(4) (2014) 315-320.

[94] R. Khalil, M. A. Horani, A. Yousef , M. Sababheh, A new definition of fractional derivative, J. Comput. Appl. Math., 264 (2014) 65–70.

[95] F. Mahmud, M. Samsuzzoha, M. A. Akbar, The generalized Kudryashov method to obtain exact traveling wave solutions of the PHI-four equation and the Fisher equation, Results Phys., 7 (2017) 4296-4302.

[96] A. M. Wazwaz, New solitons and kinks solutions to the Sharma-Tasso-Olver equation, Appl. Math. Comput., 188 (2007) 1205–1213.

[97] Y. Uğurlu, D. Kaya, Analytic method for solitary solutions of some partial differential equations, Phys. Lett. A, 370 (2007) 251–259.

[98] J. T. Pan, W. Z. Chen, A new auxiliary equation method and its application to the Sharma-Tasso-Olver model, Phys. Lett. A, 373 (2009) 3118–3121.

[99] A. Bekir, A. Boz, Exact solutions for nonlinear evolution equations using exp-function method, Phys. Lett. A, 372 (2008) 1619–1625.

[100] Y. He, S. Li, Y. Long, Exact solutions to the Sharma-Tasso-Olver equation by using improved (G'/G)-expansion method, J. Appl. Math., (2013) 247234.

Partial Differential Equations in Applied Mathematics 3 (2021) 100017

Contents lists available at ScienceDirect

Partial Differential Equations in Applied Mathematics

journal homepage: www.elsevier.com/locate/padiff

Novel dynamics of wave solutions for Cahn–Allen and diffusive predator–prey models using MSE scheme

Mohammad Safi Ullah [a,b,*], Harun-Or-Roshid [b,c], M. Zulfikar Ali [b], N.F.M. Noor [d]

[a] Department of Mathematics, Comilla University, Cumilla 3506, Bangladesh
[b] Department of Mathematics, Rajshahi University, Rajshahi 6205, Bangladesh
[c] Department of Mathematics, Pabna University of Science and Technology, Pabna 6600, Bangladesh
[d] Institute of Mathematical Sciences, Faculty of Science, University of Malaya, 50603 Kuala Lumpur, Malaysia

ARTICLE INFO

Keywords:
The MSE scheme
The Cahn–Allen model
Diffusive predator–prey model
Traveling wave
Solitary wave

ABSTRACT

By employing modified simple equation (MSE) scheme, we estimate the presence of stable kink soliton and kinky-periodic rogue wave solutions; unstable singular kink wave solutions of the biological dynamical models as a Cahn–Allen model and a diffusive predator–prey model. This model frequently occurs in various nonlinear science including quantum physics, plasmas and biophysics. We present some novel exact explicit solutions of the exponential form of both Cahn–Allen and diffusive predator–prey models with some free parametric values. We also derive particular solutions from the explicit solutions selecting some definite values of the free parametric values. As a result, kink, singular kink and kinky-periodic lump wave surfaces are achieved of the solutions. Lastly, the variety and graphic representations of the composition make the models dynamic. Stable and unstable situations are explained in detail from the analysis of the profiles.

1. Introduction

The mathematical representing of happenings in nature can be revealed by differential equations. It is well familiar that abundant categories of the physical occurrences in the field of fluid dynamics, quantum physics, chemical physics, electricity and plasmas are demonstrated by nonlinear models and the existence of solitary waves in nature is frequently. However, nonlinear behavior is a challenging due to some minor changes in time-related parametric values; it is not comfortable to manage the non-linear representative of the organism very quickly. Nonlinearity is responsible for the development of local waves and has the ability to carry energy without wastage which is a very fascinating matter.[1,2] Otherwise, rapidly growing the spread of infection may cause a disaster state in a community. To tackle the unavailable state or to remain a suitable state, we have to learn the dissimilar types of solutions of the dynamical system in a model of Cahn–Allen or any type of predator–prey model. As in tragedy state waves or to keep emerges location, the height and width of population size is very essential. If we resolve the model of dynamical systems of such difficulties by applying diverse approaches, we can find the best approach of appreciative such potential disasters and then earnings necessary precautions. Thus, the concern becomes more challenging and hence decisive solutions are needed. The solutions of the equation have a crucial impression on mathematical physics and engineering. Recently, there has been a tremendous increased to find the exact solutions of nonlinear models. Various effective schemes have been reputed and enriched, such as the $\tan(\varphi(\xi)/2)$-expansion scheme,[3] the generalized Kudryshov scheme,[4] the (G'/G)-expansion scheme,[5] the sine–Gordon expansion scheme,[6–8] the F-expansion scheme,[9] the exp-function scheme,[10,11] the MSE scheme,[12–15] first integral scheme,[16] Simple equation scheme,[17] Bilinear scheme,[18–21] the Exp-$(-\phi(\xi))$-expansion scheme,[22] the tanh scheme[23] and so on.[24–35] All most all of the above schemes are contingent on computational software except the MSE scheme. The MSE scheme is a very effective and reliable procedure settled successfully by Vitanov[12] and the reference therein.[12–15]

The ambition of this manuscript is to seek novel exact solutions together with topological soliton, periodic cusp soliton, periodic bell solutions of the well-recognized Cahn–Allen model[11,16,35] and diffusive predator–prey model[33,34] via MSE scheme.

2. Description of the MSE scheme

Consider a general form of a nonlinear model as

$$H(u, u_t, u_x, u_{xt}, u_{xx}, \ldots \quad \ldots) = 0, \tag{2.1}$$

with real function $u(\xi) = u(x,t)$ and H is a polynomial of $u(x,t)$. We present the key steps of the scheme as follows:

* Corresponding author at: Department of Mathematics, Comilla University, Cumilla 3506, Bangladesh.
E-mail addresses: safi.ru1985@gmail.com (M.S. Ullah), harunorroshidmd@gmail.com (H.O. Roshid), zulfi1022002@yahoo.com (M.Z. Ali), drfadiya@um.edu.my (N.F.M. Noor).

https://doi.org/10.1016/j.padiff.2020.100017
Received 31 August 2020; Received in revised form 11 December 2020; Accepted 14 December 2020

Step 1: Let us combine the real variables x and t by a combined variable ξ as

$$u(\bar{r},t) = u(\xi),\ \xi = \overline{P}.\bar{r} \pm wt, \tag{2.2}$$

where $\overline{P} = l\hat{i} + m\hat{j} + n\hat{k}$ and $\bar{r} = x\hat{i} + y\hat{j} + z\hat{k}$ with real constants l, m, n, wave amount k and wave velocity w.

By the above relation the Eq. (2.1) converted to the ordinary differential equation as follows

$$G(u, u', u'' \ldots \ \ldots \ \ldots) = 0, \tag{2.3}$$

where G is a polynomial in $u(\xi)$ and its derivatives.

Step 2: Consider the trial solution of Eq. (2.3) as

$$u(\xi) = \sum_{i=0}^{n} A_i \left(\frac{S'(\xi)}{S(\xi)}\right)^i, \tag{2.4}$$

with real constants $A_i (i = 0, 1, \ldots, n)$ and unknown function $S(\xi)$.

Step 3: By balancing the derivative of highest order and nonlinear terms in Eq. (2.3), we can find the value of n in Eq. (2.4).

Step 4: From Eqs. (2.4) and (2.3), we get a polynomial of $(S'(\xi)/S(\xi))$ and its derivatives and $(S(\xi))^{-i}, (i = 0, 1, 2, \ldots, n)$, and then equating the coefficients of $(S(\xi))^{-i}, (i = 0, 1, 2, \ldots, n)$ equal to zero. This produces gives an algebraic system which can be solved to obtain $A_i (i = 0, 1, 2, \ldots, n)$,$S(\xi)$. Then we can find the solution of the Eq. (2.1).

Remark. In comparison the MSE scheme with the simple equation scheme,[17] it is seen that simple equation scheme depend upon an auxiliary equation (Riccati equation) but MSE scheme is independent and can perform directly without help of any auxiliary equation. On the other hand, Simple equation gives results which are special case of Modified equation scheme.

3. Illustrative examples

Here, we include two examples to make clear the suitability of the MSE scheme to solve nonlinear models declared above.

3.1. Example-1: Traveling wave solution of Cahn–Allen model

Let us consider nonlinear model given as

$$u_t = u_{xx} - u^m + u. \tag{3.1}$$

For $m = 3$, Eq. (3.1) suits to Cahn–Allen model.[11,16,35] This model occurs in various scientific areas including biophysics, quantum physics and plasmas. To solve this model, we use transformation $\xi = kx + wt$, for wave amount k and wave velocity w. Taking help of this transformation, Eq. (3.1) converts to an ordinary differential equation

$$wu' - k^2u'' + u^3 - u = 0. \tag{3.2}$$

Balancing u^3 with u'' we receive the unknown order of solution as $n = 1$. Hence the trial solution Eq. (2.4) takes the form as

$$u(\xi) = A_0 + A_1 \frac{S'(\xi)}{S(\xi)}. \tag{3.3}$$

Now, we can compute the terms:

$$u'(\xi) = A_1 \frac{S''(\xi)}{S(\xi)} - A_1 \left(\frac{S'(\xi)}{S(\xi)}\right)^2, \tag{3.4}$$

$$u''(\xi) = A_1 \frac{S'''(\xi)}{S(\xi)} - 3A_1 \frac{S''(\xi)S'(\xi)}{S^2(\xi)} + 2A_1 \left(\frac{S'(\xi)}{S(\xi)}\right)^3. \tag{3.5}$$

Putting Eqs. (3.3)–(3.5) in the Eq. (3.2) and equating coefficients of same powers of $\frac{S'(\xi)}{S(\xi)}$, we gain:

$$\text{Coefficient of } (S(\xi))^0 : A_0^3 - A_0 = 0, \tag{3.6}$$

$$\text{Coefficient of } (S(\xi))^{-1} : -k^2A_1S'''(\xi) + 3A_0^2A_1S'(\xi) + wA_1S''(\xi) - A_1S'(\xi) = 0, \tag{3.7}$$

$$\text{Coefficient of } (S(\xi))^{-2} : -wA_1\left(S'(\xi)\right)^2 + 3k^3A_1S'(\xi)S''(\xi) + 3A_0A_1^2\left(S'(\xi)\right)^2 = 0, \tag{3.8}$$

$$\text{Coefficient of } (S(\xi))^{-3} : A_1(A_1^2 - 2k^2)\left(S'(\xi)\right)^3 = 0. \tag{3.9}$$

From Eq. (3.6), we achieve $A_0 = 0, 1, -1$ and from Eq. (3.9) we can receive the values $A_1 \neq 0$ and thus $A_1 = \pm\sqrt{2}k$ and

$$\frac{S'''}{S''} = \frac{3k^2(3A_0^2 - 1) + w(w - 3A_0A_1)}{k^2(w - 3A_0A_1)}. \tag{3.10}$$

Integrating we have

$$S'' = c_1 \exp\left(\frac{3k^2(3A_0^2 - 1) + w(w - 3A_0A_1)}{k^2(w - 3A_0A_1)}\xi\right). \tag{3.11}$$

From Eq. (3.8), we also get,

From Eq. (3.8), we also get,

$$S' = \frac{3c_1k^2}{w - 3A_0A_1} \exp\left(\frac{3k^2(3A_0^2 - 1) + w(w - 3A_0A_1)}{k^2(w - 3A_0A_1)}\xi\right). \tag{3.12}$$

Integrating Eq. (3.12) one time, we have

$$S = \frac{3c_1k^4}{3k^2(3A_0^2 - 1) + w(w - 3A_0A_1)} \times \exp\left(\frac{3k^2(3A_0^2 - 1) + w(w - 3A_0A_1)}{k^2(w - 3A_0A_1)}\xi\right) + c_2. \tag{3.13}$$

Using Eqs. (3.12) and (3.13), we attain to the solution

$$u = A_0 + \frac{3c_1A_1k^2}{w - 3A_0A_1} \times \frac{\exp\left(\frac{3k^2(3A_0^2-1)+w(w-3A_0A_1)}{k^2(w-3A_0A_1)}\xi\right)}{\frac{3c_1k^4}{3k^2(3A_0^2-1)+w(w-3A_0A_1)} \exp\left(\frac{3k^2(3A_0^2-1)+w(w-3A_0A_1)}{k^2(w-3A_0A_1)}\xi\right) + c_2}, \tag{3.14}$$

where $\xi = k(x \pm \frac{3}{\sqrt{2}}t)$ with $w = \pm\frac{3}{\sqrt{2}}k$. Here c_1 and c_2 are arbitrary constants.

Case-I: For the set $A_0 = 0, A_1 = \pm\sqrt{2}k$, we get

$$u = \pm\frac{3\sqrt{2}c_1k^3}{w} \times \frac{\exp\left(\frac{(w^2-3k^2)}{(k^2w)}\xi\right)}{\frac{3c_1k^4}{w^2-3k^2} \exp\left(\frac{(w^2-3k^2)}{(k^2w)}\xi\right) + c_2}, \tag{3.15}$$

where $\xi = k(x \pm \frac{3}{\sqrt{2}}t)$ with $w = \pm\frac{3}{\sqrt{2}}k$.

If we choose $c_2 = \frac{3k^4c_1}{w^2-3k^2}$, then we arrive to the solution

$$u = \pm\frac{w^2 - 3k^2}{\sqrt{2}wk}\left\{1 + \tanh\left(\frac{w^2 - 3k^2}{2wk^2}\xi\right)\right\}, \tag{3.16}$$

where $\xi = k(x \pm \frac{3}{\sqrt{2}}t)$ with $w = \pm\frac{3}{\sqrt{2}}k$.

If we choose $c_2 = -\frac{3k^4c_1}{w^2-3k^2}$, then we arrive to the solution

$$u = \pm\frac{w^2 - 3k^2}{\sqrt{2}wk}\left\{1 + \cot\mathrm{h}\left(\frac{w^2 - 3k^2}{2wk^2}\xi\right)\right\}, \tag{3.17}$$

where $\xi = k(x \pm \frac{3}{\sqrt{2}}t)$.

Since c_1 and c_2 are free parameters, for various selections of c_1 and c_2 it provides abundant novel exact solutions of the Cahn–Allen model. The achieved solutions from Eqs. (3.16) and (3.17) are depicted graphically in Figs. 1 and 2.

Case-II: For the set $A_0 = \pm1, A_1 = \pm\sqrt{2}k$, we get

$$u = \pm1 \pm \frac{3\sqrt{2}c_1k^3}{w - 3\sqrt{2}k} \times \frac{\exp\left(\frac{(6k^2+w(w-3\sqrt{2}k))}{k^2(w-3\sqrt{2}k)}\xi\right)}{\frac{3c_1k^4}{6k^2+w(w-3\sqrt{2}k)} \exp\left(\frac{(6k^2+w(w-3\sqrt{2}k))}{k^2(w-3\sqrt{2}k)}\xi\right) + c_2}, \tag{3.18}$$

for $\xi = k(x \pm \frac{3}{\sqrt{2}}t)$ with $w = \pm\frac{3}{\sqrt{2}}k$. Here c_1 and c_2 are arbitrary parametric values.

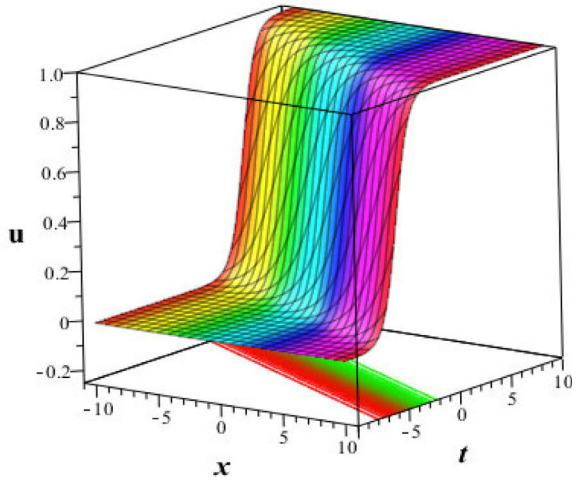

Fig. 1. Kink wave of the solution Eq. (3.16) with $k = 1$.

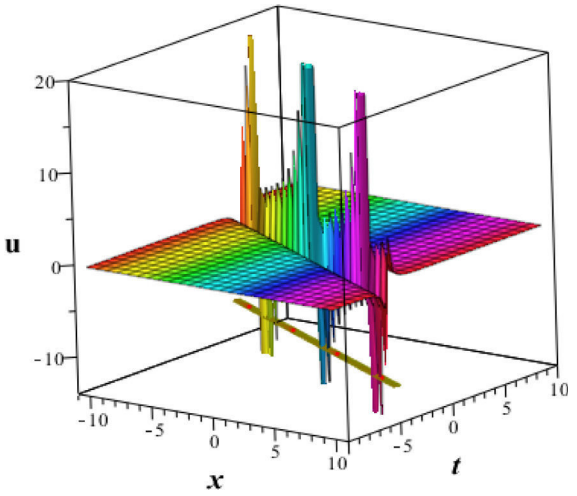

Fig. 2. Single-kink wave solution of the Eq. (3.17) with $k = 1$.

If we choose $c_2 = \frac{3k^4c_1}{6k^2+w(w-3\sqrt{2}k)}$, then we attain to the solution as

$$u = \pm 1 \pm \frac{\sqrt{2}\{6k^2 + w(w-3\sqrt{2}k)\}}{k(w-3\sqrt{2}k)}\left\{1 + \tanh\left(\frac{6k^2 + w(w-3\sqrt{2}k)}{k^2(w-3\sqrt{2}k)}\xi\right)\right\}, \tag{3.19}$$

where $\xi = k(x \pm \frac{3}{\sqrt{2}}t)$ with $w = \pm\frac{3}{\sqrt{2}}k$.

If we choose $c_2 = -\frac{3k^4c_1}{6k^2+w(w-3\sqrt{2}k)}$, then we attain to the solution as

$$u = \pm 1 \pm \frac{\sqrt{2}\{6k^2 + w(w-3\sqrt{2}k)\}}{k(w-3\sqrt{2}k)}\left\{1 + \tanh\left(\frac{6k^2 + w(w-3\sqrt{2}k)}{k^2(w-3\sqrt{2}k)}\xi\right)\right\}, \tag{3.20}$$

where $\xi = k(x \pm \frac{3}{\sqrt{2}}t)$ with $w = \pm\frac{3}{\sqrt{2}}k$.

Since c_1 and c_2 are free parameters, for different selections of c_1 and c_2 it provides abundant novel exact solutions of the Cahn–Allen model. The achieved solutions from Eqs. (3.19) and (3.20) are similar in diagrams Fig. 1 and Fig. 2 respectively. So, we exclude these equations for convenience.

Again with commercial software, we can also get various solutions of the Cahn–Allen model (solving from Eqs. (3.7) and (3.8)).

For the set of solution $A_0 = 0, A_1 = \pm\sqrt{2}k$, we get $S(\xi) = a + b\exp(\pm\xi/\sqrt{2}k)$.

Thus arrive to the solution

$$u(x,t) = \pm\frac{b}{a\left\{\cosh\frac{\xi}{\sqrt{2}k} \mp \sinh\frac{\xi}{\sqrt{2}k}\right\} + b} \text{ with } \xi = k\left(x \pm 3t/\sqrt{2}\right). \tag{3.21}$$

If we consider $a/b = \exp(2c)$, then Eq. (3.21) reduces to well known solution

$$u(x,t) = \pm\frac{1}{2}\left\{1 + \tanh\left(\pm\frac{1}{\sqrt{2}}x + \frac{3}{2}t + c\right)\right\}. \tag{3.22}$$

For the set $A_0 = 1, A_1 = \pm\sqrt{2}k$, we get $S(\xi) = a + b\exp(\pm\xi/\sqrt{2}k)$.

Hence arrive to the solution

$$u(x,t) = 1 - \frac{b}{a\left\{\cosh\frac{\xi}{\sqrt{2}k} \pm \sinh\frac{\xi}{\sqrt{2}k}\right\} + b} \text{ with } \xi = k\left(x \pm 3t/\sqrt{2}\right). \tag{3.23}$$

If we consider $a/b = \exp(2c)$, then Eq. (3.23) reduces to well known solution

$$u(x,t) = \frac{1}{2}\left\{1 + \tanh\left(\pm\frac{1}{\sqrt{2}}x + \frac{3}{2}t + c\right)\right\}. \tag{3.24}$$

For the set $A_0 = -1, A_1 = \pm\sqrt{2}k$, we get $S(\xi) = a + b\exp(\mp\xi/\sqrt{2}k)$.

Hence we attain to the solution

$$u(x,t) = -1 - \frac{b}{a\left\{\cosh\frac{\xi}{\sqrt{2}k} \mp \sinh\frac{\xi}{\sqrt{2}k}\right\} + b} \text{ with } \xi = k\left(x \mp 3t/\sqrt{2}\right). \tag{3.25}$$

If we consider $a/b = \exp(2c)$, then Eq. (3.22) gives to well known solution

$$u(x,t) = -\frac{1}{2}\left\{1 + \tanh\left(\pm\frac{1}{\sqrt{2}}x + \frac{3}{2}t + c\right)\right\}. \tag{3.26}$$

Since a and b are free parameters, for different selections of a and b it provides abundant novel exact solutions of the Cahn–Allen model. Choosing $a/b = \exp(2c)$ we get special type solution like Eqs. (3.24) and (3.26), but for other choose a and b in different way we can get dissimilar type of solutions. Thus Eqs. (3.24) and (3.26) are particular type of our solutions.

Graphs of the solutions Eqs. (3.21), (3.23) and (3.25) represent kink type wave propagation (like Fig. 1) for same positive/negative values of the arbitrary constants c_1 and c_2. But to get single soliton like wave propagation (like Fig. 2) from the same solution, we have to pick opposite values of arbitrary constants c_1 and c_2.

3.2. Example 2: A diffusive predator–prey model

In the predator–prey model including any type of natural disaster, the cycle can be reflected as a flow that may be periodic or remain unchanged like soliton and may be considered as a nonlinear wave phenomenon allied to a large amount of significance in modern biophysics. Here, we deliberate a model of two combined nonlinear models relating the spatio-temporal kinetics of a predator–prey model,[33]

$$\begin{cases} u_t = u_{xx} - \beta u + (1+\beta)u^2 - u^3 - uv \\ v_t = v_{xx} + kuv - mv - \delta v^3 \end{cases}, \tag{3.27}$$

with positive constants k, δ, m and β. Research has been done from several angles to find a solution to the predator–prey model.[33,34] For further convenience, to visualize the kinetics of the dispersive predator–prey model have expected the relations as $m = \beta$ and $k + 1/\sqrt{\delta} = \beta + 1$.

Hence the Eq. (3.27) converted to

$$\begin{cases} u_t = u_{xx} - \beta u + (k + 1/\sqrt{\delta})u^2 - u^3 - uv \\ v_t = v_{xx} + kuv - \beta v - \delta v^3 \end{cases}. \tag{3.28}$$

Analogously, we bring in the variable $\eta = x - wt$, and make the transformation $u(x,t) = u(\eta)$, to convert Eq. (3.28) as the following form:

$$\begin{cases} u'' + cu' - \beta u + (k + 1/\sqrt{\delta})u^2 - u^3 - uv = 0 \\ v'' + cv' + kuv - \beta v - \delta v^3 = 0 \end{cases}, \tag{3.29}$$

for $c \neq 0$.

To solve the Eq. (3.29), consider the relation $v = u/\sqrt{\delta}$ to convert the system to a single equation and we finally attain,

$$u'' + cu' - \beta u + ku^2 - u^3 = 0. \tag{3.30}$$

Balancing u^3 and u'' in Eq. (3.30), yields $m + 2 = 3m \to m = 1$. So Eq. (3.30) has the following solution

$$u(\eta) = a_0 + a_1 \frac{\Omega'(\eta)}{\Omega(\eta)} \text{ and } a_1 \neq 0, \tag{3.31}$$

where a_0 and a_1 are constants and need to be determined. Inserting Eq. (3.31) in Eq. (3.30) and equating the coefficient of same powers of $(\Omega(\eta))^{-i}$, $i = 0, 1, \ldots, 3$ and setting each of them is identical to zero; we have an algebraic system as below

$$\begin{aligned} & ka_0^2 - \beta a_0 - a_0^3 = 0 \\ & wa_1\Omega''(\eta) - (\beta a_1 + 3a_0^2 a_1 - 2ka_0 a_1)\Omega'(\eta) + a_1\Omega'''(\eta) = 0 \\ & -3a_1\left(\Omega'(\eta)\right)\left(\Omega''(\eta)\right) - (wa_1 - ka_1^2 + 3a_0 a_1^2)\left(\Omega'(\eta)\right)^2 = 0, \\ & \left(2a_1 - a_1^3\right)\left(\Omega'(\eta)\right)^3 = 0. \end{aligned}$$

From first and last equation of the above algebraic system, we get three types of solutions $a_0 = 0, a_1 = \pm\sqrt{2}$ and $a_0 = \frac{1}{2}(k + \sqrt{k^2 - 4\beta})$, $a_1 = \pm\sqrt{2}$ and $a_0 = \frac{1}{2}(k - \sqrt{k^2 - 4\beta})$, $a_1 = \pm\sqrt{2}$.

Case1: When we consider $a_0 = 0$ and $a_1 = \pm\sqrt{2}$.

Set-1: For the solution $a_0 = 0$ and $a_1 = \sqrt{2}$, we get other parametric values $w = \frac{\sqrt{2}}{4}(k \pm 3\sqrt{k^2 - 4\beta})$ and $\Omega(\eta) = c_1 + c_2 e^{-\frac{1}{3}(w - \sqrt{2}k)\eta}$.

Using these parametric values in Eq. (3.31), we can find the solution of the Eq. (3.28) as follows

$$u = -\frac{\sqrt{2}}{3}\frac{c_2(w - \sqrt{2}k)}{c_2 + c_1(\cosh\vartheta + \sin h\vartheta)}, \tag{3.32}$$

where $\eta = x - \frac{\sqrt{2}}{4}(k \pm 3\sqrt{k^2 - 4\beta})t$ and $\vartheta = \frac{1}{3}(w - \sqrt{2}k)\eta$.

Set-2: For the solution $a_0 = 0$ and $a_1 = -\sqrt{2}$, we get remaining parametric values $w = -\frac{\sqrt{2}}{4}(k \pm 3\sqrt{k^2 - 4\beta})$ and $\Omega(\eta) = c_1 + c_2 e^{-\frac{1}{3}(w + \sqrt{2}k)\eta}$.

Using these parametric values in Eq. (3.31), we can find the solution of the Eq. (3.28) as follows

$$u = \frac{\sqrt{2}}{3}\frac{c_2(w + \sqrt{2}k)}{c_2 + c_1(\cosh\vartheta + \sin h\vartheta)}, \tag{3.33}$$

where $\eta = x + \frac{\sqrt{2}}{4}(k \pm 3\sqrt{k^2 - 4\beta})t$ and $\vartheta = \frac{1}{3}(w + \sqrt{2}k)\eta$.

Case-2: When we consider $a_0 = \frac{1}{2}(k + \sqrt{k^2 - 4\beta})$ and $a_1 = \pm\sqrt{2}$.

Set-1: For the solution $a_0 = \frac{1}{2}(k + \sqrt{k^2 - 4\beta})$ and $a_1 = \sqrt{2}$, we get remaining parametric values

$w = -\frac{1}{\sqrt{2}}k, \frac{\sqrt{2}}{4}(k - 3\sqrt{k^2 - 4\beta})$ and $\Omega(\eta) = c_1 + c_2 e^{-\frac{\sqrt{2}}{6}(\sqrt{2}w + k + 3\sqrt{k^2 - 4\beta})\eta}$.

Using these parametric values in Eq. (3.31), we can find the solution of the Eq. (3.28) as follows

$$u = \frac{1}{2}(k + \sqrt{k^2 - 4\beta}) - \frac{1}{3}\frac{c_2(\sqrt{2}w + k + 3\sqrt{k^2 - 4\beta})}{c_2 + c_1(\cosh\vartheta + \sin h\vartheta)}, \tag{3.34}$$

where $\eta = x - \frac{\sqrt{2}}{4}(k - 3\sqrt{k^2 - 4\beta})t$ or $\eta = x + \frac{1}{\sqrt{2}}kt$ and $\vartheta = \frac{\sqrt{2}}{6}(\sqrt{2}w + k + 3\sqrt{k^2 - 4\beta})\eta$.

Set-2: For the solution $a_0 = \frac{1}{2}(k + \sqrt{k^2 - 4\beta})$ and $a_1 = -\sqrt{2}$, we get remaining parametric values

$w = \frac{1}{\sqrt{2}}k, -\frac{\sqrt{2}}{4}(k - 3\sqrt{k^2 - 4\beta})$ and $\Omega(\eta) = c_1 + c_2 e^{-\frac{\sqrt{2}}{6}(\sqrt{2}w - k - 3\sqrt{k^2 - 4\beta})\eta}$.

Using these parametric values in Eq. (3.31), we can find the solution of the Eq. (3.28) as follows

$$u = \frac{1}{2}(k + \sqrt{k^2 - 4\beta}) + \frac{1}{3}\frac{c_2(\sqrt{2}w - k - 3\sqrt{k^2 - 4\beta})}{c_2 + c_1(\cosh\vartheta + \sin h\vartheta)}, \tag{3.35}$$

where $\eta = x + \frac{\sqrt{2}}{4}(k - 3\sqrt{k^2 - 4\beta})t$ or $\eta = x - \frac{1}{\sqrt{2}}kt$ and $\vartheta = \frac{\sqrt{2}}{6}(\sqrt{2}w - k - 3\sqrt{k^2 - 4\beta})\eta$.

Case-3: When we consider $a_0 = \frac{1}{2}(k - \sqrt{k^2 - 4\beta})$ and $a_1 = \pm\sqrt{2}$.

Set-1: For the solution $a_0 = \frac{1}{2}(k - \sqrt{k^2 - 4\beta})$ and $a_1 = \sqrt{2}$, we get remaining parametric values

$w = -\frac{1}{\sqrt{2}}k, \frac{\sqrt{2}}{4}(k + 3\sqrt{k^2 - 4\beta})$ and $\Omega(\eta) = c_1 + c_2 e^{-\frac{\sqrt{2}}{6}(\sqrt{2}w + k - 3\sqrt{k^2 - 4\beta})\eta}$.

Using these parametric values in Eq. (3.31), we can find the solution of the Eq. (3.28) as follows

$$u = \frac{1}{2}(k - \sqrt{k^2 - 4\beta}) - \frac{1}{3}\frac{c_2(\sqrt{2}w + k - 3\sqrt{k^2 - 4\beta})}{c_2 + c_1(\cosh\vartheta + \sin h\vartheta)}, \tag{3.36}$$

where $\eta = x - \frac{\sqrt{2}}{4}(k + 3\sqrt{k^2 - 4\beta})t$ or $\eta = x + \frac{1}{\sqrt{2}}kt$ and $\vartheta = \frac{\sqrt{2}}{6}(\sqrt{2}w + k - 3\sqrt{k^2 - 4\beta})\eta$.

Set-2: For the solution $a_0 = \frac{1}{2}(k - \sqrt{k^2 - 4\beta})$ and $a_1 = -\sqrt{2}$, we get remaining parametric values

$w = \frac{1}{\sqrt{2}}k, -\frac{\sqrt{2}}{4}(k + 3\sqrt{k^2 - 4\beta})$ and $\Omega(\eta) = c_1 + c_2 e^{-\frac{\sqrt{2}}{6}(\sqrt{2}w - k + 3\sqrt{k^2 - 4\beta})\eta}$.

Using these parametric values in Eq. (3.31), we can find the solution of the Eq. (3.28) as follows

$$u = \frac{1}{2}(k - \sqrt{k^2 - 4\beta}) + \frac{1}{3}\frac{c_2(\sqrt{2}w - k + 3\sqrt{k^2 - 4\beta})}{c_2 + c_1(\cosh\vartheta + \sin h\vartheta)}, \tag{3.37}$$

where $\eta = x + \frac{\sqrt{2}}{4}(k + 3\sqrt{k^2 - 4\beta})t$ or $\eta = x - \frac{1}{\sqrt{2}}kt$ and $\vartheta = \frac{\sqrt{2}}{6}(\sqrt{2}w - k + 3\sqrt{k^2 - 4\beta})\eta$.

If we plot Eq. (3.32) with particular choose of the constants such that $k^2 - 4\beta > 0$, then we achieved progress of spaces as kink type that is population density is stable and lies between two asymptotic state $u = 0$ to $u = 0.85$ with $c_1 = c_2 = w = \beta = 1, k = 2$ (see Fig. 3a). But if we set the constants such that $k^2 - 4\beta < 0$, then most of the times population are stable except some times and periodic (see Fig. 3b with $c_1 = c_2 = w = \beta = 1, k = 1$). On the other hand when c_1 *or* c_2 negative, then density of species unstable and increases unexpectedly (see Fig. 3c with $c_1 = -1, c_2 = w = \beta = 1, k = 2$). Fig. 3d: perspective view of Eq. (3.33) for $c_1 = c_2 = w = \beta = 1, k = 1$. The other solution gives the same type of situation with similar conditions on the parametric values. So we avoid the similar figures again.

4. Comparison

Here, we compare our solutions with the solutions of other researchers obtained by some renowned schemes as exp-function scheme, first integral scheme and Bernoulli sub-equation function scheme. The details are included as follows:

(a) Comparison with Exp-function scheme Ref. 11**:** Ugurlu[11] obtained some solutions of the Cahn–Allen model via exp-function scheme in which solutions u_8, u_9 are identical with our solution Eq. (3.21) when $b = 1, a = b_0$ and the other solutions are different with their solutions (For more see the Ref. 14).

(b) Comparison with first integral scheme Ref. 16**:** Tascan and Bekir[16] obtained some solutions of the Cahn–Allen model via first

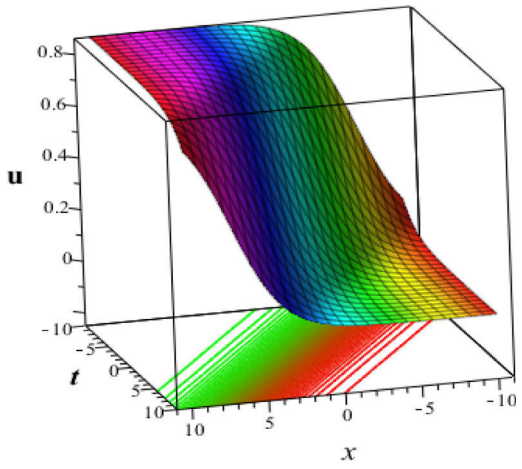

Fig. 3a. Kink wave view of Eq. (3.32) for $c_1 = c_2 = w = \beta = 1, k = 2$.

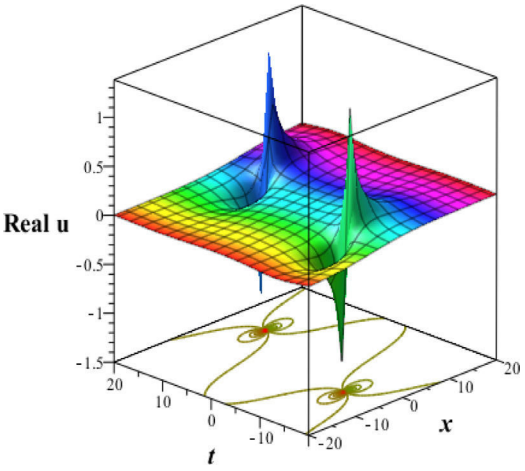

Fig. 3b. Kinky-periodic lump wave view of Eq. (3.32) for $c_1 = c_2 = w = \beta = 1, k = 1$.

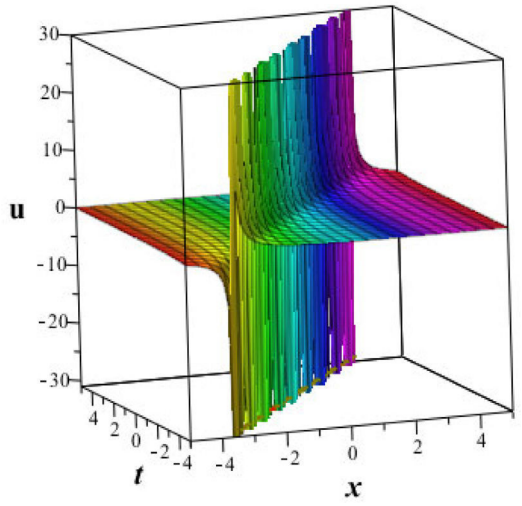

Fig. 3c. Singular-kink soliton view of Eq. (3.32) for $c_1 = -1, c_2 = w = \beta = 1, k = 2$.

integral scheme in which solutions Eq. (3.16) are identical with our solutions Eq. (3.21) (when in our study $a = b = 1, k = -1/\sqrt{2}$ and in their study $c_0 = 0$) and u_8, u_9 are identical with our solutions Eq.

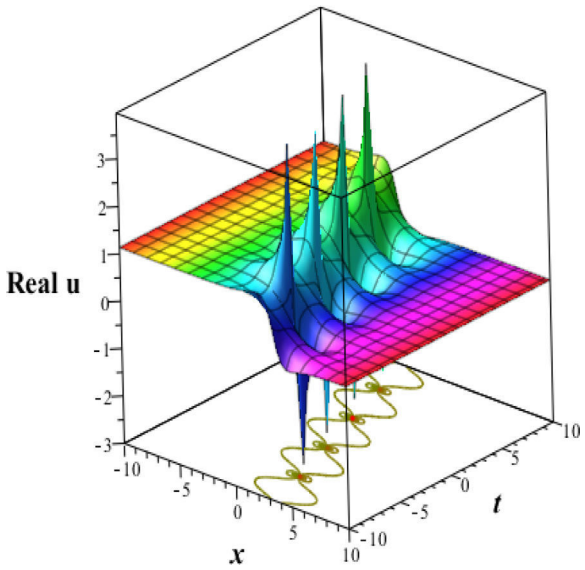

Fig. 3d. Kinky-periodic lump wave view of Eq. (3.33) for $c_1 = c_2 = w = \beta = 1, k = 1$.

(3.21) when $b = 1, a = b_0$ and the other solutions are different with their solutions.

(c) Comparison with the Bernoulli sub-equation function scheme Ref. 35**:** Bulut et al.[35] derived six solutions of Cahn–Allen model and all of these are special case of our solutions. When we put $k = -\sqrt{2}/3, c_2 = a_2, 2c_1k^2 = E$; $k = -\sqrt{2}/3, c_2 = 2\sqrt{2}d, 2c_1k^2 = E$ and $k = -\sqrt{2}/3, c_2 = 3\sqrt{2}d, 2c_1k^2 = E$ in our solution (**Case-I** i.e., Eq. (3.15)) reduces to solutions u_1, u_4 and u_5 of Ref. 35 respectively. Similarly, we see that the solutions u_2, u_3, u_6 are special case of our solution (**Case-II** i.e., Eq. (3.18)). Our results have more free parameters which can be converted to diverse types of dynamical behavior for diverse choices of free parameters.

In contrast, by employing the MSE scheme in this manuscript we have achieved four solutions with simple calculations.

5. Conclusions

In this paper, the MSE scheme has been effectively employed for finding the exact solutions and dynamics of the Cahn–Allen model and the dispersive predator–prey model. We presented abundant new exact explicit solutions of the exponential form of both Cahn–Allen and diffusive predator–prey models with some free parametric values. We derived particular solutions from the general exponential function such as stable kink soliton and kinky-periodic rogue wave solutions; unstable singular kink wave solutions of both models. We also derive particular solutions from the explicit solutions selecting some definite values of the free parametric values. Lastly, the variety and graphic representations of the composition make the models dynamic. Stable and unstable situations are explained in detail from the analysis of the profiles. By comparing the MSE scheme with different schemes, we can claim that the MSE scheme is frank, simple, proficient, and can be applied in numerous nonlinear models. In existing schemes, for example, the (G'/G)-expansion scheme, the Exp-function scheme and the tanh-function scheme, it is essential to employ suggestive calculation software like Mathematica or Maple to solve the intricate algebraic equation. No auxiliary equations are needed to solve non-linear models by using the MSE scheme.

Funding statement

This research did not receive any particular offer from funding agencies.

Additional information

No additional information is available for this paper.

CRediT authorship contribution statement

Mohammad Safi Ullah: Methodology, Software. **Harun-Or-Roshid:** Supervision. **M. Zulfikar Ali:** Supervision. **N.F.M. Noor:** Validation.

Declaration of competing interest

The authors declare that they have no known competing financial interests or personal relationships that could have appeared to influence the work reported in this paper.

Acknowledgments

The authors are real glad to the referees for their constructive comments, recommendations, valuable suggestions that tremendously improved the quality of the manuscript.

References

1. Aguero M, Najera M, Carrillo M. Non classic solitonic structures in DNA's vibrational dynamics. *Int J Mod Phys B*. 2008;22:2571–2582. http://dx.doi.org/10.1142/S021797920803968X.
2. Alka W, Goyal A, Kumar CN. Nonlinear dynamics of dna-riccati generalized solitary wave solutions. *Phys Lett A*. 2011;375:480–483. http://dx.doi.org/10.1016/j.physleta.2010.11.017.
3. Hammouch Z, Mekkaoui T, Agarwal P. Optical solitons for the Calogero–Bogoyavlenskii–Schiff equation in (2 + 1) dimensions with time-fractional conformable derivative. *Eur Phys J Plus*. 2018;133(7):248. http://dx.doi.org/10.1140/epjp/i2018-12096-8.
4. Ullah MS, Roshid HO, Ali MZ, Rahman Z. Novel exact solitary wave solutions for the time fractional generalized Hirota–Satsuma coupled KdV model through the generalized Kudryshov method. *Contemp Math*. 2019;1(1):25–32. http://dx.doi.org/10.37256/cm.11201936.25-33.
5. Roshid HO, Alam MN, Hoque MF, Akbar MA. A new extended (G'/G)-expansion method to find exact traveling wave solutions of nonlinear evolution equations. *Math Stat*. 2013;1(3):162–166. http://dx.doi.org/10.13189/ms.2013.010308.
6. Guirao JLG, Baskonus HM, Kumar A. Regarding new wave patterns of the newly extended nonlinear (2+1)-dimensional Boussinesq equation with fourth order. *Mathematics*. 2020;8(3):341. http://dx.doi.org/10.3390/math8030341.
7. Yel G, Baskonus HM, Gao W. New dark-bright soliton in the shallow water wave model. *AIMS Math*. 2020;5(4):4027–4044. http://dx.doi.org/10.3934/math.2020259.
8. Gao W, Senel M, Yel G, Baskonus HM, Senel B. New complex wave patterns to the electrical transmission line model arising in network system. *AIMS Math*. 2020;5(3):1881–1892. http://dx.doi.org/10.3934/math.2020125.
9. Abdou MA. The extended F-expansion method and its application for a class of nonlinear evolution equations. *Chaos Solitons Fractals*. 2007;31(1):95–104. http://dx.doi.org/10.1016/j.chaos.2005.09.030.
10. Mahmoudi J, Tolou N, Khatami I, Barari A, Ganji DD. Explicit solution of nonlinear ZK-BBM wave equation using Exp-function method. *J Appl Sci*. 2008;8(2):358–363. http://dx.doi.org/10.3923/jas.2008.358.363.
11. Ugurlu Y. Exp-function method for the some nonlinear partial differential equations. *Math Aeter*. 2013;3(1):57–70.
12. Vitanov NK, Dimitrova ZI, Kantz H. Modified method of simplest equation and its application to nonlinear PDEs. *Appl Math Comput*. 2010;216(9):2587–2595. http://dx.doi.org/10.1016/j.amc.2010.03.102.
13. Jawad AJM, Petkovic MD, Biswas A. Modified simple equation method for nonlinear evolution equations. *Appl Math Comput*. 2010;217(2):869–877. http://dx.doi.org/10.1016/j.amc.2010.06.030.
14. Zayed EME. A note on the modified simple equation method applied to Sharma–Tasso–Olver equation. *Appl Math Comput*. 2011;218(7):3962–3964. http://dx.doi.org/10.1016/j.amc.2011.09.025.
15. Zayed EME, Ibrahim SAH. Exact solutions of nonlinear evolution equations in mathematical physics using the modified simple equation method. *Chin Phys Lett*. 2012;29(6). 060201. http://dx.doi.org/10.1088/0256-307X/29/6/060201.
16. Tascan F, Bekir A. Traveling wave solutions of the Cahn–Allen equation by using first integral method. *Appl Math Comput*. 2007;207(1):279–282. http://dx.doi.org/10.1016/j.amc.2008.10.031.
17. Jafari H, Kadkhoda N. Application of simplest equation method to the (2+1)-dimensional nonlinear evolution equations. *NTMSCI*. 2014;2(2):64–68.
18. Ma WX. Generalized bilinear differential equations. *Stud Nonlinear Sci*. 2011;2(4):140–144.
19. Chen SJ, Yin YH, Ma WX, Lü X. Abundant exact solutions and interaction phenomena of the (2 + 1)-dimensional YTSF equation. *Anal Math Phys*. 2019;9:2329–2344. http://dx.doi.org/10.1007/s13324-019-00338-2.
20. Ma WX. Lump and interaction solutions to linear PDEs in 2 + 1 dimensions via symbolic computation. Mod. *Phys Lett B*. 2019;33:1950457. http://dx.doi.org/10.1142/S0217984919504578.
21. Ma WX, Zhang L. Lump solutions with higher-order rational dispersion relations. *Pramana J Phys*. 2020;94:43. http://dx.doi.org/10.1007/s12043-020-1918-9.
22. Roshid HO, Rahman MA. The $\exp(-\Phi(\eta))$-expansion method with application in the (1+1)-dimensional classical Boussinesq equations. *Results Phys*. 2014;4:150–155. http://dx.doi.org/10.1016/j.rinp.2014.07.006.
23. Wazwaz AM. The extended tanh method for new compact and noncompact solutions for the KP-BBM and the ZK-BBM equations. *Chaos Solitons Fractals*. 2008;38(5):1505–1516. http://dx.doi.org/10.1016/j.chaos.2007.01.135.
24. Yomba E. The modified extended fan sub-equation method and its application to the (2+1)-Dimensional Broer–Kaup–Kuperschmidt equations. *Chaos Solitons Fractals*. 2006;27(1):187–196. http://dx.doi.org/10.1016/j.chaos.2005.03.021.
25. Zayed EME, Zedan HA, Gepreel KA. On the solitary wave solutions for nonlinear Hirota–Sasuma coupled KDV equations. *Chaos Solitons Fractals*. 2004;22:285–303. http://dx.doi.org/10.1016/j.chaos.2003.12.045.
26. Yan Z. Abundant families of Jacobi elliptic function solutions of the (2+1)-dimensional integrable Davey–Stewartson- type equation via a new method. *Chaos Solitons Fractals*. 2003;18(2):299–309. http://dx.doi.org/10.1016/S0960-0779(02)00653-7.
27. Ullah MS, Roshid HO, Ma WX, Ali MZ, Rahman Z. Interaction phenomena among lump, periodic and kink wave solutions to a (3+1)-dimensional Sharma–Tasso–Olver-like equation. *Chin J Phys*. 2020;68:699–711. http://dx.doi.org/10.1016/j.cjph.2020.10.009.
28. Ma WX, Fuchssteiner B. Explicit and exact solutions to a Kolmogorov-Petrovskii–Piskunov equation. *Int J Non-Linear Mech*. 1996;31(3):329–338. http://dx.doi.org/10.1016/0020-7462(95)00064-X.
29. Ullah MS, Roshid HO, Ali MZ, Rahman Z. Dynamical structures of multi-soliton solutions to the Bogoyavlenskii's breaking soliton equations. *Eur Phys J Plus*. 2020;135(3):282. http://dx.doi.org/10.1140/epjp/s13360-020-00289-9.
30. Sirendaoreji. Auxiliary equation method and new solutions of Klein-Gordon equations. *Chaos Solitions Fract*. 2007;31:943–950. http://dx.doi.org/10.1016/j.chaos.2005.10.048.
31. Wazwaz AM. The sine-cosine method for obtaining solutions with compact and noncompact structures. *Appl Math Comput*. 2004;159(2):559–576. http://dx.doi.org/10.1016/j.amc.2003.08.136.
32. Ma WX, Lee JH. A transformed rational function method and exact solutions to the 3+1 dimensional Jimbo–Miwa equation. *Chaos Solitons Fractals*. 2009;42(3):1356–1363. http://dx.doi.org/10.1016/j.chaos.2009.03.043.
33. Petrovskii SV, Malchow H, Li BL. An exact solution of a diffusive predator–prey system. *Proc R Soc A*. 2005;461:1029–1053. http://dx.doi.org/10.1098/rspa.2004.1404.
34. Kraenkel RA, Manikandan K, Senthivelan M. On certain new exact solutions of a diffusive predator–prey system. *Commun Nonlinear Sci Numer Simul*. 2013;18:1269–1274. http://dx.doi.org/10.1016/j.cnsns.2012.09.019.
35. Bulut H, Atas SS, Baskonus HM. Some novel exponential function structures to the Cahn–Allen equation. *Cogent Phys*. 2016;3(1). 1240886. http://dx.doi.org/10.1080/23311940.2016.1240886.

Results in Physics 22 (2021) 103958

Contents lists available at ScienceDirect

Results in Physics

journal homepage: www.elsevier.com/locate/rinp

Optical soliton polarization with Lakshmanan–Porsezian–Daniel model by unified approach

Mohammad Safi Ullah [a,b], Harun-Or-Roshid [c], M. Zulfikar Ali [b], Anjan Biswas [d,e,f,g], Mehmet Ekici [h,*], Salam Khan [d], Luminita Moraru [i], Abdullah Khamis Alzahrani [e], Milivoj R. Belic [j]

[a] Department of Mathematics, Comilla University, Cumilla 3506, Bangladesh
[b] Department of Mathematics, Rajshahi University, Rajshahi 6205, Bangladesh
[c] Department of Mathematics, Pabna University of Science and Technology, Pabna 6600, Bangladesh
[d] Department of Physics, Chemistry and Mathematics, Alabama A&M University, Normal, AL 35762–4900, USA
[e] Mathematical Modeling and Applied Computation (MMAC) Research Group, Department of Mathematics, King Abdulaziz University, Jeddah 21589, Saudi Arabia
[f] Department of Applied Mathematics, National Research Nuclear University, 31 Kashirskoe Hwy, Moscow 115409, Russian Federation
[g] Department of Mathematics and Applied Mathematics, Sefako Makgatho Health Sciences University, Medunsa-0204, Pretoria, South Africa
[h] Department of Mathematics, Faculty of Science and Arts, Yozgat Bozok University, 66100 Yozgat, Turkey
[i] Faculty of Sciences and Environment, Department of Chemistry, Physics and Environment, Dunarea de Jos University of Galati, 47 Domneasca Street, 800008, Romania
[j] Science Program, Texas A&M University at Qatar, PO Box 23874, Doha, Qatar

ARTICLE INFO

OCIS:
060.2310
060.4510
060.5530
190.3270
190.4370

Keywords:
Unified method
LPD model
Optical solitons

ABSTRACT

This work retrieves polarized optical soliton solutions for pulses in birefringent fibers that are modeled by the Lakshmanan–Porsezian–Daniel model. The unified approach recovers singular solitons only. This approach fails to retrieve the much needed bright and dark soliton solutions. These singular solitons exist with restricted parametric conditions that are also exhibited.

Introduction

Optical soliton dynamics is an engineering marvel in telecommunications industry [1–10]. An inherent problem with the dynamics of pulse propagation across trans-oceanic and trans-continental distances is its polarization. This is attributed to several factors such as the randomness of fiber diameter, rough handling of optical fibers and many others. These factors occasionally lead to hi-bi fibers. It is often a challenging task to retrieve the soliton solutions to the models that are studied in the context of high birefringence.

One such model that has been around for a fairly long period is the Lakshmanan–Porsezian–Daniel (LPD) model that was first reported in 1988 and later gained a lot of popularity [11]. A wide range of integration algorithms have been implemented to secure soliton and other solutions to LPD model in the context of polarization-preserving fibers [12], including $\exp(-\phi(\xi))$-expansion scheme [13], trial equation scheme [14] and many more [15–18]. Today's work will retrieve soliton solutions to LPD model with differential group delay by unified approach that was first reported during 2018 [19]. As it will be revealed, the algorithm could only expose singular solitons. The details are jotted in the rest of the paper after a quick re-visitation of the model and the integration algorithm.

Governing model

The dimensionless LPD model with Kerr law nonlinearity has the following form [15,16,20]:

$$i\psi_t + a\psi_{xx} + b\psi_{xt} + c\,|\psi|^2\psi = \sigma\psi_{xxxx} + p\psi_x^2\psi^* + q\,|\psi_x|^2\psi + r\,|\psi|^2\psi_{xx} + \lambda\psi^2\psi_{xx}^* + s\,|\psi|^4\psi. \quad (1)$$

In Eq. (1), x and t represent independent spatial and temporal variables, respectively. The dependent variable ψ represents the complex wave

* Corresponding author.
E-mail address: mehmet.ekici@bozok.edu.tr (M. Ekici).

https://doi.org/10.1016/j.rinp.2021.103958
Received 20 November 2020; Received in revised form 4 February 2021; Accepted 5 February 2021
Available online 11 February 2021

function. Next, the parameters a, b, c, σ and s signify group velocity dispersion, spatio-temporal dispersion, the coefficient of Kerr law nonlinearity, the coefficient of fourth order dispersion and the two-photon absorption, respectively. Finally, the p, q, r and λ terms account for several forms of the nonlinear dispersion. Solitons are possible for a sustained delicate balance of dispersion with the nonlinear terms.

For birefringent fibers, the model can be divided into two parts of a vector representation. Avoiding the properties of 4WM, the above model reduces to [13,14]:

$$\begin{aligned} &iu_t + a_1u_{xx} + b_1u_{xt} + \left(c_1|u|^2 + d_1|v|^2\right)u \\ &= \sigma_1u_{xxxx} + \left(p_1u_x^2 + q_1v_x^2\right)u^* + \left(r_1|u_x|^2 + s_1|v_x|^2\right)u \\ &+ \left(\lambda_1|u|^2 + \theta_1|v|^2\right)u_{xx} + \left(\chi_1u^2 + \eta_1v^2\right)u_{xx}^* \\ &+ \left(f_1|u|^4 + \phi_1|u|^2|v|^2 + \vartheta_1|v|^4\right)u \end{aligned} \tag{2}$$

$$\begin{aligned} &iv_t + a_2v_{xx} + b_2v_{xt} + \left(c_2|v|^2 + d_2|u|^2\right)v \\ &= \sigma_2v_{xxxx} + \left(p_2v_x^2 + q_2u_x^2\right)v^* + \left(r_2|v_x|^2 + s_2|u_x|^2\right)v \\ &+ \left(\lambda_2|v|^2 + \theta_2|u|^2\right)v_{xx} + \left(\chi_2v^2 + \eta_2u^2\right)v_{xx}^* \\ &+ \left(f_2|v|^4 + \phi_2|v|^2|u|^2 + \vartheta_2|u|^4\right)v. \end{aligned} \tag{3}$$

In Eqs. (2) and (3), c_j, f_j for $j = 1,2$ represent the self-phase and d_j, ϕ_j, ϑ_j with $j = 1,2$ stand for the cross-phase modulation effects, respectively.

Mathematical analysis

Consider the following transformation of this coupled system

$$u(x,t) = H_1(\zeta)\exp(i\varphi) \tag{4}$$

$$v(x,t) = H_2(\zeta)\exp(i\varphi) \tag{5}$$

where H_1 and H_2 are the soliton amplitude components and

$$\zeta = x - \varpi t \tag{6}$$

is the traveling wave variable with the soliton speed ϖ. The phase component φ is as below:

$$\varphi = -kx + wt + \varepsilon \tag{7}$$

with frequency k, wave number w and phase shift ε. Inserting Eqs. (4) and (5) into Eqs. (2) and (3) and sorting out the real and imaginary parts leads to the following equations. The real part is

$$\begin{aligned} &(w + a_nk^2 - b_nkw + k^4\sigma_n)H_n - (c_n + k^2(p_n - r_n + \lambda_n + \chi_n))H_n^3 \\ &+ f_nH_n^5 - (d_n + k^2(q_n - s_n + \eta_n + \theta_n))H_n(H_{\bar{n}})^2 + \phi_n(H_n)^3(H_{\bar{n}})^2 \\ &+ \vartheta_nH_n(H_{\bar{n}})^4 + (p_n + r_n)H_n(H_n')^2 + (q_n + s_n)H_n(H_{\bar{n}}')^2 \\ &- (a_n - b_n\varpi + 6k^2\sigma_n)H_n'' + (\lambda_n + \chi_n)H_n^2H_n'' \\ &+ (\eta_n + \theta_n)(H_{\bar{n}})^2H_n'' + \sigma_nH_n^{(4)} = 0 \end{aligned} \tag{8}$$

while the imaginary part is

$$\begin{aligned} &(\varpi + 2a_nk - b_n(k\varpi + w) + 4k^3\sigma_n)H_n' - 2k(p_n + \lambda_n - \chi_n)H_n^2H_n' \\ &+ 2k(\eta_n - \theta_n)H_n'(H_{\bar{n}})^2 - 2q_nkH_nH_{\bar{n}}H_{\bar{n}}' - 4k\sigma_nH_n^{(3)} = 0 \end{aligned} \tag{9}$$

with $n = 1,2$ and $\bar{n} = 3 - n$. By the balancing principle, one can write

$$H_{\bar{n}} = H_n. \tag{10}$$

From Eqs. (8) and (10), we can rewrite

$$\begin{aligned} &(w + a_nk^2 - b_nkw + k^4\sigma_n)H_n - (c_n + d_n + k^2(h_n + R_n))H_n^3 + J_nH_n^5 \\ &+ L_nH_n(H_n')^2 - (a_n - b_n\varpi + 6k^2\sigma_n)H_n'' + R_nH_n^2H_n'' + \sigma_nH_n^{(4)} = 0 \end{aligned} \tag{11}$$

where

$$J_n = f_n + \phi_n + \vartheta_n, \quad h_n = p_n + q_n - r_n - s_n,$$

$$L_n = p_n + q_n + r_n + s_n, \quad R_n = \eta_n + \theta_n + \lambda_n + \chi_n. \tag{12}$$

From Eqs. (9) and (10), one can rewrite

$$\begin{aligned} &(\varpi + 2a_nk - b_n(k\varpi + w) + 4k^3\sigma_n)H_n' \\ &- 2k(p_n + q_n - \eta_n + \theta_n + \lambda_n - \chi_n)H_n^2H_n' - 4k\sigma_nH_n^{(3)} = 0. \end{aligned} \tag{13}$$

Thus, the third expression of Eq. (13) gives $\sigma_n = 0$. Hence the solutions of the coupled system Eqs. (2) and (3) will be presented for the fourth order dispersion omitted. The other terms in Eq. (13), yield the following relation

$$\eta_n + \chi_n = p_n + q_n + \theta_n + \lambda_n \tag{14}$$

and therefore the soliton speed is

$$\varpi = \frac{v_nw - 2a_nk}{1 - v_nk} \tag{15}$$

for $b_n = \frac{1}{k}$. Comparing the values of the soliton velocity, Eq. (15) gives

$$(1 - b_1k)(b_2w - 2a_2k) = (1 - b_2k)(b_1w - 2a_1k). \tag{16}$$

Therefore Eq. (11) can be written as

$$\begin{aligned} &(w + a_nk^2 - b_nkw)H_n - (c_n + d_n + k^2(h_n + R_n))H_n^3 + J_nH_n^5 + L_nH_n(H_n')^2 \\ &- (a_n - b_n\varpi)H_n'' + R_nH_n^2H_n'' = 0. \end{aligned} \tag{17}$$

Application of unified method to LPD model

Assume the trial solution of Eq. (17) is

$$H_n(\zeta) = \sum_{i=0}^{N} A_i^{(n)}S(\zeta)^i + B_i^{(n)}S(\zeta)^{-i} \tag{18}$$

where $A_0^{(n)}, A_i^{(n)}$ and $B_i^{(n)}$ for $i = 1,2,\ldots,N$ are real constants and $S(\zeta)$ satisfies Riccati equation:

$$S'(\zeta) = S^2(\zeta) + l. \tag{19}$$

Eq. (19) has nine solution categories according to three cases:

Case-1: Hyperbolic functions (when $l < 0$):

$$S(\zeta) = \begin{cases} \dfrac{\sqrt{-(C^2+D^2)l} - C\sqrt{-l}\cosh(2\sqrt{-l}(\zeta+E))}{C\sinh(2\sqrt{-l}(\zeta+E)) + D}, \\ \dfrac{-\sqrt{-(C^2+D^2)l} - C\sqrt{-l}\cosh(2\sqrt{-l}(\zeta+E))}{C\sinh(2\sqrt{-l}(\zeta+E)) + D}, \\ \sqrt{-l} + \dfrac{2C\sqrt{-l}}{C + \cosh(2\sqrt{-l}(\zeta+E)) - \sinh(2\sqrt{-l}(\zeta+E))}, \\ -\sqrt{-l} + \dfrac{2C\sqrt{-l}}{C + \cosh(2\sqrt{-l}(\zeta+E)) - \sinh(2\sqrt{-l}(\zeta+E))}, \end{cases} \tag{20}$$

Case-2: Trigonometric functions (when $l > 0$):

$$S(\zeta) = \begin{cases} \dfrac{\sqrt{(C^2-D^2)l} - C\sqrt{l}\cos(2\sqrt{l}(\zeta+E))}{C\sin(2\sqrt{l}(\zeta+E)) + D}, \\ \dfrac{-\sqrt{(C^2-D^2)l} - C\sqrt{l}\cos(2\sqrt{l}(\zeta+E))}{C\sin(2\sqrt{l}(\zeta+E)) + D}, \\ i\sqrt{l} + \dfrac{-2iC\sqrt{l}}{C + cos(2\sqrt{l}(\zeta+E)) - i\sin(2\sqrt{l}(\zeta+E))}, \\ -i\sqrt{l} + \dfrac{2iC\sqrt{l}}{C + cos(2\sqrt{l}(\zeta+E)) - i\sin(2\sqrt{l}(\zeta+E))}, \end{cases} \tag{21}$$

where $C \neq 0$ and D, E are real arbitrary constants.

Case-3: Rational function solution (when $l = 0$):

$$S(\zeta) = \frac{1}{\zeta + E}. \tag{22}$$

To identify the value of N in Eq. (18), balancing $H_n^2 H_n''$ with H_n^5 yields $N = 1$. Eq. (18) takes the form

$$H_n(\zeta) = A_0^{(n)} + A_1^{(n)} S(\zeta) + B_1^{(n)} S(\zeta)^{-1}. \tag{23}$$

Then putting Eq. (23) along with Eq. (19) into Eq. (17) and after some calculations, we pose the following sets of solutions:

Set-1: $A_0^{(n)} = 0,\ A_1^{(n)} = M_n,\ B_1^{(n)} = 0$

$$\begin{aligned} w =\ & (k^3 J_n a_n b_n - k\lambda^2 L_n^2 b_n - 2kl^2 L_n R_n b_n + 2klJ_n a_n b_n - k^2 J_n a_n \\ & + l^2 L_n^2 + 2l^2 L_n R_n + 2lJ_n a_n)/(J_n(k^2 b_n^2 + 2lb_n^2 - 2kb_n + 1)) \end{aligned}$$

$$\begin{aligned} c_n =\ & -(k^4 h_n L_n b_n^2 + 2k^4 h_n R_n b_n^2 + k^4 L_n R_n b_n^2 + 2k^4 R_n^2 b_n^2 + 2k^2 lh_n L_n b_n^2 \\ & + 4k^2 lh_n R_n b_n^2 - 2k^2 lL_n^2 b_n^2 - 4k^2 lL_n R_n b_n^2 - 2k^3 h_n L_n b_n - 4k^3 h_n R_n b_n \\ & - 2k^3 L_n R_n b_n - 4k^3 R_n^2 b_n + k^2 L_n b_n^2 d_n + 2k^2 R_n b_n^2 d_n - 2l^2 L_n^2 b_n^2 \\ & - 8l^2 L_n R_n b_n^2 - 8l^2 R_n^2 b_n^2 + 4klL_n^2 b_n + 12klL_n R_n b_n + 8klR_n^2 b_n + 2lL_n b_n^2 d_n \\ & + 4lR_n b_n^2 d_n + k^2 h_n L_n + 2k^2 h_n R_n + k^2 L_n R_n + 2k^2 R_n^2 - 2kL_n b_n d_n \\ & - 4kR_n b_n d_n - 2lL_n^2 - 6lL_n R_n - 4lR_n^2 - 2J_n a_n + L_n d_n + 2R_n d_n)/(k^2 L_n b_n^2 \\ & + 2k^2 R_n b_n^2 + 2lL_n b_n^2 + 4lR_n b_n^2 - 2kL_n b_n - 4kR_n b_n + L_n + 2R_n) \end{aligned}$$

Set-2: $A_0^{(n)} = 0,\ A_1^{(n)} = 0,\ B_1^{(n)} = M_n l$

$$\begin{aligned} w =\ & (k^3 J_n a_n b_n - k\lambda^2 L_n^2 b_n - 2kl^2 L_n R_n b_n + 2klJ_n a_n b_n - k^2 J_n a_n + l^2 L_n^2 \\ & + 2l^2 L_n R_n + 2lJ_n a_n)/(J_n(k^2 b_n^2 + 2lb_n^2 - 2kb_n + 1)) \end{aligned}$$

$$\begin{aligned} c_n =\ & -(k^4 h_n L_n b_n^2 + 2k^4 h_n R_n b_n^2 + k^4 L_n R_n b_n^2 + 2k^4 R_n^2 b_n^2 + 2k^2 lh_n L_n b_n^2 \\ & + 4k^2 lh_n R_n b_n^2 - 2k^2 lL_n^2 b_n^2 - 4k^2 lL_n R_n b_n^2 - 2k^3 h_n L_n b_n - 4k^3 h_n R_n b_n \\ & - 2k^3 L_n R_n b_n - 4k^3 R_n^2 b_n + k^2 L_n b_n^2 d_n + 2k^2 R_n b_n^2 d_n - 2l^2 L_n^2 b_n^2 \\ & - 8l^2 L_n R_n b_n^2 - 8l^2 R_n^2 b_n^2 + 4klL_n^2 b_n + 12klL_n R_n b_n + 8klR_n^2 b_n + 2lL_n b_n^2 d_n \\ & + 4lR_n b_n^2 d_n + k^2 h_n L_n + 2k^2 h_n R_n + k^2 L_n R_n + 2k^2 R_n^2 - 2kL_n b_n d_n \\ & - 4kR_n b_n d_n - 2lL_n^2 - 6lL_n R_n - 4lR_n^2 - 2J_n a_n + L_n d_n + 2R_n d_n)/(k^2 L_n b_n^2 \\ & + 2k^2 R_n b_n^2 + 2lL_n b_n^2 + 4lR_n b_n^2 - 2kL_n b_n - 4kR_n b_n + L_n + 2R_n) \end{aligned}$$

Set-3: $A_0^{(n)} = 0,\ A_1^{(n)} = M_n,\ B_1^{(n)} = M_n l$

$$\begin{aligned} w =\ & -(8M_n^2 l^2 kJ_n L_n^2 b_n + 16M_n^2 l^2 kJ_n L_n R_n b_n - 6M_n^2 lkJ_n^2 a_n b_n - k^3 J_n L_n a_n b_n \\ & - 2k^3 J_n R_n a_n b_n + 8kl^2 L_n^3 b_n + 32l^2 L_n^2 R_n b_n + 32kl^2 L_n R_n^2 b_n - 8M_n^2 l^2 J_n L_n^2 \\ & - 16M_n^2 l^2 J_n L^n R_n - 2klJ_n L_n a_n b_n - 4klJ_n R_n a_n b_n - 6M_n^2 lJ_n^2 a_n + k^2 J_n a_n \\ & + 2k^2 J_n R_n a_n - 8l^2 L_n^3 - 32l^2 L_n^2 R_n - 32l^2 L_n R_n^2 - 2lJ_n L_n a_n - 4lJ_n R_n a_n) \\ & /(J_n(6J_n b_n^2 M_n^2 l + k^2 L_n b_n^2 + 2k^2 R_n b_n^2 + 2lL_n b_n^2 + 4lR_n b_n^2 - 2kL_n b_n \\ & - 4kR_n b_n + L_n + 2R_n)) \end{aligned}$$

$$\begin{aligned} c_n =\ & -(6k^2 h_n J_n b_n^2 M_n^2 - 6k^2 J_n L_n b_n^2 M_n^2 l + 12kJ_n L_n b_n M_n^2 l + 12kJ_n R_n b_n M_n^2 l \\ & + 2k^2 lh_n L_n b_n^2 + 4k^2 lh_n R_n b_n^2 - 4k^2 lL_n R_n b_n^2 + 12klL_n R_n b_n - 6J_n L_n M_n^2 l \\ & - 6J_n R_n M_n^2 l - 2a_n J_n + 2k^2 R_n^2 - 2lL_n^2 - 4lR_n^2 + L_n d_n + 2R_n d_n - 24l^2 L_n^2 b_n^2 \\ & + 2k^4 R_n^2 b_n^2 - 4k^3 R_n^2 b_n - 80l^2 R_n^2 b_n^2 + k^2 h_n L_n + 2k^2 h_n r_n + k^2 L_n R_n - 6lL_n R_n \\ & - 88l^2 L_n R_n b_n^2 + k^4 h_n L_n b_n^2 + 2k^4 h_n R_n b_n^2 + k^4 L_n R_n b_n^2 - 2k^2 lL_n^2 b_n^2 - 2k^3 h_n L_n b_n \\ & - 4k^3 h_n R_n b_n - 2k^3 L_n R_n b_n + k^2 L_n b_n^2 d_n + 2k^2 R_n b_n^2 d_n + 4klL_n^2 b_n + 8klR_n^2 b_n \\ & + 2lL_n b_n^2 d_n + 4lR_n b_n^2 d_n - 2kL_n b_n d_n - 4kR_n b_n d_n - 8l^2 J_n b_n^2 M^2 - 24l^2 J_n R_n b_n^2 M_n^2 \\ & + 6J_n b_n^2 d_n M_n^2 l)/(6J_n b_n^2 M_n^2 l + k^2 L_n b_n^2 + 2k^2 R_n b_n^2 + 2lL_n b_n^2 + 4lR_n b_n^2 - 2kL_n b_n \\ & - 4kR_n b_n + L_n + 2R_n) \end{aligned}$$

for

$$M_n = \pm \frac{\sqrt{-J_n(L_n + 2R_n)}}{J_n}.$$

Using Eqs. (20)–(21)–(22) and Eqs. (4)–(5), with the help of the solution Set-1, we obtain the following eighteen exact solutions of Eqs. (2) and (3):

$$u_{1,1}(x,t) = M_1 \left(\frac{\sqrt{-(C^2+D^2)l} - C\sqrt{-l}\cosh(2\sqrt{-l}(\zeta+E))}{C\sinh(2\sqrt{-l}(\zeta+E)) + D} \right) \exp[i\varphi]$$

$$v_{1,1}(x,t) = M_2 \left(\frac{\sqrt{-(C^2+D^2)l} - C\sqrt{-l}\cosh(2\sqrt{-l}(\zeta+E))}{C\sinh(2\sqrt{-l}(\zeta+E)) + D} \right) \exp[i\varphi]$$

$$u_{1,2}(x,t) = M_1 \left(\frac{-\sqrt{-(C^2+D^2)l} - C\sqrt{-l}\cosh(2\sqrt{-l}(\zeta+E))}{C\sinh(2\sqrt{-l}(\zeta+E)) + D} \right) \exp[i\varphi]$$

$$v_{1,2}(x,t) = M_2 \left(\frac{-\sqrt{-(C^2+D^2)l} - C\sqrt{-l}\cosh(2\sqrt{-l}(\zeta+E))}{C\sinh(2\sqrt{-l}(\zeta+E)) + D} \right) \exp[i\varphi]$$

$$u_{1,3}(x,t) = M_1 \left(\sqrt{-l} + \frac{2C\sqrt{-l}}{C + \cosh(2\sqrt{-l}(\zeta+E)) - \sinh(2\sqrt{-l}(\zeta+E))} \right) \exp[i\varphi]$$

$$v_{1,3}(x,t) = M_2 \left(\sqrt{-l} + \frac{2C\sqrt{-l}}{C + \cosh(2\sqrt{-l}(\zeta+E)) - \sinh(2\sqrt{-l}(\zeta+E))} \right) \exp[i\varphi]$$

$$u_{1,4}(x,t) = M_1 \left(-\sqrt{-l} + \frac{2C\sqrt{-l}}{C + \cosh(2\sqrt{-l}(\zeta+E)) - \sinh(2\sqrt{-l}(\zeta+E))} \right) \exp[i\varphi]$$

$$v_{1,4}(x,t) = M_2 \left(-\sqrt{-l} + \frac{2C\sqrt{-l}}{C + \cosh(2\sqrt{-l}(\zeta+E)) - \sinh(2\sqrt{-l}(\zeta+E))} \right) \exp[i\varphi]$$

which are all singular soliton pairs. Further, one arrives at the following periodic solutions:

$$u_{1,5}(x,t) = M_1 \left(\frac{\sqrt{(C^2-D^2)l} - C\sqrt{l}\cos(2\sqrt{l}(\zeta+E))}{C\sin(2\sqrt{l}(\zeta+E)) + D} \right) \exp[i\varphi]$$

$$v_{1,5}(x,t) = M_2 \left(\frac{\sqrt{(C^2-D^2)l} - C\sqrt{l}\cos(2\sqrt{l}(\zeta+E))}{C\sin(2\sqrt{l}(\zeta+E)) + D} \right) \exp[i\varphi]$$

$$u_{1,6}(x,t) = M_1 \left(\frac{-\sqrt{(C^2-D^2)l} - C\sqrt{l}\cos(2\sqrt{l}(\zeta+E))}{C\sin(2\sqrt{l}(\zeta+E)) + D} \right) \exp[i\varphi]$$

$$v_{1,6}(x,t) = M_2 \left(\frac{-\sqrt{(C^2-D^2)l} - C\sqrt{l}\cos(2\sqrt{l}(\zeta+E))}{C\sin(2\sqrt{l}(\zeta+E)) + D} \right) \exp[i\varphi]$$

$$u_{1,7}(x,t) = M_1 \left(i\sqrt{l} + \frac{-2iC\sqrt{l}}{C + \cos(2\sqrt{l}(\zeta+E)) - i\sin(2\sqrt{l}(\zeta+E))} \right) \exp[i\varphi]$$

$$v_{1,7}(x,t) = M_2 \left(i\sqrt{l} + \frac{-2iC\sqrt{l}}{C + \cos(2\sqrt{l}(\zeta+E)) - i\sin(2\sqrt{l}(\zeta+E))} \right) \exp[i\varphi]$$

$$u_{1,8}(x,t) = M_1 \left(-i\sqrt{l} + \frac{2iC\sqrt{l}}{C + \cos(2\sqrt{l}(\zeta+E)) - i\sin(2\sqrt{l}(\zeta+E))} \right) \exp[i\varphi]$$

$$v_{1,8}(x,t) = M_2 \left(-i\sqrt{l} + \frac{2iC\sqrt{l}}{C + \cos(2\sqrt{l}(\zeta+E)) - i\sin(2\sqrt{l}(\zeta+E))} \right) \exp[i\varphi]$$

$$u_{1,9}(x,t) = \frac{M_1}{\zeta + E} \exp[i\varphi]$$

$$v_{1,9}(x,t) = \frac{M_2}{\zeta + E} \exp[i\varphi]$$

where M_n and w are come from Set-1 and $\varphi = -kx + wt + \varepsilon$. Here $u_{1,9}$ and $v_{1,9}$ are the rational solutions to the model.

Using Eqs. (20)–(21)–(22) and Eqs. (4)–(5), with the help of the solution Set-2, we obtain the following eighteen exact solutions of Eqs. (2) and (3):

$$u_{2,1}(x,t) = \frac{M_1 l}{\dfrac{\sqrt{-(C^2+D^2)l} - C\sqrt{-l}\cosh(2\sqrt{-l}(\zeta+E))}{C\sinh(2\sqrt{-l}(\zeta+E)) + D}} \exp[i\varphi]$$

$$v_{2,1}(x,t) = \frac{M_2 l}{\dfrac{\sqrt{-(C^2+D^2)l} - C\sqrt{-l}\cosh(2\sqrt{-l}(\zeta+E))}{C\sinh(2\sqrt{-l}(\zeta+E)) + D}} \exp[i\varphi]$$

$$u_{2,2}(x,t) = \frac{M_1 l}{\dfrac{-\sqrt{-(C^2+D^2)l} - C\sqrt{-l}\cosh(2\sqrt{-l}(\zeta+E))}{C\sinh(2\sqrt{-l}(\zeta+E)) + D}} \exp[i\varphi]$$

$$v_{2,2}(x,t) = \frac{M_2 l}{\dfrac{-\sqrt{-(C^2+D^2)l} - C\sqrt{-l}\cosh(2\sqrt{-l}(\zeta+E))}{C\sinh(2\sqrt{-l}(\zeta+E)) + D}} \exp[i\varphi]$$

$$u_{2,3}(x,t)=\frac{M_1 l}{\sqrt{-l}+\frac{2C\sqrt{-l}}{C+\cosh(2\sqrt{-l}(\zeta+E))-\sinh(2\sqrt{-l}(\zeta+E))}}\exp[i\varphi]$$

$$v_{2,3}(x,t)=\frac{M_2 l}{\sqrt{-l}+\frac{2C\sqrt{-l}}{C+\cosh(2\sqrt{-l}(\zeta+E))-\sinh(2\sqrt{-l}(\zeta+E))}}\exp[i\varphi]$$

$$u_{2,4}(x,t)=\frac{M_1 l}{-\sqrt{-l}+\frac{2C\sqrt{-l}}{C+\cosh(2\sqrt{-l}(\zeta+E))-\sinh(2\sqrt{-l}(\zeta+E))}}\exp[i\varphi]$$

$$v_{2,4}(x,t)=\frac{M_2 l}{-\sqrt{-l}+\frac{2C\sqrt{-l}}{C+\cosh(2\sqrt{-l}(\zeta+E))-\sinh(2\sqrt{-l}(\zeta+E))}}\exp[i\varphi]$$

These constitute another set of singular solitons. Next, the periodic solution pairs are

$$u_{2,5}(x,t)=\frac{M_1 l}{\frac{\sqrt{(C^2-D^2)l}-C\sqrt{l}\cos(2\sqrt{l}(\zeta+E))}{C\sin(2\sqrt{l}(\zeta+E))+D}}\exp[i\varphi]$$

$$v_{2,5}(x,t)=\frac{M_2 l}{\frac{\sqrt{(C^2-D^2)l}-C\sqrt{l}\cos(2\sqrt{l}(\zeta+E))}{C\sin(2\sqrt{l}(\zeta+E))+D}}\exp[i\varphi]$$

$$u_{2,6}(x,t)=\frac{M_1 l}{\frac{-\sqrt{(C^2-D^2)l}-C\sqrt{l}\cos(2\sqrt{l}(\zeta+E))}{C\sin(2\sqrt{l}(\zeta+E))+D}}\exp[i\varphi]$$

$$v_{2,6}(x,t)=\frac{M_2 l}{\frac{-\sqrt{(C^2-D^2)l}-C\sqrt{l}\cos(2\sqrt{l}(\zeta+E))}{C\sin(2\sqrt{l}(\zeta+E))+D}}\exp[i\varphi]$$

$$u_{2,7}(x,t)=\frac{M_1 l}{i\sqrt{l}+\frac{-2iC\sqrt{l}}{C+\cos(2\sqrt{l}(\zeta+E))-i\sin(2\sqrt{l}(\zeta+E))}}\exp[i\varphi]$$

$$v_{2,7}(x,t)=\frac{M_2 l}{i\sqrt{l}+\frac{-2iC\sqrt{l}}{C+\cos(2\sqrt{l}(\zeta+E))-i\sin(2\sqrt{l}(\zeta+E))}}\exp[i\varphi]$$

$$u_{2,8}(x,t)=\frac{M_1 l}{-i\sqrt{l}+\frac{2iC\sqrt{l}}{C+\cos(2\sqrt{l}(\zeta+E))-i\sin(2\sqrt{l}(\zeta+E))}}\exp[i\varphi]$$

$$v_{2,8}(x,t)=\frac{M_2 l}{-i\sqrt{l}+\frac{2iC\sqrt{l}}{C+\cos(2\sqrt{l}(\zeta+E))-i\sin(2\sqrt{l}(\zeta+E))}}\exp[i\varphi]$$

$$u_{2,9}(x,t)=M_1 l(\zeta+E)\exp[i\varphi]$$

$$v_{2,9}(x,t)=M_2 l(\zeta+E)\exp[i\varphi]$$

where M_n and w are come from Set-2 and $\varphi=-kx+wt+\varepsilon$.

Similarly, using Eqs. (20)–(21) and Eqs. (4)–(5), with the help of the solution Set-3, we obtain the sixteen exact solutions of Eqs. (2) and (3). But, Eq. (22) does not provide any exact solution of Eqs. (2) and (3) for the solution Set-3.

Conclusions

This paper revealed soliton solutions to LPD model with differential group delay. The polarized solitons are thus retrieved and exhibited. The scheme implemented is the unified approach which yielded singular soliton solutions only. Singular solitons are applicable to model optical rogons, but not optical solitons, and the algorithm, evidently, has a few drawbacks. The method fails to retrieve the much-needed bright solitons and dark solitons. Also, this scheme is unable to produce N-soliton solutions to the governing model. Moreover, a profound drawback is its inability to locate soliton radiation that is inevitably present once linear and nonlinear dispersion terms are embedded in the model. Thus, to conclude, the unified approach is not of much use in the study of governing models that give rise to optical solitons. From the applications perspective, this integration algorithm cannot be applied to obtain bright or dark solitons in any model. It can only be used to address optical rogons that are supposedly modeled with singular solitons. In addition, singular solitons cannot be plotted. This paper therefore concludes with analytical results for only singular solitons obtained by the aid of the unified method.

CRediT authorship contribution statement

Mohammad Safi Ullah: Methodology, Software. **Harun-Or-Roshid:** Methodology, Software. **M. Zulfikar Ali:** Methodology, Software. **Anjan Biswas:** Supervision. **Mehmet Ekici:** Investigation. **Salam Khan:** Supervision. **Luminita Moraru:** Validation. **Abdullah Khamis Alzahrani:** Validation. **Milivoj R. Belic:** Funding acquisition.

Declaration of competing interest

The authors declare that they have no known competing financial interests or personal relationships that could have appeared to influence the work reported in this paper.

Acknowledgment

The research work of the ninth author (MRB) was supported by the grant NPRP 11S-1126-170033 from QNRF, Qatar and he is thankful for it.

References

[1] Triki H, Biswas A, Moshokoa SP, Belic M. Optical solitons and conservation laws with quadratic–cubic nonlinearity. Optik 2017;28:63–70.
[2] Li BQ, Ma YL. Periodic solutions and solitons to two complex short pulse (CSP) equations in optical fiber. Optik 2017;144:149–55.
[3] Arshad M, Seadawy AR, Lu D. Exact bright–dark solitary wave solutions of the higher–order cubic–quintic nonlinear Schrödinger equation and its stability. Optik 2017;138:40–9.
[4] Kibler B, Fatome J, Finot C, Millot G, Dias F, Genty G, et al. The Peregrine soliton in nonlinear fiber optics. Nat Phys 2010;6:790–5.
[5] Li BQ, Sun JZ, Ma YL. Soliton excitation for a coherently coupled nonlinear Schrödinger system in optical fibers with two orthogonally polarized components. Optik 2018;175:275–83.
[6] Li BQ, Ma YL. Periodic and N–kink–like optical solitons for a generalized Schrödinger equation with variable coefficients in an inhomogeneous fiber system. Optik 2019;179:854–60.
[7] Yang JW, Gao YT, Su CQ, Zuo DW, Feng YJ. Solitons and quasi–periodic behaviors in an inhomogeneous optical fiber. Commun Nonlinear Sci Numer Simul 2017;42:477–90.
[8] Hoque MF, Roshid HO. Optical soliton solutions of the Biswas–Arshed model by the expansion method. Phys Scr 2020;95:075219.
[9] Ullah MS, Roshid HO, Ali MZ, Rahman Z. Novel exact solitary wave solutions for the time fractional generalized Hirota–Satsuma coupled KdV model through the generalized Kudryshov method. Contemp Math 2019;1:25–32.
[10] Ullah MS, Roshid HO, Ali MZ, Rahman Z. Dynamical structures of multi–soliton solutions to the Bogoyavlenskii's breaking soliton equations. Eur Phys J 2020;135(3):282.
[11] Lakshmanan M, Porsezian K, Daniel M. Effect of discreteness on the continuum limit of the Heisenberg spin chain. Phys Lett A 1988;133(9):483–8.
[12] Al-Qarni AA, Ebaid A, Alshaery AA, Bakodah HO, Biswas A, Khan S, et al. Optical solitons for Lakshmanan–Porsezian–Daniel model by Riccati equation approach. Optics 2019;182:922–9.
[13] Arshed S, Biswas A, Majid FB, Zhou Q, Moshokoa SP, Belic M. Optical solitons in birefringent fibers for Lakshmanan–Porsezian–Daniel model using $\exp(-\phi(\xi))$–expansion method. Optik 2018;170:555–60.
[14] Biswas A, Yildirim Y, Yasar E, Alqahtani RT. Optical solitons for Lakshmanan–Porsezian–Daniel model with dual–dispersion by trial equation method. Optik 2018;168:432–9.

[15] Bansal A, Biswas A, Triki H, Zhou Q, Moshokoa SP, Belic M. Optical solitons and group invariant solutions to Lakshmanan–Porsezian–Daniel model in optical fibers and PCF. Optik 2018;160:86–91.
[16] Alqahtani RT, Babatin MM, Biswas A. Bright optical solitons for Lakshmanan–Porsezian–Daniel model by semi–inverse variational principle. Optik 2018;154:109–14.
[17] Biswas A, Ekici M, Sonmezoglu A, Babatin MM. Optical solitons with differential group delay and dual–dispersion for Lakshmanan–Porsezian–Daniel model by extended trial function method. Optik 2018;170:512–9.
[18] Guzman JV, Alqahtani RT, Zhou Q, Mahmood MF, Moshokoa SP, Ullah MZ, et al. Optical solitons for Lakshmanan–Porsezian–Daniel model with spatio–temporal dispersion using the method of undetermined coefficients. Optik 2017;144:115–23.
[19] Akcagil S, Aydemir T. A new application of the unified method. NTMSCI 2018;6:185–99.
[20] Zayed EME, Shohib RMA, El-Horbaty MM, Biswas A, Ekici M, Alshomrani AS, et al. Optical solitons in birefringent fibers with Lakshmanan–Porsezian–Daniel model by the aid of a few insightful algorithms. Optik 2020;200:163281.

UNIVERSAL WISER
PUBLISHER

Novel Exact Solitary Wave Solutions for the Time Fractional Generalized Hirota–Satsuma Coupled KdV Model Through the Generalized Kudryshov Method

[1,2,*]Mohammad Safi Ullah, [2,3]Harun-Or-Roshid, [2]M. Zulfikar Ali and [1,2]Zillur Rahman

[1]Department of Mathematics, Comilla University, Cumilla-3506, Bangladesh
[2]Department of Mathematics, Rajshahi University, Rajshahi-6205, Bangladesh
[3]Department of Mathematics, Pabna University of Science and Technology, Pabna-6600, Bangladesh
Email: safi.ru1985@gmail.com and Email: harunorroshidmd@gmail.com

Abstract: In the current article, the generalized Kudryshov method is applied to determine exact solitary wave solutions for the time fractional generalized Hirota–Satsuma coupled KdV model. Here, fractional derivative is illustrated in the conformable derivative. Therefore, plentiful exact traveling wave solutions are achieved for this model, which encourage us to enlarge, a novel technique to gain unsteady solutions of autonomous nonlinear evolution models those occurs in physical and engineering branches. The obtained traveling wave solutions are expressed in terms of the exponential and rational functions. It is effortless to widen that this method is powerful and will be applied in further tasks to create advance exclusively innovative solutions to other higher-order nonlinear conformable fractional differential model in engineering problems.

Keywords: The generalized Kudryshov method; exact solitary wave solutions; time fractional generalized Hirota-Satsuma coupled (HSC) KdV system; conformable fractional derivative

1. Introduction

Nearby, great interest in fractional calculus applied in various fields such as electrical networks, control theory of dynamics, statistics, electro-chemistry of oxidization, acoustics, nonlinear optical fibre, plasma and solid state physics, chemical kinetics and geochemistry phenomena, signal processing and data mining can be effectively formed by means of nonlinear fractional order differential systems [1-6]. Modeling of a range of physical phenomena in terms of nonlinear time fractional evolution equations has played a significant factor in numerous efficient applications in the above mentioned fields.

The time fractional generalized HSC KdV system is vital nonlinear model occurs in the Toda lattice equation, a recognized (1+1) dimension soliton equation. This system can also be utilized as the model of interaction of neighboring particles of the same mass in a lattice formation with a crystal as well as illustrated basic characteristics of string dynamics in constant curvature space [13].

The more general form of time fractional generalized HSC KdV system can be written as follows [10, 11, 22]:

$$\begin{cases} \dfrac{\partial^{\alpha} h}{\partial t^{\alpha}} = \dfrac{1}{4} h_{xxx} + 3hh_x + 3(w - v^2)_x \\ \dfrac{\partial^{\alpha} v}{\partial t^{\alpha}} = -\dfrac{1}{2} v_{xxx} - 3hv_x, \qquad 0 < \alpha \le 1. \\ \dfrac{\partial^{\alpha} w}{\partial t^{\alpha}} = -\dfrac{1}{2} w_{xxx} - 3hw_x \end{cases} \tag{1}$$

Recently, searching exact solutions of the system Eq.(1) was found by renowned researchers [12, 13].Guo et. al. [12]

DOI: https://doi.org/10.37256/cm.11201936.25-33

applied the improved fractional sub-equation method to construct analytical solutions to the space–time fractional equations arises in fluid mechanics. The exact and complex traveling wave solutions to the time fractional generalized Hirota-Satsuma coupled KdV system are deliberated by Neirameh [13] using the direct algebraic method.

Considerable effort have been paid by many dynamical researchers to investigate exact solutions for FDEs such as the impulsive fractional differential equations with different boundary conditions [14, 15, 16], nonlinear impulsive hybrid boundary value problems involving fractional differential equations [17], Space–Time fractional Burgers equation [18], time fractional Burgers equation in fluid flow [19], the fractional coupled viscous Burgers' equation [20], Time-fractional KdV equations [21] and so on.

The objective of this paper is to apply the generalized Kudryashov method for finding the exact solitary wave solutions of the time fractional generalized HSC KdV system, which take part in a key task in mathematical physics.

This paper is organized as follows: fundamental properties of conformable fractional derivative are presented in section 2. The brief description of the generalized Kudryashov methods is given in section 3. Then in section 4, this method has been applied to establish exact solutions for the time fractional general HSC KdV system. The obtained results are presented graphically and the relevant physical illustrations are provided in section 5. Finally, concluding remarks are drawn in section 6.

2. Conformable fractional derivative and its properties

For a function $\phi:(0,\infty)\to\Re$, the conformable fractional derivative of ϕ for order α is defined [23] as

$$\frac{\partial^{\alpha}\phi}{\partial t^{\alpha}}=\lim_{\varepsilon\to 0^{+}}\frac{\phi(t+\varepsilon t^{1-\alpha})-\phi(t)}{\varepsilon}\quad,\quad t>0\quad\text{and}\quad 0<\alpha\le 1$$

Some important properties of the conformable fractional derivative are as follows:

$$\frac{\partial^{\alpha}}{\partial t^{\alpha}}(a\phi+b\varphi)=a\frac{\partial^{\alpha}}{\partial t^{\alpha}}(\phi)+b\frac{\partial^{\alpha}}{\partial t^{\alpha}}(\varphi),\forall a,b\in\Re.$$

$$\frac{\partial^{\alpha}}{\partial t^{\alpha}}(t^{\beta})=\beta t^{\beta-\alpha},\forall\beta\in\Re\ \textbf{\textit{and}}\ \frac{\partial^{\alpha}}{\partial t^{\alpha}}(\lambda)=0,\lambda=const.$$

$$\frac{\partial^{\alpha}}{\partial t^{\alpha}}(\phi\circ\varphi)(t)=t^{1-\alpha}\phi'(\varphi(t))\varphi'(t).$$

3. The Method

Let us assume a general nonlinear evolution equation in *x* and *t* as

$$\aleph(h,h_t,h_x,h_{\boldsymbol{x}}\ ,...)=0,x\in\Re,t>0\ , \tag{2}$$

where the function $h = h(x,t)$ is unknown and $\aleph$ is a polynomial function with respect to some functions or specified variables, which have nonlinear terms and highest order derivatives of the unknown function. The key steps of the generalized Kudryashov method are as [7, 9, 21]:

Step 1: Consider the following traveling wave transformation

$$h(x,t)=H(\zeta),\zeta=x-\frac{ct^{\alpha}}{\alpha} \tag{3}$$

where *c* is the velocity of the relative wave mode. By using the above transformation the nonlinear partial differential equation (3) is reduced to a nonlinear ordinary differential equation (ODE)

$$\chi(H,H',H'',...)=0\ , \tag{4}$$

where the prime denotes the derivative of H with respect to ζ and χ is a polynomial of $H(\zeta)$.

Step 2: Let us assume that the solution of Eq. (4) has the following form:

$$H(\zeta)=\frac{\sum_{i=0}^{N} a_i \phi^i(\zeta)}{\sum_{j=0}^{M} b_j \phi^j(\zeta)} \tag{5}$$

where a_i and b_j are real constants, N and M are positive integers such that $a_N, b_M \neq 0$ and $\phi(\zeta)$ satisfies the following ordinary differential equation:

$$\phi'(\zeta)=\phi^2(\zeta)-\phi(\zeta). \tag{6}$$

The general solution of Eq. (6) is of the following form:

$$\phi(\zeta)=\frac{1}{1+Ae^{\zeta}}, \tag{7}$$

where A is any arbitrary constant.

Step 3: Determine the positive integers N and M in Eq. (5) by balancing the highest order derivative term with the nonlinear term of $H(\zeta)$ in Eq. (2) or Eq. (4). Moreover, we define the degree of $H(\zeta)$ as $D(H(\zeta)=N-M$, which gives rise to the degree of other expression as

$$D\left(\frac{d^q H}{d\zeta^q}\right)=N-M+q, D\left(H^p\left(\frac{d^q H}{d\zeta^q}\right)^s\right)=(N-M)p+s(N-M+q),$$

where p, q, s are integer numbers.

Thus, we can find the value of N and M in Eq. (5).

Step 4: Inserting Eq. (5) along with Eq. (6) into Eq. (4) and collect all terms with the same powers of ϕ together. Setting each coefficients of this polynomial ϕ to zero, we obtain a system of algebraic equations for a_i, b_j and c.

Step 5: By inserting the values of parameters gained in previous step and $\phi(\zeta)$ into the Eq. (5), then the solutions of Eq. (2) can be constructed.

4. Applications

Consider the following traveling wave transformation:

$$\begin{cases} h(x,t)=\frac{1}{c}H^2(\xi) \\ v(x,t)=-c+H(\xi) \\ w(x,t)=2c^2-2cH(\xi) \end{cases}, \tag{8}$$

where $\xi=x-\frac{c}{\alpha}.t^{\alpha}$.

Inserting Eq. (8) into Eq. (1) reduced into ordinary differential equations

$$c(H_{\xi})^2+cHH_{\xi}+3H^4-4c^2H^2+6c^4+2c^2R=0 \tag{9}$$

and $cH_{\xi\xi} + 2H^3 - 2c^2H = 0.$ (10)

where R is an integration constant to be evaluated later.

Case 1: By balancing the highest order derivative term $HH_{\xi\xi}$ with the nonlinear term H^4 in Eq. (9) gives $N = M+ 1$ Setting $M = 1$, we have $N = 2$. Therefore Eq. (5) reduces to

$$H(\xi) = \frac{a_0 + a_1\phi + a_2\phi^2}{b_0 + b_1\phi} \tag{11}$$

Inserting Eq.(11) along with Eq.(6) into Eq.(9), we have a polynomial of $\phi^k, (k = 0,1,2,...)$. Equating the coefficients of this polynomial of the same powers of ϕ to zero, we obtain a system of equations yields the values for R,c, a_0, a_1, a_2, b_0 and b_1.

Set 1: $R = -\frac{5}{32}, c = -\frac{1}{4}, a_0 = -\frac{1}{4}b_0, a_1 = -\frac{1}{4}b_1 + \frac{1}{2}b_0, a_2 = \frac{1}{2}b_1, b_0, b_1 = const.$

Set 2: $R = -\frac{5}{2}, c = -1, a_0 = \frac{1}{2}b_1, a_1 = -b_1, a_2 = b_1, b_0 = -\frac{1}{2}b_1, b_1 = const.$

Set 3: $R = -\frac{5}{2}, c = -1, a_0 = -\frac{1}{2}b_1, a_1 = b_1, a_2 = -b_1, b_0 = -\frac{1}{2}b_1, b_1 = const.$

Set 4: $R = -\frac{5}{32}, c = -\frac{1}{4}, a_0 = \frac{1}{4}b_0, a_1 = \frac{1}{4}b_1 - \frac{1}{2}b_0, a_2 = -\frac{1}{2}b_1, b_0, b_1 = const.$

Set 5: $R = -\frac{3}{4}, c = \frac{1}{2}, a_0 = 0, a_1 = \mp\frac{i}{\sqrt{2}}b_1, a_2 = \mp\frac{i}{\sqrt{2}}b_1, b_0 = -\frac{1}{2}b_1, b_1 = const.$

For set 1, the time fractional generalized HSC KdV equations hold the solution as:

$$\begin{cases} h(x,t) = -\frac{1}{4}\left\{\frac{1 - Ae^{\xi}}{1 + Ae^{\xi}}\right\}^2 \\ v(x,t) = \frac{1}{2(1 + Ae^{\xi})} \\ w(x,t) = \frac{1}{4(1 + Ae^{\xi})} \end{cases}, \tag{12}$$

where $\xi = x + \frac{t^{\alpha}}{4\alpha}$

For set 2, the time fractional generalized HSC KdV equations hold the solution as:

$$\begin{cases} h(x,t) = -\left\{\frac{1 + A^2e^{2\xi}}{1 - A^2e^{2\xi}}\right\}^2 \\ v(x,t) = \frac{2}{1 - A^2e^{2\xi}} \\ w(x,t) = \frac{4}{1 - A^2e^{2\xi}} \end{cases} \tag{13}$$

where $\xi = x + \frac{t^{\alpha}}{\alpha}$.

For set 3, the time fractional generalized HSC KdV equations hold the solution as:

$$\begin{cases} h(x,t) = -\left\{\frac{1+A^2e^{2\xi}}{1-A^2e^{2\xi}}\right\}^2 \\ v(x,t) = -\frac{2A^2e^{2\xi}}{1-A^2e^{2\xi}} \\ w(x,t) = -\frac{4A^2e^{2\xi}}{1-A^2e^{2\xi}} \end{cases} \tag{14}$$

where $\xi = x + \frac{t^{\alpha}}{\alpha}$

For set 4, the time fractional generalized HSC KdV equations hold the solution as:

$$\begin{cases} h(x,t) = -\frac{1}{4}\left\{\frac{1-Ae^{\xi}}{1+Ae^{\xi}}\right\}^2 \\ v(x,t) = \frac{Ae^{\xi}}{2(1+Ae^{\xi})} \\ w(x,t) = \frac{Ae^{\xi}}{4(1+Ae^{\xi})} \end{cases}, \tag{15}$$

where $\xi = x + \frac{t^{\alpha}}{4\alpha}$.

For set 5, the time fractional generalized HSC KdV equations hold the solution as:

$$\begin{cases} h(x,t) = -4\left\{\frac{\pm(1+Ae^{\xi})\mp 1}{1+A^2e^{2\xi}}\right\}^2 \\ v(x,t) = \frac{-(1-A^2e^{2\xi})\mp i2\sqrt{2}(1+Ae^{\xi})\pm i2\sqrt{2}}{2(1-A^2e^{2\xi})}, \\ w(x,t) = \frac{1-A^2e^{2\xi}\mp i2\sqrt{2}(1+Ae^{\xi})\pm i2\sqrt{2}}{1-A^2e^{2\xi}} \end{cases} \tag{16}$$

where $\xi = x - \frac{t^{\alpha}}{2\alpha}$.

Case 2: Balancing HH_{xx} with H^4 in equation (10) gives $N = M + 1$, Setting $M = 1$, we obtain $N = 2$. Therefore Eq. (5) reduces to

$$H(\xi) = \frac{a_0 + a_1\phi + a_2\phi^2}{b_0 + b_1\phi} \tag{17}$$

Inserting Eq.(17) along with Eq.(5) into Eq.(10), we get a polynomial of $\phi^k, (k = 0,1,2,...)$. Equating the coefficients of this polynomial of the same powers of ϕ to zero, we obtain a system of equations yields the values for$c$, a_0, a_1, a_2, b_0 and b_1 .

Set 1: $c = -\frac{1}{4}, a_0 = -\frac{1}{4}b_0, a_1 = -\frac{1}{4}b_1 + \frac{1}{2}b_0, a_2 = \frac{1}{2}b_1, b_0, b_1 = const.$

Set 2: $c = -1, a_0 = \frac{1}{2}b_1, a_1 = -b_1, a_2 = b_1, b_0 = -\frac{1}{2}b_1, b_1 = const.$

Set 3: $c = -1, a_0 = -\frac{1}{2}b_1, a_1 = b_1, a_2 = -b_1, b_0 = -\frac{1}{2}b_1, b_1 = const.$

Set 4: $c = -\frac{1}{4}, a_0 = \frac{1}{4}b_0, a_1 = \frac{1}{4}b_1 - \frac{1}{2}b_0, a_2 = -\frac{1}{2}b_1, b_0, b_1 = const.$

Set 5: $c = \frac{1}{2}, a_0 = 0, a_1 = \pm i\sqrt{2}b_0, a_2 = \mp i\sqrt{2}b_0, b_0 = const,\ b_1 = 2b_0$.

From some simplification, we see that the set-1 to set-4 gives the same results as in case-1. But only set-5 is different which gives solution as

$$\begin{cases} h(x,t) = -4\left\{\dfrac{\pm(1+Ae^{\xi})\mp 1}{-1+A^2e^{2\xi}}\right\}^2 \\ v(x,t) = \dfrac{1-A^2e^{2\xi} \pm i2\sqrt{2}(1+Ae^{\xi}) \mp i2\sqrt{2}}{2(-1+A^2e^{2\xi})}, \\ w(x,t) = \dfrac{-1+A^2e^{2\xi} \mp i\sqrt{2}(1+Ae^{\xi}) \pm i\sqrt{2}}{2(-1+A^2e^{2\xi})} \end{cases} \tag{18}$$

where $\xi = x - \frac{t^{\alpha}}{2\alpha}$.

5. Graphical representations

Ten set of results are achieved in this research. All of the results are analyzed and some of them depicted in the Figs. 1–2. The graphs signify the change of amplitude, shape of wave and nature of the solitary waves for each acquired wave solutions in space x at time t. The solution h (x,t) of Eq.(12) represents bright bell solitary wave (Fig-1(a)) for the physical parameters A=0.5, α=0.67 The solution both v (x,t) and w (x,t) of Eq.(12) represents similar kink solitary wave. Fig-1(b) expressed the shape of the kink wave v (x,t) of Eq.(12) for the physical parameters A=0.5, α=0.67.

The solutions h (x,t)of Eq.(15) represent bright bell solitary wave solutions and all of them are similar like to the graph Fig-1(a) of h (x,t) in Eq.(12). We also see that the solutions v (x,t), w (x,t) of Eq.(15) represent kink solitary wave solutions and all of them are similar like to the graph Fig-1(b) of h (x,t) in Eq.(12). So we omit the similar type of figures.

The solution h (x,t) of Eq.(13) represents dark solitary wave (see Fig-2(a)) for the physical parameters A=0.5, α=0.5 in space x at time t. The solution both v (x,t) and w (x,t) of Eq.(13) represents similar singular kink solitary wave. Fig-2(b) expressed the shape of the singular kink solitary wave v (x,t) of Eq.(13) for the physical parameters A=0.5, α=0.5.

The solutions h (x,t) of Eq.(14), Eq.(16) and Eq.(18) represent dark bell solitary wave solutions and all of them are similar to the graph Fig-2(a) of h (x,t) in Eq.(13). We also see that the solutions v (x,t), w (x,t) of Eq.(14) and complex part of v (x,t), w (x,t) of Eq.(16) and v (x,t), w (x,t) of Eq.(18) represent singular kink solitary wave solutions and all of them are similar like to the graph Fig-2(b) of h (x,t) in Eq.(13). So we omit the similar type of figures. Real part of in Eq.(16) and

Eq.(18) gives constant solution that represent in *xt* plane.

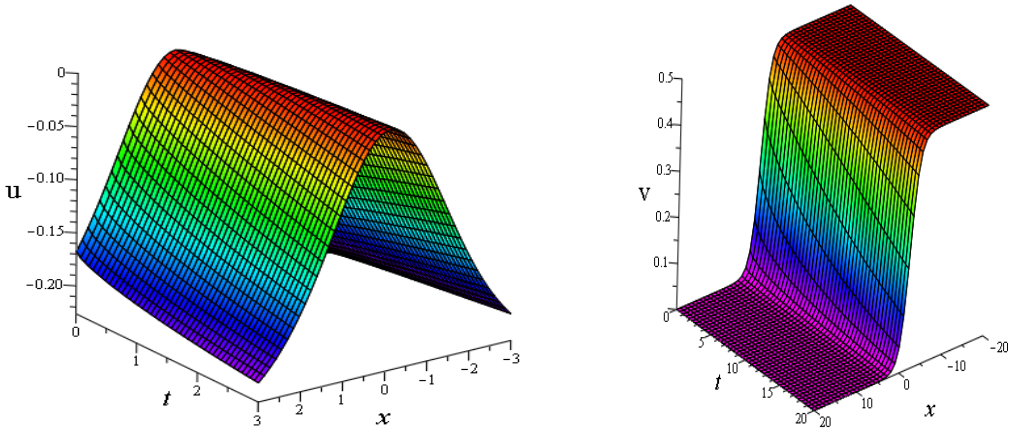

(a) (b)

Figure 1 (a) Represent bright bell solitary wave solution *h (x,t)* of Eq.(12) for the physical parametric values *A*=0.5, *α*=0.67 and (b) Represent kink solitary wave solution *v (x,t)* of Eq.(12) for the physical parametric values *A*=0.5, *α*=0.67.

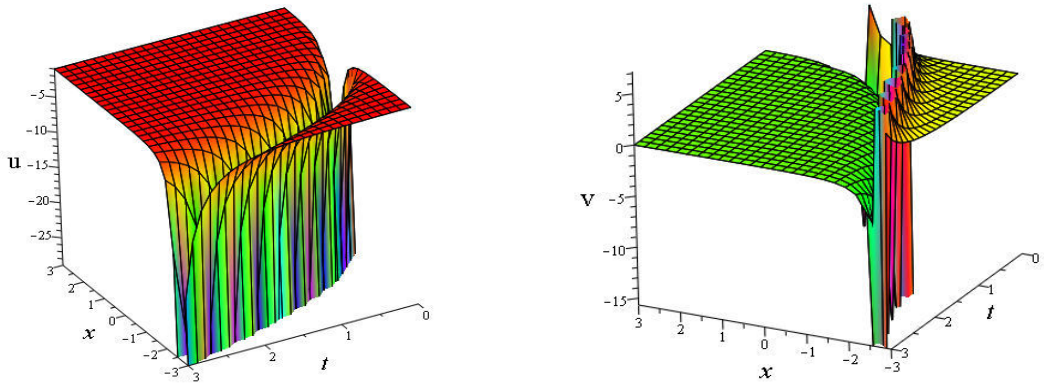

(a) (b)

Figure 2 (a) Represent dark bell solitary wave solution *h (x,t)* of Eq.(13) for the physical parametric values *A*=0.5, *α*=0.67 and (b) Represent kink solitary wave solution *v (x,t)* of Eq.(13) for the physical parametric values *A*=0.5, *α*=0.67.

6. Conclusions

In this article, we have successfully used a mathematical apparatus named the generalized Kudryashov method for creating exact solitary wave solutions to the time fractional generalized Hirota-Satsuma coupled KdV system. The achieved solitary wave solutions are expressed in terms of the exponential and rational functions. The acquired results will serve as a very important milestone in the study of interaction of neighboring particles of the same mass in a lattice formation with a crystal and long water wave phenomena. We also have demonstrated that the generalized Kudryashov method is an effective solvable tool for large classes of system of conformable nonlinear fractional differential equations.

Conflict of Interest: The authors declare that they have no conflict of interest.

References

[1] K.B. Oldham, J. Spanier. *The Fractional Calculus*. New York: Academic Press; 1974.

[2] I. Podlubny. Numerical solution of ordinary fractional differential equations by the fractional difference method. In Elaydi, S., Gyori, I. and Ladas, G. (Eds.) *Advances in Difference Equations*. Amsterdam: Gordon and Breach; 1997.

[3] I. Podlubny. *Fractional Differential Equations*. New York: Academic Press; 1999.
[4] S.G. Samko, A.A. Kilbas, O.I. Marichev. *Fractional Integrals and Derivatives: Theory and Applications*. Yverdon: Gordon and Breach; 1993.
[5] K.S. Miller, B. Ross. *An Introduction to the Fractional Calculus and Fractional Differential Equations*. New York: Wiley; 1993.
[6] M. Caputo. Linear models of dissipation whose Q is almost frequency independent. *J. Roy. Astr. Soc*., 1967; 13: 529-539.
[7] M.R. Islam, H.O. Roshid. Application of Generalized Kudryashov Method to the Burger Equation. *Int. J. Math. Trends and Tech*. (IJMTT), 2017; 38(2): 111-113.
[8] M.J. Ablowitz, H. Segur. Solitons and Inverse Scattering Transform. Philadephia: SIAM; (1981).
[9] S.T. Demiray, Y. Pandir, H. Bulut. Generalized Kudryashov method for time-fractional differential equations. In: *Abstract and applied analysis*. 2014; 2014 (Article ID 901540).
[10] Z.Z. Ganji, D.D. Gangi, Y. Rostamiyan. Solitary wave solutions for a time-fraction generalized Hirota–Satsuma coupled KdV equation by an analytical technique. *Appl. Math. Model*. 2009; 33 (7): 3107-3113.
[11] M. Shateri, D.D. Ganji. Solitary Wave Solutions for a Time-Fraction Generalized Hirota-Satsuma Coupled KdV Equation by a New Analytical Technique. *Int. J. Differ. Equ*. 2010; 2010: 117-223. Article ID 954674.
[12] S. Guo , L. Mei , Y. Li , Y. Sun . The improved fractional sub-equation method and its applications to the space–time fractional differential equations in fluid mechanics. *Phys. Lett. A* 2012;376 (4): 407–411.
[13] A. Neirameh. Soliton Solutions of the Time Fractional Generalized Hirota-satsuma Coupled KdV System. *Appl. Math. Inf. Sci.* 2015; 9(4): 1847-1853.
[14] G.M. Mophou. Existence and uniqueness of mild solutions to impulsive fractional differential equations . *Nonlinear Anal*. 2010; 72: 1604-1615.
[15] G. Wang, B. Ahmad, L. Zhang, Some existence results for impulsive nonlinear fractional differential equations with mixed boundary conditions. *Comput. Math. Appl*. 2011; 62(3): 1379-1397.
[16] X. Zhang, X. Huang, Z. Liu. The existence and uniqueness of mild solutions for impulsive fractional equations with nonlocal conditions and infinite delay. *Nonlinear Anal. Hybrid Syst*.2010; 4: 775-781.
[17] B. Ahmad, S. Sivasundaram. Existence results for nonlinear impulsive hybrid boundary value problems involving fractional differential equations. *Nonlinear Anal.: Hybrid Syst*. 2009; 3: 251-258.
[18] A. B. Emad, Abdel-Salamand, J. H. Ahmed. Solutions of the (2+1) Space–Time Fractional Burgers equation. *American Journal of Computational and Applied Mathematics*. 2016; 6(2): 109-117.
[19] A. Yokus, D. Kaya. Numerical and exact solutions for time fractional Burgers' equation. *J. Nonlinear Sci. Appl*. 2017; 10: 3419–3428.
[20] T. A. Sulaiman, M.Yavuz, H. Bulut, H. M. Baskonus. Investigation of the fractional coupled viscous Burgers' equation involving Mittag-Leffler kernel. *Physica A: Statistical Mechanics and its Applications*, 2019; 527(1): 121-126.
[21] H. Bulut, Y. Pandir, S. T. Demiray. Exact Solutions of Time-Fractional KdV Equations by Using Generalized Kudryashov Method. *International Journal of Modeling and Optimization*, 2014; 4(4): 315-320.
[22] A.S. Arife, S.K. Vanani, A. Yildirim. Numerical Solution of Hirota-Satsuma Couple Kdv and a Coupled MKdv Equation by Means of Homotopy Analysis Method. *World Appl. Sci. J*. 2011; 01(13): 2271-2276.
[23] R. Khalil , M.A. Horani , A. Yousef , M. Sababheh. A new definition of fractional derivative. *Journal of Computational and Applied Mathematics* 2014; 264: 65–70.

Physics Letters A 397 (2021) 127263

Contents lists available at ScienceDirect

Physics Letters A

www.elsevier.com/locate/pla

Collision phenomena among lump, periodic and soliton solutions to a (2+1)-dimensional Bogoyavlenskii's breaking soliton model

Mohammad Safi Ullah [b,c,*], M. Zulfikar Ali [c], Harun-Or-Roshid [e], A.R. Seadawy [d], Dumitru Baleanu [a]

[a] Department of Mathematics, Cankaya University, 06530 Ankara, Turkey
[b] Department of Mathematics, Comilla University, Cumilla-3506, Bangladesh
[c] Department of Mathematics, Rajshahi University, Rajshahi-6205, Bangladesh
[d] Department of Applied Mathematics, Taibah University, Al-Ula, Saudi Arabia
[e] Department of Mathematics, Pabna University of Science and Technology, Pabna-6600, Bangladesh

ARTICLE INFO

Article history:
Received 5 February 2021
Received in revised form 19 February 2021
Accepted 25 February 2021
Available online 2 March 2021
Communicated by B. Malomed

Keywords:
BBS model
Lump wave
Periodic wave
Soliton solutions

ABSTRACT

In this manuscript, the (2+1)-dimensional Bogoyavlenskii's breaking soliton (BBS) model is considered. At-first, we reduce the model into its bilinear form using the Hirota bilinear approach. We then analytically construct lump waves and collision of lump with periodic waves via the Hirota scheme. We also present collision between lump wave and single-, double-kink soliton solutions, and the collision among lump, periodic and single-, double-kink soliton solutions of the model. In addition, we explain the fission properties of the collisions. It is noticed that collision of lump-kink waves split into double kinky-lump waves and gradually increases the number of such waves as the increase of λ, which was not found in the previous literature. Finally, we graphically present the nature of the collision solutions of the model in 3D and contour plots. The derived such wave solutions may have much more important for controlling unpredictable harmful waves arises in nature.

1. Introduction

The soliton theory, which is one of the three sections of nonlinear science, is broadly used in various areas of physical science such as fluid mechanics, nonlinear optics, mathematical biology, ecology, chemical kinetics, plasma waves and others [1–8]. Various reliable and effective approaches have been suggested to address the solitary waves such as the (G'/G)-expansion method [9], the generalized Kudryashov method [10], the Hirota bilinear method [11], the tan-cot method [12], the tanh-coth method [13], the direct algebraic method [14], the Modified simple equation method [15], F expansion method [16], the sine-Gordon expansion method [17,18], etc. Lump wave is one of the most important parts of solitary waves and have diverse properties [19–25]. In 1977, the simplest lump wave solution was primary reported by Manakov et al. [26]. The study of lump wave solutions has been used in optical fiber [3], oceanic science [27], atmospheric science [28] and so forth. Recently, the multi-type collisions between lump/rogue and periodic waves are investigated in [29], and collisions between higher-order rogue waves and diverse types of n-soliton solutions are investigated in [30] as well. Thus such studies are highly focused on the viewpoint of the combination of quadratic functions with the exponential or trigonometric or hyperbolic functions to explain the nature of the collision of kink, lump, rogue and periodic waves for produce kinky-lump, kinky-rogue, periodic-lump wave, periodic-rogue waves and kinky-periodic-rogue wave for the NLEEs [31–38]. Based on the motivation of the above study, we consider the BBS model [39–42]:

$$\phi_{xxxy} + 4\phi_y\phi_{xx} + 4\phi_x\phi_{xy} + \phi_{xt} = 0 \tag{1}$$

where ϕ is the function of spatial variables x, y and time variable t; for the study of new dynamic phenomena and the physical behavior of different collisions among lump, periodic and soliton solutions.

Such interaction was not studied in the previous literature of the BBS model. Fission phenomena of kinky-lump wave were not derived in any nonlinear models and it is the first step of this model. These type studies of the model are still unexplored and have much scientific interest.

* Corresponding author.
E-mail addresses: safi.ru1985@gmail.com (M.S. Ullah), harunorroshidmd@gmail.com (H.-O. Roshid).

https://doi.org/10.1016/j.physleta.2021.127263
0375-9601/

We will here firstly obtain the bilinear formation of the model Eq. (1) to construct lump and periodic wave solutions and their various collision solutions. Then the dynamics of those solutions will be clearly illustrated.

2. The bilinear formation of the BBS model

Consider the conversion relation as below

$$\phi = \frac{3}{2}(\ln\psi)_x, \tag{2}$$

with real function $\psi(x, y, t)$ to be determined.

Inserting the relation Eq. (2), in Eq. (1), then we can write

$$(\ln\psi)_{xxxxy} + 6(\ln\psi)_{xy}(\ln\psi)_{xxx} + 6(\ln\psi)_{xx}(\ln\psi)_{xxy} + (\ln\psi)_{xxt} = 0. \tag{3}$$

Integrating the Eq. (3) with respect to x, then we have

$$(\ln\psi)_{xt} + (\ln\psi)_{xxxy} + 6(\ln\psi)_{xy}.(\ln\psi)_{xx} = 0. \tag{4}$$

By considering the linear terms of Eq. (4), we have

$$(\ln\psi)_{xt} + (\ln\psi)_{xxxy} = 0. \tag{5}$$

By using the bilinear operator D, the Eq. (5) can be written as

$$(D_x D_t + D_y {D_x}^3) f.f = 0, \tag{6}$$

when the D-operator [11] is defined by

$$(D_x{}^m D_y{}^k D_t{}^n) f.g = \left(\frac{\partial}{\partial x_1} - \frac{\partial}{\partial x_2}\right)^m \left(\frac{\partial}{\partial y_1} - \frac{\partial}{\partial y_2}\right)^k \left(\frac{\partial}{\partial t_1} - \frac{\partial}{\partial t_2}\right)^n \times \left[f(x_1, y_1, t_1).g(x_2, y_2, t_2)\right].$$

Thus Eq. (5) reduces to

$$\psi\psi_{xt} - \psi_t\psi_x + 3\psi_{xx}\psi_{xy} - 3\psi_x\psi_{xxy} + \psi\psi_{xxxy} - \psi_{xxx}\psi_y = 0. \tag{7}$$

Clearly if ψ satisfies Eq. (1), then $\phi = \frac{3}{2}(\ln\psi)_x$ directly generates the solutions of the governing model Eq. (1).

3. Lump wave solution of BBS model

To obtain the lump wave solutions of the BBS model, consider an ansatz of the following form

$$\psi = (p_1x + p_2y + p_3t)^2 + (q_1x + q_2y + q_3t)^2 + l, \tag{8}$$

where $p_1, p_2, p_3, q_1, q_2, q_3$ and l are free parameters. Setting Eq. (8) in Eq. (7), we have an algebraic system in $p_1, p_2, p_3, q_1, q_2, q_3$ and l. By solving this system via Maple 18, we have $p_3 = q_3 = 0$, $p_1 = p_1$, $p_2 = -\frac{q_1q_2}{p_1}$, $q_1 = q_1$, $q_2 = q_2$, $l = l$, then the Eq. (8) can be written as

$$\psi = \left(p_1x - \frac{q_1q_2}{p_1}y\right)^2 + (q_1x + q_2y)^2 + l. \tag{9}$$

By combining Eq. (9) and Eq. (7) and putting $p_1 = q_1 = q_2 = l = 1$, we have the solution of Eq. (1) as depicted in Fig. 1. Due to guarantee ϕ is localized in every direction, l have to be considered as a positive constant. In this case, the optimum amplitude of the solution ϕ is occurred at the points $(\pm\sqrt{\frac{l}{{p_1}^2+{q_1}^2}}, 0)$ with the amplitudes $\frac{3}{2}\sqrt{\frac{{p_1}^2+{q_1}^2}{l}}$ and $-\frac{3}{2}\sqrt{\frac{{p_1}^2+{q_1}^2}{l}}$.

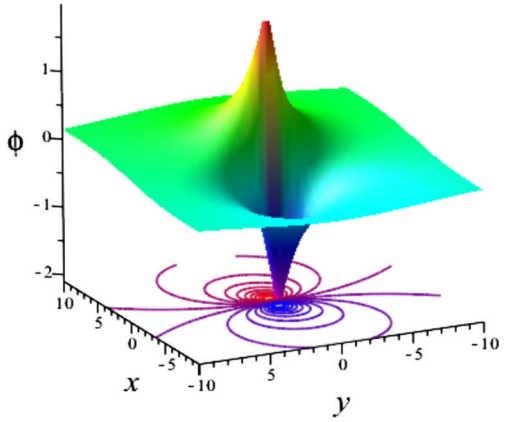

Fig. 1. Profiles of the lump solution ϕ Eq. (1) for $p_1 = q_1 = q_2 = l = 1$.

4. Collision among lumps, periodic waves, and soliton solutions

4.1. Collision between lumps and periodic waves

To study the collision scenarios between lump and periodic waves, consider a function constructed by double quadratic form and a sinusoidal function

$$\psi = (\alpha_1x + \alpha_2y + \alpha_3t)^2 + (\beta_1x + \beta_2y + \beta_3t)^2 + l + \lambda\cos(\gamma_1x + \gamma_2y + \gamma_3t), \tag{10}$$

where $\alpha_1, \alpha_2, \alpha_3, \beta_1, \beta_2, \beta_3, \gamma_1, \gamma_2, \gamma_3, l$ and λ are free parameters. Inserting Eq. (10) in Eq. (7), we have an algebraic system in $\alpha_1, \alpha_2, \alpha_3, \beta_1, \beta_2, \beta_3, \gamma_1, \gamma_2, \gamma_3, l$ and λ. By solving this system via Maple 18, we get the following results:

Case 1: $\alpha_2 = \alpha_3 = \beta_2 = \beta_3 = \gamma_2 = \gamma_3 = 0, \lambda = \lambda, \alpha_1 = \alpha_1, \beta_1 = \beta_1, \gamma_1 = \gamma_1, l = l.$

Case 2: $\alpha_1 = \alpha_1, \alpha_2 = -\frac{\beta_1\beta_2}{\alpha_1}, \alpha_3 = \beta_3 = \gamma_1 = \gamma_3 = 0, \lambda = \lambda, \beta_1 = \beta_1, \beta_2 = \beta_2,\ \gamma_2 = \gamma_2, l = l$

For **case 1**, the Eq. (10) can be written as

$$\psi = (\alpha_1x)^2 + (\beta_1x)^2 + l + \lambda\cos(\gamma_1x). \tag{11}$$

For **case 2**, the Eq. (10) can be written as

$$\psi = \left(\alpha_1x - \frac{\beta_1\beta_2}{\alpha_1}y\right)^2 + (\beta_1x + \beta_2y)^2 + l + \lambda\cos(\gamma_2y). \tag{12}$$

Using Eq. (11) and Eq. (7) and selecting $\alpha_1 = \beta_1 = \gamma_1 = l = 1$, we have the solution of Eq. (1) (see Fig. 2). Fig. 2 exhibits as a single kinky-lump wave for $\lambda = 1$ (see Fig. 2(a)) but it is going to split into double kinky-lump waves even large number of kinky-lump waves due to fission of wave for the increase of λ (see the Fig. 2(b-d)) gradually. Beside this, by choosing $\alpha_1 = \beta_1 = \beta_2 = \gamma_2 = l = 1$ and setting Eq. (12) in Eq. (7), we have the solution of Eq. (1) (see Fig. 3). The solution in **case-2** exhibits as a single lump wave for $\lambda = 1$ (see Fig. 3(a)) but it is going to split into double lump waves due to fission of lump wave for the increase of λ (see the Fig. 3(b-d)) gradually. The energy distribution is symmetric over all the periodic lump waves while it travels (see Fig. 3).

4.2. Collision between a lump and a single-kink soliton

To construct the collision of lump wave and a single kink soliton, we consider a function constructed by double quadratic form and an exponential function

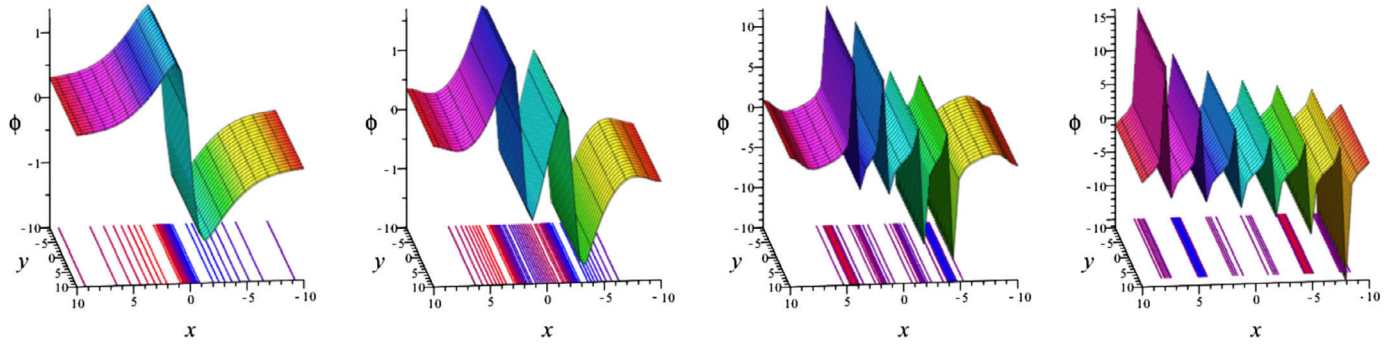

Fig. 2. Profiles of the kinky-lump wave degenerate into periodic kinky-lump wave gradually via solution ϕ of Eq. (1) for $\alpha_1 = \beta_1 = \gamma_1 = l = 1$.

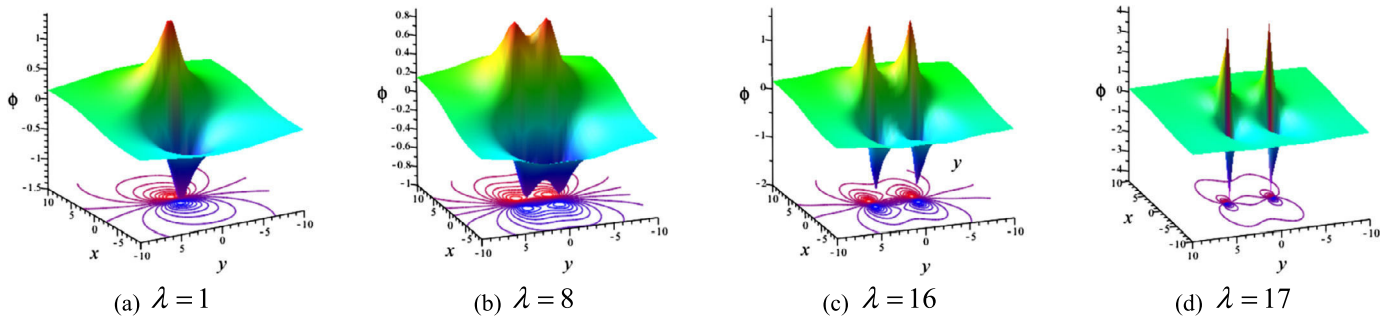

Fig. 3. Profiles of collision solution ϕ of Eq. (1) for $\alpha_1 = \beta_1 = \beta_2 = \gamma_2 = l = 1$.

$$\psi = (\alpha_1 x + \alpha_2 y + \alpha_3 t)^2 + (\beta_1 x + \beta_2 y + \beta_3 t)^2 + l + \lambda \exp(m_1 x + m_2 y + m_3 t), \tag{13}$$

where $\alpha_1, \alpha_2, \alpha_3, \beta_1, \beta_2, \beta_3, m_1, m_2, m_3, l$ and λ are real free constants. Setting Eq. (13) into the Eq. (7), we have an algebraic system in $\alpha_1, \alpha_2, \alpha_3, \beta_1, \beta_2, \beta_3, m_1, m_2, m_3, l$ and λ. By solving these equations via Maple 18, we get $\alpha_1 = \alpha_1, \alpha_2 = -\frac{\beta_1\beta_2}{\alpha_1}$, $\alpha_3 = \beta_3 = m_1 = m_3 = 0$, $\beta_1 = \beta_1$, $\beta_2 = \beta_2$, $m_2 = m_2$, $l = l$, $\lambda = \lambda$, then the Eq. (13) can be written as

$$\psi = \left(\alpha_1 x - \frac{\beta_1\beta_2}{\alpha_1} y\right)^2 + (\beta_1 x + \beta_2 y)^2 + l + \lambda \exp(m_2 x). \tag{14}$$

Using Eq. (14) and Eq. (7) and selecting $\alpha_1 = \beta_1 = \beta_2 = m_2 = l = 1$, $\lambda = 10$, we have the solution of Eq. (1) (see Fig. 4). The Fig. 4 exhibits the dynamic processes of collision between lump waves with a single kink wave solution. We observe that the lump wave is downed and consumed by the kink compare with single lump wave Fig. 1 and flow pattern being congested from one side.

4.3. Collision between a lump and a double kink soliton

To make the collision of lump wave and a two-kink soliton, we assume a function constructed by double quadratic form and a cosine hyperbolic function

$$\psi = (\alpha_1 x + \alpha_2 y + \alpha_3 t)^2 + (\beta_1 x + \beta_2 y + \beta_3 t)^2 + l + \lambda \cosh(\delta_1 x + \delta_2 y + \delta_3 t), \tag{15}$$

where $\alpha_1, \alpha_2, \alpha_3, \beta_1, \beta_2, \beta_3, \delta_1, \delta_2, \delta_3, l$ and λ are free parameters. Setting Eq. (15) in Eq. (7), we have a system of algebraic equations in $\alpha_1, \alpha_2, \alpha_3, \beta_1, \beta_2, \beta_3, \delta_1, \delta_2, \delta_3, l$ and λ. By solving these equations via Maple 18, we obtain $\alpha_1 = \alpha_1$, $\alpha_2 = -\frac{\beta_1\beta_2}{\alpha_1}$, $\alpha_3 = \beta_3 = \delta_1 = \delta_3 = 0$, $\lambda = \lambda\beta_1 = \beta_1$, $\beta_2 = \beta_2$, $\delta_2 = \delta_2$, $l = l$, then the Eq. (15) can be written as

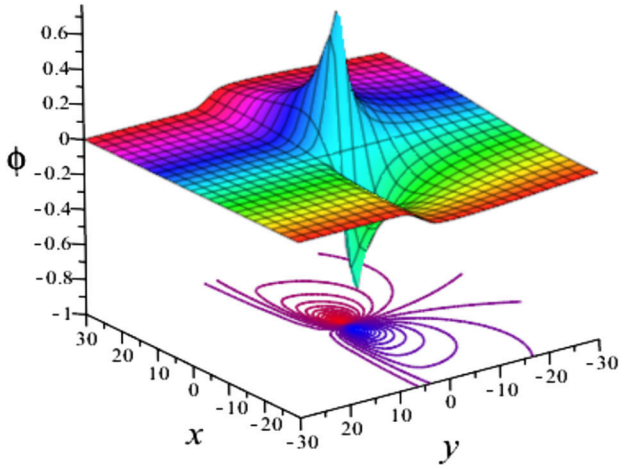

Fig. 4. Profiles of collision lump solution ϕ of Eq. (1) for $\alpha_1 = \beta_1 = \beta_2 = m_2 = l = 1$, $\lambda = 10$.

$$\psi = \left(\alpha_1 x - \frac{\beta_1\beta_2}{\alpha_1} x\right)^2 + (\beta_1 x + \beta_2 y)^2 + l + \lambda \cosh(\delta_2 y). \tag{16}$$

By combining Eq. (16) and Eq. (7) and setting $\alpha_1 = \beta_1 = \beta_2 = \delta_2 = l = 1$, $\lambda = 10$ and inserting, we have the solution of Eq. (1) (see Fig. 5). The Fig. 5 exhibits the dynamic processes of collision between lump waves with two kink waves. We observe that the lump wave is downed and consumed by the kink waves compare with lump wave (see Fig. 1 and Fig. 4) and flow pattern being congested from two sides.

4.4. Collision among lump, periodic and a single kink wave

To achieve the collision among a lump wave, a periodic and a single kink solution of Eq. (1), we assume a function constructed by double quadratic form, a cosine and an exponential function

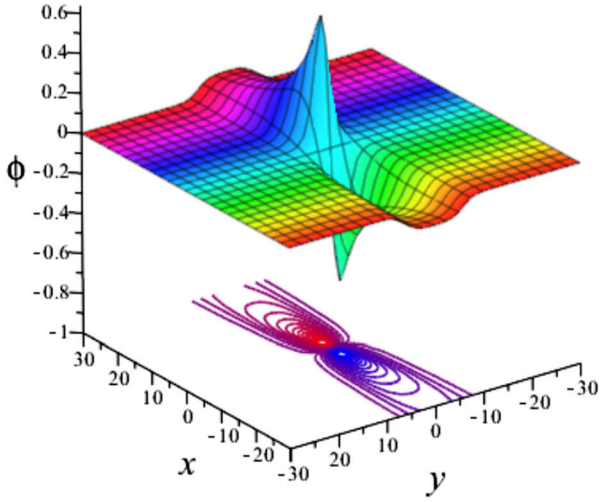

Fig. 5. Profiles of collision lump solution ϕ of Eq. (1) for $\alpha_1 = \beta_1 = \beta_2 = \delta_2 = l = 1$, $\lambda = 10$.

$$\psi = (\alpha_1 x + \alpha_2 y + \alpha_3 t)^2 + (\beta_1 x + \beta_2 y + \beta_3 t)^2 + l + \lambda_1 \cos(\gamma_1 x + \gamma_2 y + \gamma_3 t) + \lambda_2 \exp(m_1 x + m_2 y + m_3), \tag{17}$$

where $\alpha_1, \alpha_2, \alpha_3, \beta_1, \beta_2, \beta_3, \gamma_1, \gamma_2, \gamma_3, m_1, m_2, m_3, l, \lambda_1$ and λ_2 are real free constants. Setting Eq. (17) in Eq. (7), we have a system of algebraic equations in $\alpha_1, \alpha_2, \alpha_3, \beta_1, \beta_2, \beta_3, \gamma_1, \gamma_2, \gamma_3, m_1, m_2, m_3, l, \lambda_1$ and λ_2. By solving these equations via Maple 18, we have $\alpha_1 = \alpha_1$, $\alpha_2 = -\frac{\beta_1\beta_2}{\alpha_1}$, $\alpha_3 = \beta_3 = \gamma_1 = \gamma_3 = m_1 = m_3 = 0$, $\lambda_1 = \lambda_1$, $\lambda_2 = \lambda_2$, $\alpha_2 = \alpha_2$, $\beta_1 = \beta_1$, $\beta_2 = \beta_2$, $\gamma_2 = \gamma_2$, $m_2 = m_2$, $l = l$, then the Eq. (17) can be written as

$$\psi = \left(\alpha_1 x - \frac{\beta_1\beta_2}{\alpha_1} y\right)^2 + (\beta_1 x + \beta_2 y)^2 + l + \lambda_1 \cos(\gamma_2 y) + \lambda_2 \exp(m_2 y). \tag{18}$$

Using Eq. (18) and Eq. (7) and putting $\alpha_1 = \beta_1 = \beta_2 = \gamma_2 = m_2 = l = 1, \lambda_2 = 2$, we achieve the solution of Eq. (1) (see Fig. 6). The Fig. 6 exhibits the dynamic processes of collision among lump waves with single kink and periodic wave solution. We observe that the lump wave is downed and consumed by the kink wave compare with lump wave (see Fig. 1 and Fig. 4) and flow pattern being congested from one sides. Besides this, effect of periodic function makes the fission phenomena. The solution (see Fig. 6) exhibits as a single lump wave for $\lambda_1 = 1$ (see Fig. 6(a)) but it is going to split into double lump waves with $\lambda_1 = 15$ (see the Fig. 6(b, c) and Fig. 6(e, f)). In fact, it is shown that one lump of them goes to diminish and another one still unchanged for $\lambda_1 = 17$ or more increasing values.

4.5. Collision among lump, periodic and a double kink soliton

To construct the collision among a lump wave, a periodic and a two-kink soliton, we assume a function constructed by double quadratic form, a cosine and cosine hyperbolic functions

$$\psi = (\alpha_1 x + \alpha_2 y + \alpha_3 t)^2 + (\beta_1 x + \beta_2 y + \beta_3 t)^2 + l + \lambda_1 \cos(\gamma_1 x + \gamma_2 y + \gamma_3 t) + \lambda_2 \cosh(\delta_1 x + \delta_2 y + \delta_3 t), \tag{19}$$

where $\alpha_1, \alpha_2, \alpha_3, \beta_1, \beta_2, \beta_3, \gamma_1, \gamma_2, \gamma_3, \delta_1, \delta_2, \delta_3, l, \lambda_1$ and λ_2 are free parameters. Setting Eq. (19) into the Eq. (7), we have an algebraic system in $\alpha_1, \alpha_2, \alpha_3, \beta_1, \beta_2, \beta_3, \gamma_1, \gamma_2, \gamma_3, \delta_1, \delta_2, \delta_3, l, \lambda_1$ and λ_2. By solving this system via Maple 18, we have $\alpha_1 = \alpha_1, \alpha_2 = -\frac{\beta_1\beta_2}{\alpha_1}, \alpha_3 = \beta_3 = \gamma_1 = \gamma_3 = \delta_1 = \delta_3 = 0, \lambda_1 = \lambda_1, \lambda_2 = \lambda_2, \beta_1 = \beta_1, \beta_2 = \beta_2, \gamma_2 = \gamma_2, \delta_2 = \delta_2, l = l$, then the Eq. (19) can be written as

$$\psi = \left(\alpha_1 x - \frac{\beta_1\beta_2}{\alpha_1} y\right)^2 + (\beta_1 x + \beta_2 y)^2 + l + \lambda_1 \cos(\gamma_2 y) + \lambda_2 \cosh(\delta_2 y). \tag{20}$$

By using Eq. (20) and Eq. (7) and putting $\alpha_1 = \beta_1 = \beta_2 = \gamma_2 = \delta_2 = l = 1, \lambda_2 = 2$, then we acquire the solution of Eq. (1) (see Fig. 7). The Fig. 7 exhibits the dynamic processes of collision among lump waves with double kink and a periodic wave solution. We observe that the lump wave is downed and consumed by the kink compare with lump wave (see Fig. 1 and Fig. 4) and flow pattern being congested from two sides. Besides this, effect of periodic function makes the fission phenomena. The solution Fig. 7 exhibits as a single lump for $\lambda_1 = 1$ (see Fig. 7(a)), but it is going to split into double lump with the increase of λ_1 (see the Fig. 7(b-f)) gradually.

5. Conclusion

The main result in this paper is the procedure of obtaining the lump wave solutions and a class of interactions among lump, periodic and the soliton solutions of the BBS model by using different ansatz functions. In particular, for the double quadratic polynomials in the structure of the solution provide a lump wave solution that profiles are depicted in Fig. 1. We explicitly present interactions between lump and periodic waves, lump and single-, double-kink soliton solutions of the model. We also show how to interact lump with periodic waves, and single-, double- kink solitons, and to produce dynamical various structures such as periodic kinky-lump waves, periodic lump waves, lump-single, -double kink solitons, periodic-single, -double kink solitons. All interaction solitons are depicted in figures Fig. 2 to Fig. 7. It is observed that the results are much interesting as they present the causes of fission properties of the lump waves, which are presented in the figures Fig. 3, Fig. 6 and Fig. 7. It is included that the new dynamics may be enriched by the nonlinear behavior of the model and even can be found in other nonlinear models.

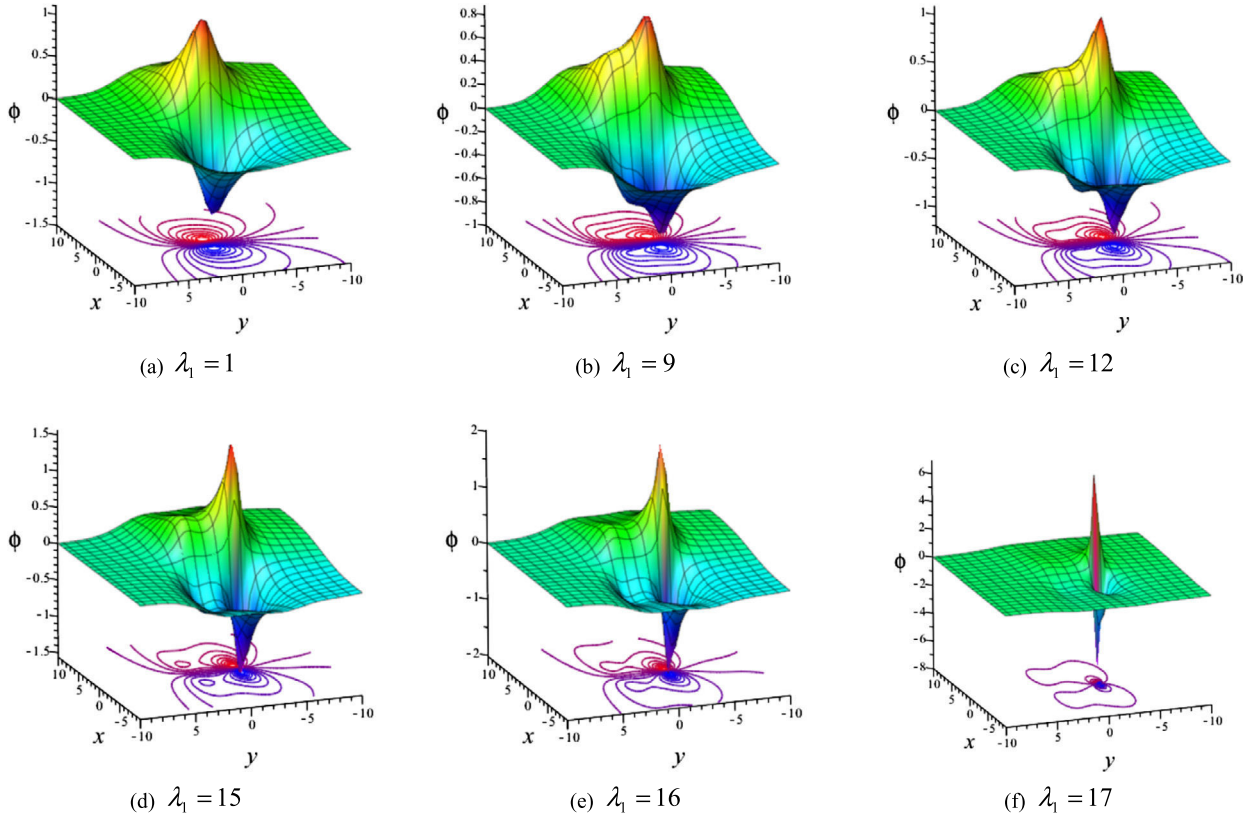

(a) $\lambda_1 = 1$ (b) $\lambda_1 = 9$ (c) $\lambda_1 = 12$

(d) $\lambda_1 = 15$ (e) $\lambda_1 = 16$ (f) $\lambda_1 = 17$

Fig. 6. Profiles of collision solution ϕ of Eq. (1) for $\alpha_1 = \beta_1 = \beta_2 = \gamma_2 = m_2 = l = 1$, $\lambda_2 = 2$.

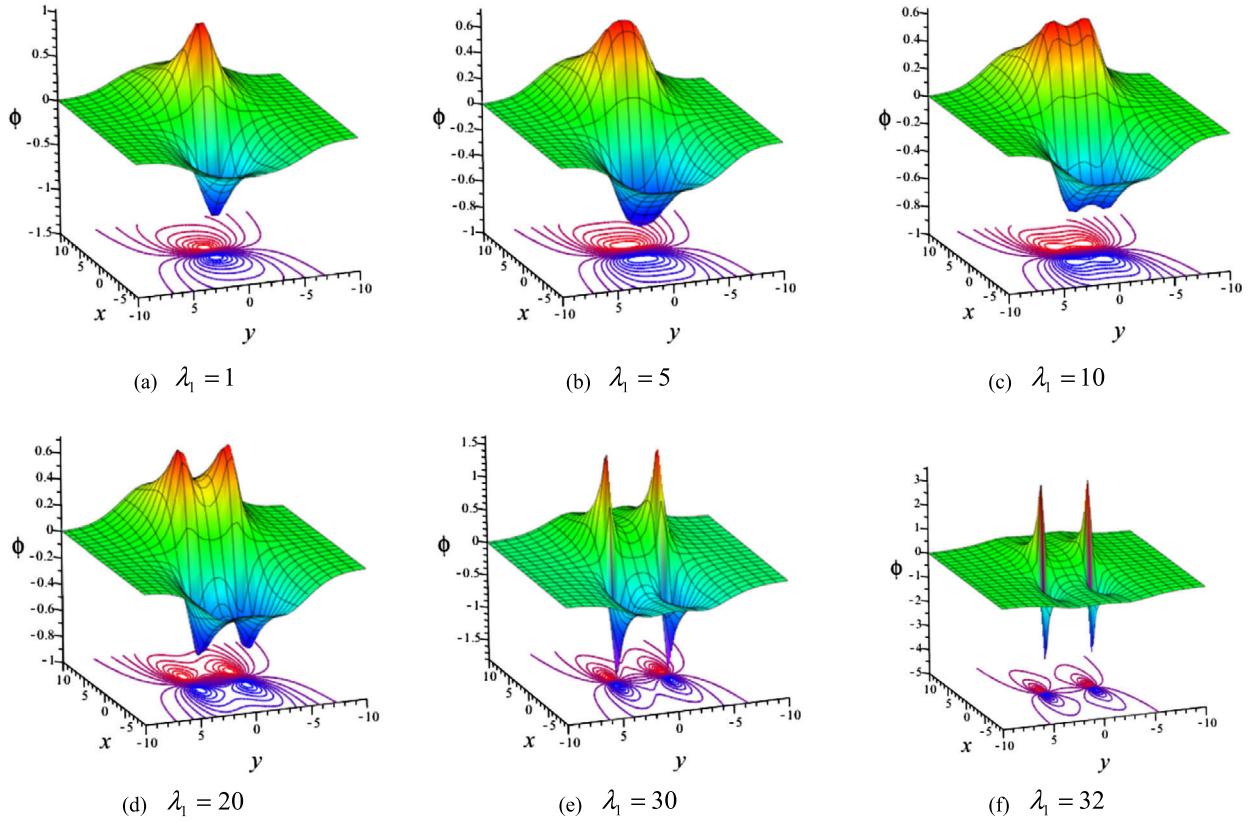

(a) $\lambda_1 = 1$ (b) $\lambda_1 = 5$ (c) $\lambda_1 = 10$

(d) $\lambda_1 = 20$ (e) $\lambda_1 = 30$ (f) $\lambda_1 = 32$

Fig. 7. Profiles of collision solution ϕ of Eq. (1) for $\alpha_1 = \beta_1 = \beta_2 = \gamma_2 = \delta_2 = l = 1$, $\lambda_2 = 2$.

Declaration of competing interest

The authors declare that they have no known competing financial interests or personal relationships that could have appeared to influence the work reported in this paper.

References

[1] A. Biswas, 1-soliton solution of the generalized Camassa–Holm Kadomtsev–Petviashvili equation, Commun. Nonlinear Sci. Numer. Simul. 14 (2009) 2524–2527.
[2] H.I. Abdel-Gawad, M. Tantawy, M.S. Osman, Dynamic of DNA's possible impact on its damage, Math. Methods Appl. Sci. 39 (2) (2016) 168–176.
[3] M.S. Ullah, H.O. Roshid, M.Z. Ali, N.F.M. Noor, Novel dynamics of wave solutions for Cahn-Allen and diffusive predator-prey models using MSE scheme, Partial Differ. Equ. Appl. Math. 3 (2021) 100017.
[4] O.A. Ilhan, T.A. Sulaiman, H. Bulut, H.M. Baskonus, On the new wave solutions to a nonlinear model arising in plasma physics, Eur. Phys. J. Plus 133 (1) (2018) 27.
[5] C. Lu, C. Fu, H. Yang, Time-fractional generalized Boussinesq equation for Rossby solitary waves with dissipation effect in stratified fluid and conservation laws as well as exact solutions, Appl. Math. Comput. 327 (2018) 104–116.
[6] A. Esen, T.A. Sulaiman, H. Bulut, H.M. Baskonus, Optical solitons to the space-time fractional (1+1)-dimensional coupled nonlinear Schrödinger equation, Optik 167 (2018) 150–156.
[7] A. Jhangeer, H.M. Baskonus, G. Yel, W. Gao, New exact solitary wave solutions, bifurcation analysis and first order conserved quantities of resonance nonlinear Schrödinger's equation with Kerr law nonlinearity, J. King Saud Univ., Sci. 33 (1) (2021) 101180.
[8] M.S. Ullah, H.O. Roshid, M.Z. Ali, A. Biswas, M. Ekici, S. Khan, L. Moraru, A.K. Alzahrani, M.R. Belic, Optical soliton polarization with Lakshamanan-Porsezian-Daniel model by unified approach, Results Phys. 22 (2021) 103958.
[9] M.L. Wang, X.Z. Li, J.L. Zhang, The (G'/G)-expansion method and travelling wave solutions of nonlinear evolution equations in mathematical physics, Phys. Lett. A 372 (4) (2008) 417–423.
[10] M.S. Ullah, H.O. Roshid, M.Z. Ali, Z. Rahman, Novel exact solitary wave solutions for the time fractional generalized Hirota–Satsuma coupled KdV model through the generalized Kudryshov method, Contemp. Math. 1 (1) (2019) 25–32.
[11] R. Hirota, The Direct Method in Soliton Theory, Camb. Uni. Press, Cambridge, 2004.
[12] R. Kumar, M. Kumar, A. Kumar, Some soliton solutions of non linear partial differential equations by tan-cot method, IOSR J. Math. 6 (6) (2013) 23–28.
[13] A.M. Wazwaz, The tanh-coth method for solitons and kink solutions for nonlinear parabolic equations, Appl. Math. Comput. 188 (2007) 1467–1475.
[14] A.R. Seadawy, The solutions of the Boussinesq and generalized fifth-order KdV equations by using the direct algebraic method, Appl. Math. Sci. 6 (2012) 4081–4090.
[15] A.J.M. Jawad, M.D. Petkovic, A. Biswas, Modified simple equation method for nonlinear evolution equations, Appl. Math. Comput. 217 (2) (2010) 869–877.
[16] R. Silambarasan, H.M. Baskonus, R.V. Anand, M. Dinakaran, B. Balusamy, W. Gao, Longitudinal strain waves propagating in an infinitely long cylindrical rod composed of generally incompressible materials and its Jacobi elliptic function solutions, Math. Comput. Simul. 182 (C) (2021) 566–602.
[17] A. Kumar, E. Ilhan, A. Ciancio, G. Yel, H.M. Baskonus, Extractions of some new travelling wave solutions to the conformable Date-Jimbo-Kashiwara-Miwa equation, AIMS Math. 6 (5) (2021) 4238–4264.
[18] J.L.G. Guirao, H.M. Baskonus, A. Kumar, Regarding new wave patterns of the newly extended nonlinear (2+1)-dimensional Boussinesq equation with fourth order, Mathematics 8 (3) (2020) 341.
[19] H.O. Roshid, Lump solutions to a (3+ 1)-dimensional potential-Yu–Toda–Sasa–Fukuyama (YTSF) like equation, Int. J. Appl. Comput. Math. 3 (2017) 1455–1461.
[20] W.X. Ma, Lump solutions to the Kadomtsev–Petviashvili equation, Phys. Lett. A 379 (2015) 1975–1978.
[21] J.P. Yu, Y.L. Sun, Study of lump solutions to dimensionally reduced generalized KP equations, Nonlinear Dyn. 87 (2017) 2755–2763.
[22] S.T. Chen, W.X. Ma, Lump solutions to a generalized Bogoyavlensky-Konopelchenko equation, Front. Math. China 13 (3) (2018) 525–534.
[23] Z. Xu, H. Chen, Z. Dai, Rogue wave for the (2+1)-dimensional Kadomtsev–Petviashvili equation, Appl. Math. Lett. 37 (2014) 34–38.
[24] J.Y. Yang, W.X. Ma, C.M. Khalique, Determining lump solutions for a combined soliton equation in (2+1)-dimensions, Eur. Phys. J. Plus 135 (2020) 494.
[25] W.X. Ma, Y. Zhang, Y. Tang, Symbolic computation of lump solutions to a combined equation involving three types of nonlinear terms, East Asian J. Appl. Math. 10 (4) (2020) 732–745.
[26] S.V. Manakov, V.E. Zakharov, L.A. Bordag, A.R. Its, V.B. Matveev, Two-dimensional solitons of the Kadomstev-Petviashvili equation and their interaction, Phys. Lett. A 63 (3) (1977) 205–206.
[27] C. Kharif, E. Pelinovsky, A. Slunyaev, Rogue Waves in the Ocean, Springer, Berlin, Germany, 2009.
[28] L. Stenflo, M. Marklund, Rogue waves in the atmosphere, Plasma Phys. 76 (3–4) (2010) 293–295.
[29] M.F. Hoque, H.O. Roshid, Optical soliton solutions of the Biswas-Arshed model by the $\tan(\theta/2)$ expansion approach, Phys. Scr. 95 (2020) 075219.
[30] M.F. Hoque, H.O. Roshid, F.S. Alshammari, Dynamical interactions between higher-order rogue waves and various forms of n-soliton solutions $(n \to \infty)$ of the (2+1)-dimensional ANNV equation, Chin. Phys. B 29 (11) (2020) 114701.
[31] M.S. Ullah, H.O. Roshid, W.X. Ma, M.Z. Ali, Z. Rahman, Interaction phenomena among lump, periodic and kink wave solutions to a (3+1)-dimensional Sharma-Tasso-Olver-like equation, Chin. J. Phys. 68 (2020) 699–711.
[32] H.O. Roshid, W.X. Ma, Dynamics of mixed lump-solitary waves of an extended (2 + 1)-dimensional shallow water wave model, Phys. Lett. A 382 (2018) 3262–3268.
[33] J.B. Zhang, W.X. Ma, Mixed lump-kink solutions to the BKP equation, Comput. Math. Appl. 74 (3) (2017) 591–596.
[34] H.Q. Zhao, W.X. Ma, Mixed lump-kink solutions to the KP equation, Comput. Math. Appl. 74 (6) (2017) 1399–1405.
[35] W.X. Ma, Interaction solutions to the Hirota-Satsuma-Ito equation in (2+1)-dimensions, Front. Math. China 14 (3) (2019) 619–629.
[36] X.E. Zhang, Y. Chen, X.Y. Tang, Rogue wave and a pair of resonance stripe solitons to KP equation, Comput. Math. Appl. 76 (8) (2018) 1938–1949.
[37] W.X. Ma, X. Yong, H.Q. Zhang, Diversity of interaction solutions to the (2+1)-dimensional Ito equation, Comput. Math. Appl. 75 (1) (2018) 289–295.
[38] W.X. Ma, R. Zhou, L. Gao, Exact one-periodic and two-periodic wave solutions to Hirota bilinear equations in (2+1) dimensions, Mod. Phys. Lett. A 24 (21) (2009) 1677–1688.
[39] W. Yong-Qi, Bilinear Bäcklund transformation and explicit solutions for a nonlinear evolution equation, Chin. Phys. B 19 (4) (2010).
[40] E. Fan, Y.C. Hon, Quasi-periodic waves and asymptotic behavior for Bogoyavlenskii's breaking soliton equation in (2+1) dimensions, Phys. Rev. E 78 (3) (2008).
[41] T. Xia, S. Xiong, Exact solutions of (2+1)-dimensional Bogoyavlenskii's breaking soliton equation with symbolic computation, Comput. Math. Appl. 60 (3) (2010) 919–923.
[42] M.S. Ullah, H.O. Roshid, M.Z. Ali, Z. Rahman, Dynamical structures of multi-soliton solutions to the Bogoyavlenskii's breaking soliton equations, Eur. Phys. J. Plus 135 (3) (2020) 282.

Chinese Journal of Physics 68 (2020) 699–711

Contents lists available at ScienceDirect

Chinese Journal of Physics

journal homepage: www.sciencedirect.com/journal/chinese-journal-of-physics

Interaction phenomena among lump, periodic and kink wave solutions to a (3 + 1)-dimensional Sharma-Tasso-Olver-like equation

Mohammad Safi Ullah [a,b], Harun-Or Roshid [c,*], Wen-Xiu Ma [d,e,f,g], M. Zulfikar Ali [b], Zillur Rahman [a,b]

[a] Department of Mathematics, Comilla University, Cumilla-3506, Bangladesh
[b] Department of Mathematics, Rajshahi University, Rajshahi-6205, Bangladesh
[c] Department of Mathematics, Pabna University of Science and Technology, Pabna-6600, Bangladesh
[d] Department of Mathematics and Statistics, University of South Florida, Tampa, FL 33620, USA
[e] Department of Mathematics, Zhejiang Normal University, Jinhua 321004, Zhejiang, China
[f] College of Mathematics and Systems Science, Shandong University of Science and Technology, Qingdao 266590, Shandong, China
[g] Department of Mathematical Sciences, North-West University, Mafikeng Campus, Mmabatho 2735, South Africa

ARTICLE INFO

Keywords:
Sharma–Tasso–Olver-like (STOL) equation
Soliton
Lump wave
rogue wave
kinky periodic wave

PACS Nos:
02.30.Jr
02.70.Wz
05.45.Yv
94.05.Fg

ABSTRACT

In this article, we consider a (3 + 1)-dimensional Sharma–Tasso–Olver-like (STOL) model describing dynamical propagation of nonlinear dispersive waves in inhomogeneous media. Applying Hirota's bilinear technique and a trial function, we explore nonlinear dynamical properties of basic solutions to the STOL model. We find that the fission fusion pattern occurs in the collision between the lump and kink waves, the collision between the lump and periodic waves, and the collision among the lump, kink and periodic waves, which is a novel fascinating collision pattern. We also observe that a large value of the coefficient in the periodic function produces a hybrid lump wave by fission in the collision solution. To better understand the dynamic properties of the obtained collision solutions, we plot a number of 3D and contour diagrams by choosing suitable parametric values with the aid of the computational software Maple 18.

1. Introduction

Nonlinear evolution equations (NLEEs) applicable not only the areas of mathematical physics, but also other branches of nonlinear science for instance optics, plasma physics, atmospheric, geochemistry and oceanic sciences etc. [1-4]. Complication of NLEES and challenges in their analytical study has engrossed a lots of effort from renowned scientists who are involved with nonlinear dynamics. As a result, exploration of exact solutions of NLEEs is a vital anxiety for dynamical researchers. There are diverse categories of exact solutions mainly soliton, multi-soliton, rational, periodic, breather line, breather kinky, lump and rogue wave solutions [5-12]. For investigating the characteristics of solitary waves, there are various reliable and fruitful approaches such as inverse scattering scheme [13], tanh function method [14], exp-function method [15,16], Darboux method [17], direct algebraic method [18], first integral

* Corresponding author.
E-mail addresses: harun_math@pust.ac.bd (H.-O. Roshid), mawx@cas.usf.edu (W.-X. Ma).

https://doi.org/10.1016/j.cjph.2020.10.009
Received 11 April 2020; Received in revised form 12 September 2020; Accepted 25 October 2020
Available online 28 October 2020

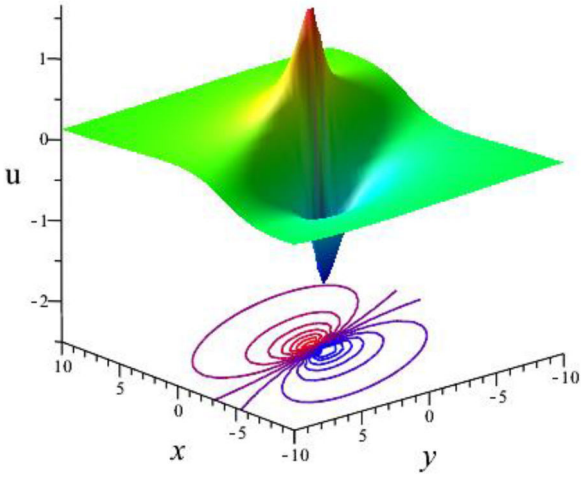

Fig. 1.. (Color online) Outlook of lump wave solution u_1 of the Eq. (6) (For interpretation of the references to color in the text, the reader is referred to the web version of this article.).

method [19, 20], exp $(-\phi(\xi))$expansion method [21], Hirota's bilinear method [22-24] etc. Though, soliton should have elastic property yet fission-fusion type non-elastic properties have been existed in few nonlinear models and investigated by many researchers [12, 23-25].

In mathematical physics, the interaction of rogue wave with other soliton/periodic wave is a kind of remarkable task in nonlinear sciences which are localized both in position and time, while lump wave is localized in every spaces only. Recently, combination of positive quadratic polynomial functions with the exponential/trigonometric functions i.e. collision of kink, lump, rogue and periodic waves produce kinky-lump, kinky-rogue, periodic-lump wave, periodic-rogue waves and kinky-periodic rogue wave for the NLEEs and their nonlinear dynamics concerned a lot of interest [26-41]. In the existed literature, we observed that interactions as mixed lump-kink [27, 28], lump solitons and the interaction phenomena [29-36], lump-stripe soliton solutions [37-38], non-elastic fusion phenomena of multi-solitons [39], N th-order rogue waves [40], two lump solitons [41] are studied by recent dynamical researchers. But it is still unexplored that both bright and dark kinks give the fission phenomena even produce hybrid lump waves, double kinky-periodic-lump type wave exhibits as hybrid lump wave, fission and fusion properties exist in presence and without presence of sinusoidal function and produces hybrid lump waves, both fission-fusion phenomena occurrences in both x-and y-periodic lump waves into a double kink wave and produce hybrid lump waves, annihilations of lump-kink wave.

Motivated by the above works and new properties, we would like to derive novel higher order collision solutions which are not reported in the previous literature for the (3 + 1)-dimensional classical STOL equation [42, 43]:

$$\begin{aligned} &u_t + a\left[\left(3uu_x + u^3\right)_x + u_{xxx}\right] + b\left[\left(2uu_y + u_x\partial_x^{-1}u_y + u^2\partial_x^{-1}u_y\right)_x + u_{xxy}\right] \\ &+c\left[\left(2uu_z + u_x\partial_x^{-1}u_z + u^2\partial_x^{-1}u_z\right) + u_{xxz}\right] = 0. \end{aligned} \tag{1}$$

with real function $u(x,y,z,t)$and real constants a,b,c. Here ∂_x^{-1}indicate integral operator and inverse of ∂_x.

In this article, our main goal is to construct more novel exact collision among lump, periodic and kinky wave solutions that degenerate into periodic line breather waves, kinky periodic waves, double kinky periodic waves, periodic lump waves, double kinky lump waves, kinky periodic lump waves, hybrid lump waves and fission fusion properties of the Eq. (1).

2. Interaction solutions and dynamics of the solutions for STOL equation

Through the relation $u = (\ln f)_x$, the Eq. (1)can be expressed as the form

$$aff_{xxxx} + bff_{xxxy} + cff_{xxxz} - af_xf_{xxx} - bf_xf_{xxy} - cf_xf_{xxz} + ff_{xt} - f_xf_t = 0, \tag{2}$$

with real function $f(x,y,z,t)$to be determined. When $f$satisfies Eq. (2), $u = (\ln f)_x$directly generates a solution of the main Eq. (1).

In order to evaluate $f$explicitly, we assume an ansatz of the following form

$$\begin{aligned} f &= (m_1x + m_2y + m_3z + m_4t + m_5)^2 + (m_6x + m_7y + m_8z + m_9t + m_{10})^2 \\ &+m_{11} + l_1\cos(m_{12}x + m_{13}y + m_{14}z + m_{15}t + m_{16}) \\ &+l_2\cosh(m_{17}x + m_{18}y + m_{19}z + m_{20}t + m_{21}), \end{aligned} \tag{3}$$

where $m_1, m_2, m_3, \ldots\ldots m_{16}$, $l_1$and $l_2$are real free constants, $m_{17}, \ldots\ldots m_{21}$are real/completely imaginary constants. Inserting Eq. (3) to Eq. (2), collect every coefficients of $x,y,z,t,\cos,\sin,\cosh,\sinh$together and setting each of these expression equal to zero, we gain a system of equations in $m_1, m_2, m_3, \ldots\ldots m_{21}$, $l_1$and l_2. Solving this system of algebraic equations by using Maple 18, we obtain the following four

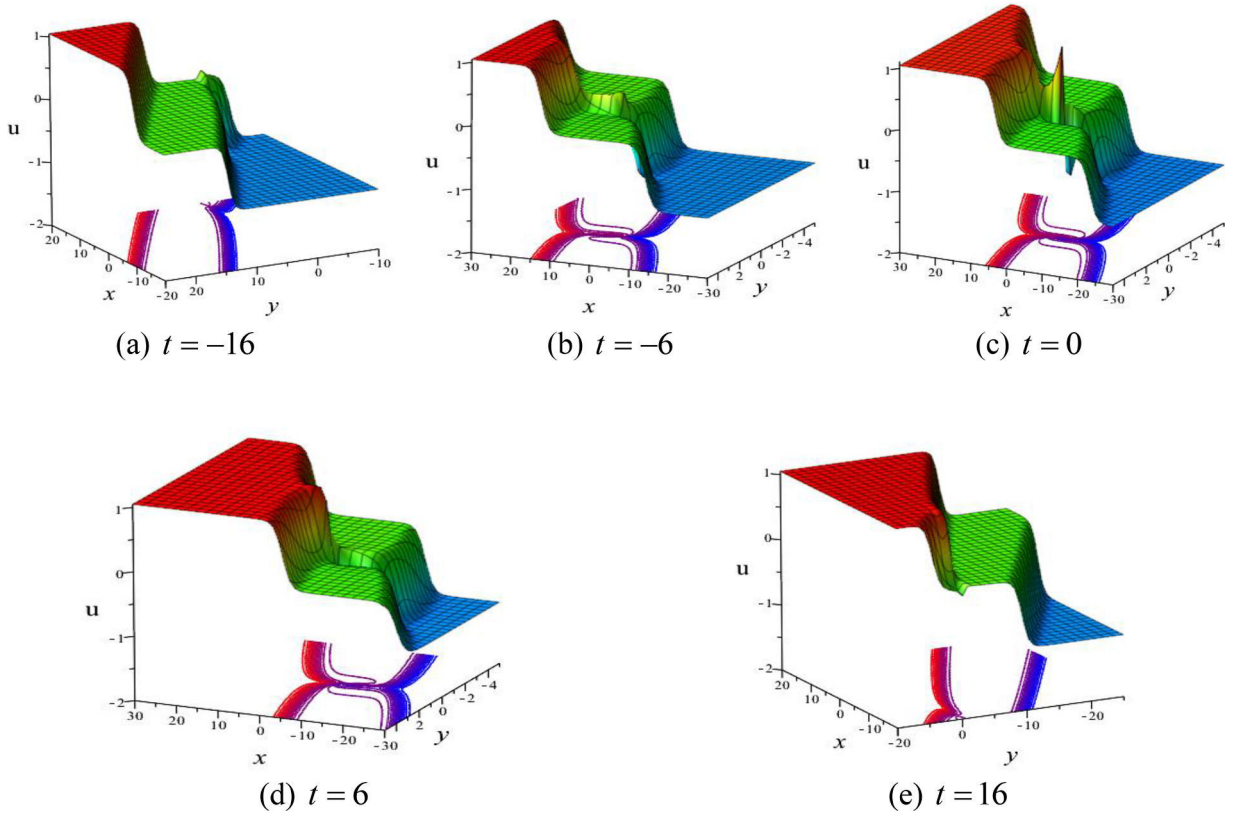

Fig. 2.. (Color online) Fission-fusion profiles of the lump wave get into a duel kinky waves for the solutions Eq. (9) with $l_2 = a = b = 1, c = -1, m_1 = 3, m_2 = -146, m_3 = -4.4, m_5 = 4, m_6 = 3, m_7 = -3.9, m_8 = 10.24, m_{10} = 1, m_{11} = 8.82, m_{17} = 1.05, m_{18} = 2.1, m_{19} = 4.6, m_{21} = 0$at $z = 0$(For interpretation of the references to color in the text, the reader is referred to the web version of this article.).

results,

Case 1:

$$l_1 = 0, l_2 = 0, m_4 = 0, m_9 = 0, \quad m_i = m_i (i = 1, 2, 3, 5, 6, 7, 8, 10, 11, \cdots, 21). \tag{4}$$

Inserting Eq. (4) into the Eq. (3), we obtain

$$f = (m_1 x + m_2 y + m_3 z + m_5)^2 + (m_6 x + m_7 y + m_8 z + m_{10})^2 + m_{11}. \tag{5}$$

Using the relation $u = (\ln f)_x$, Eq. (5)offers the result

$$u_1 = [2(m_1 x + m_2 y + m_3 z + m_5)m_1 + 2(m_6 x + m_7 y + m_8 z + m_{10})m_6]/ \left[(m_1 x + m_2 y + m_3 z + m_5)^2 + (m_6 x + m_7 y + m_8 z + m_{10})^2 + m_{11}\right]. \tag{6}$$

The result Eq. (6) contains nine free arbitrary constants and exhibits lump wave with the condition $m_{11} > 0$ in the xyplane. The line soliton solution that is definitely dissimilar starting a moving line soliton, arise very quickly and disappear in the constant background within tiny time but in the intermediate time it gives highest peak. It is well known that $u \to 0$as the two quadratic functions tend to positive or negative infinity. It maximum minimum amplitude occurs at the points $\left(\frac{m_2 m_{10} - m_5 m_7}{m_1 m_7 - m_2 m_6} \pm \sqrt{\frac{m_{11}}{{m_1}^2 + {m_6}^2}}, \frac{m_5 m_6 - m_1 m_{10}}{m_1 m_7 - m_2 m_6}\right)$when $z = 0$. The Fig.1 represents stretch of the lump wave solution Eq. (6), consists of one deep hole and one high crest for the particular values $m_1 = 2$, $m_2 = 3, m_3 = 2, m_5 = 1, m_6 = 5, m_7 = 1, m_8 = 5, m_{10} = 1, m_{11} = 10$, in the xyplane with $t = 0, z = 0$. The peak of the lump wave locates at $\left(-\frac{2}{13} + \frac{\sqrt{290}}{29}, -\frac{3}{13}\right)$, the valley locates at $\left(-\frac{2}{13} - \frac{\sqrt{290}}{29}, -\frac{3}{13}\right)$and maximum amplitude is $\frac{\sqrt{290}}{10}$and deep is equal distance i.e. $-\frac{\sqrt{290}}{10}$.

Case 2:

$$\begin{aligned} &l_1 = 0, m_4 = 0, m_9 = 0, \; m_{20} = -m_{17}^2 (a m_{17} + b m_{18} + c m_{19}) \\ &l_2 = l_2, m_i = m_i \, (i = 1, 2, 3, 5, 6, 7, 8, 10, 11, 17, 18, 19, 21), \end{aligned} \tag{7}$$

where $a, b$and $c$can take arbitrary values.

Inserting Eq. (7) into the Eq. (3), we emerge to

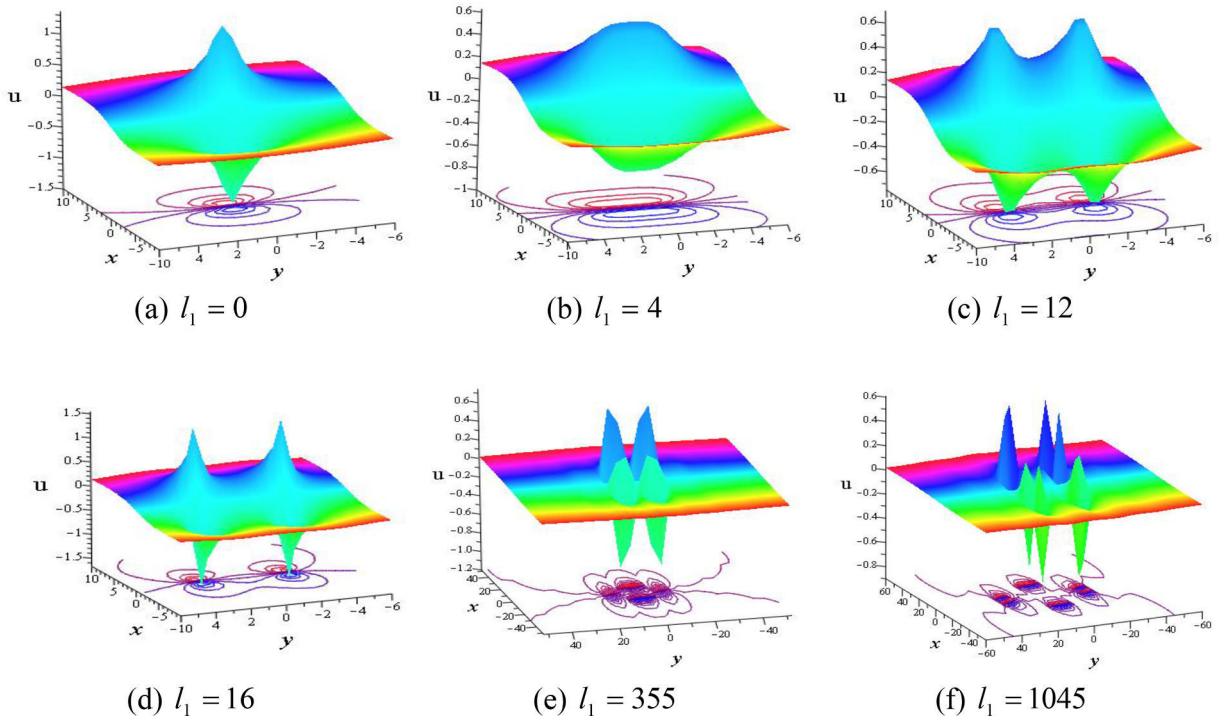

Fig. 3.. (Color online) Diagrams of collision solution u_3 of Eq. (12) for the values $a = 3, b = 3, c = -4, m_1 = -1, m_2 = 1, m_3 = -2, m_5 = -0.1, m_6 = 1, m_7 = 1, m_8 = 2, m_{10} = 0.1, m_{11} = 1, m_{12} = 0, m_{13} = 1, m_{14} = -2, m_{16} = 0$(For interpretation of the references to color in the text, the reader is referred to the web version of this article.).

$$f = (m_1x + m_2y + m_3z + m_5)^2 + (m_6x + m_7y + m_8z + m_{10})^2 + m_{11} + l_2\cosh\{m_{17}x + m_{18}y + m_{19}z - m_{17}^2(am_{17} + bm_{18} + cm_{19})t + m_{21}\}. \tag{8}$$

Using the relation $u = (\ln f)_x$, Eq. (8)provides the result

$$u_2 = \left[\begin{array}{c} 2(m_1x + m_2y + m_3z + m_5)m_1 + 2(m_6x + m_7y + m_8z + m_{10})m_6 \\ +l_2m_{17}\sinh\{m_{17}x + m_{18}y + m_{19}z - m_{17}^2(am_{17} + bm_{18} + cm_{19})t + m_{21}\} \end{array}\right] / \left[\begin{array}{c} (m_1x + m_2y + m_3z + m_5)^2 + (m_6x + m_7y + m_8z + m_{10})^2 + m_{11} \\ +l_2\cosh\{m_{17}x + m_{18}y + m_{19}z - m_{17}^2(am_{17} + bm_{18} + cm_{19})t + m_{21}\} \end{array}\right]. \tag{9}$$

In the solutions Eq. (9), we explore collision of the lump and a double kink waves through demonstration of the Fig. 2. It is seen that only a double kink waves is visible in Fig. 2(a) at the time $t = -16$and a small wave initiate at the lower kink (see from contour plot of Fig. 2(a)) but in its propagation a lump wave come out at the time $t = -6$from the lower kink (see Fig. 2(b)). So, the fission phenomenon of lower kink is happened. As time goes, it moves to the upper kink and then get highest amplitude at $t = 0$as well as lump reach in the middle of the two kinks (see Fig. 2(c)). After then the lump wave goes to the upper kink and amplitude of lump decreases again as time increases (see Fig. 2(d)) and finally diminished to the upper kink at $t = 16$(see Fig. 2(e)). So, the fusion phenomenon of upper kink is occurred. From the overall observation, we see the height of the double kink waves remain same in the overall propagation before and after the collision.

Case 3:

$$l_2 = 0, m_4 = 0, m_9 = 0, m_{15} = m_{12}^2(am_{12} + bm_{13} + cm_{14})$$
$$l_1 = l_1, m_i = m_i\,(i = 1, 2, 3, 5, 6, 7, 8, 10, 11, 12, 13, 14, 16), \tag{10}$$

where $a, b$and $c$can take arbitrary real values.

Setting Eq. (10) to the Eq. (3), we acquire

$$f = (m_1x + m_2y + m_3z + m_5)^2 + (m_6x + m_7y + m_8z + m_{10})^2 + m_{11} + l_1\cos\{m_{12}x + m_{13}y + m_{14}z + m_{12}^2(am_{12} + bm_{13} + cm_{14})t + m_{16}\}. \tag{11}$$

Using the relation$u = (\ln f)_x$, Eq. (11)offers the result

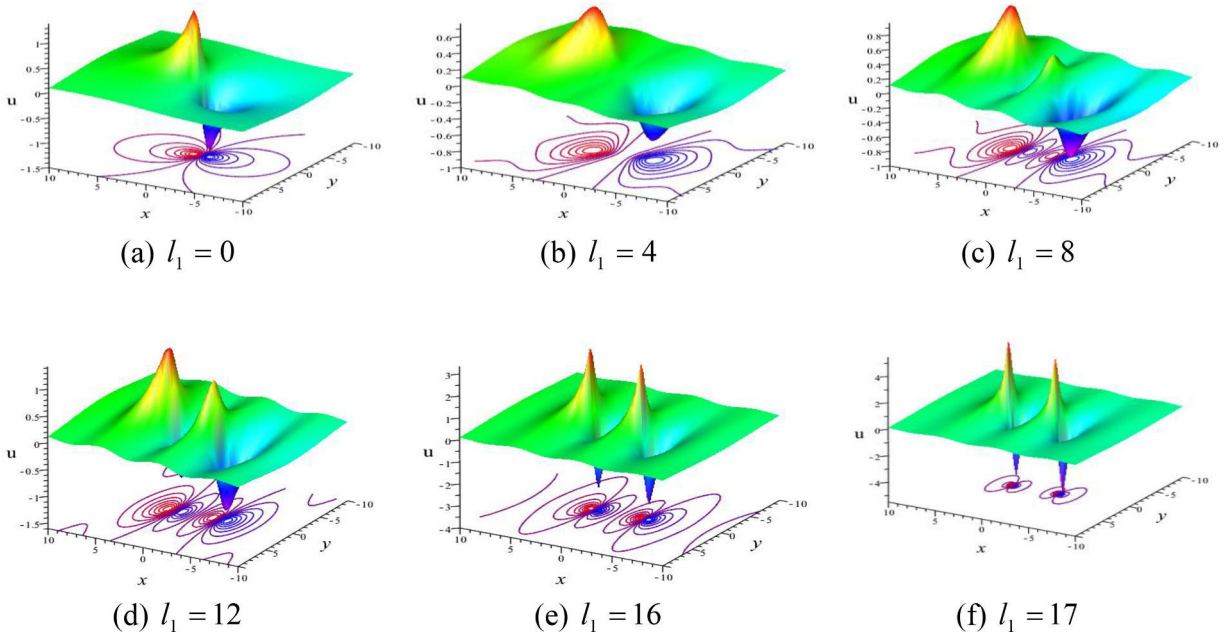

Fig. 4.. (Color online) Diagrams of the collision solution $u_3$of Eq. (12) for the values $a = 3, b = 3, c = -4,\ m_1 = -1, m_2 = 1, m_3 = -2, m_5 = -0.1, m_6 = 1, m_7 = 1, m_8 = 2, m_{10} = 0.1, m_{11} = 1, m_{12} = 1, m_{13} = 0, m_{14} = -2, m_{16} = 0$(For interpretation of the references to color in the text, the reader is referred to the web version of this article.).

$$u_3 = \begin{bmatrix} 2(m_1x + m_2y + m_3z + m_5)m_1 + 2(m_6x + m_7y + m_8z + m_{10})m_6 \\ -l_1 m_{12}\sin\{m_{12}x + m_{13}y + m_{14}z + m_{12}^2(am_{12} + bm_{13} + cm_{14})t + m_{16}\}m_{12} \end{bmatrix} / \begin{bmatrix} (m_1x + m_2y + m_3z + m_5)^2 + (m_6x + m_7y + m_8z + m_{10})^2 + m_{11} \\ +l_1\cos\{m_{12}x + m_{13}y + m_{14}z + m_{12}^2(am_{12} + bm_{13} + cm_{14})t + m_{16}\} \end{bmatrix}. \tag{12}$$

For $l_1 = 0$, $u_3$reduces to single lump only like **case-1** but for $l_1 \neq 0$, $u_3$comes in-terms of two quadratic polynomials and a sinusoidal function (i.e. collision of lump and periodic wave), as depicted in the Figs. 3–5. Here, three sub cases are arising in the followings.

(i) When $m_{12} = 0$and $m_{13} \neq 0$, $u_3$reduces to collision solution with following dynamics:

It is well-known that the lump form with a crest and a trough (observe Fig. 3(a)). But as the value of $l_1$increases, the collision of lump and periodic waves create a fission of lump wave i.e. a crest and a trough progressively split into two crests and two troughs having the same height (observe Fig. 3(b)–3(d)) and propagate along y-direction initially. Thus the fission of lump wave is happened. We also observe that fission of the lump wave is continuous process as for large values of $l_1 = 355$, the lump wave again generate fission and split into four lump waves propagate along both in the $x$and y-directions, even if for $l_1 = 1045$, it gives six lump (hybrid lump) waves (see Fig.3(e, f)) and so on.

(ii) When $m_{12} \neq 0$and $m_{13} = 0$, $u_3$reduces to collision solution with following dynamics:

It gives the similar collision solution (fission of lump) in the figures Fig. 4(b)–4(f) and produces more lump waves propagate periodically toward the x-axis and also the extreme amplitude of the crests and the troughs gradually enlarges as $l_1$increases. In contrast the Fig. 3 with Fig. 4, we observe that the lump wave in the collision solution locates toward the y-axis in Fig. 3but the lump wave in the collision solution locates toward the x-axis in the Fig. 4.

(iii) When $m_{12} \neq 0$and $m_{13} \neq 0$, $u_3$reduces to collision solution with following dynamics:

In fact, some interesting phenomenon can also be observed when both $m_{12} \neq 0$and $m_{13} \neq 0$and the value of coefficient $l_1$increases the trigonometric function that dominate on the values of coefficients in quadratic functions (lump wave) as depicted in Fig. 5(a)-(d). We display the corresponding 3D plot (3D as in upper and contour plot as in lower), density and 2D profile in the xyplane (for $y = -3, 0, 3$in Fig. 5(c)) of the lump-periodic wave. Anyone can see that at $y = 0$amplitude of the lump gives highest peak (observe Fig. 5(c)). On the other hand, another periodic-rogue wave can be observed in xtplane as in the Fig. 5(d).

Case 4:

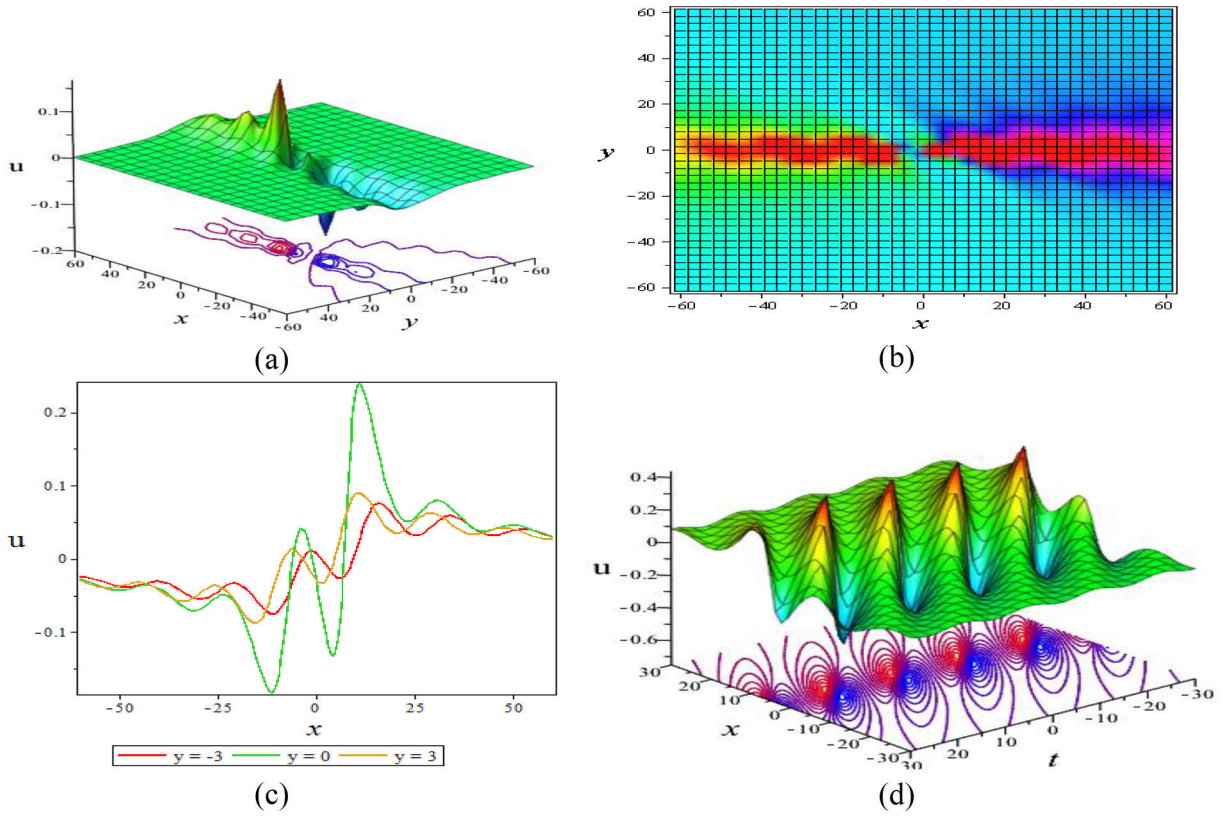

Fig. 5.. (Color online) Profile of the collision of lump and periodic waves solution $u_3$of Eq. (12) for $l_1 = 15, a = 1, b = 2, c = -4, m_1 = 0.5, m_2 = -1, m_3 = 1, m_5 = -0.5, m_6 = -0.25, m_7 = -3, m_8 = -3.5, m_{10} = 1, m_{11} = 20, m_{12} = \frac{1}{3}, m_{13} = \frac{4}{15}, m_{14} = -0.8, m_{16} = 0$: (a) the 3D plot, (b) the density plot and (c) the similar curve plot at $z = 0, t = 0$; (d) Periodic rogue wave at $z = 0, y = 0$(For interpretation of the references to color in the text, the reader is referred to the web version of this article.).

$$\begin{aligned} &m_4 = 0, m_9 = 0, m_{15} = m_{12}^2(am_{12} + bm_{13} + cm_{14}), m_{20} = -m_{17}^2(am_{17} + bm_{18} + cm_{19}) \\ &l_1 = l_1, l_2 = l_2, m_i = m_i\ (i = 1, 2, 3, 5, 6, 7, 8, 10, 11, 12, 13, 14, 16, 17, 18, 19, 21), \end{aligned} \tag{13}$$

where $a, b$and $c$can take any arbitrary values.

Putting Eq. (13) into the Eq. (3), offers the result

$$\begin{aligned} f = &(m_1x + m_2y + m_3z + m_5)^2 + (m_6x + m_7y + m_8z + m_{10})^2 + m_{11} \\ &+l_1\cos\{m_{12}x + m_{13}y + m_{14}z + m_{12}^2(am_{12} + bm_{13} + cm_{14})t + m_{16}\} \\ &+l_2\cosh\{m_{17}x + m_{18}y + m_{19}z - m_{17}^2(am_{17} + bm_{18} + cm_{19})t + m_{21}\}. \end{aligned} \tag{14}$$

Using the relation$u = (\ln f)_x$, Eq. (14)offers the result

$$\begin{aligned} u_4 = &\begin{bmatrix} 2(m_1x + m_2y + m_3z + m_5)m_1 + 2(m_6x + m_7y + m_8z + m_{10})m_6 \\ -l_1m_{12}\sin\{m_{12}x + m_{13}y + m_{14}z + m_{12}^2(am_{12} + bm_{13} + cm_{14})t + m_{16}\} \\ +l_2m_{17}\sinh\{m_{17}x + m_{18}y + m_{19}z - m_{17}^2(am_{17} + bm_{18} + cm_{19})t + m_{21}\} \end{bmatrix} / \\ &\begin{bmatrix} (m_1x + m_2y + m_3z + m_5)^2 + (m_6x + m_7y + m_8z + m_{10})^2 + m_{11} \\ +l_1\cos\{m_{12}x + m_{13}y + m_{14}z + m_{12}^2(am_{12} + bm_{13} + cm_{14})t + m_{16}\} \\ +l_2\cosh\{m_{17}x + m_{18}y + m_{19}z - m_{17}^2(am_{17} + bm_{18} + cm_{19})t + m_{21}\} \end{bmatrix}. \end{aligned} \tag{15}$$

In the solution Eq. (15), comes in terms of two quadratic polynomials, a periodic and a hyperbolic function which exhibits double kinky-periodic-lump type wave propagation for$l_2 \neq 0,\ l_1 \neq 0$. In this case, three clusters are arising in the followings.

Cluster-1 - Taking $l_2$very small as$l_2 \to 0$:

Taking $l_2$very small, a dynamical situation viewed in the Figs.6–7 for the values $a = 5, b = 1, c = -1, m_3 = m_5 = m_8 = m_{10} = m_{11} = m_{14} = 1, m_{16} = 0.1, m_{19} = 7, m_{21} = 1$at $z = 0$. The solution $u_4$provides double kinky-periodic lump wave in which some$x$-periodic-

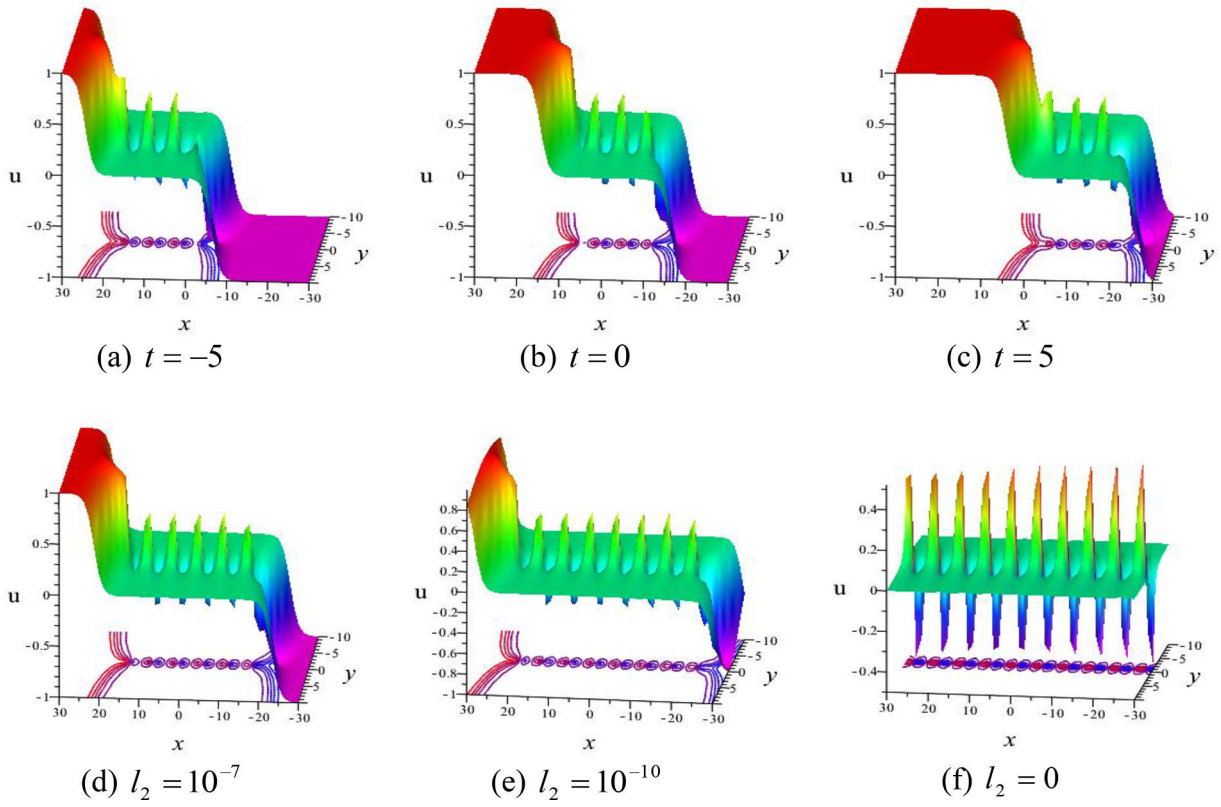

Fig. 6.. (Color online) Profiles of collision solution $u_4$of Eq. (15) for the parameters $m_1 = m_6 = m_{13} = m_{18} = 0, m_2 = m_7 = m_{12} = m_{17} = 1$, $l_1 = 0.5$: (a)-(c) the periodic lump get into the double kinky wave for $l_2 = 10^{-4}$; (d)-(e) increases of periodic lump into the double kinky wave for $l_2 \to 0$; (f) x- periodic lump wave for $l_2 = 0$(For interpretation of the references to color in the text, the reader is referred to the web version of this article.).

lump with period $2\pi/m_{12}$get into the double kink and kinky wave moves through $x$axis with time increases for the values as depicted in the Fig. 6(a)-(c). In this case number of lump wave remains same with the same value of $l_2 = 0.0001$. But when$l_2 \to 0$, the number of lump wave gradually increases as the values of $l_2$decreases (observe Fig. 6(d)-(e)), even if, kink vanishes and only periodic lump exist for $l_2 = 0$(observe Fig. 6(f)) at $t = 0$.Actually, changing different parametric constraint of the solution Eq. (15) distinguish characteristics again exhibits in Fig. 7(a)-(d) as $y-$ periodic lump with period $2\pi/m_{13}$get into the kink that arises with a constant background and decay go back to the same previous background at a longer time. On the other hand, same behavior can be observed in line soliton in the Fig. 7(e)-(h). Interesting characteristics can also be experienced when constant coefficients vanishes (i.e., $m_5 = m_{10} = m_{11} = m_{16} = m_{21} = 0$) as depicted in the Fig.8(a)-(c) that behaved $y-$ periodic bright-dark lump waves get into the double kink waves with period $2\pi/m_{13}$. The bright lumps get into the lower kink and dark lumps get into the upper kink. Both kinks give the fission phenomena and produce hybrid lump waves in which height and number of lump increases as $l_1$increase (observe Fig. 8(a)-(c)). These novel nonlinear phenomena are the first reported for the (3 + 1)-dimension STOL equation.

Cluster-2 - Taking $l_2$not so small:

Taking $l_2$not so small, a dynamical situation viewed to the solutionu_4, provides double kinky waves in which two lump waves periodically get into the kink waves and exhibits fission fusion phenomena. Solution Eq. (15), exhibits fission-fusion phenomena as depicted in the Figs.9(a)-(f) and 10(a)-(f) which are similar to the fission-fusion phenomena of the Fig. 2. But the only different is that $y$periodic two lumps causes fission from the upper kink and then fused into the lower kink when $m_{12} = 0, m_{13} \neq 0$(observe Fig. 9(a)-(e)) and $x$periodic two lumps causes fission from the upper kink and then fused into the lower kink when $m_{12} \neq 0, m_{13} = 0$(observe Fig. 10(a)-(f)). Both the figures Figs. 9(a)-(f) and 10(a)-(f) are sketch with specific parameters $l_1 = 16, l_2 = 0.5, a = -3, b = 2, c = 1, m_1 = -1, m_2 = 1, m_3 = -2, m_5 = 0, m_6 = 1, m_7 = 1, m_8 = 4, m_{10} = 0, m_{11} = 1, m_{14} = 1, m_{16} = 0, m_{17} = 1, m_{18} = 0, m_{19} = 2, m_{21} = 0$at $z = 0$. These novel nonlinear phenomenon is the first reported for the (3 + 1)-dimension STOL equation.

Cluster-3 - Taking lump vanish (i.e., $m_i = 0; i = 1, 2, 3, 5, 6, 7, 10$):

When $m_i = 0\,(i = 1, 2, 3, 5, 6, 7, 10)$; lump waves being diminished and then collision between the kinky and periodic wave are appeared in the solution Eq. (15), then we find

$$f = m_{11} + l_1\cos\{m_{12}x + m_{13}y + m_{14}z + m_{12}^2(am_{12} + bm_{13} + cm_{14})t + m_{16}\} + l_2\cosh\{m_{17}x + m_{18}y + m_{19}z - m_{17}^2(am_{17} + bm_{18} + cm_{19})t + m_{21}\}. \tag{16}$$

The solution Eq. (16) can convert to diverse collision solutions, selecting the constants $m_{17}, m_{18}, m_{19}, m_{21}$are real/purely imaginary

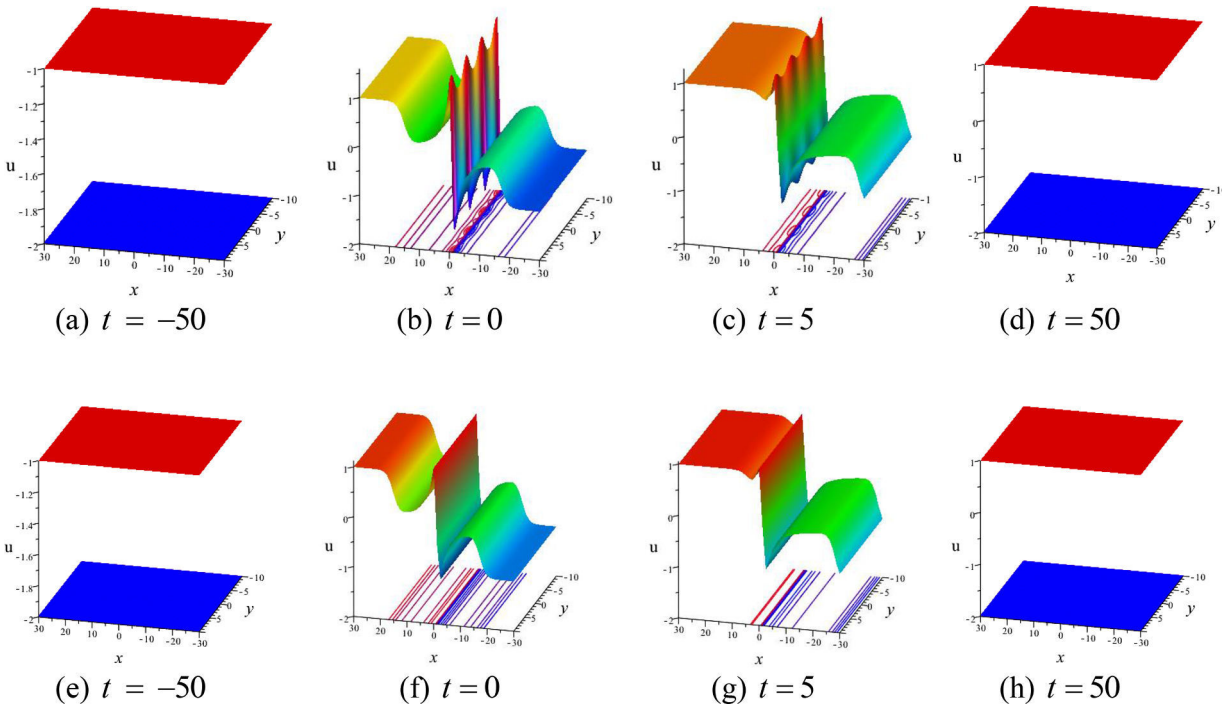

Fig. 7.. (Color online) Annihilation properties of collision solution $u_4$of Eq. (15) for $l_1 = 0.5, l_2 = 10^{-4}$at $z = 0$; (a)-(d) y – periodic lump wave get into the kinky wave for $m_2 = m_7 = m_{12} = m_{18} = 0, m_1 = m_6 = m_{13} = m_{17} = 1$; (e)-(h) x- periodic lump get into the kink wave for $m_2 = m_7 = m_{13} = m_{18} = 0, m_1 = m_6 = m_{12} = m_{17} = 1$(For interpretation of the references to color in the text, the reader is referred to the web version of this article.).

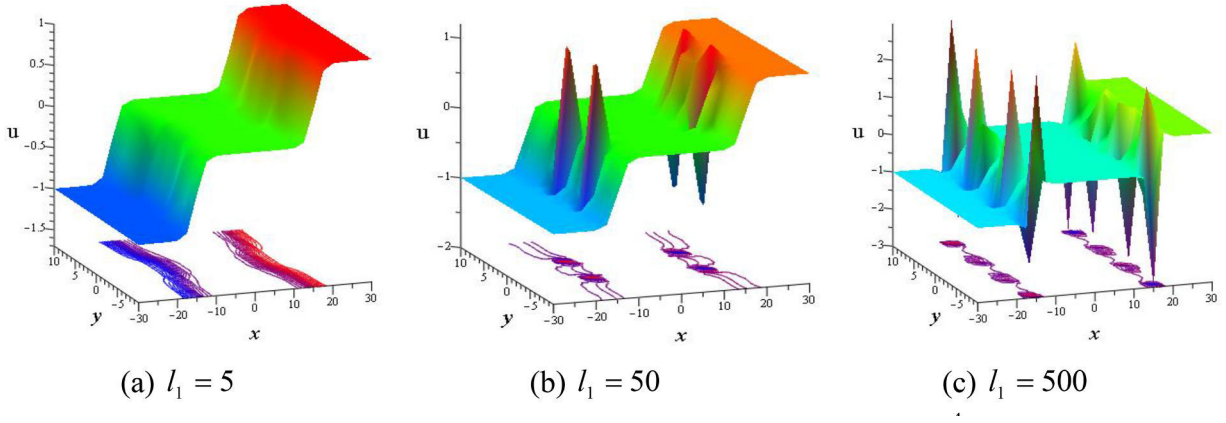

Fig. 8.. (Color online) Profiles of collision solution $u_4$of Eq. (15) for $l_2 = 10^{-4}, a = 5, b = 1, c = -1, m_1 = m_6 = m_{12} = m_{18} = 0, m_{19} = 7, m_2 = m_3 = m_7 = m_8 = m_{13} = m_{14} = m_{17} = 1$at $t = 0, z = 0$(For interpretation of the references to color in the text, the reader is referred to the web version of this article.).

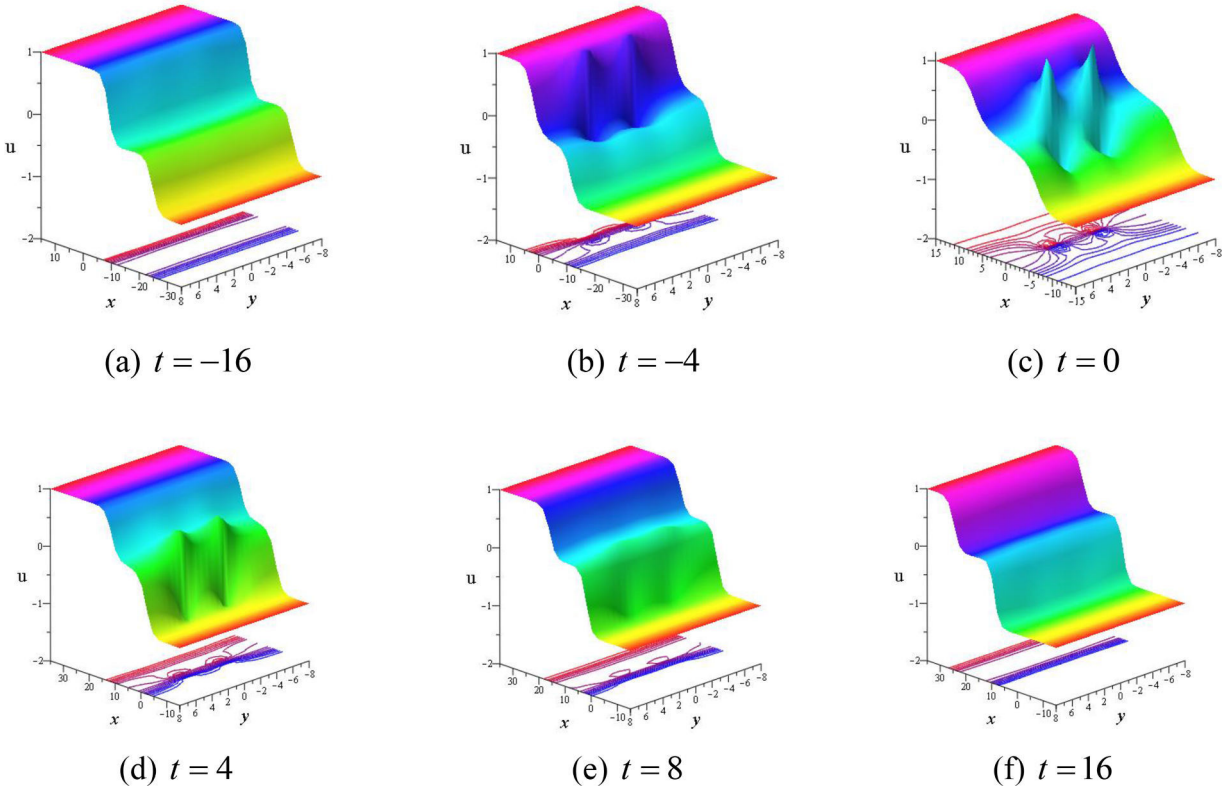

Fig. 9.. (Color online) Fission-fusion profile of y-periodic lump wave with the double kink wave of solution Eq. (15)for $m_{13}=1$(For interpretation of the references to color in the text, the reader is referred to the web version of this article.).

value.

(i) For $m_{17}, m_{18}, m_{19}, m_{21}$are real valued, we acquire a collision wave of the Eq. (1) using the relation $u=(\ln f)_x$as:

$$u_5=\begin{bmatrix}-l_1m_{12}\sin\{m_{12}x+m_{13}y+m_{14}z+m_{12}^2(am_{12}+bm_{13}+cm_{14})t+m_{16}\}\\+l_2m_{17}\sinh\{m_{17}x+m_{18}y+m_{19}z-m_{17}^2(am_{17}+bm_{18}+cm_{19})t+m_{21}\}\end{bmatrix}/$$
$$\begin{bmatrix}m_{11}+l_1\cos\{m_{12}x+m_{13}y+m_{14}z+m_{12}^2(am_{12}+bm_{13}+cm_{14})t+m_{16}\}\\+l_2\cosh\{m_{17}x+m_{18}y+m_{19}z-m_{17}^2(am_{17}+bm_{18}+cm_{19})t+m_{21}\}\end{bmatrix}. \quad (17)$$

Characteristics of the solution $u_5$for the Eq. (17) are explained for diverse choose of the involve parametric values in the figure Fig. 11 and corresponding contour line of the diagram are drawn bellow of the figures in Fig. 11(a)–11(d). For $l_1=0$, $u_5$reduces to double kinky waves (see Fig. 11(a)) but for $l_1\neq 0$, $u_5$is collision of a y- kinky periodic breather wave (see Fig. 11(b)–(d)). Evidently, as $t$changes the collision wave moves toward the $x-$ axis and the phase of the periodic wave changes after $\frac{2\pi}{m_{13}}$along y-axis.

In this case, we also observe that changing different parametric constraint in the solution Eq. (17) distinguish characteristics again exhibits which are periodic line breather waves proceed in various directions as depicted in the Fig. 11(e)-(h), (i)-(l), (m)-(p). Each group of periodic line breather waves begins with a constant background and decay return to the same previous background at a longer time.

(i) For $m_{17}, m_{18}, m_{19}, m_{21}$are pure imaginary valued, i.e., $m_{17}=i\tilde{m}_{17}, m_{18}=i\tilde{m}_{18}, m_{19}=i\tilde{m}_{19}, m_{21}=i\tilde{m}_{21}$with $\tilde{m}_{17}, \tilde{m}_{18}, \tilde{m}_{19}$and $\tilde{m}_{21}$are real valued, we acquire a collision of two breather waves of the Eq. (1) using the relation $u=(\ln f)_x$as:

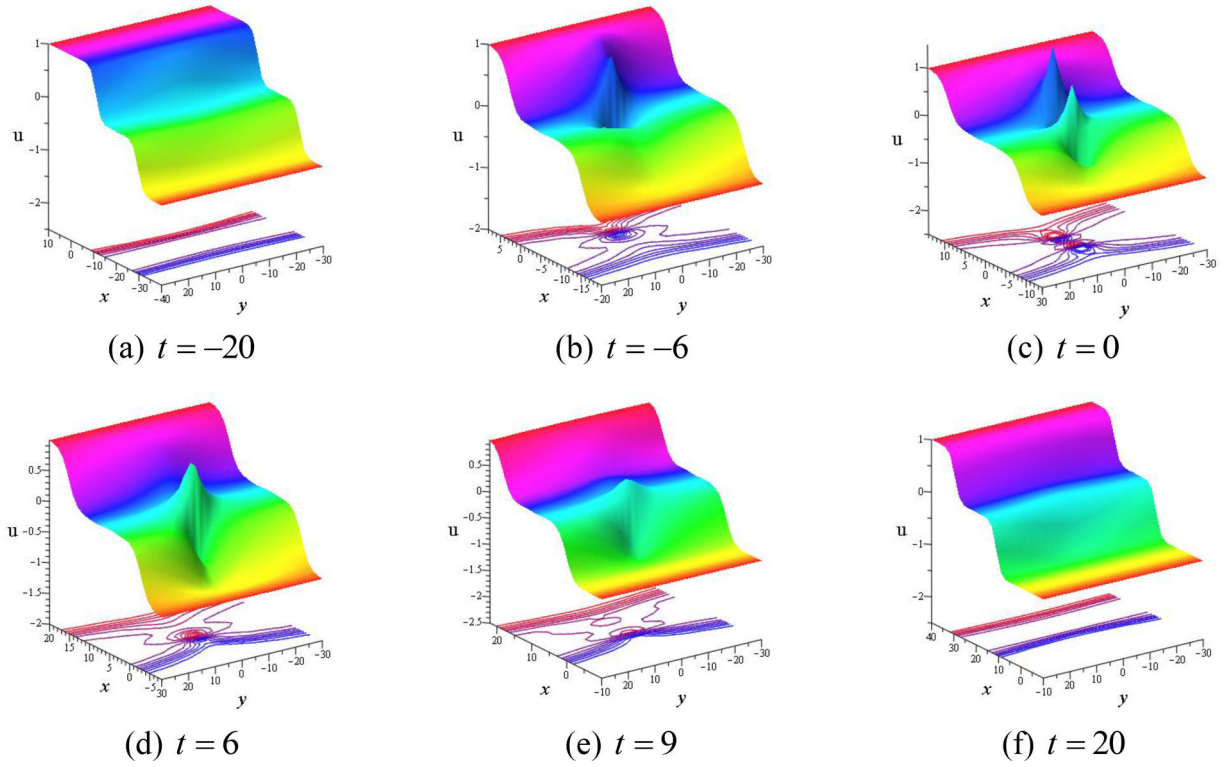

Fig. 10.. (Color online) Fission-fusion profile of x-periodic lump wave with the double kink wave of solution Eq. (15)for $m_{12} = 1$(For interpretation of the references to color in the text, the reader is referred to the web version of this article.).

$$\tilde{u}_5 = \begin{bmatrix} -l_1 m_{12}\sin\{m_{12}x + m_{13}y + m_{14}z + m_{12}^2(am_{12} + bm_{13} + cm_{14})t + m_{16}\} \\ -l_2\tilde{m}_{17}\sin\left\{\tilde{m}_{17}x + \tilde{m}_{18}y + \tilde{m}_{19}z + \tilde{m}_{17}^2\left(a\tilde{m}_{17} + b\tilde{m}_{18} + c\tilde{m}_{19}\right)t + \tilde{m}_{21}\right\} \end{bmatrix} / \begin{bmatrix} m_{11} + l_1\cos\{m_{12}x + m_{13}y + m_{14}z + m_{12}^2(am_{12} + bm_{13} + cm_{14})t + m_{16}\} \\ +l_2\cos\left\{\tilde{m}_{17}x + \tilde{m}_{18}y + \tilde{m}_{19}z + \tilde{m}_{17}^2\left(a\tilde{m}_{17} + b\tilde{m}_{18} + c\tilde{m}_{19}\right)t + \tilde{m}_{21}\right\} \end{bmatrix}. \tag{18}$$

Lastly, the solution represented by Eq. (18) are different periodic waves for different chooses of parameters in $\tilde{u}_5$. When $l_1 = 0$, $\tilde{u}_5$is a one periodic wave that confine in the position and time directions (observe Fig. 12(a)). Otherwise, when $l_1 \neq 0$, then $\tilde{u}_5$exhibits the dual periodic waves in both $xy$and xz- planes (observe Fig. 12(b) and (c)).

3. Conclision

In summary, interaction solutions of the (3 + 1)-dimensional STOL equation have been determined successfully. With the aid of Maple software, a test function is carefully used to derive different nonlinear dynamical properties. As a result, some novel collision solutions among the lump, periodic and kinky waves are derived of the STOL model. We also established fission fusion properties for the collision of lump and kink waves, lump and periodic waves and among the collision of lump, kink and periodic waves. We also observed that fission and fusion properties exist in presence and without presence of sinusoidal function and produces hybrid lump waves. By taking purely imaginary values of some parameters, we derived line breather and double periodic breather wave solutions. To better understand the dynamic natures of the obtained collision solutions, we depict adequate 3d plots and contour diagrams by choosing suitable parametric values with the aid of computational software Maple 18. It is expected that our achieved solutions can improve the dynamical characteristics of the other higher order models.

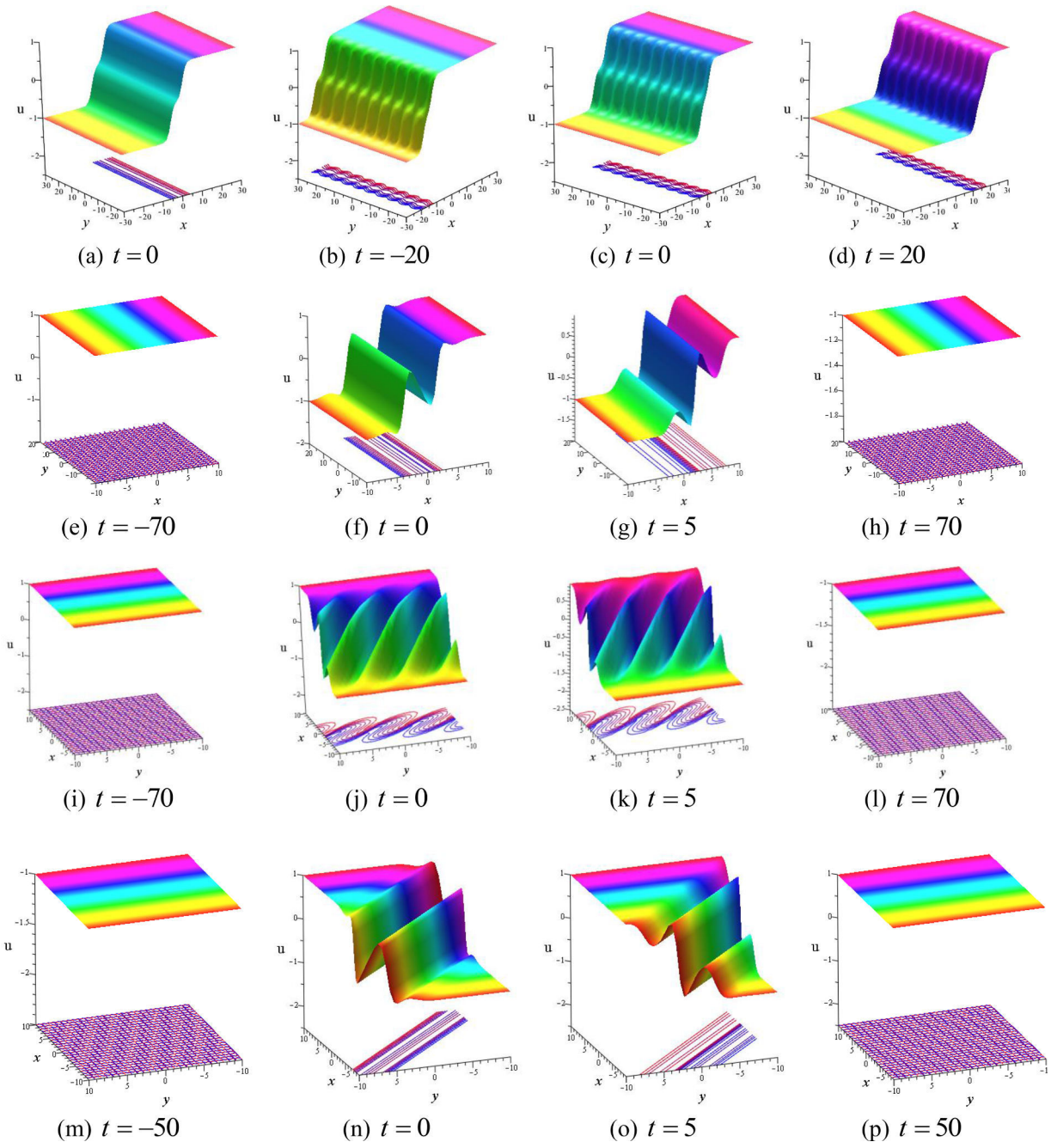

Fig. 11.. (Color online) Annihilation properties of the collision solution u_5 of Eq. (17) for $a=1, b=-2, c=3, m_{11}=1500, m_{14}=-2, m_{16}=1, m_{17}=1, m_{19}=-1/12, m_{21}=1$ and $l_2=100$: (a) double kinky waves for $l_1=m_{12}=m_{18}=0, m_{13}=1$; (b)-(d) y- periodic and double kinky waves for $l_1=1000, m_{12}=m_{18}=0, m_{13}=1$; (e)-(h) x- periodic and double kinky waves for $l_1=1000, m_{13}=m_{18}=0, m_{12}=1$; (i)-(l) (x,y)- periodic and double kinky waves for $l_1=1000, m_{18}=0, m_{12}=m_{13}=1$; (m)-(p) (x,y)- periodic and double kinky waves for $l_1=1000, m_{12}=m_{13}=m_{18}=1$(For interpretation of the references to color in the text, the reader is referred to the web version of this article.).

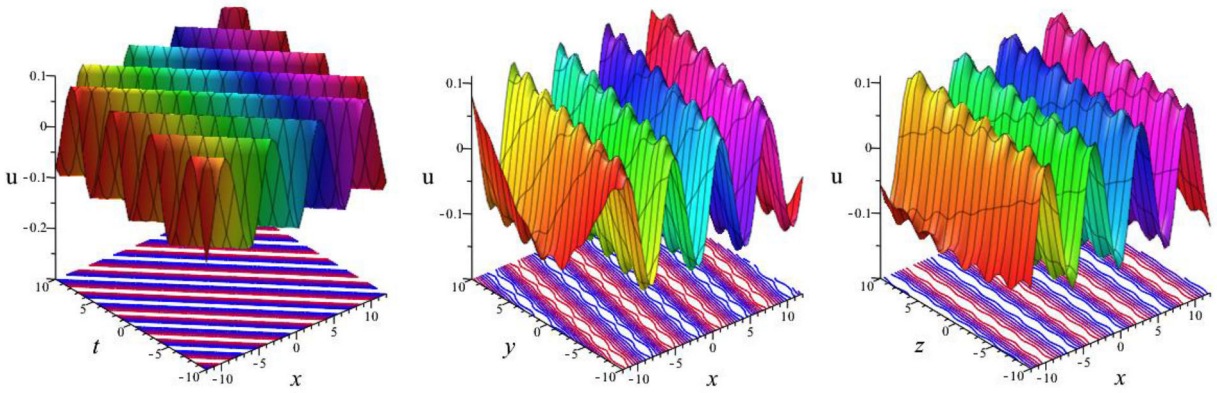

Fig. 12.. (Color online) Diagrams of the collision solution $\tilde{u}_5$of Eq. (18) for $a = -1, b = 1, c = -0.6, m_{11} = 1, m_{12} = 0, m_{13} = 2, m_{14} = -2, m_{16} = 1, l_2 = 0.1$ and $\tilde{m}_{17} = 1, \tilde{m}_{18} = -0.25, \tilde{m}_{19} = -1/12, \tilde{m}_{21} = 1$: (a) one periodic wave at $l_1 = 0$; (b)-(c) dual periodic wave at $l_1 = 0.1$(For interpretation of the references to color in the text, the reader is referred to the web version of this article.).

Declaration of Competing Interest

The researchers have no conflict of interest.

References

[1] A.R. Seadawy, Stability analysis for Zakharov-Kuznetsov equation of weakly nonlinear ion-acoustic waves in a plasma, Comput. Math. Appl. 67 (2014) 172–180.
[2] H. Triki, A. Biswas, S.P. Moshokoa, M. Belic, Optical solitons and conservation laws with quadratic-cubic nonlinearity, Optik 128 (2017) 63–70.
[3] B.Q. Li, Y.L. Ma, Periodic solutions and solitons to two complex short pulse (CSP) equations in optical fiber, Optik 144 (2017) 149–155.
[4] H.W. Yang, X. Chen, M. Guo, Y.D. Chen, A new ZK-BO equation for three-dimensional algebraic Rossby solitary waves and its solution as well as fission property, Nonlinear Dynam. 91 (2018) 2019–2032.
[5] W.Q. Peng, S.F. Tian, T.T. Zhang, Dynamics of the soliton waves, breather waves, and rogue waves to the cylindrical Kadomtsev-Petviashvili equation in pair-ion-electron plasma, Phys. Fluid 31 (2019), 102107.
[6] W.Q. Peng, S.F. Tian, X.B. Wang, T.T. Zhang, Y. Fang, Riemann-Hilbert method and multi-soliton solutions for three-component coupled nonlinear Schrödinger equations, J. Geom. Phys. 146 (2019), 103508.
[7] L.D. Zhang, S.F. Tian, W.Q. Peng, T.T. Zhang, X.J. Yan, The dynamics of lump, lump-off and rogue wave solutions of (2+1)-dimensional Hirota-Satsuma-Ito equations, East Asian J. Appl. Math. 10 (2020) 243–255.
[8] W.Q. Peng, S.F. Tian, T.T. Zhang, Y. Fang, Rational and semi-rational solutions of a nonlocal (2+ 1)-dimensional nonlinear Schrödinger equation, Math. Meth. Appl. Sci. 42 (2019) 6865–6877.
[9] A.C. Cevikel, A. Bekir, New solitons and periodic solutions for (2+1)-dimensional Davey-Stewartson equations, Chin. J. Phys. 51 (1) (2013) 1–13.
[10] A. Bekir, M. Kaplan, Exponential rational function method for solving nonlinear equations arising in various physical models, Chin. J. Phys. 54 (3) (2016) 365–370.
[11] E. Tala-Tebue, H. Rezazadeh, M. Eslami, A. Bekir, New approach to model coupled nerve fibers and exact solutions of the system, Chin. J. Phys. 62 (2019) 179–186.
[12] M.S. Ullah, H.O. Roshid, M.Z. Ali, Z. Rahman, Dynamical structures of multi-soliton solutions to the Bogoyavlenskii's breaking soliton equations, Eur. Phys. J. Plus 135 (2020) 282.
[13] M.J. Ablowitz, M.A. Ablowitz, P.A. Clarkson, Solitons, Nonlinear Evolution Equations and Inverse Scattering, Cambridge university press, 1991.
[14] A.M. Wazwaz, The tanh method for traveling wave solutions of nonlinear equations, Appl. Math. Comput. 154 (2004) 713–723.
[15] X.H. Wu, J.H. He, Exp-function method and its application to nonlinear equations, Chaos, Solitons and Fractals 38 (2008) 903–910.
[16] A. Bekir, Application of the Exp-function method for nonlinear differential-difference equations, Appl. Math. Comput. 215 (11) (2010) 4049–4053.
[17] V.B. Matveev, M.A. Salle, Darboux Transformation and Solitons, Springer-Verlag, Berlin, 1991.
[18] R. Hirota, Direct Methods in Soliton Theory, Cambridge University Prees, 2004.
[19] Z. Feng, The first-integral method to study the Burgers–Korteweg–de Vries equation, J. Phys. A: Math. Gen. 35 (2002) 343–349.
[20] A. Bekir, Ö. Ünsal, Analytic treatment for nonlinear evolution equations by using first integral method, Pramana – J. Phys. 79 (1) (2012) 3–17.
[21] H.O. Roshid, M.A. Rahman, The exp (− Φ (η))-expansion method with application in the (1+ 1)-dimensional classical Boussinesq equations, Result Phys. 4 (2014) 150–155.
[22] M.B. Hossen, H.O. Roshid, M.Z. Ali, Characteristics of the solitary waves and rogue waves with interaction phenomena in a (2+ 1)-dimensional Breaking Soliton equation, Phys. Lett. A 382 (2018) 1268–1274.
[23] S. Wang, X.Y. Tang, S.Y. Lou, Soliton fission and fusion: burgers equation and Sharma-Tasso-Olver equation, Chaos, Solitons and Fractals 21 (2004) 231–239.
[24] A.H. Chen, Multi-kink solutions and soliton fission and fusion of Sharma-Tasso-Olver equation, Phys. Lett. A 374 (2010) 2340–2345.
[25] H.O. Roshid, M.M. Rashidi, Multi-soliton fusion phenomenon of Burgers equation and fission, fusion phenomenon of Sharma–Tasso–Olver equation, J. Ocea. Eng. Sci. 2 (2017) 120–126.
[26] H.O. Roshid, Lump solutions to a (3+ 1)-dimensional potential-Yu–Toda–Sasa–Fukuyama (YTSF) like equation, Int. J. Appl. Comput. Math. 3 (2017) 1455–1461.
[27] J.B. Zhang, W.X. Ma, Mixed lump-kink solutions to the BKP equation, Comput. Math. Appl. 74 (2017) 591–596.
[28] H.Q. Zhao, W.X. Ma, Mixed lump–kink solutions to the KP equation, Comput. Math. Appl. 74 (2017) 1399–1405.
[29] Y. Tang, S. Tao, Q. Guan, Lump solitons and the interaction phenomena of them for two classes of nonlinear evolution equations, Comput. Math. Appl. 72 (2016) 2334–2342.
[30] X. Zhang, Y. Chen, Rogue wave and a pair of resonance stripe solitons to a reduced (3+1)-dimensional Jimbo-Miwa equation, Commun. Nonlinear Sci. Numer. Simulat. 52 (2017) 24–31.

[31] B. Ren, W.X. Ma, J. Yu, Rational solutions and their interaction solutions of the (2+1)-dimensional modified dispersive water wave equation, Comput. Math. Appl. 77 (2019) 2086–2095.
[32] A.S. Fokas, D.E. Pelinovsky, C. Sulaem, Interaction of lumps with a line soliton for the DSII equation, Physica D 152–153 (2001) 189–198.
[33] H.O. Roshid, W.X. Ma, Dynamics of mixed lump-solitary waves of an extended (2 + 1)-dimensional shallow water wave model, Phys. Lett. A 382 (2018) 3262–3268.
[34] W.X. Ma, X. Yong, H.Q. Zhang, Diversity of interaction solutions to the (2+1)-dimensional Ito equation, Comput. Math. Appl. 75 (2018) 289–295.
[35] Y. Tang, S. Tao, M. Zhou, Q. Guan, Interaction solutions between lump and other solitons of two classes of nonlinear evolution equations, Nonlinear Dynam. 89 (2017) 1–14.
[36] Z.H. Xu, H.L. Chen, Z.D. Dai, Rogue wave for the (2+1)-dimensional Kadomtsev-Petviashvili equation, Appl. Math. Lett. 37 (2014) 34–38.
[37] J.Y. Yang, W.X. Ma, Z.Y. Qin, Lump and lump-soliton solutions to the (2+1)-dimensional Ito equation, Anal. Math. Phys. 8 (2017) 427–436.
[38] M. Shahriari, J. Manafian, Analytical behaviour of lump solution and interaction phenomenon to the Kadomtsev–Petviashvili-like equation, Pramana – J. Phys. 93 (2019) 3.
[39] M.S. Khatun, M.F. Hoque, M.A. Rahman, Multisoliton solutions, completely elastic collisions and non-elastic fusion phenomena of two PDEs, Pramana – J. Phys. 88 (2017) 86.
[40] H. Gao, Dynamics of N th-order rogue waves in (2+1)-dimensional Hirota equation, Pramana – J. Phys. 88 (2017) 84.
[41] Z. Lu, E.M. Tian, R. Grimshaw, Interaction of two lump solitons described by the Kadomtsev–Petviashvili I equation, Wave Motion 40 (2004) 123–135.
[42] Z.J. Lian, S.Y. Lou, Symmetries and exact solutions of the Sharma-Tasso-Olver equation, Nonlinear Anal. 63 (2005) 1167–1177.
[43] A.M. Wazwaz, S.A.E. Tantawy, New (3+1)-dimensional equations of Burgers type and Sharma-Tasso-Olver type: multiple-soliton solutions, Nonlinear Dynam. 87 (2017) 2457–2461.

Eur. Phys. J. Plus (2020) 135:282
https://doi.org/10.1140/epjp/s13360-020-00289-9

THE EUROPEAN PHYSICAL JOURNAL PLUS

Regular Article

Dynamical structures of multi-soliton solutions to the Bogoyavlenskii's breaking soliton equations

Mohammad Safi Ullah[1,2,a], **Harun-Or Roshid**[2,3,b], **M. Zulfikar Ali**[2], **Zillur Rahman**[1,2]

[1] Department of Mathematics, Comilla University, Cumilla 3506, Bangladesh
[2] Department of Mathematics, Rajshahi University, Rajshahi 6205, Bangladesh
[3] Department of Mathematics, Pabna University of Science and Technology, Pabna 6600, Bangladesh

Received: 9 December 2019 / Accepted: 21 February 2020

Abstract We derive a multi-soliton solution for the Bogoyavlenskii's breaking soliton equation by utilizing the simplified Hirota's approach. From this multi-soliton solution, we investigate various forms of single kinky–lump-type breather solitons, double kinky–lump-type breather solitons, collision of a kink line soliton with a kinky-type breather soliton, and collision of a pair of double kinky–lump breather solitons by the appropriate selection of the involved parameters. These breathers hold unlike features in various planes even in various times. Elastic and non-elastic collisions for double kinky-type lump breather are experienced in various planes and in various times. The effect and control of the propagation direction, energies, phase shifts and shape of waves by the parameters are also analyzed. Some figures are given to illustrate the dynamics of the achieved solutions. The acquired results can enrich the dynamical properties of the higher-dimensional nonlinear scenarios in the engineering fields.

1 Introduction

Nonlinear partial differential models are extensively employed to interpret many complicated areas of sciences and engineering issue, for instance, optical connections, oceanic scientific problems, fluid dynamics, atmospheric, geochemistry, chemical physics and plasma physics and others [1–5]. It has three sections specifically soliton, chaos and fractal. Concepts of solitons are very significant and effective research area in nonlinear science. The hot topics of solitons are lump, kink, rogue and breather solitary waves. To explore the features of solitary wave, numerous reputed scientists have been developed by various reliable and fruitful approaches mainly Exp-function method [6,7], (G'/G)-expansion method [8], homogeneous balance method [9,10], homotopy perturbation method [11], F-expansion method [12], direct algebraic method [13], Tan-Cot method [14], the inverse scattering transform [15], Darboux transformation [16], and so forth. In 2004, a well-known approach called Hirota bilinear method was firstly discovered by Hirota [17]. This method becomes effective and reliable

[a] e-mail: safi.ru1985@gmail.com
[b] e-mail: harunorroshidmd@gmail.com (corresponding author)

within the short time and used to derive soliton, multi-soliton, lump waves, rogue waves, breather waves and exciting localized formations of soliton solutions [17–20,24–28]. More recently, Ma [29–31] determined lump wave solutions and their interactions with various solitons for both linear and nonlinear PDEs. Ma [32] also derived long-time asymptotes for a three-competent coupled mKdV model, and he used inverse scattering transforms [33] to derive soliton solutions for nonlocal reverse-time nonlinear Schrödinger equations.

The prime aim of this work is to determine multi-soliton solutions and then construct various new kinds of localized wave solutions to the following Bogoyavlenskii's breaking soliton (BBS) equation [21–23] via the Hirota bilinear technique.

$$\Phi_{xxxy} + 4\Phi_y\Phi_{xx} + 4\Phi_x\Phi_{xy} + \Phi_{xt} = 0 \tag{1}$$

To reach our goal, this paper is arranged as follows: we employ the Hirota bilinear technique to determine the n-soliton solutions of the BBS equation in Sect. 2. Section 3 offers the lump, breather soliton and their collision solutions of the BBS equation. Finally, some conclusions are drawn in Sect. 4.

2 Multi-soliton of the BBS equation

Dispersion relation for the BBS Eq. (1) can be evaluated considering a trial solution in an exponential form as:

$$\Phi(x, y, t) = \exp(\vartheta_i), \quad \vartheta_i = a_i x + b_i y - \varpi_i t. \tag{2}$$

Exerting Eq. (2) into the linear terms of Eq. (1), we get hold of the dispersion relation ϖ_i as

$$\varpi_i = a_i^2 b_i, \quad i = 1, 2, \cdots \cdots, n \tag{3}$$

and the resultant variables take place as

$$\vartheta_i = a_i x + b_i y - a_i^2 b_i t, \quad i = 1, 2, \cdots \cdots, n. \tag{4}$$

Let us consider the conversion relation

$$\Phi(x, y, t) = R(\ln \tau(x, y, t))_x. \tag{5}$$

Now exerting Eq. (5) with $\tau(x, y, t) = 1 + \exp(\vartheta)$ into Eq. (1) and then resolving R, we acquire

$$R = \frac{3}{2}. \tag{6}$$

To evaluate n-soliton solution, we must consider the supplementary function $\tau(x, y, t)$ in the following:

$$\begin{aligned}\tau(x, y, t) = 1 &+ \sum_{i=1}^{n} \exp(\vartheta_i) + \sum_{i<j}^{n} A_{ij} \exp(\vartheta_i + \vartheta_j) \\ &+ \sum_{i<j<k}^{n} A_{ij} A_{ik} A_{jk} \exp(\vartheta_i + \vartheta_j + \vartheta_k) \\ &+ \cdots + \left(\prod_{i<j} A_{ij}\right) \exp\left(\sum_{i=1}^{n} \vartheta_i\right).\end{aligned} \tag{7}$$

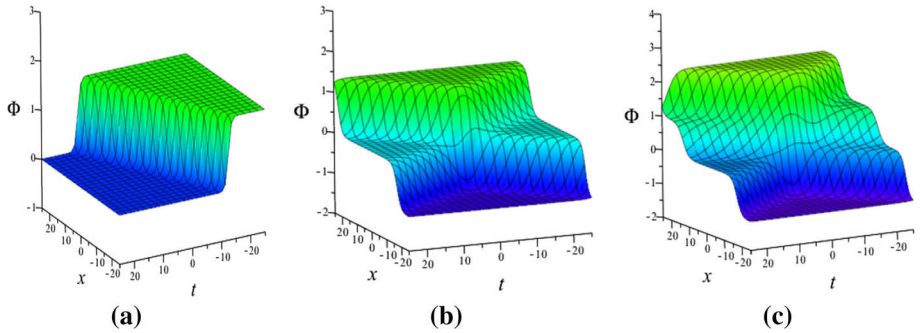

Fig. 1 Sketch of Eq. (5) with Eq. (7) and Eq. (10) for the values $l_1 = 1, m_1 = -1, p_1 = 1, q_1 = 1$. **a** 3D shape of single-kink soliton ($n = 1$); **b** 3D shape of double-kink or two solitons ($n = 2$); **c** 3D shape of triple-kink or three solitons ($n = 3$)

Here we consider trial solution for two solitons as

$$\tau(x, y, t) = 1 + \exp(\vartheta_1) + \exp(\vartheta_2) + A_{12}\exp(\vartheta_1 + \vartheta_2). \tag{8}$$

Setting Eq. (8) with Eq. (5) and Eq. (6) into Eq. (1) and then solving for unknown A_{12}, we gain

$$A_{12} = \frac{(a_1 - a_2)(a_1^2 b_2 + 2a_1 b_1 a_2 - 2a_1 a_2 b_2 - b_1 a_2^2)}{(a_1 + a_2)(a_1^2 b_2 + 2a_1 b_1 a_2 + 2a_1 a_2 b_2 + b_1 a_2^2)}. \tag{9}$$

In the similar way, we can get three, four and more soliton solutions from Eq. (7), where the unknowns are given by

$$A_{ij} = \frac{(a_i - a_j)(a_i^2 b_j + 2a_i b_i a_j - 2a_i a_j b_j - b_i a_j^2)}{(a_i + a_j)(a_i^2 b_j + 2a_i b_i a_j + 2a_i a_j b_j + b_i a_j^2)}, i, j = 1, 2, \cdots, n \tag{10}$$

providing $(a_i + a_j)(a_i^2 b_j + 2a_i b_i a_j + 2a_i a_j b_j + b_i a_j^2) \neq 0$.

Profile of the solution Eq. (7) with Eq. (5) and Eq. (10) exhibits multi-soliton solutions or n-kink soliton solutions as depicted in Fig. 1. Taking $n = 1,\ 2$ and $n = 3$, we get single-kink wave (Fig. 1a), double-kink solitons (Fig. 1b) and triple-kink solitons (Fig. 1c), respectively. It is evidently observed from Fig. 1b, c that before ($t < 0$) and after ($t > 0$) collision multi-kink solitons remain their own properties (height, width and speed) which are same. That is, the collisions are elastic.

3 Lump and breather soliton solution of the BBS equation

This section recalls the multi-soliton solutions to derive lump-type breather solution; collision of a soliton and a lump-type breather soliton; and collision between two lump-type breather solitons in the succeeding subsections.

3.1 Two-soliton and lump-type breather soliton solutions

Here, we would like to create lump-type breather wave propagation. To perform that, we have to assume at least two soliton solutions by putting $n = 2$ and then let $a_1 = l_1 + im_1, a_2 = l_1 - im_1, b_1 = p_1 + iq_1, b_2 = p_1 - iq_1$, into Eq. (8) and Eq. (9) and then Eq. (5) gives

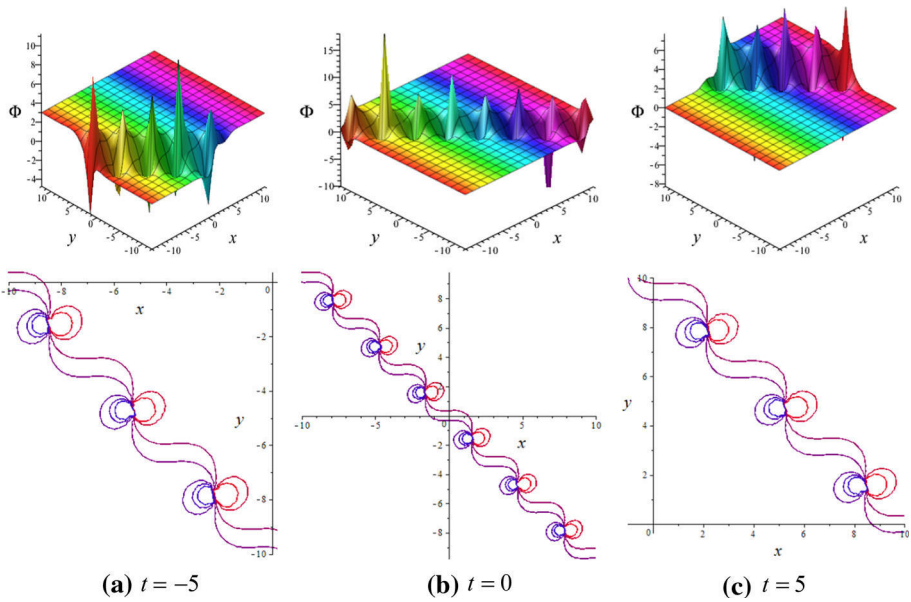

(a) $t = -5$ **(b)** $t = 0$ **(c)** $t = 5$

Fig. 2 Outlook of Eq. (11) with the parametric values $l_1 = 1, m_1 = -1, p_1 = 1, q_1 = 1$: 3D plot (upper) and its contour plot (below)

$$\Phi(x, y, t) = \frac{3}{2}\{\ln(1 + 2\exp(M_1)\cos(\sigma_1) + A_{12}\exp(2\sigma_1)\}_x. \tag{11}$$

where $M_1 = l_1 x + p_1 y - (l_1^2 p_1 - m_1^2 p_1 - 2l_1 m_1 q_1)t$, $\sigma_1 = m_1 x + q_1 y - (l_1^2 q_1 - m_1^2 q_1 + 2l_1 m_1 p_1)t$ and $A_{12} = -\frac{m_1(2p_1 l_1 m_1 + q_1 l_1^2 + 3q_1 m_1^2)}{l_1(2q_1 l_1 m_1 + p_1 m_1^2 + 3p_1 l_1^2)}$.

The solution Eq. (11) comes from two-soliton solution and gives lump-type breather propagation. Features of the solution Eq. (11) (Fig. 2 3D (upper) and its contour (below)) for the values $l_1 = 1, m_1 = -1, p_1 = 1, q_1 = 1$. Figures show that the solution exhibits as lump-type breather propagations along the paradox in the xy-plane at $t = 0$ (Fig. 2b), for different times ($t \neq 0$) it propagates not along paradox in the xy-plane but parallel to the paradox (Fig. 2a, c) and in every case all lump gets into a kink wave. We also observe that the kink waves as well as periodic lump lie in the negative quadrant for $t < 0$, move toward the paradox with time increase and reach along paradox at $t = 0$, and then move away from the paradox into the positive quadrant for as $t > 0$ with an increase in time. Its swiftness, breadth and direction remain unchanged on the whole dynamical system and periodic lump occurs equidistance from each other in each system.

Alternatively, we experience different phenomena when profile observes in the xt-plane. In this case, the solution Eq. (11) exhibits as multi-lump waves periodically get into a single-kink wave when $y \neq 0$ (Fig. 3a, c), but exhibits double kinky wave at $y = 0$ (Fig. 3b) and periodic lump-type scratch is also viewed in both kink waves.

3.2 Interaction of a soliton and a lump-type breather soliton from three-soliton solutions

In this case, we would like to determine a collision solution between periodic lump-type breather waves that comes from two solitons and a kink soliton. In this regard, consider the three-soliton solutions by putting $n = 3$ into Eq. (7) with Eq. (10), and then let $a_1 =$

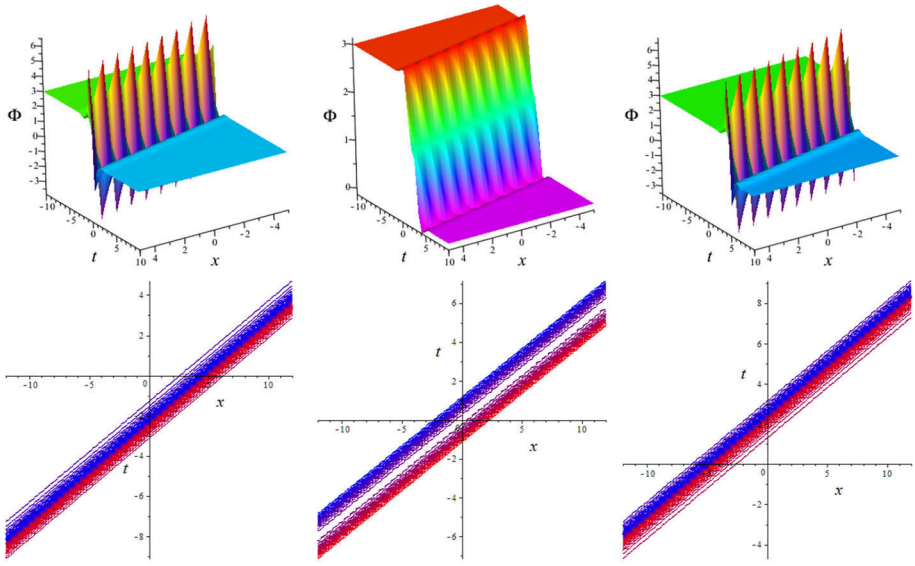

(a) $y = -5$ **(b)** $y = 0$ **(c)** $y = 5$

Fig. 3 Outlook of Eq. (11) with the parametric values $l_1 = 1, m_1 = -1, p_1 = 1, q_1 = 1$: 3D plot (upper) and its contour plot (below)

$l_1 + im_1, a_2 = l_1 - im_1, a_3 = c, b_1 = p_1 + iq_1, b_2 = p_1 - iq_1, b_3 = d$ into Eq. (7) together with Eqs. (5, 6, 10) which gives the resultant solution as

$$\begin{aligned}\Phi(x, y, t) = \frac{3}{2} \ln\{&1 + 2\exp(M_1)\cos(\sigma_1) + A_{12}\exp(2\sigma_1) + \exp(cx + \mathrm{d}y - c^2\mathrm{d}t) \\ &+ 2\rho_1 \exp(M_1 + cx + \mathrm{d}y - c^2\mathrm{d}t)\cos(\sigma_1 + \xi_1) + A_{12}\rho_1^2 \exp(2M_1 \\ &+ cx + \mathrm{d}y - c^2\mathrm{d}t)\}_x, \end{aligned} \tag{12}$$

where $A_{12} = -\frac{m_1(2p_1l_1m_1 + q_1l_1^2 + 3q_1m_1^2)}{l_1(2q_1l_1m_1 + p_1m_1^2 + 3p_1l_1^2)}$, $M_1 = l_1x + p_1y - (l_1^2p_1 - m_1^2p_1 - 2l_1m_1q_1)t$, $\sigma_1 = m_1x + q_1y - (l_1^2q_1 - m_1^2q_1 + 2l_1m_1p_1)t$ and $A_{23} = P_1 + iQ_1 = \rho_1 \exp(i\xi_1)$(say), then $A_{13} = P_1 - iQ_1 = \rho_1 \exp(-i\xi_1)$ in which $\rho_1 = \sqrt{P_1^2 + Q_1^2}$ and $\xi_1 = \tan^{-1}(\frac{Q_1}{P_1})$.

In Eq. (12), solution comes in terms of the combination of exponential and periodic sinusoidal function exhibiting collision of a kinky periodic lump-type breather soliton and a kink-shaped line soliton, as viewed in Figs. 4, 5 and 6 for the values $l_1 = 1, m_1 = -1, p_1 = 1, q_1 = 1, c = 1$. There are two sub-cases existed depending on the interaction direction.

Case (i): For $d > 0$, we observe (Fig. 4 3D (upper) and its contour (below)) that the two waves are always parallel to each other, even at the time of interaction (see the contour plots in Fig. 4 (below)). We also observe that the two waves (display as a double-kink wave) contain periodically lump waves to get into the lower kink (Fig. 4a (upper)) before ($t < 0$) collision and upper kink (Fig. 4c (upper)) after ($t > 0$) collision in the xy-plane, respectively. They are overlapped entirely at $t = 0$ where highest amplitude comes into sight (Fig. 4b (upper)). Actually the whole collision processes are completely elastic which is evidently observed in the contour plots in Fig. 4 (below) in the same plane.

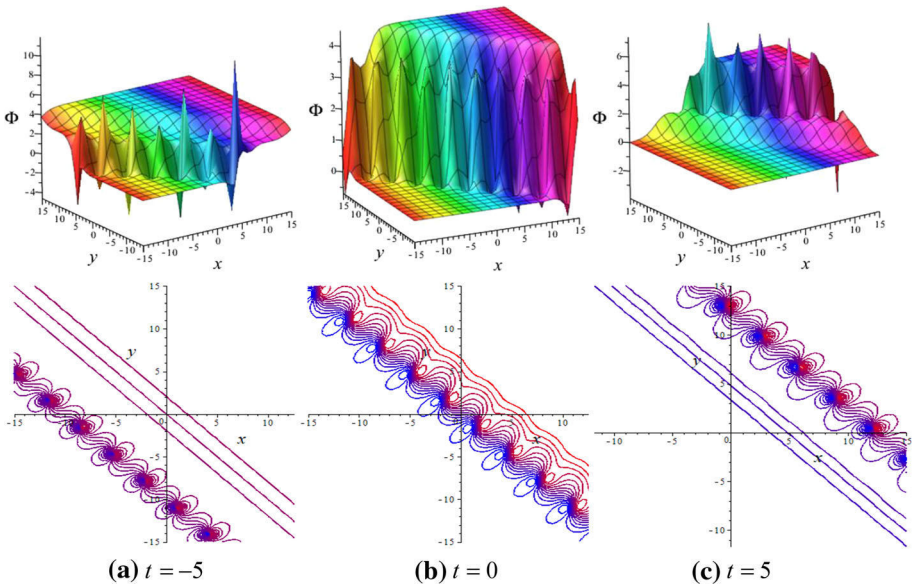

Fig. 4 Collision between breather lump soliton and kink line soliton of Eq. (12) for $l_1 = 1, m_1 = -1$, $p_1 = 1, q_1 = 1, c = 1, d = 1$: 3D plot (upper) and its contour plot (below)

Case (ii): For $d < 0$, we observe (Fig. 5 3D (upper) and its contour (below)) that the two waves (a kinky periodic lump-type breather soliton and a kink-shaped line soliton) interact at a certain angle. We see that a kink wave interacts with the breather wave and shifting of the collision changes along negative of y-axis (Fig. 5a) to positive of y-axis (Fig. 5c), but at the intermediate time they interact at the origin (Fig. 5b). The overall propagation process is elastic. Beside this, when we take the plot into the xt-plane, similar elastic collisions are also observed in the double-kink waves with the same parametric values (Fig. 6 3D (upper) and its contour (below)).

3.3 Four solitons and interaction of two lump-type breather solitons

To determine interaction of two lump-type breather solitons, we have to consider at four soliton solutions. In this regard, consider the three-soliton solution by putting $n = 4$ in Eq. (7) with Eq. (10), and then let $a_1 = l_1 + im_1, a_2 = l_1 - im_1, a_3 = l_2 + im_2, a_4 = l_2 - im_2$, $b_1 = p_1 + iq_1, b_2 = p_1 - iq_1, b_3 = p_2 + iq_2, b_4 = p_2 - iq_2$ into Eq. (7) together with Eqs. (5, 6, 10) giving the resultant solution as

$$\begin{aligned}\Phi(x, y, t) = \frac{3}{2} \ln\{&1 + 2\exp(M_1)\cos(\sigma_1) + +2\exp(M_2)\cos(\sigma_2) + A_{12}\exp(2M_1) \\ &+ A_{34}\exp(2M_2) + 2\rho_1\cos(\xi_1 + \sigma_1 + \sigma_2)\exp(M_1 + M_2) \\ &+ 2\rho_2\cos(\xi_2 + \sigma_1 - \sigma_2)\exp(M_1 + M_2) \\ &+ 2A_{12}\rho_1\rho_2\exp(2\sigma_1 + \sigma_2)\cos(M_2 + \xi_1 - \xi_2) \\ &+ 2A_{34}\rho_1\rho_2\exp(\sigma_1 + 2\sigma_2)\cos(M_1 + \xi_1 + \xi_2) + A_{12}A_{34}\exp(2\sigma_1 + 2\sigma_2)\}_x\end{aligned} \tag{13}$$

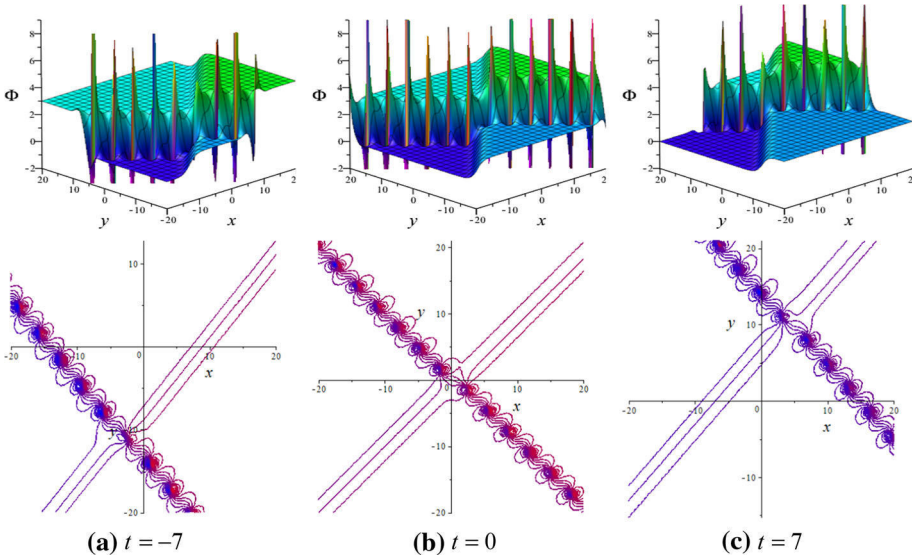

Fig. 5 Collision between breather lump soliton and kink line soliton of Eq. (12) for $l_1 = 1, m_1 = -1, p_1 = 1, q_1 = 1, c = 1, d = -1$: 3D plot (upper) and its contour plot (below)

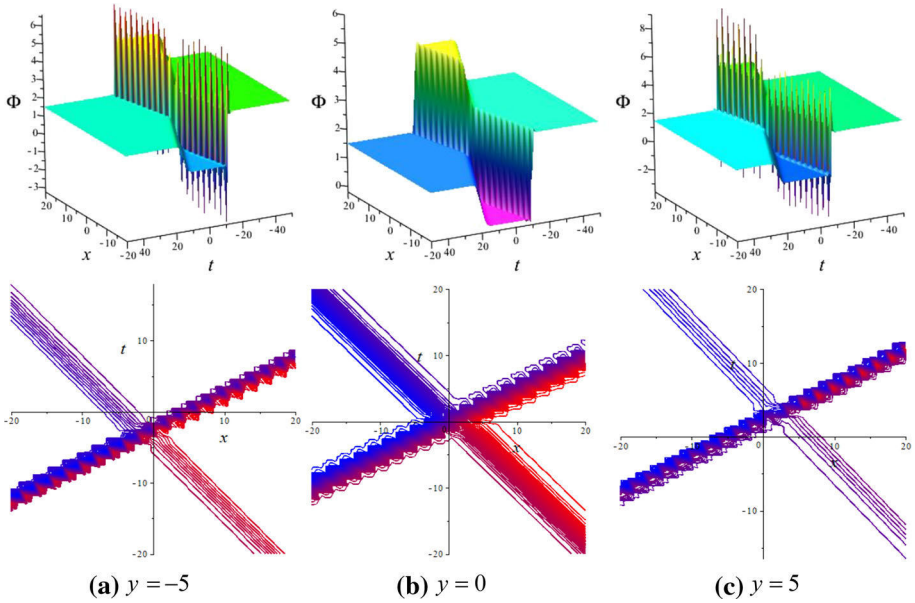

Fig. 6 Collision between breather lump soliton and kink line soliton of Eq. (12) for $l_1 = 1, m_1 = -1, p_1 = 1, q_1 = 1, c = 1, d = -1$: 3D plot (upper) and its contour plot (below)

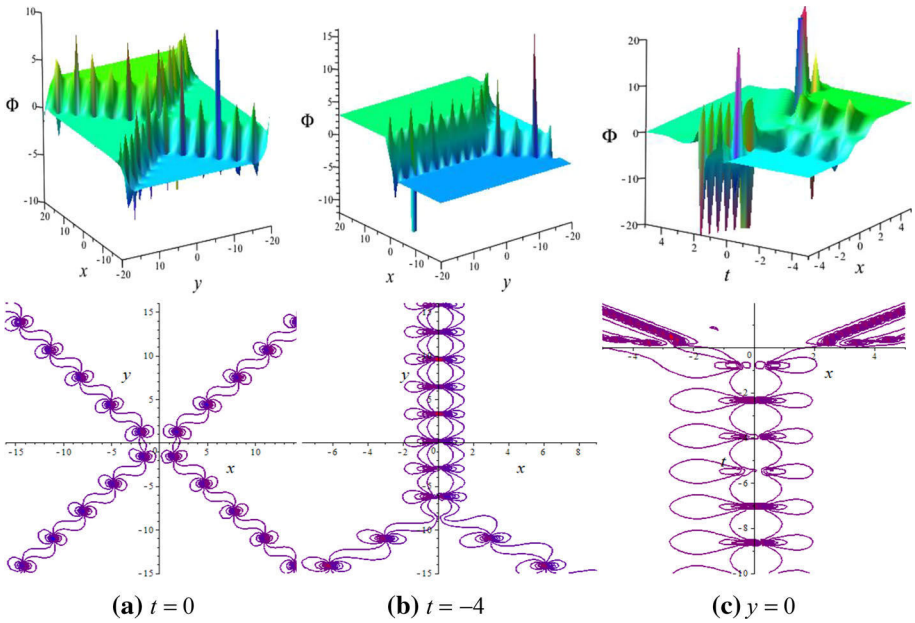

(a) $t = 0$ **(b)** $t = -4$ **(c)** $y = 0$

Fig. 7 Collision of periodic lump and periodic line waves of Eq. (13) for $l_1 = 1, m_1 = -1, p_1 = 1, q_1 = 1, l_2 = -1.001, m_2 = 1, p_2 = 1, q_2 = 1$: 3D plot (upper) and its contour plot (below)

where $M_1 = l_1 x + p_1 y - (l_1^2 p_1 - m_1^2 p_1 - 2 l_1 m_1 q_1)t$, $\sigma_1 = m_1 x + q_1 y - (l_1^2 q_1 - m_1^2 q_1 + 2 l_1 m_1 p_1)t$,

$$M_2 = l_2 x + p_2 y - (l_2^2 p_2 - m_2^2 p_2 - 2 l_2 m_2 q_2)t,$$
$$\sigma_2 = m_2 x + q_2 y - (l_2^2 q_2 - m_2^2 q_2 + 2 l_2 m_2 p_2)t,$$
$$A_{12} = -\frac{m_1(2 p_1 l_1 m_1 + q_1 l_1^2 + 3 q_1 m_1^2)}{l_1(2 q_1 l_1 m_1 + p_1 m_1^2 + 3 p_1 l_1^2)}, \quad A_{34} = -\frac{m_2(2 p_2 l_2 m_2 + q_2 l_2^2 + 3 q_2 m_2^2)}{l_2(2 q_2 l_2 m_2 + p_2 m_2^2 + 3 p_2 l_2^2)}$$

$A_{24} = P_1 + i Q_1 = \rho_1 \exp(i\xi_1)$ (say) and $A_{14} = P_2 + i Q_1 = \rho_2 \exp(i\xi_1)$ (say), then $A_{13} = P_1 - i Q_1 = \rho_1 \exp(-i\xi_1)$ and $A_{23} = P_2 - i Q_2 = \rho_2 \exp(-i\xi_1)$.

To find the values of ρ_1, ρ_2, ϑ_1 and ϑ_2, we apply $\rho = \sqrt{P^2 + Q^2}$ and $\vartheta = \tan^{-1}(\frac{Q}{P})$.

In the solution Eq. (13), comes in terms of exponential and periodic sinusoidal function exhibits collision of a pair of periodic lump-type breather waves, as viewed in Fig. 7 with the values $l_1 = 1, m_1 = -1, p_1 = 1, q_1 = 1, l_2 = -1.001, m_2 = 1, p_2 = 1, q_2 = 1$ at $t = 0$. It is fascinating that collision of these breathers owns unlike dynamic natures in distinct planes. Both elastic (Fig. 7a 3D (upper) and its contour (below)) and non-elastic (Fig. 7b, c 3D (upper) and its contour (below)) collision own different times and different planes. Figure 7a exhibits double-kink-type X-shaped breather soliton for elastic collision as before and after collision each lump-type breather wave remains their same solitonic natures and interacts at the origin coming along opposite paradox in the xy-plane. It is observed that the some lump waves are periodically got into each soliton, being at equal distance from each other. On the other hand, when we take the same plot in the same xy-plane but in different times at $t = -4$ it exhibits non-elastic fusion phenomena after collision as propagated from negative to positive along y direction (Fig. 7b 3D (upper) and its contour (below)). Other behavior also owns the collision when observed in the xt-plane. It is seen that a breather lump wave

interacts at $t = 0$ and then causes fission as it is split into two breather-type lump waves (Fig. 7c 3D (upper) and its contour (below)) time goes by.

4 Conclusions

In the summary, we have successfully used Hirota bilinear method to gain multi-soliton solutions Eq. (7) of the BBS equation; see Fig. 1. Various parametric values have been selected to get distinguish dynamical characteristics of single kinky–lump-type breather solitons (Figs. 2, 3a, c), double kinky–lump-type breather solitons (Figs. 3b, 4, 5, 6, 7a), collision of a kink line soliton with a kinky-type breather soliton (Figs. 4, 5, 6), and collision of a pair of kinky–lump breather solitons (Fig. 7a) by the appropriate selection of involved parameters from the multi-soliton solutions of the models. These breathers hold unlike features in various planes even in various times. Elastic (Figs. 1, 2, 3, 4, 5, 6, 7a) and non-elastic (Fig. 7b, c) collisions for double kinky–lump-type breather are experienced in various plane and in various times. Some figures are given to illustrate the dynamics of the achieved solutions. This will also prompt us to explore new approach to obtain more extensive and accurate solution to the models. The acquired results can enhance the dynamical properties of higher-dimensional nonlinear scenarios in the engineering fields.

Compliance with ethical standards

Conflict of interest The authors have no conflict of interest.

References

1. A.R. Seadawy, Stability analysis for Zakharov–Kuznetsov equation of weakly nonlinear ion-acoustic waves in a plasma. Comput. Math. Appl. **67**(1), 172–180 (2014)
2. H. Triki, A. Biswas, S.P. Moshokoa, M. Belic, Optical solitons and conservation laws with quadratic-cubic nonlinearity. Optik **128**, 63–70 (2017)
3. B.Q. Li, Y.L. Ma, Periodic solutions and solitons to two complex short pulse (CSP) equations in optical fiber. Optik **144**, 149–155 (2017)
4. H.W. Yang, X. Chen, M. Guo, Y.D. Chen, A new ZK–BO equation for three-dimensional algebraic Rossby solitary waves and its solution as well as fission property. Nonlinear Dyn. **91**(3), 2019–2032 (2018)
5. A. Biswas, 1-Soliton solution of the generalized Camassa–Holm Kadomtsev–Petviashvili equation. Commun. Nonlinear Sci. Numer. Simul. **14**, 2524–2527 (2009)
6. J.H. He, M.A. Abdou, New periodic solutions for nonlinear evolution equations using Exp-function method. Chaos Solitons Fractals **34**, 1421–1429 (2007)
7. X.H. Wu, J.H. He, Exp-function method and its application to nonlinear equations. Chaos Solitons Fractals **38**(3), 903–910 (2008)
8. M. Wang, X. Li, J. Zhang, The G'/G-expansion method and travelling wave solutions of nonlinear evolution equations in mathematical physics. Phys. Lett. A **372**, 417–423 (2008)
9. E. Fan, H. Zhang, A note on the homogeneous balance method. Phys. Lett. A **246**, 403–406 (1998)
10. M. Senthilvelan, On the extended applications of homogenous balance method. Appl. Math. Comput. **123**, 381–388 (2001)
11. D. Arseven, T. Zi, An analytical study for fisher type equations by using Homotopy perturbation method. Comput. Math. Appl. **60**(3), 602–609 (2010)
12. M.A. Abdou, The extended F-expansion method and its application for a class of nonlinear evolution equations. Chaos Solitons Fractals **31**(1), 95–104 (2007)
13. A.R. Seadawa, The solutions of the boussinesq and generalized fifth-order KdV equations by using the direct algebraic method. Appl. Math. Sci. **6**(82), 4081–4090 (2012)
14. R. Kumar, M. Kumar, A. Kumar, Some soliton solutions of non linear partial differential equations by tan–cot method. IOSR J. Math. **6**, 23–28 (2013)

15. M.J. Ablowitz, M.A. Ablowitz, P.A. Clarkson, *Solitons, Nonlinear Evolution Equations and Inverse Scattering* (Cambridge University Press, Cambridge, 1991)
16. Y. Li, J.E. Zhang, Darboux transformations of classical Boussinesq system and its multi-soliton solutions. Phys. Lett. A **284**(6), 253–258 (2001)
17. R. Hirota, *The Direct Method in Soliton Theory* (Cambridge University Press, Cambridge, 2004)
18. M.B. Hossen, H.O. Roshid, M.Z. Ali, Characteristics of the solitary waves and rogue waves with interaction phenomena in a (2+ 1)-dimensional breaking soliton equation. Phys. Lett. A **382**, 1268–1274 (2018)
19. W.X. Ma, Y. Zhou, Lump solutions to nonlinear partial differential equations via Hirota bilinear forms. J. Differ. Equ. **264**, 2633–2659 (2018)
20. H.Q. Zhao, W.X. Ma, Mixed lump–kink solutions to the KP equation. Comput. Math. Appl. **74**, 1399–1405 (2017)
21. W. Yong-Qi, Bilinear Bäcklund transformation and explicit solutions for a nonlinear evolution equation. Chin. Phys. B **19**(4), 040304 (2010)
22. E. Fan, Y.C. Hon, Quasiperiodic waves and asymptotic behavior for Bogoyavlenskii's breaking soliton equation in (2 + 1) dimensions. Phys. Rev. E **78**(3), 036607 (2008)
23. T. Xia, S. Xiong, Exact solutions of (2 + 1) -dimensional Bogoyavlenskii's breaking soliton equation with symbolic computation. Comput. Math. Appl. **60**(3), 919–923 (2010)
24. H.O. Roshid, W.X. Ma, Dynamics of mixed lump-solitary waves of an extended (2 + 1)-dimensional shallow water wave model. Phys. Lett. A **382**, 3262–3268 (2018)
25. H.O. Roshid, Lump solutions to a (3 + 1)-dimensional potential-Yu–Toda–Sasa–Fukuyama (YTSF) like equation. Int. J. Appl. Comput. Math. **3**, 1455–1461 (2017)
26. W. Liu, Y. Zhang, Multiple rogue wave solutions for a (3+1)-dimensional Hirota bilinear equation. Appl. Math. Lett. **98**, 184–190 (2019)
27. Z. Xu, H. Chen, Z. Dai, Rogue wave for the (2+1)-dimensional Kadomtsev–Petviashvili equation. Appl. Math. Lett. **37**, 34–38 (2014)
28. G.F. Deng, Y.T. Gao, J.J. Su, C.C. Ding, Multi-breather wave solutions for a generalized (3 + 1)-dimensional Yu–Toda–Sasa–Fukuyama equation in a two-layer liquid. Appl. Math. Lett. **98**, 177–183 (2019)
29. W.X. Ma, A search for lump solutions to a combined fourth-order nonlinear PDE in (2 + 1)-dimensions. J. Appl. Anal. Comput. **9**(4), 1319–1332 (2019)
30. W.X. Ma, Interaction solutions to the Hirota–Satsuma-Ito equation in (2 + 1)-dimensions. Front. Math. China **14**(3), 619–629 (2019)
31. W.X. Ma, Lump and interaction solutions to linear PDEs in 2 + 1 dimensions via symbolic computation. Mod. Phys. Lett. B **33**(36), 1950457 (2019)
32. W.X. Ma, Long-time asymptotics of a three-component coupled mKdV system. Mathematics **7**(7), 573 (2019)
33. W.X. Ma, Inverse scattering for nonlocal reverse-time nonlinear Schrödinger equations. Appl. Math. Lett. **102**, 106161 (2020)